Directed sortase evolution for site-specific protein engineering and surface functionalization

Von der Fakultät für Mathematik, Informatik und Naturwissenschaften der RWTH Aachen
University zur Erlangung des akademischen Grades einer
Doktorin der Naturwissenschaften genehmigte Dissertation

vorgelegt von

Zhi Zou

Master of Biochemistry and Molecular Biology

aus

Huanggang, Hubei, P.R. China

Berichter: Univ.-Prof. Dr. rer. nat. Ulrich Schwaneberg

Univ.-Prof. Dr. rer. nat. Andrij Pich

Tag der mündlichen Prüfung: 26.02.2019

Diese Dissertation ist auf den Internetseiten der Universitätsbibliothek verfügbar.

Table of Contents

Table of Contents

Table of Contents

Table of Contents

Acknowledgements

First of all I would like to thank my supervisor, Prof. Dr. Ulrich Schwaneberg, for giving me this opportunity to work in his group and for all his unwavering encouragements and guidance for my study and research during the last four years. He has given all his best to teach me everything he knows which helped me a lot in order to become an independent researcher. I am also glad to thank Prof. Dr. Andrij Pich and Prof. Dr. Lothar Elling for spending their time to read and evaluate my PhD thesis and serving as members in my PhD defence committee. Furthermore, I would like to thank Prof. Dr. Jan Schirawski for being in my PhD defence committee as the chairman.

I would to thank my supervisors, Dr. Felix Jakob and Dr. Diana M. Mate, for their guidance and supports for my research and life in the past four years. Thank you, Diana, for your supports in first year which enabled me to get the projects into the correct direction. Many appreciations to Felix, who took over the supervision after Diana, he did an excellent job during the last three years and I enjoyed a lot for working with him. Especially, I sincerely thank him for his continuous support and guidance for writing of manuscripts and PhD thesis. I wish to thank our senior postdoctoral colleague Dr. Islam Elawaad, who helped me a lot for correcting and optimizing the manuscripts and PhD thesis. I also would like to say my thanks to our collaborators, Prof. Dr. Andrij Pich and Elisabeth Gau, for their solid support in microgel syntheses as well as fruitful discussions for writing of manuscripts.

I also want to thank all members of the Biohybrid System subgroup in DWI–Leibniz-Institute for Interactive Materials and the entire Schwaneberg group for their help and assistance to my life and study. The friendly and international working atmosphere made me feel no pressure in Aachen. Special thanks to Hoda Alibiglou and Dr. Mehdi Davari for their help in computational analysis and the fruitful scientific discussions. And also, I want to give my thankfulness to our lab managers, our scientific coordinator (Dr. Nursen Sözer) and all the technicians in our lab, for their great technical supports and organizations.

Last but not least, I thank my beloved parents and elder sister in China, for the love, education, and encouragements. I would like to give a big hug to my wife Dou Hu (Chara) who always stays with me no matter where I am. I sincerely appreciate her for her accompanying, care, understanding and dedication with me in Aachen in the last three years. My dear families, your love and contributions can be found on every single page of this thesis.

I acknowledge China Scholarship Council (CSC), DWI – Leibniz-Institute for Interactive Materials and RWTH Aachen University for financial supports.

Abbreviations and acronyms

Å	Ångström
AA	Amino acid
ABTS	2,2'-azino-bis (3-ethylbenzothiazoline-6-sulphonic acid)
Abz	2-aminobenzoyl
Amp	Ampicillin
BCCE	7-benzoxy-3-carboxycoumarin ethyl ester
bp	Base pairs
CYP	Cytochrome P450 monooxygenase
CV	Coefficient of variation
Da	Dalton
ddH_2O	Double-distilled water
DNA	Deoxyribonucleic acid
Dnp	2,4-dinitrophenyl
DTT	Dithiothreitol
DMSO	Dimethyl sulfoxide
DMF	Dimethyl sulfoxide
E. coli	*Escherichia coli*
e.g.	*exempli gratia* (for example)
eGFP	enhanced green fluorescent protein
epPCR	Error-prone polymerase chain reaction
et al.	*et alli*
EV	Empty vector
Fw	Forward
g	Gravitational force
GMA	Glycidyl methacrylate
h	Hour(s)
H-bond	Hydrogen bond
HPLC	High-performance liquid chromatography
HTS	High-throughput screening
IC_{50}	The half maximal inhibitory concentration
IPTG	Isopropyl ß-D-thiogalactopyranoside
IVC	*In vitro* compartmentalization
Kan	Kanamycin
kb	Kilobase(s)
k_{cat}	Catalytic activity
kDa	Kilodalton
K_M	Substrate affinity constant
LB	Lysogeny broth
MALDI	Matrix-assisted laser desorption/ionization
Min	Minute
mM	Millimolar
µM	Micromolar
MTP	Microtiter plate
MD	Molecular dynamics
MS	Mass Specturm
NADPH	Nicotinamide adenine dinucleotide phosphate (reduced form)
No.	Number
OD_{600}	Optical density at a wavelength of 600 nm

Abbreviations and acronyms

PAGE	Polyacrylamide gel electrophoresis
PCR	Polymerase chain reaction
PDB	Protein data bank
PEG	Polyethylene glycol
pH	Decimal logarithm of the reciprocal of the hydrogen ion activity
pK_a	Logarithmic measure of the acid dissociation constant
PLICing	Phosphorothioate-based ligase-independent gene cloning
pNBP	p-nitrophenylbutyrate
PP	Polypropylene
PP-MTP	Polypropylne microtiter plate
PS	Polystyrene
PVCL	Poly (*N*-Vinylcaprolactam)
pmol	Picomole
Rev	Reverse
RMSD	root mean square deviations
RMSF	root mean square fluctuations
rpm	Revolutions per minute
RT	Room temperature
RFU	Relative fluorescence units
s	Second
SASA	Solvent-accessible surface area
Sa-SrtA	*Staphylococcus aureus* Sortase A
Sa-SrtB	*Staphylococcus aureus* Sortase B
SDM	Site-Directed Mutagenesis
SDS-PAGE	Sodium dodecyl sulfate polyacrylamide gel electrophoresis
SeSaM	Sequence Saturation Mutagenesis
SSM	Site-Saturation Mutagenesis
SrtA	Sortase A
SrtB	Sortase B
SrtC	Sortase C
T_m	Half-inactivation temperature
Ts	Transition
Tv	Transversion
U	Unit
UPLC-MS	Ultra-Perfermance Liquid Chromatography Mass Spectrum
UV	Ultraviolet
VCL	Vinylcaprolactam
vs.	*versus*
WT	Wild type
°C	Degree Celsius
3-CCE	7-hydroxy-3-carboxycoumarin ethyl ester
4-MUC	4-methylumbelliferyl-β-D-cellobioside
4-MUP	4-methylumbelliferylphosphate
11-PCA	11-Phenoxyundecanoic acid
2,6-DMP	2,6-Dimethoxyphenol
4-TFB amine	4-(Trifluoromethyl)-benzylamine

Abstract

Sortase-mediated ligation (SML) has emerged as a improtant tool for site-specific bioconjugation in protein engineering and material functionalization. Sortase A from *Staphylococcus aureus* (Sa-SrtA) specifically recognizes an LPxTG (in which x means any amino acid) motif in the target protein 1 and cleaves the scissile amide bond between threonine and glycine. The generated thioester intermediate subsequently ligates to the target protein 2 with oligo glycine at N-terminal. Despite many highlights in applications, wild type Sa-SrtA suffers from several notable limitations (e.g. a relatively low catalytic efficiency (high $K_{m\ (LPxTG)} \approx 6.5$ mM), a strict specificity for the LPxTG motif and dependency on calcium cofactor).

Directed evolution is a powerful tool to tailor enzyme properties towards user-defined goals. Directed sortase A evolution requires the development of a robust high-throughput assay which directly detects the formed conjugated products. Several conjugated product-based high-throughput screening strategies (e.g. cell surface display and *in vitro* compartmentalization) of Sa-SrtA have been established. Variants with enhanced activities, altered substrate specificities (rather than LPxTG motif) and calcium-independence were identified. However, these strategies are rather specific for engineering of one property of sortase A and usually limited in versatilities. For such purpose, it was essential to establish a general, robust and reliable screening system in microtiter plate (MTP) format which is applicable to perform directed Sa-SrtA evolution campaigns for different properties (e.g. thermos-stability and solvent resistance). In order to advance research of sortase engineering, this thesis was focused on the development of a general high-throughput screening system of sortase A, directed evolution of sortase A for efficient site-specific ligations in organic solvents, and applications of sortase A for covalent immobilization of multiple proteins on microgel.

In the first section, a general directed sortase evolution platform (SortEvolve) was developed in in 96-well MTP made of polypropylene (PP-MTP). Two applications were carried out for SortEvolve. In Application 1, SortEvolve was validated for the directed Sa-SrtA evolution. In Application 2, SortEvolve was validated for the directed evolution of CueO laccase with minimized background noise (20-fold decreased). SortEvolve ensures a comparable amount/semi-purified enzyme through immobilization in PP-MTP. The latter is beneficial to avoid false positives during screening and also suited for directed evolution campaigns in which background activity (or noise) from crude lysate has to be minimized in order to identify beneficial variants

In the next section, directed Sa-SrtA evolution campaign (KnowVolution) towards organic solvents was implemented. Organic solvents (e.g. DMSO, DMF) are routinely used to dissolve

Abstract

hydrophobic compounds. Engineering of Sa-SrtA for improved resistance/activity in organic co-solvents facilitates SML for more broad range of substrates. A random mutagenesis library (SeSaM library) of Sa-SrtA was screened in DMSO co-solvent by a modified SortEvolve protocol. Sa-SrtA variant M1 (R159G) with 2.2-fold improved resistance and variant M3 (D165Q/D186G/K196V) with 6.3-fold catalytic efficiency in 45% (v/v) DMSO co-solvent were obtained when compared with Sa-SrtA WT, respectively. Interactions of between Sa-SrtA and DMSO were investigated by molecular dynamic (MD) simulations. The MD simulations revealed that conformational mobility of Sa-SrtA is important for the gained resistance and activities in the co-solvent of DMSO. Application of Sa-SrtA M3 has exploited in site-specific conjugation in organic co-solvents. Versatility of SML in organic co-solvents was demonstrated by generating peptide-amines conjugates. Sa-SrtA M3 showed an up to 4.7-fold increased specific activity (vs Sa-SrtA WT) for site-specific conjugation of peptide/primary amines in DMSO and DMF co-solvents.

In the last section, a general covalent immobilization platform of enzymes on the surface of Poly (*N*-vinylcaprolactam)/Glycidyl methacrylate (PVCL/GMA) microgel was developed using sortase-mediated ligation. Versatility of the platform was proved by immobilization of five enzymes (lipase A, phytase, laccase, cellulase, and monooxygenase) with either N-terminal GGG motif or C-terminal LPxTG on surface of pVCL/GMA microgel. The kinetic parameters, solvents resistance, pH profile, thermo-stability and reusability of immobilized CueO laccase and P450-BM3 monooxygenase on PVCL/GMA microgel were subsequently investigated. Impressively, immobilized CueO and P450 BM3 showed an up to 4-fold improved resistance in the co-solvent of DMSO in comparison to corresponding free enzymes (e.g. P450 BM3 monooxygenase, CueO laccase). The highly stable immobilized CueO was further exploited in decolourization of aromatic dyes with high efficiency and reusability.

1. Chapter I: Introduction

1.1. Sortases: sources, classes, and functions

Sortases are an array of sequence-specific membrane-associated transpeptidases present mainly in Gram-positive bacteria.[1-2] *In vivo*, sortases directly sort the specific proteins in the cell and covalently attach them cell wall, such as pili and multi-subunit hair-like fibers.[1, 3] Since the discovery of sortase A in 1999,[4] a large number of sortase genes have been found in different kinds of microorganisms.[2] Sortases from Gram-positive bacteria have been partitioned into six distinct classes: classes A – F (**Table 1**). Except for class C which is mainly involved in the assembly of bacterial pili, the major function of other sortase classes is the attachment of proteins to the bacterial cell wall.[2-3, 5] Therefore, they play a major role in bacterial adhesion and virulence.[2]

Table 1. Classification of sortases and substrate recognition motifs with species specificities.

Sortase class	Sorting motif *		Bacteria source
A	**LPxTG**		*S. aureus, S. pyogenes, S. epidermidis, S. gordonil B. anthracis, B. cereus, E. facium, L. monocytogenes, L. innocua*
B	**NPQTN**		*S. aureus, S. pyogenes, B. anthracis, B. cereus, B. halodurans, C. difficile, L. monocytogenes, L. innocua*
C	**LPLTG** **QVPTG**	or	*Naeslundii, S. agalactiae. S. equi, B. cereus, C. diphteriae, E. faecium, R. albus.*
D	**LPNTA** **LAETG**	or	*B. anthracis, B. cereus, B. halodurans, B. subtilis, C. botulinum, G. steraronthermophilus*
E	**LPxTG**		*B. longum, C. diphteriae, C. glutamicum, C. efficiens. T. fusca, T. whipplei, S. avermitilis, S. coelicolor*
F	unknown		*S. coelicolor, S. avermitilis, T. fusca*

* x denotes any amino acid. Table is adapted from Spirig et.al.[2]

1.1.1 Class A sortases: sortase A

Class A sortases (SrtAs) are housekeeping proteins involved in diverse functions in Gram-positive bacteria (e.g. host cell invasion, bacterial adhesion and nutrient acquisition).[3, 5-6] Based on this fact, SrtAs have gained considerable attention as targets for anti-infective therapy.[7-8] SrtA from *Staphylococcus aureus* (Sa-SrtA) is a typical example to explain the processes of sortase-mediated attachment of cell wall surface proteins (**Figure 1**). A substrate protein containing a C-terminal LPxTG motif (where x is any amino acid residues) is secreted to the membrane. Sortase A recognizes this sorting motif and cleaves the scissile amide bond between threonine and glycine. The generated protein-sortase A intermediate is subsequently attacked by oligo-glycine located in the N terminus of the lipid. Subsequent bond-formation between the carbonyl group of the threonine in the sorting motif and the primary amino group of the cross bridged glycine results in the attachment of the protein to cell wall peptidoglycans.[9] Sortases from other families catalyze similar transpeptidase reactions, but join different sorting motifs and amine donors.
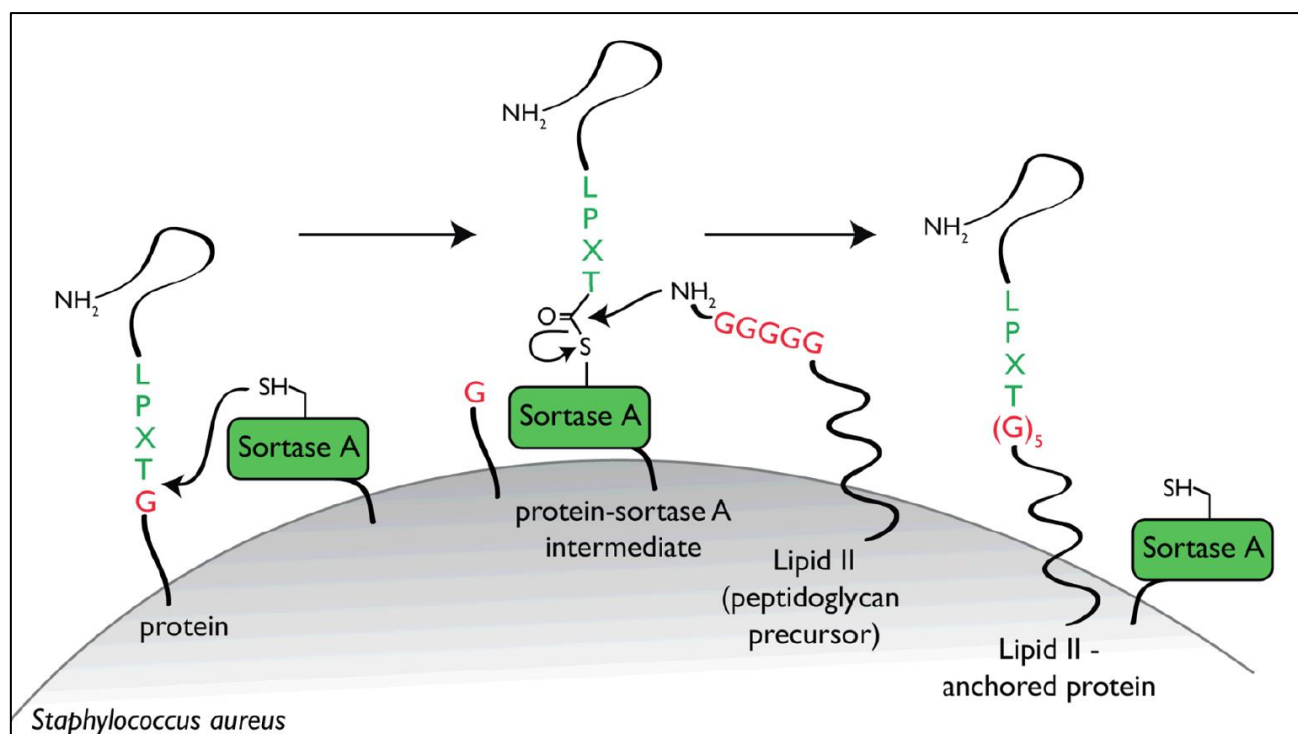
Figure 1. Schematic representation of sortase A-mediated bioconjugation of surface proteins in Gram-positive bacteria. The figure is adapted from Guimaraes *et al*.[9]

1.1.1.1. Structure and transpeptidation mechanism of SrtA

Biochemical and structural experiments have demonstrated that Sa-SrtA owns an eight-stranded barrel backbone structure and holds three prerequisite active site residues (Cys184, His120, and Arg197) in the LPxTG substrate binding pocket (**Figure 2a**).[10] A ping-pong mechanism is supposed to be involved in the transpeptidation reaction.[11-12] Same mechanism of catalysis is hypothesized for all sortases, since active site cysteine, histidine, and arginine are strictly conserved. Clubb and his co-workers revealed that the binding of LPxTG substrate to Sa-SrtA occurs through an induced-fit mechanism.[10] Upon the encapsulation of leucine residue in LPxTG motif, the β6/β7 loop in Sa-SrtA undergoes a disordered–ordered transition (**Figure 2 b/c/d**).[10] An extensive displacement (10 Å) of the β6/β7 loop toward the active site was observed (**Figure 2d**). *In vitro*, Sa-SrtA activity is stimulated by the calcium ion (Ca^{2+}). It was reported that Ca^{2+} enhances the activity of Sa-SrtA 8-fold[13] by altering the mobility of β6/β7 loop resulting in a decrease in the K_m value for LPxTG motif binding.[14]

Structure of sortase A from *Streptococcus pyogenes* (Spy-SrtA) was also studied to understand the mechanism of catalysis and substrate recognition. The overall structure of Spy-SrtA adopts a highly similar eight-stranded barrel backbone structure to Sa-SrtA even though only a 24% sequence identity was shared (**Figure 3a**).[15] Likewise, three residues (Cys^{208}, His^{142}, and Arg^{216}) are served as the active sites (**Figure 3b**). Despite the core of beta-barrel fold is highly conserved as the structure of Sa-SrtA, remarkable differences exist in loop regions (e.g. β6/β7 and β7/β8) and N/C termini.[15] Interestingly, activity of Spy-SrtA is not promoted by Ca^{2+}, which indicates the presence of Ca^{2+} does not effects the

structure of enzymes. In comparison to Sa-SrtA, there is a significant reduction of catalytic activity of Spy-SrtA. Around 80- and 8-fold reductions of k_{cat} and catalytic efficiency were reported for Spy-SrtA when compared to Sa-SrtA, respectively.[15]
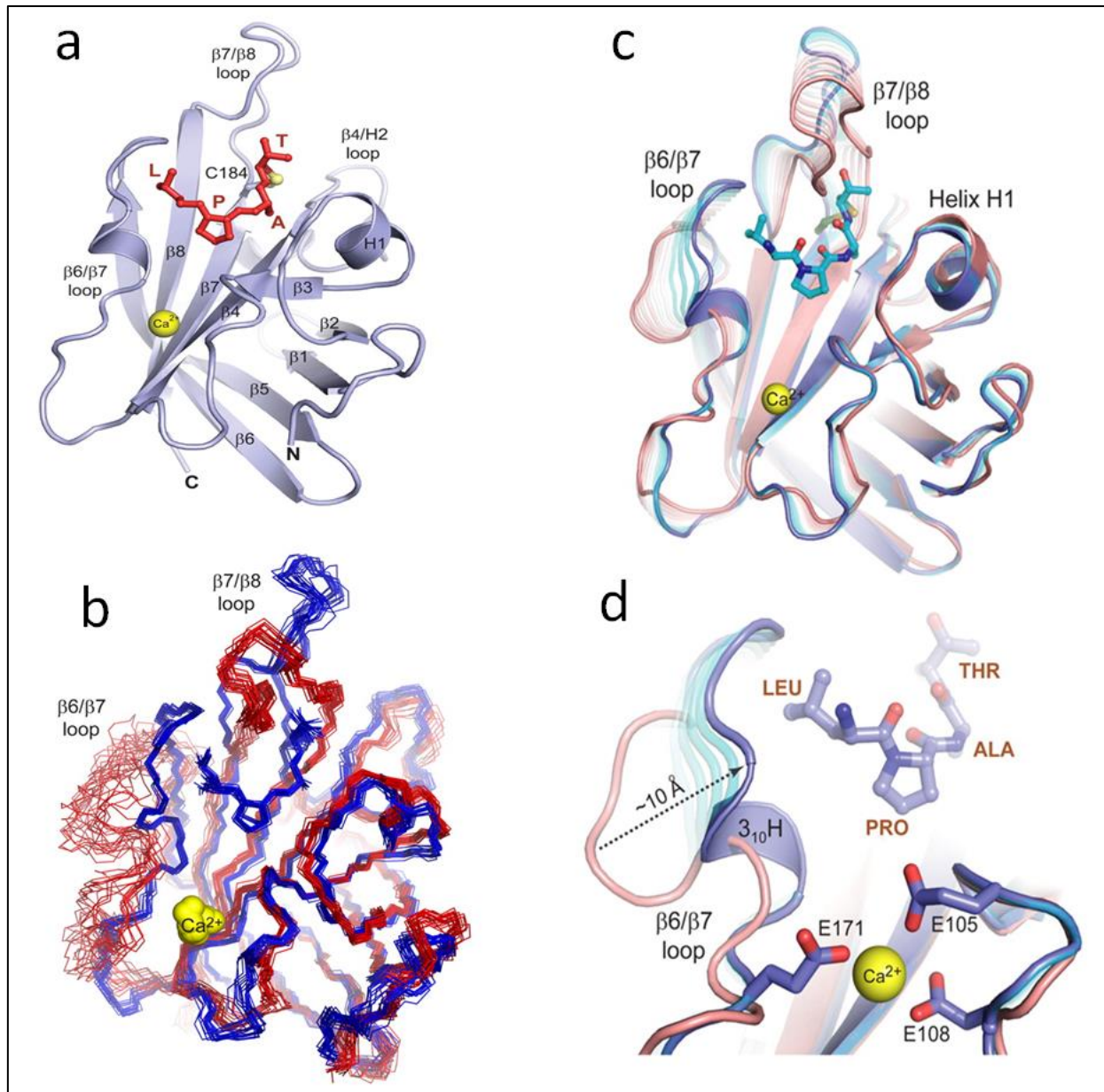
Figure 2. NMR structure of the Sa-SrtA-LPAT complex. a) Ribbon drawing of the structure of the Sa-SrtA-LPAT complex. The LPAT peptide is shown in a red ball-and-stick representation. b) Overlay of the ensemble of NMR structures of Sa-SrtA (red colour, PDB code:1ija) and the Sa-SrtA-LPAT complex (blue colour). The comparison shows that the structurally disordered β6/β7 loop becomes ordered upon binding the LPAT peptide. c) Superposition of the average NMR structures of the Sa-SrtA-LPAT complex (blue colour) and Sa-SrtA (pink colour). The significantly substrate-induced conformational changes occur in positions located within the β6/β7 and β7/β8 loops. d) Zoom in for (c) to emphasize the shift of the β6/β7 loop over the sorting signal and the role that Ca^{2+} plays in stabilizing the closed conformation of the β6/β7 loop. The figure is adapted from Suree et al.[10]
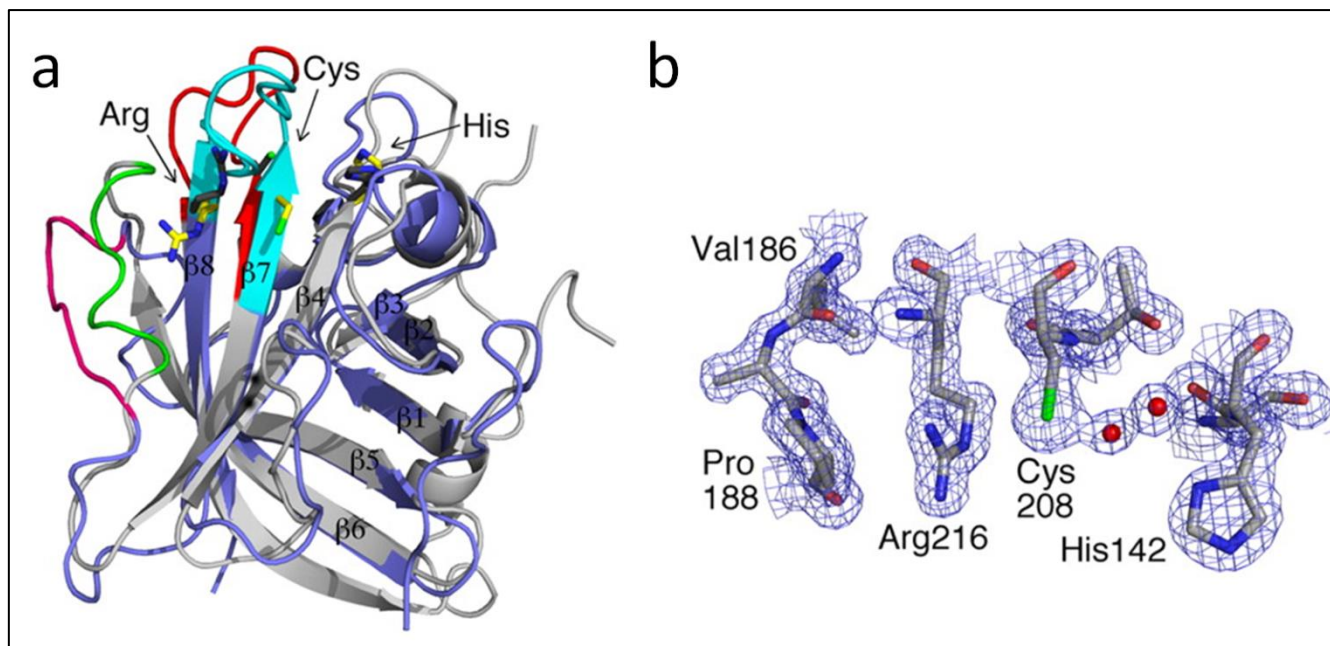
Figure 3. a) Overlay of Spy-SrtA (in *gray*) with Sa-SrtA (in *blue*). Active sites are colored *dark gray* and *yellow* for Spy-SrtA and Sa-SrtA, respectively. The β_6/β_7 and β_7/β_8 loops are colored *red*/*green* in Spy-SrtA and *cyan*/*magenta* in Sa-SrtA respectively. b) Stereoview showing the arrangement of active sites (Cys^{208}, His^{142}, and Arg^{216}) in the structure of Spy-SrtA. The figures are adapted from Race et.al.[16]

1.1.1.2 Specificity of SrtA

While different sortase classes have distinct sorting motifs (**Table 1**), nearly all the SrtAs can recognize an identical LPxTG sequence as the sorting tag.[2] The specificity of Sa-SrtA regarding each residues in LPxTG motif was studied by MaCafferty and his co-workers (**Figure 4**).[17] Sa-SrtA showed a strict LPxTG sequence-based transpeptidase activity. The narrow substrate scope of Sa-SrtA enables the highly site-specific transpeptidation, and is applicable in ligations requiring high selectivity. However, the constraint precludes the applications of Sa-SrtA to modify proteins lacking this particular sequence.[18] Unlike Sa-SrtA, Spy-SrtA not only recognizes LPxTG motif but also shows a comparable specificity towards LPxTA/LPxLG motif and accepts alanine as nucleophile donor in the transpeptidase reaction.[15, 19] The latter is important since it enables the usage of SrtAs in more complex bioconjugations in which diverse orthogonal substrates can be attached onto a single protein target or onto multiple cargos simultaneously.[20]
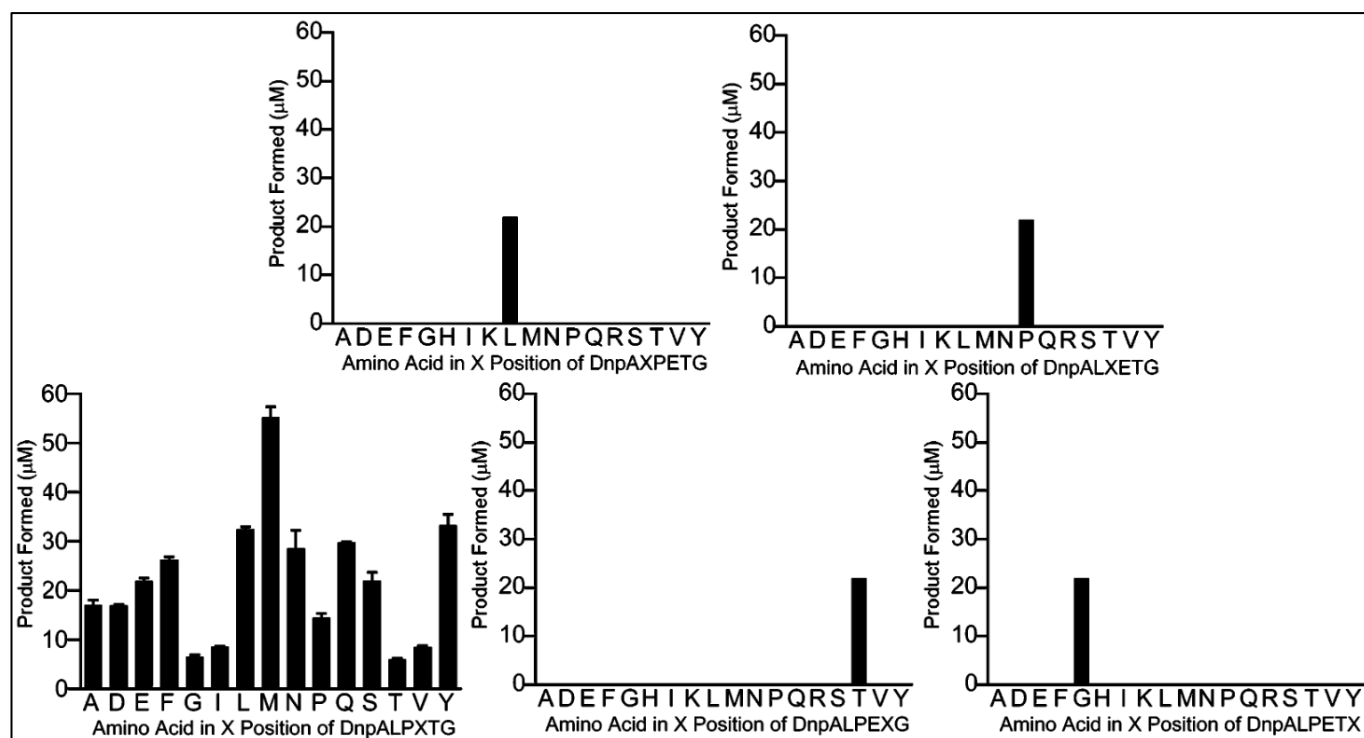
Figure 4. Specificity analyses of the sortase substrate libraries (assays were performed in 100 μL reaction mixtures containing 15 μM Sa-SrtA, 2 mM $CaCl_2$, and 300 μM peptide substrate). Reactions were initiated by the addition of enzyme, mixtures were incubated (37 °C, 30 min) and quenched by supplementing of HCl (1M, 50 μL). The figures are adapted from Kruger *et al.*[17]

In addition to the well-established Sa-SrtA and Spy-SrtA, many homologs of SrtAs have been identified in Gram-positive bacteria and their substrate specificities have been investigated.[19, 21] Schwarzer and his co-workers reported that sortases of *Streptococci* origin displayed a more relaxed specificity for donor and acceptor substrates than their *Staphylococci* counterparts. In general, *Streptococci* sortases prefer a hydrophobic LPKLG motif compared to the canonical LPKTG. However, activities of *Streptococci* sortases are relatively low in comparison to *Staphylococci* sortase. These observations provide a special view to understand the structure-function relationship of SrtAs and might facilitate the engineering of SrtAs with altered/reprogrammed specificities.

1.1.2. Class B sortase: sortase B

Class B sortases (SrtBs) are routinely found in *Staphylococcus* and *Firmicutes* species. Despite the significant primary sequence homology that SrtBs share, the functions of the members of this class are quite diverse.[2] SrtBs were firstly found for assembling of hemeprotein onto the cell wall.[22-24] Recently, sortase B was found to play a key role in assembling of pili in *Streptococcus pyogenes*.[16] Unlike Sa-SrtA, sortase B in *Staphylococcus aureus* (Sa-SrtB) recognizes a penta NPQTN sequence as a sorting motif and is only expressed in the absence of iron.[22, 25] Structure and computational studies of Sa-SrtB have been recently performed by Clubb and his coworker.[26] Overall, Sa-SrtB harbors a highly conserved backbone structure as Sa-SrtA, but shows significant differences in loop regions (e.g. β6/β7 and β7/β8 loops,

Figure 5a). The results indicate that an oxyanion hole was generated with amino acid residues Arg[223], Glu[224] and stabilized the high energy enzyme-NPQT intermediate. Additionally, the threonine within the NPQT motif promotes the construction of oxyanion hole by stabilizing the active site Arg[223] with a hydrogen bond (**Figure 5b**).[26]
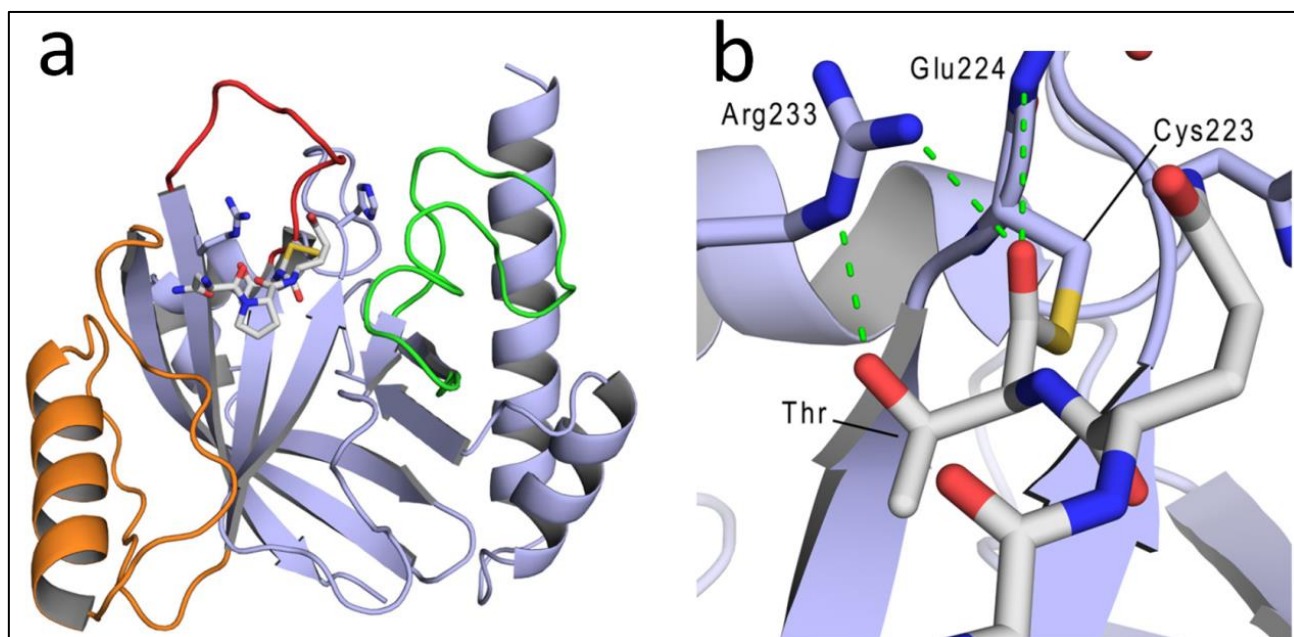
Figure 5. Struture of Sa-SrtB-NPQT* complex. a) Ribbon diagram of the Sa-SrtB-NPQT*complex. Loop regions are **colored with** Green (β2/β3 loop), orange (β6/β7 loop) and red (β7/β8 loop). NPQT Substrate analog and active sites are shown as sticks. b) Expanded view of the energy minimized model of Sa-SrtB-NPQT* thioacyl intermediate. Interaction between threonine in NPQT motif and Sa-SrtB are shown. The figures are adapted from Jacobitz et al.[26]

Transpeptidase activities of wild-type and mutant Sa-SrtBs were investigated. In comparison with Sa-SrtA, Sa-SrtB is far less active (**Table 2**). A 520-fold lower of turnover (k_{cat}) was obtained of Sa-SrtB when compared to Sa-SrtA. K_m value Sa-SrtB stays at a similar level as Sa-SrtA. Interestingly, a more recently study has performed a similar kinetics experiment with new identified k_{cat} (= 1×10^{-4} s^{-1}) and K_m (=1.8 mM) values.[26] Both reports have confirmed the low catalytic activity of Sa-SrtB. Specificity of Sa-SrtB was investigated. As in the prototypical SrtAs, Sa-SrtB is tolerant to substitution of alanine to glutamine residue in NPQTN. Furthermore, Sa-SrtB is also tolerant to alanine substitution following the scissile peptide bond distinguishing the enzyme from Sa-SrtA, which strictly specific for glycine at this site.[17, 19, 21]

Table 2. Kinetic parameters of Sa-SrtA and Sa-SrtB using LPETG and NPQTN motif as substrates. The table is adapted from Bentley et.al.[27]

Sortase	k_{cat} (s^{-1})		K_m (mM)		k_{cat}/K_m (M^{-1}s^{-1})	
	LPETG	NPQTN	LPETG	NPQTN	LPETG	NPQTN
Sa-SrtA	0.28 ± 0.02	/	8.7 ± 1.0	/	37 ± 3	$8.7 \pm 0.6 \times 10^{-4}$
Sa-SrtB	/	$5.4 \pm 0.5 \times 10^{-4}$	/	7.8 ± 2.0	/	0.063 ± 0.01

1.1.3. Class C, D, E, F sortases

In Gram-positive bacteria, class C sortases are widely distributed and function as pilin polymerases involved in the synthesis of pili which facilitate microbial adhesion and biofilm formation. The assembly of pili typically occurs in a two-stage process. In the first stage, the long thin shaft of the pilus is synthesized by one or more class C enzymes by linking together pilin subunits via iso-peptide bonds. In the second stage, the generated base of the pilus is attached to the cell wall by a housekeeping sortase.[2] Unlike the extensive studies for SrtAs, there are limited reports for the structure analysis of SrtCs. In 2009, Achour and his coworkers revealed that SrtC from *S. pneumonia* harbors an additional loop that closes the active site in comparison with the Sa-SrtA.[28] The lid interacts with key catalytic residues in the active site and plays an important role in enzyme activity and substrate specificity. Across the diverse species and pilin synthesis systems studied to date, the pilin assembling class C sortases show a unique variance in their competence to recognize a variety of sorting motifs. A SrtC2 from *Streptococcus pyogenes* was found to anchor QVPTGV tagged surface proteins to the cell wall.[29]

In comparison to the considerable knowledge available for sortase A, B, and C, much less information is known about members of class D, E, and F sortases. Class D enzymes exist in bacilli and have only been characterized in *B. anthracis.* Sortase D from *B. anthracis* (Ba-SrtD) anchors two proteins (BasH and BasI) to the cell wall. Gene knockout of this enzyme lead to a reduction in spore formation under low oxygen conditions.[30] Interestingly, SrtA and SrtD in *B. anthracis* recognize similar sorting signals. The substrates (BasH and BasI) of Ba-SrtD contain an LPNTA sorting motif that differs only slightly from the canonical LP[A/N/K]TG sorting motif recognized by *B. anthracis* SrtA. These findings indicate that these may have evolved a high degree of specificity *in vivo*. The genes encoding sortase D in other bacilli are frequently clustered with genes encoding proteins with an LPNTA sorting signal motif, which may suggested that these enzymes retained the same LPNTA motif as *B. anthracis* SrtA.[31]

In some high G + C Gram-positive bacteria, class E sortases may be used as their housekeeping sortase.[32] This assumption is inspired by the finding that genes encoding sortase A and sortase E are never found in the same microorganism.[33] Class E sortases are supposed to recognize an LAXTG sorting motif based on the comparative genome analysis.[33] SrtE was firstly characterized in *C. diphtheria* which attaches assembled pili to the cell wall, a function shared by some SrtA enzymes.[2] In *S. coelicolor*, SrtEs assemble chaplin surface proteins tagged with LAXTG sorting motif.[2] Class F enzymes (SrtFs) are present in *S. coelicolor* as well as other Actinobacteria. The Function of SrtFs is yet to be investigated [2]

1.1.4. Applications of sortase-mediated ligation in protein engineering and polymer functionalization

Since the first application of Sa-SrtA in protein-protein ligation demonstrated in 2004,[34] sortase-mediated ligation (SML) has been employed in a wide variety of bioconjugate chemistry and protein engineering applications. Those include N-/C-terminal labeling of proteins, protein-sugar modification, protein-lipid modification, protein-protein fusion, peptide/protein cyclization, and cell-surface labelling. More recent applications have extended the SML toolbox to surface functionalization, hydrogel modification, biomolecules PEGylation, virus-like particles decoration, versatile protein immobilization/purification as well as *in vivo* protein labelling. In most cases, Sa-SrtA and its engineered variants were used. To meet the ongoing demands for various SML applications, sortases from different bacterial sources with varied recognition motifs have been reported. A few examples of SML are discussed in detail below.

1.1.4.1 Sortase-mediated N-/C-terminal labelling of proteins

Genetic constructs for recombinant expression of green fluorescence protein (eGFP) in bacteria and yeast are powerful tools for protein labeling *in vivo*, however they are limited by the weak tolerance of protein in fusion format as well as lack the precision of genetically encoded tags. By using SML, diverse probes can be site-specifically conjugated to N-, C- or both N- and C-termini of protein *in vitro*, in principle, without any limitations (**Figure 6**). On the basis of this fact, a lot of studies have demonstrated the successful labeling of proteins.[35-36] The first proof to ligate PEG to eGFP was reported by Parthasarathy et al.[37] Ploegh and his co-workers have successfully conjugated biotin, tetramethylrhodamine (TAMRA), phenylazide photocrosslinker, FITC, 3-amino-3-(*o*-nitrophenyl) propionic acid to mouse class I major histocompatibility complex (MHC) H-2K molecules.[38] Notably, further studies have proved the versatility of SML by coupling many types of biomacromulecules (e.g. nucleic acid,[39] lipid,[40] and sugars[41]).
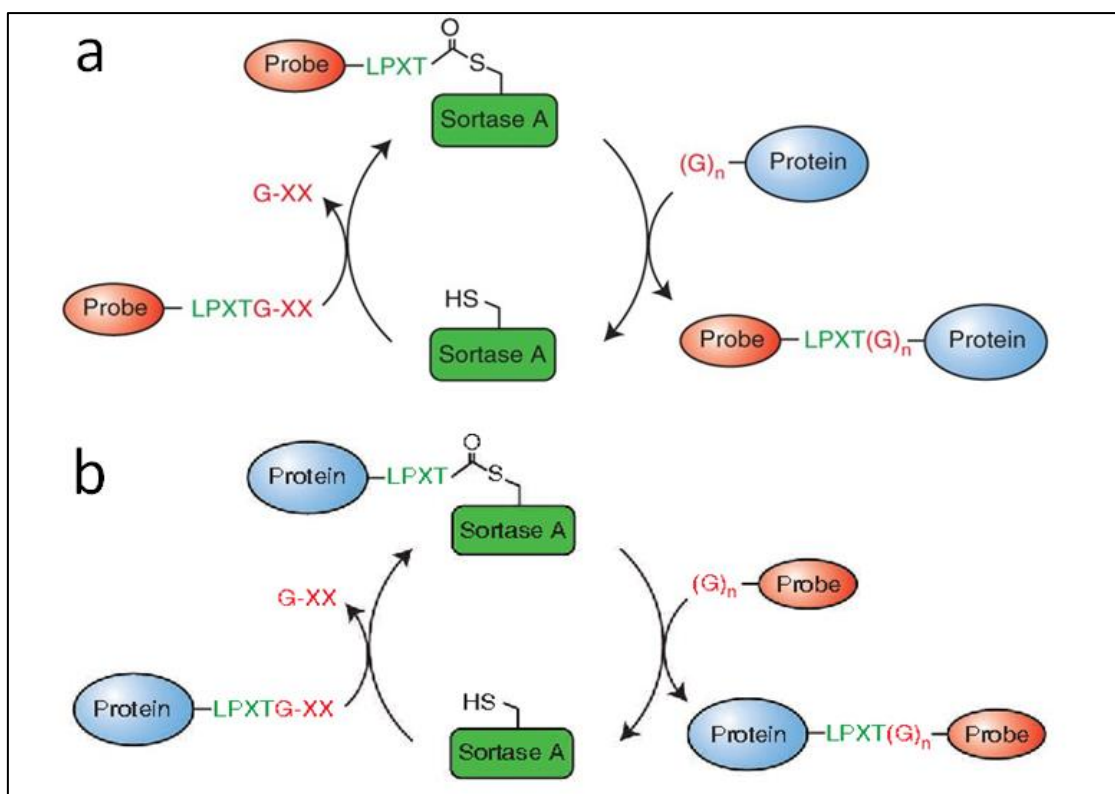
Figure 6. Sortase-medited modifications of protein termini. a) N-terminal labeling of protein b) C-terminal labelling of proteins. The figures are adapted from Guimaraes et.al and Thiele et.al.[9, 42]

1.1.4.2 Sortase-mediated surface functionalization

Surface modification to generate functionalized polymers is gaining growing interest in polymer synthesis, membrane science, and nano materials. A critical step for surface functionalization is the development of methodologies that can firmly immobilized the biomolecules on the solid surface but with little risk to their biofunctions. SML offers a gentle, simple, and site-specific approach for such purposes. Chan et al have firstly ligated eGFP and the sequence specific DNA binding protein Tus on Glycidyl methacrylate (GMA) beads.[43] Highly oriented unstable protein β1,4-galactosyltranseferase or recombinant *Helicobacter pylori* α1,3-fucosyltransferase (rHFucT) were displayed on surface of EAH-Sepharose (**Figure 7**).[44] Kinetic parameters of immobilized rHFucT were determined. Interestingly, higher k_{cat} values were observed for the immobilized enzyme when compared to its soluble counterpart.[44] Recently, the capacity of SML to repeatedly regenerate a covalently coated monomolecular film of thrombomodulin (TM) molecules was demonstrated.[45] This work is likely to open up many potentials of SML toolbox to extend the lifetime of bioactive surface, films, and membranes.
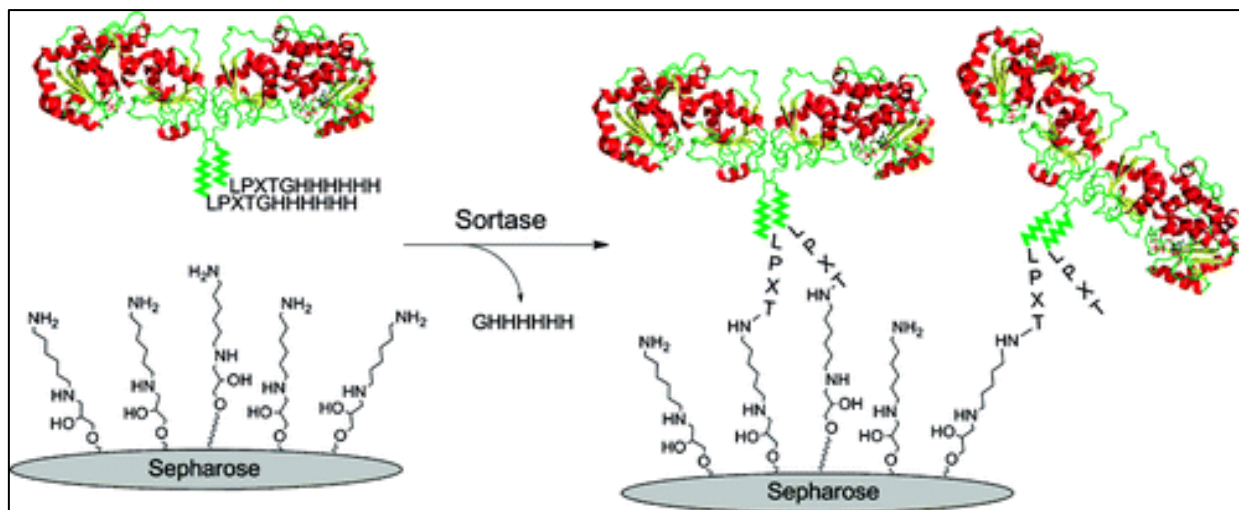
Figure 7. Highly oriented immobilization of unstable membrane protein on solid surface via sortase-mediated ligation. The figure is adapted from Guimaraes et.al and Ito et.al.[44]

1.1.4.3 Sortase-mediated protein immobilization/purification

  Although SML has enabled the multiple labeling of proteins, a common challenge is to efficiently separate the desired conjugated products from the reaction mixture which contains enzyme, salts, and unconjugated substrates. By means of affinity tags (e.g. hexahistidine, Strep-tag), sortase can be immobilized on respective resins. Within the possible design of substrates, immobilized sortase could facilitate protein purification and site-specific bioconjugation into a single step. With this motivation, Tsourkas and co-workers have developed a sortase-tag expressed protein ligation (STEPL) technique in 2013 (**Figure 8a**).[46] Ligands were fused with the sorting motif LPXTG, a space linker of $(GGS)_5$, Sa-SrtA and a hexahistidine and was purified on a nickel column. In presence of calcium ions and cargo with amino groups, Sa-SrtA simultaneously catalyzed ligand release and peptide ligation.[46] An optimized continuous-flow system for sortase-mediated modification and purification was performed by Ploegh and his co-workers (**Figure 8b**).[47] In this system, a highly active and calcium independent Sa-SrtA variant was used with a limited amount. More importantly, the immobilized Sa-SrtA variant was reused for multiple cycles.[47] More recently, a proximity-based sortase-mediated ligation (PBSL) strategy was carried out by Tsourkas and his coworkers by combining the sortase-mediated tool and SpyTag–SpyCatcher technique. By using this new system, improved ligation efficiency to over 95% was achieved.[48] In summary, sortase-mediated protein purification provides a straightforward method for protein modifications and minimized the efforts for subsequent purification of the conjugated products. The high efficiency and simplicity enables a wider range of applications in biochemical synthesis and protein engineering.
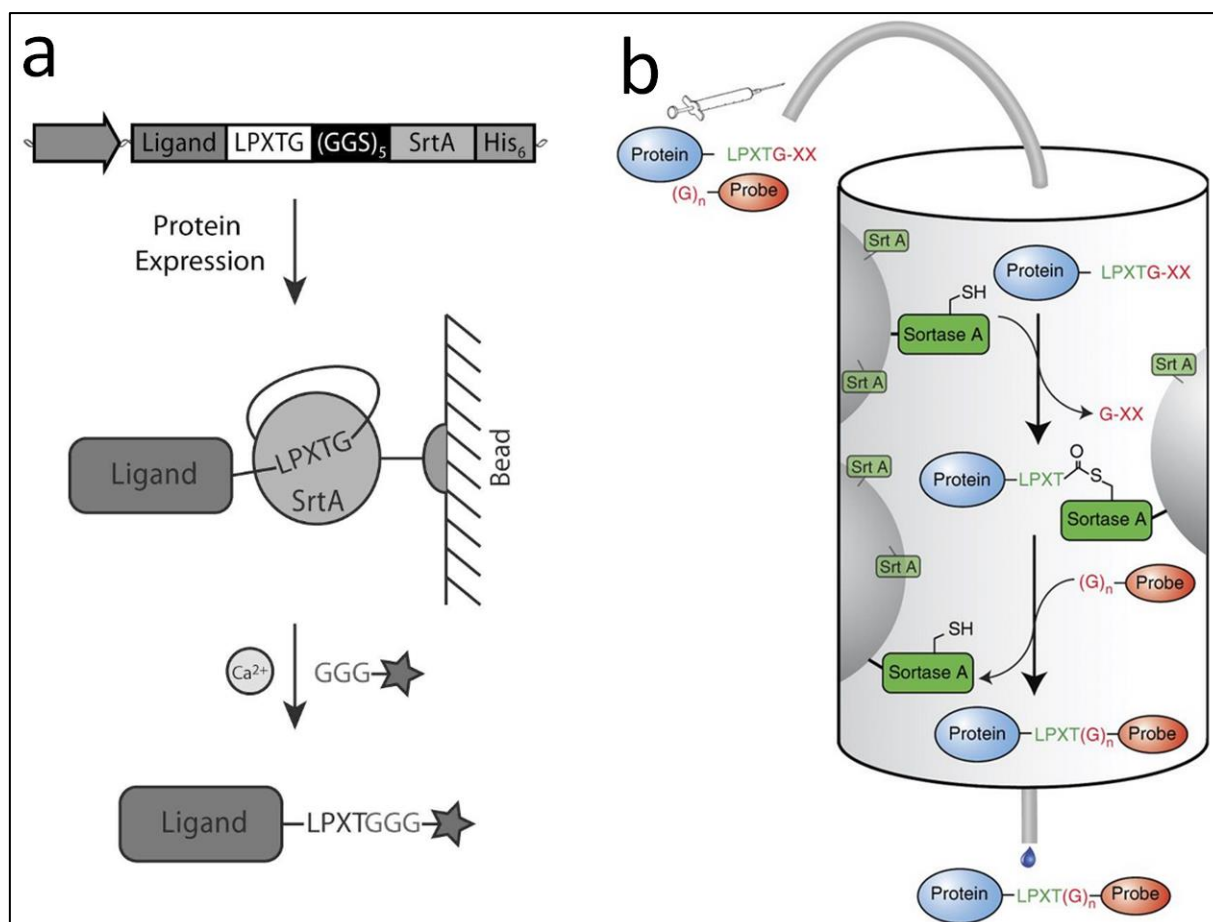
Figure 8. Sortase-mediated protein modification/purification. a) Sortase-tag expressed protein ligation (STEPL) technique for protein purification and site-specific bioconjugation into a single step; b) Sortase-mediated site-specific protein modification and separation in batch and continuous-flow systems. The figures are adapted from Warden-Rothman[46] and Witte et.al[47].

1.1.4.4 Sortase-mediated in vivo protein labelling

The high versatility of SML for protein modification *in vitro* and on the surface of living cells suggested that it might be possible to extend their applications for *in vivo* protein ligations. The first proof of principle was demonstrated by Ploegh and his coworker in 2012.[49] The calcium-independent Spy-SrtA instead of Sa-SrtA was used. The authors demonstrated that SMLs could be achieved in both *Saccharomyces cerevisiae* and in mammalian HEK293T cells. Another application for *in vivo* labeling of proteins in *Caenorhabditis elegans* cell using engineered calcium-independent Sa-SrtA was reported.[50] As aforementioned, SML is not limited to the N-terminal glycine substrates; other primary amine molecules were also proved to be suitable substrates for efficient ligations.[44] Inspired by these findings, *in vivo* protein labeling with diverse group of amines was demonstrated by Cochran and his co-workers (Figure **9a**).[51] Specificities of Sa-SrtA towards amines were firstly investigated by employing an array of small size amine compounds. It was concluded from this work that Sa-SrtA can theoretically use any unbranched primary amine as a substrate. Several model proteins (e.g superfolder GFP (sfGFP), GST, anti-HER2 nanobody 5f7) were co-expressed with Sa-SrtA in a culture medium with 3-azido-1-propanamine Azp amine. Azp-labeled proteins were efficiently produced during

the cultivation process (**Figure 9b**).[51] This study enables a simple, inexpensive production of modified proteins with no additional purification steps.
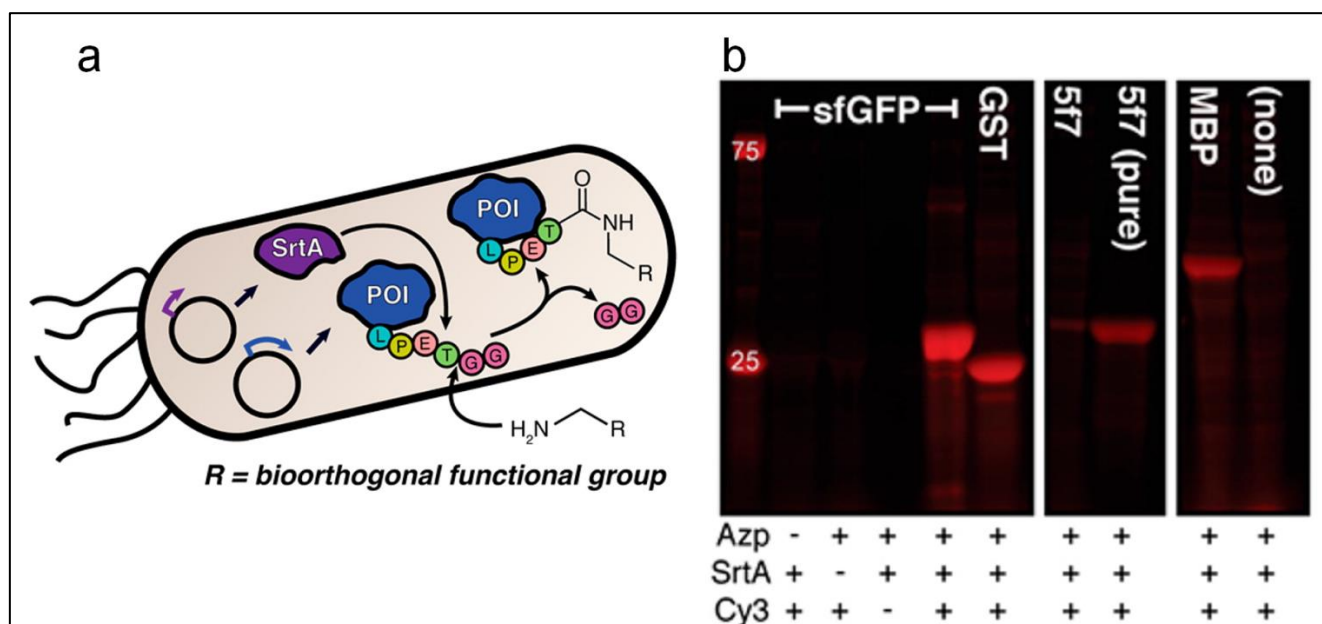
Figure 9. a) Schematic representation of *in vivo* protein conjugation with amines via sortase-mediated ligation. b) Fluorescence detection of *in vivo* produced and Azp labeled proteins by Cy3-DBCO dyes (fluorescent staining was achieved by click chemistry between Azp and DBCO). The figures are adapted from Glasgow et.al .[51]

In conclusion, SMLs have been extensively employed for site-specific protein engineering both *in vitro* and *in vivo*. Especially that Sa-SrtA not only recognizes N-terminal glycine tagged peptides, but also performs efficient ligations with side chain of lysine as well as unbranched amines. The latter will likely bring SMLs a step closer to a variety of applications, such as *in vivo* protein engineering, site-specific internal protein labeling, selective surface/membrane decorations, and multiple polymer functionalizations.

1.2. Directed evolution

1.2.1 State of the Art

The sequence of the amino acids within a protein affects both its structure and function. Therefore, the approach to alter the sequence, and hence modify the structure and activity of proteins, opens many opportunities, both in scientific research and exploitation of biocatalysis in industrial applications. However, the complexity of finding a direct relationship between protein sequence and function has precluded the widespread design for this goal. Directed evolution begins with the construction of a library of mutated genes and subsequent screening towards the desired function. This methodology differs from the traditional rational design approaches which involve computer design and site-directed mutagenesis depending on the full understanding of detailed structural and mechanistic information of the target protein. Due to this great advantage, directed evolution has attracted in the past decades a huge interest as a powerful tool for protein engineering.[52-54]

Chapter I: Introduction

In general directed evolution campaigns consist of three major steps: (1) generation of random mutagenesis libraries, (2) identification of improved variants with a suitable screening system and (3) isolation of gene(s) encoding the best variants, which are used for the next rounds of directed enzyme evolution (iterative cycles) until the desired property improvements are reached (**Figure 10**).

An array of methods can be employed for t generation of random mutagenesis libraries, such as error-prone PCR (epPCR), sequence saturated mutagenesis,[55] DNA shuffling,[56] or site saturated mutagenesis (SSM). Mutated gene libraries are cloned into a suitable plasmid vector and transformed into an adequate expression host microorganism with subsequent production of library of protein variants.
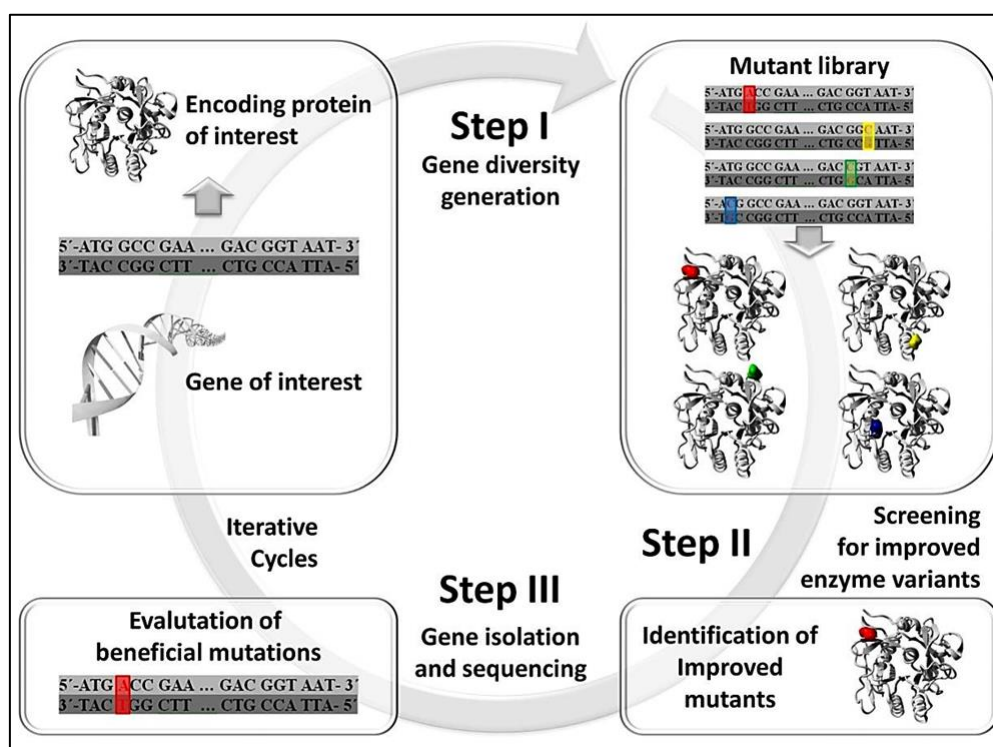
Figure 10. Schematic representation of a directed evolution campaign. Three main steps are included. Step I: Generation of random mutagenesis libraries; Step II: Identification of improved variants by using a high-throughput screening assay; Step III: Isolation and sequencing of improved variants (Thanks to Dr. Felix Jakob for providing the picture).

After generation of the gene library, variants with the improved desired property will be identified by screening step. The outcome of directed evolution experiments is critically dependent on how a library is screened.[54] Due to the large number (up to $10^{9\text{-}12}$) of variants produced in the random mutagenesis, it is nearly impossible to analyze all the variants one by one within a feasible time span. Therefore, an efficient and reliable high throughput screening (HTS) system plays as a vital role for the success of a directed evolution campaign. Although screening of large libraries ($10^{6\text{-}12}$) of enzymes remains a challenge, small libraries ($10^{3\text{-}5}$) are usually screened via absorbance or fluorescence detection.

1.2.2. High throughput screening methods

   To date, many methods have been developed for high throughput screening. Typical examples of screening are discussed in detail below.

1.2.2.1 High throughput screening in microtiter plate (MTP)

   Upon the genotype-phenotype linkages, most of the screening methods can be basically classified into two strategies: screening by spatial separation and compartmentalization.[54] In spatial separation, colonies of library are screened either on solid media plate or in liquid culture medium (**Figure 11**). Screening of colonies on solid media plates is limited to special enzymes, since not all enzymes are well expressed or not all the substrates are easily distributed/detectable on solid media. Liquid cultivation of separated colonies in microtiter plate format is the most common way used. The main advantage of MTP-based screening is the good compatibility of analytical reporters (e.g. fluorescence, luminescence, and absorbance) and standardized tools/devices (e.g. HPLC, NMR, MTP reader) thus enable to keep the stable environment for the quantitative activity measurement and data set evaluation of each variant.[54]
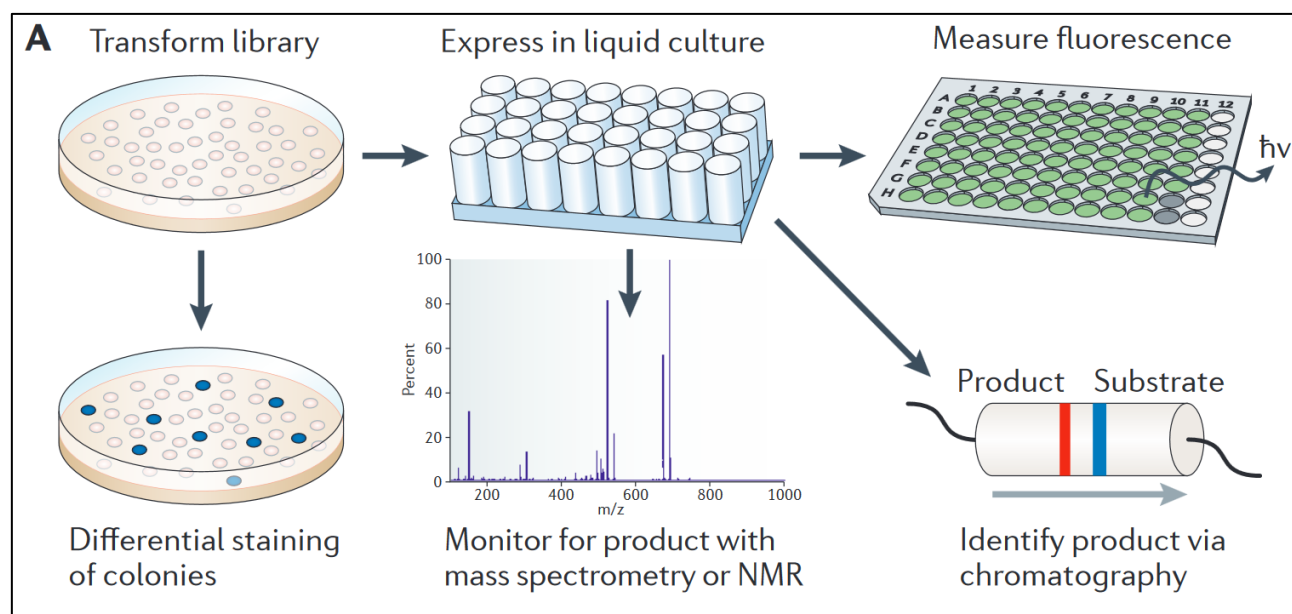
Figure 11. Spatial separation strategy of screening in directed protein evolution. Colonies of variants are individually cultivated in solid or liquid media. The figure is adapted from Liu et.al.[54]

1.2.2.2 High throughput screening by fluorescence-activated cell sorting (FACS)

   Despite the widespread applicability of spatial separation methods in high throughput screenings, a main limitation remains its relatively low throughput capacities compared to the protein diversity. In general, spatial separation methods permit the screening of fewer than 10^4 colonies per round with an acceptable time and effort.[52, 57] [54] Rather than spatially separating clones, displaying proteins on the cell wall or membrane could also maintain the genotype-phenotype linkage with individual cell. By combining the cell surface display methodology to fluorescence-activated cell sorting (FACS) technique, screening of large size libraries ($\geq 10^8$) is possible. The FACS based ultra-high throughput screening (UHTS) became

more broadly applied with the development of a yeast cell display toolbox. An array of successful applications including enhanced antibody-antigen affinities,[58] discovery of protein-protein interations,[59] and evolution of enzymes[60] were reported by using the methodology.

It is obvious that cell-constrained fluorescent signals are not applicable for every given gene and phenotype. *In vitro* compartmentalization (IVC) offers an alternative approach to implement screening by FACS.[61] Two formats of IVC enable protein evolution: 1) emulsion of single cells expressing the library member; 2) emulsion of individual DNA molecules coupled with *in vitro* transcription–translation system.[62] *In vitro* expression of proteins endows researchers a flexible way to use fluorogenic substrates and expands the phenotypes and enzymes which can be implemented by FACS. Notably, IVC system was reported to significantly reduce the time spent for screening. A whole round screening can be completed within 16 h (**Figure 12**), while at least 120 h are needed for a one round in standard spatial separation screening in MTP format.
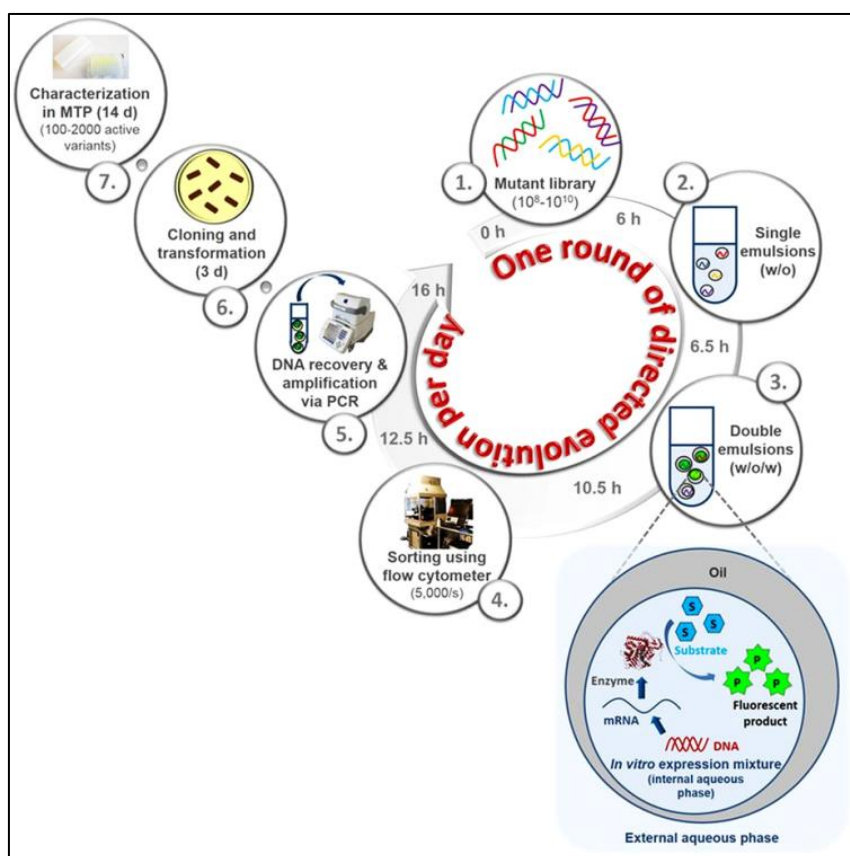
Figure 12. Principle of InvitroFlow screening methodology. A seven-step protocol was described. One round of InVitroFlow screening (including diversity generation, flow cytometry based screening, and amplification) was completed within 16 h. The figure is adapted from Körfer et.al.[62]

1.2.2.3 High throughput screening by affinity selection

In a typical affinity selection screening campaign, protein variants with desired phenotype of binding capacities and genotype are combined and captured using an immobilized target, whereas or non-binding

colonies are washed away. Cells and bacteriophage are suitable compartments which not only can be used as immobilized target but also achieve the linkage between genes and respective products. Therefore, cell/phage surface display methods are extensively used in affinity selection based HTS of functional peptide, proteins and even antibodies.[63-65] Due to the ultra-high-throughput capacity, affinity selections are often limited by the insufficient size of enzyme/protein libraries. Based on this fact, ribosome and mRNA displays were developed.[66-67]

1.2.3. Directed sortase evolution

Despite the highlights in bioconjugated applications, wild-type Sa-SrtA suffered from several notable limitations in first few years such as a low catalytic efficiency (k_{cat}/K_m = 200 $M^{-1}s^{-1}$; partly due to the high coupling concentration of LPxTG substrate, $K_m \approx$ 7 mM), activity dependency on Ca^{2+} cofactor a strict specificity for the LPxTG motif.[35] Due to the relatively low catalytic efficiency, high concentrations of substrates are often required to achieve high reaction rates in SML. The latter is challenged in applications where high concentration of substrates is not applicable (e.g. *in vivo* ligation, low solubility in water). The dependency on Ca^{2+} limited the applications of SML in phosphate buffer (precipitation generates in phosphate buffer) as well as *in vivo* protein modification. The strict recognition towards LPxTG enables high degree of specificity of Sa-SrtA. However, when SML is employed for peptide/protein semi-synthesis, the conserved selectivity becomes a downside since fewer or no amino acid substitutions need to be incorporates into the target protein. A broad specificity for diverse motif rather than LPxTG would be advantageous for such a purpose.

1.2.2.1 Directed sortase evolution for improved catalytic efficiency

The first directed evolution campaign to improve the catalytic efficiency of Sa-SrtA was reported by Liu and his coworkers in 2011.[60] A UHTS was developed for screening of Sa-SrtA as well as other bond-forming enzyme. A series of variants were identified with eight rounds of screening. Notable, two variants P94S/D160N/D165A/K196T (rM4) and P94S/D160N/D165A/K190E/K196T (M5) showed 140- and 120-fold improvement in catalytic efficiency when compared to Sa-SrtA WT (**Table 3**). Furthermore, variant M5 was successfully employed for *in vivo* protein labeling in *HeLa* cells.[60] In 2016, Liu and his co-workers further enhanced the activity of M5 via a MTP based directed evolution campaign.[68] The authors identified several beneficial positions (e.g. D124G, Y187L, and E189R) and combined them to the M5. Finally, variants 5M/D124G/Y187L/E89R and 5M/D124G/Y187L/E189A were generated and identified with up to 4.6-fold enhanced catalytic efficiency when compared to M5.

Table 3. Kinetics of Sa-SrtA variants. Abz-LPETGK-Dnp and Triglycine were used as substrates. Table was modified from Chen et.al.[60]

Sa-SrtA	k_{cat} (s^{-1})	$K_{m\ (LPETG)}$ (mM)	k_{cat}/K_m (M^{-1}s^{-1})

WT	1.5 ± 0.2	7.6 ± 0.5	200 ± 30
P94S	1.6 ± 0.1	2.5 ± 0.6	600 ± 200
D160N	2.3 ± 0.2	3.7 ± 0.5	600 ± 100
D165A	2.4 ± 0.3	3.6 ± 1.0	700 ± 200
K196T	1.2 ± 0.1	3.3 ± 0.8	400 ± 100
P94S/D160N/D165A/K196T (rM4)	4.8 ± 0.8	0.17 ± 0.03	28000 ± 7000
P94S/D160N/D165A/K190E/K196T (M5)	5.4 ± 0.4	0.23 ± 0.02	23000 ± 3000

1.2.2.2 Directed sortase evolution for Ca^{2+} independence

The first study to design Ca^{2+} independent Sa-SrtA variants was conducted in 2012 by Hirakawa et.al.[69] Alignment of protein sequences of Sa-SrtA and others SrtAs revealed amino acid residues in the Sa-SrtA that bind to Ca^{2+} are not conserved in other SrtAs. Conversely，it was observed that in Ca^{2+} independent SrtAs (e.g. Streptococcus pyogenes SrtA (SpSrtA) and Bacillus anthracis SrtA (BaSrtA)) residues in sites 105 and 108 are highly conserved to Lys and Gln, respectively. Therefore, the authors mutated Glu105 and Glu108 to Lys105 and Gln108 (or Ala105) and generated two Ca^{2+} independent Sa-SrtA variants E105K/E108Q and E105K/E108A.[69]

Even though E105K/E108Q and E105K/E108A show considerable activities in absence of Ca^{2+}, but their only show 40% activity when compared with Sa-SrtA in presence of Ca^{2+}. To further optimize the Ca^{2+} independence of Sa-SrtA, Ploegh and his co-workers have introduce the E105K/E108A to the previously identified M5 by site-directed mutagenesis and generated a hepta-mutant variant Sa-SrtA M7.[47, 50, 70] Several successful application regarding *in vivo* protein modification and surface display were reported via Sa-SrtA M7 mediated ligation.[50]

More recently, a directed Sa-SrtA evolution campaign using an IVC based screening strategy was performed.[71] A large library of Sa-SrtA with up to 10^{12} clones was screened. A variant presented a 114-fold enhancement in catalytic efficiency in the absence of Ca^{2+} compared to the wild-type was identified. Although the catalytic performance (in absence of Ca^{2+}) of newly identified variant was not compared to Sa-SrtA M7 as above mentioned, but the authors have showed that the variant harbors considerable high activity for protein labeling *in vivo*.[71]

1.2.2.3 Directed sortase evolution for altered/reprogrammed specificity

The first study regarding the specificity engineering of Sa-SrtA was investigated by McCafferty and his co-workers.[27] Researcher replaced the β6/β7 loop in Sa-SrtA with the corresponding domain from Sa-SrtB and generated a chimeric sortase enzyme (SrtLS). Interesting, it was observed that SrtLS performed a 700,000-fold enhanced activity for cleavage of NPQTN motif but did not catalyse transpeptidation stage of the reaction.[27] Directed Sa-SrtA evolution of altering specificity was firstly reported in 2011.[72] A

phage-display based screening of Sa-SrtA library upon the loop β6/β7 loop region was performed. A variant F40 was identified with broad specificity to different sort motifs (e.g. APxTG, DPxTG and SPxTG). With the altered specificity, variant F40 was successfully applied to catalyze traceless ligations of histone H3.[72]

Most recently, Liu and his workers have further evolved Sa-SrtA for broader or even reprogrammed specificities by using a modified yeast cell display based screening method.[18, 60] Random mutagenesis libraries were generated based on the reported high active variant M5. After nine rounds screening, the authors have identified several variant with specificity changes up to 51,000-fold and without loss of catalytic activity. The evolved variants with reprogrammed specificities are sufficiently orthogonal to perform the simultaneous ligation of multiple protein/peptide substrates to respective targets in a one-pot solution.[18]

1.3 Objectives

The aim of this work was to engineer Sa-SrtA for efficient bioconjugation, advancing the sortase-mediated toolbox in protein engineering, surface and polymer functionalization.

In the firstly step a sortase-mediated HTS platform for directed enzyme evolution (SortEvolve) was established in PP-MTP. Directed sortase evolution for improved activity and directed enzyme evolution coupled with a semi-purification process were validated. Organic solvents can be used to dissolve hydrophobic substrates in SML but usually not tolerant by sortase A. Therefore, the established SortEvolve system was then optimized and used in the following KnowVolution campaign to identify solvent resistant Sa-SrtA. Several variants with improved resistance and conjugated activity in presence of organic co-solvents were obtained to this end. To gain the knowledge of structure-function relationship of Sa-SrtA in the co-solvents of DMSO, molecular dynamic simulations were investigated. In the last part, SML was employed to advance the methodologies of biofunctionalization of microgel. The generated gel-enzyme hybrids were subsequently used in industrial oriented applications

The main objectives of this PhD thesis are: **i)** Establishment of a robust high throughput screening assay for evolution of Sa-SrtA **ii)** Development of sortase-mediated platform for screening of enzymes with minimized background noise **iii)** Directed Sa-SrtA evolution for efficient site-specific ligation in organic co-solvents **iv)** Understanding the structure-function relationships of Sa-SrtA in organic co-solvents **v)** Expanding applications of sortase-mediated toolbox for hydrophobic compounds conjugations in organic co-solvents **vi)** Development of a general platform for functionalization of microgel particles via sortase-mediated ligation. **vii)** Application of functionalized microgels for industrial aims (textile dye decolourization).

2. Chapter II: A sortase-mediated high throughput screening platform for directed enzyme evolution

2.1. Declaration

Parts of this chapter have been published in the journal ''*ACS Combinatorial Science*'' and are adapted to this thesis with the permission of American Chemical Society Copyright Clearance Center.

2.2. Sortase-mediated high throughput screening: challenges and applications

Directed evolution is a powerful method to tailor enzymes towards user-defined goals [53-54, 73] A robust and reliable high throughput screening assay for enzyme of interest lies in the heart for a successful directed evolution campaign.[74-75] The first fluorescence resonance energy transfer (FRET) based HTS assay for Sa-SrtA was reported in 2004 which uses Abz-LPETG-Dnp-NH$_2$ and triglycine as substrates.[76] During the transpeptidation reaction the covalent bond of Thr-Gly was cleaved and the fluorophore (Abz) and quencher (Dnp) are separated, resulting in a gain of fluorescence emission intensity. Upon the bond cleavage fluorescent signal is generated, which is independent of the sortase catalyzed transpeptidation (conjugated product formation in the second stage of the sortase-mediated ligation).

A main challenge remains for directed sortase evolution as well as the general peptide-peptide bond-forming enzymes is to develop a HTS assay which can directly detect the conjugated products. As mentioned above, attaching the conjugated products on supports surface (e.g yeast surface display,[60] phage display,[72] and IVC based selection[71]) have been reported. Most recently, FRET assays *via* protein-protein, peptide-peptide conjugation were developed in MTP-based to determine transpeptidase without separation of conjugated products and substrates were also reported Sa-SrtA.[77-78] Flow cytometry based UHTS screening requires fluorescence signals on the single cell/compartment level and are highly attractive as prescreening systems for very large libraries. In general, most beneficial variants in UHTS are usually identified in subsequent rescreening via MTP based screening assays [79-81]

..When a HTS is performed using enzyme cell-free lysate, a common drawback is the background noise which lead to the reduction of the signal-to-noise ratio. The phenomenon is especially obviously for screening of enzymes which using ATP or phosphate as substrates (e.g. cyclase, kinase, Phosphorylase). However, performing purification of enzyme of interest from cell-free lysate is always laborious and significantly reduces the throughput of screening. As aforementioned, SML have been successfully employed for the immobilization/purification of protein on different supports with high site-specificity,[35,

[43] therefore it is promising to combine an enzyme purification process in HTS assay. Sortase-mediated purification for HTS has not reported yet.

In this chapter, we describe a polymer surface based directed protein evolution assay (SortEvolve) which provides a general screening tool for improving properties of enzymes. SortEvolve enables a semi-purification of improved enzymes through immobilization of enzyme variants in PP-MTPs. Two applications of SortEvolve were performed. Application 1: directed sortase A evolution for improved activity; Application 2: directed enzyme evolution coupled with a semi-purification process. Application 2 is especially suited for directed evolution campaigns in which background activity has to be minimized in order to identify beneficial variants.

2.3. Results and discussion

The work described here was done in three phases. In the first phase, principles of the established SortEvolve screening platform for directed Sa-SrtA and CueO evolution is described (**2.3.1**). The second phase described the establishment and optimizations of SortEvolve in 96-well polypropylene microtiter plate (PP-MTP). In detail, processes include: a) Production of Sa-SrtA, GGG-eGFP-LCI and CueO-LPETGGGRR (**2.3.2**); b) Optimization of performance criteria of screening assays in Application 1 and Application 2 (**2.3.3**). In the third phase, validations of the SortEvolve screening platform in Application 1 and 2 were demonstrated by screening three site-saturation mutagenesis (SSM) libraries of Sa-SrtA (P94, D160, and D165) in order to improve the Sa-SrtA ligation efficiency (**2.3.4**) and by screening of two SSM libraries of CueO laccase (D439 and P444) in order to improve CueO activity (Application 2) (**2.3.5**).[60, 82] In the last phases, kinetic parameters of the evolved Sa-SrtA variants and CueO variants were characterized (**2.3.6**).

2.3.1 Principle of SortEvove screening platform

Figure 13 illustrates the two targeted applications in SortEvolve. In Application 1 (**Figure 13a**), three SSM libraries (SSM P94, SSM D160, and SSM D165) of Sa-SrtA were screened independently from each other (one 96-well MTP plate per position). Sa-SrtA variants catalyze conjugation of two peptides (adhesion promotor GGG-eGFP-LCI and reporter enzyme CueO-LPETGGGRR WT); Sa-SrtA and variants specifically recognize the C-terminal recognition sequence LPETGGGRR of CueO, cleave the amide bond between threonine and glycine and generates a CueO-LPET-Sa-SrtA intermediate in which the Sa-SrtA variant is covalently attached through a thioester bond to CueO. From the recognition sequence the GGGRR is cleaved. In the next reaction step, a nucleophilic attack from the N-terminal GGG tagged eGFP-LCI occurs and a fusion protein CueO-eGFP-LCI is formed through stable amide

bond with a simultaneous release of the Sa-SrtA variant. After transfer into a PP-MTP, the generated fusion protein CueO-LPETGGG-eGFP-LCI bound to the PP-MTP in which LCI acts as adhesion promoter.[83] After binding, two identical washing steps were conducted and the activity of Sa-SrtA was determined through the 2,2'-azino-bis(3-ethylbenzothiazoline-6-sulphonic acid (ABTS) assay of immobilized CueO-LPETGGG-eGFP-LCI.[84]

In SortEvolve Application 2 (**Figure 13b**), two SSM libraries (SSM D439 and SSM P444) of CueO-LPETGGGRR were individually screened. Likewise, Sa-SrtA WT catalyzes the fusion of two peptides (GGG tagged eGFP-LCI and LPETGGGRR tagged CueO variant). Sa-SrtA WT specifically recognizes CueO-LPETGGGRR variants and GGG-eGFP-LCI and a fusion protein CueO (variant)-LPETGGG-eGFP-LCI is formed similar as described in Application 1. After transfer into a PP-MTP, the generated fusion proteins CueO (variant)-LPETGGG-eGFP-LCI bound to the PP-MTP. After binding, two identical washing steps were conducted and the activity of immobilized CueO (variant)-LPETGGG-eGFP-LCI was determined by the ABTS assay. A significant result of the semi-purification process was a 20-fold reduction in background was achieved.
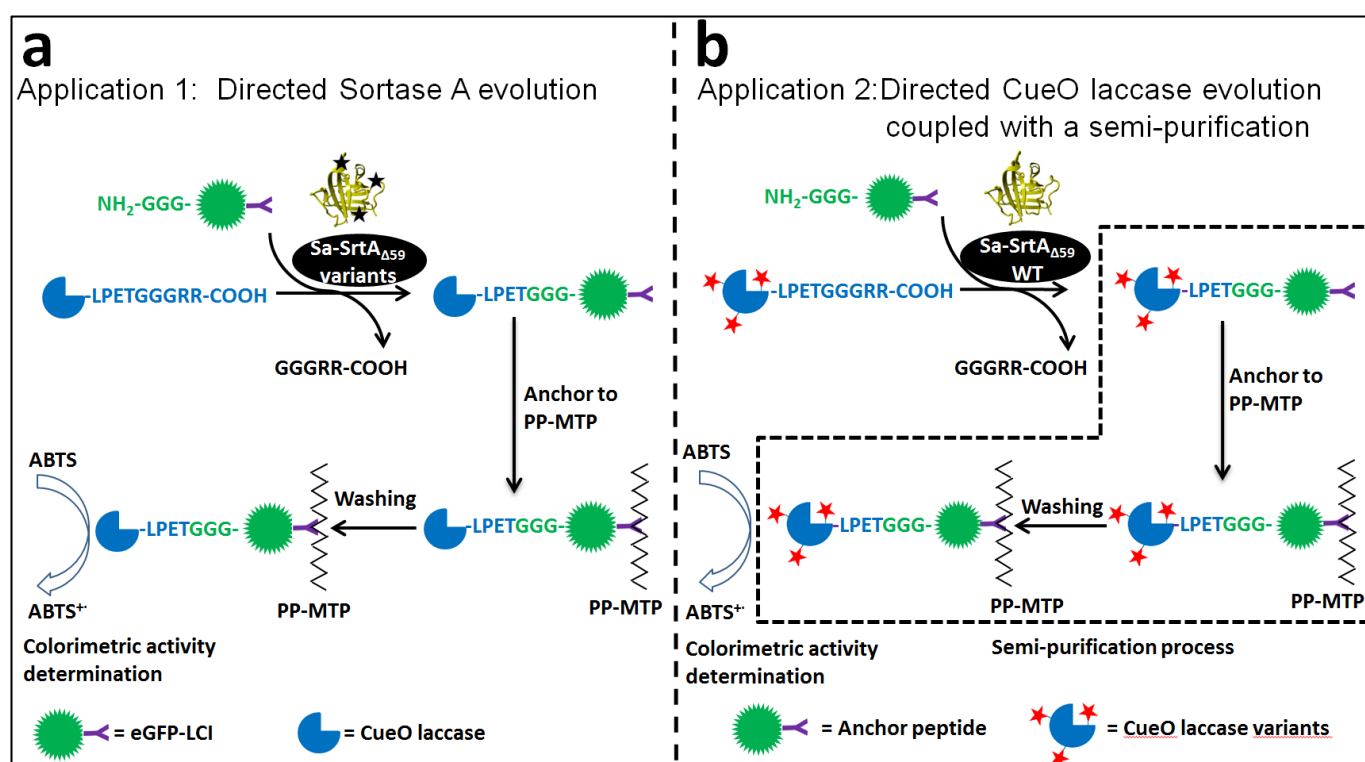
Figure 13. Schematic representation of the SortEvolve screening platform for directed SrtA evolution (a: Application 1) and directed CueO evolution (b: Application 2).

2.3.2. Production of Sa-SrtA, GGG-eGFP-LCI and CueO-LPETGGGRR

The expression of Sa-SrtA WT (and selected variants in Table 2), GGG-eGFP (control of GGG-eGFP-LCI), GGG-eGFP-LCI and CueO-LPETGGGRR in flask were performed as described in 2.4.2. In order to determine key performance parameters, Sa-SrtA, GGG-eGFP-LCI and CueO-LPETGGGRR laccase were purified to homogeneity for Application 1 and 2 (**Figure 14a**). Activity of purified was measured with a FRETassay.[76] The activity purified Sa-SrtA is comparable to the reported data (data is not shown). Comparable fluorescence was observed for eGFP, GGG-eGFP and GGG-eGFP-LCI (data is not shown). The results indicate the incorporation of GGG tagged or LCI in C- and N-terminals does not affect structure of eGFP. Activity of purified CueO and CueO-LPETGGGRR was monitored by ABTS assay. Data is given in **Figure 14b**. The incorporation of LPETGGGRR motif in the C-terminus of CueO laccase attributes a slight decrease (8 %) in its activity.
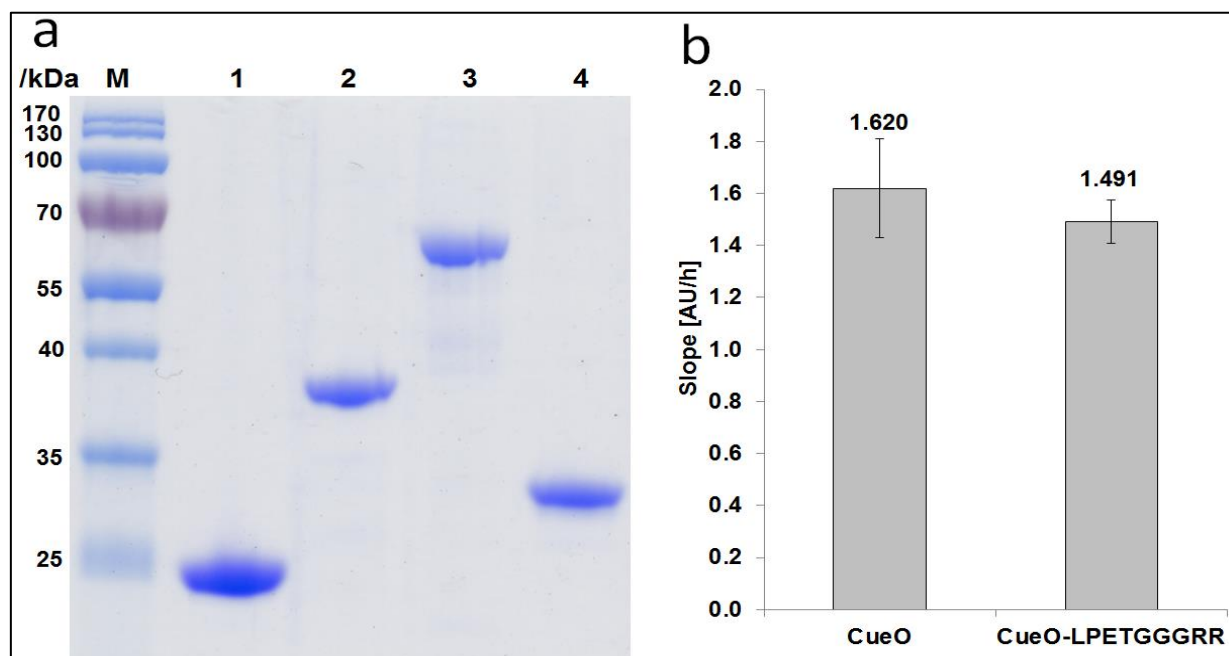
Figure 14. a)SDS-PAGE gel of purified proteins which are used in SortEvolve Application 1 (GGG-eGFP-LCI and CueO-LPETGGGRR) and Application 2 (GGG-eGFP-LCI and Sa-SrtA). M: Standard protein ladder; **1**: Sa-SrtA WT (molecular weight 18.7 kDa); **2**: GGG-eGFP-LCI (molecular weight 36.2 kDa); **3**: CueO-LPETGGGRR (molecular weight 55.9 kDa); and **4**: GGG-eGFP (molecular weight 29.7 kDa).b) Comparison of activities for CueO laccase and C-terminal modified CueO-LPETGGGRR laccase. 5 nM (280 ng/mL) purified CueO and CueO-LPETGGGRR were incubated in PP-MTP with 3 mM ABTS solution (160 μL, sodium citrate buffer pH 3.0, 100 mM). Plates were stirred briefly and the absorbance was constantly measured by Tecan Infinite M1000 PRO plate reader ($\varepsilon_{ABTS\cdot+,\ 420\ nm}$ = 36,000 $M^{-1}cm^{-1}$, room temperature, 15 min). ABTS absorbance slope (Y-axis, AU/h) was calculated.

Concentration and washing steps of GGG-eGFP-LCI (in solution) were optimized for binding in PP-MTP. Different concentrations (ranged from 3 to 200 μg/mL) of GGG-eGFP-LCI were incubated in PP-MTP. To minimize the unspecific binding, identical washing steps were performed. Protocols for binding and washing in PP-MTP are described in 2.4.3.

Fluorescence of the bound GGG-eGFP-LCI (after washing) are recorded (**Figure 15a**). Based on the fluorescence result, binding of GGG-eGFP-LCI on surface of PP-MTP was saturated when 50 ug/mL or higher concentrations GGG-eGFP-LCI were incubated in solution. Moreover, the bound GGG-eGFP-LCI on PP-MTP surface was also visualized by confocal fluorescence microscopy. A strong binding of GGG-eGFP-LCI on PP-MTP with a comparable low background of GGG-eGFP in presence of bovine serum albumin (BSA) was observed (**Figure 15 b** and **c**). The C-terminal fused anchor peptide LCI significantly promoted the binding of eGFP. A monolayer of protein was specifically immobilized on the surface of PP-MTP as described.[85]
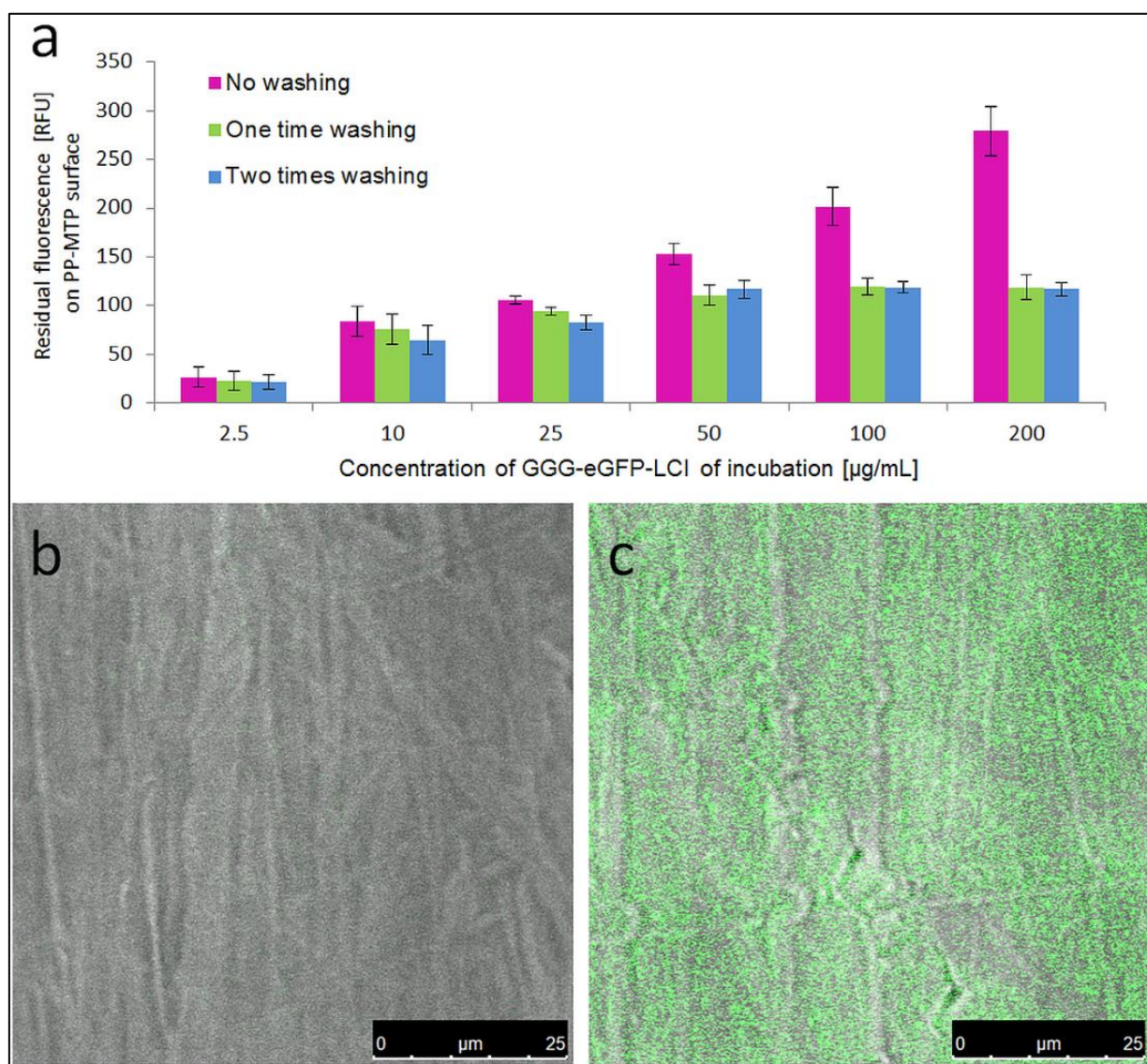
Figure 15. Optimization of GGG-eGFP-LCI binding on polypropylene microtiter plate (PP-MTP) surface. **a)** Residual binding fluorescence on the washed PP-MTP which was incubated with different concentration of purified GGG-eGFP-LCI. Steps were described above. Visualization of GGG-eGFP(**b**) and GGG-eGFP-LCI (**c**) binding on PP plates by fluorescence microscopy (PP plate was incubated 10 min at room temperature with (left) 2.75 μM (equal to 87 μg/mL) GGG-GFP, (right) 2.75 μM (equal to 100 μg/mL) GGG-eGFP-LCI in 100 μL 50 mM Tris-HCl buffer pH 7.5, washed by 10 mL dd H_2O. λ_{exc}.488 nm, λ_{em} 500-600nm, gain 600, confocal microscope TCS SP8 (Leica Microsystems CMS GmbH, Mannheim, Germany).

2.3.3. Performance criteria of screening assays in directed sortase evolution (Application 1) and directed laccase evolution coupled with a semi-purification process (Application 2)

2.3.3.1 Linear detection range of Sa-SrtA cell lysate in Application 1

The linear detection range of Sa-SrtA was determined by supplementing gradient amounts of Sa-SrtA cell-free lysate to a defined reaction mixture (200 μL, 100 μg/mL GGG-eGFP-LCI, 50 μg/mL purified CueO-LPETGGGRR in buffer A (buffer A: 5 mM $CaCl_2$, 150 mM NaCl, 50 mM Tris-HCl, pH 7.5)). The slopes (AU/h) were obtained from 16 replications within the determined linear detection range of ABTS absorbance (**Figure 16a**). A linear increase of laccase activity was shown when 20 μL to 45 μL Sa-SrtA cell-free lysate was used. Sixty microliter and higher volumes did not lead to higher bound CueO laccase activity (maximum to 0.8 AU/h slope was obtained, calculate from 1.1 AU/h subtracting the background 0.3 AU/h). The latter can likely be attributed to the limited polypropylene surface for protein's anchoring in 96-well MTP plates. In order to quantify the amount of CueO laccase is bound on the PP-MTP well, protein CueO-LPETGGG-eGFP-LCI was constructed using PLICing[86] method and purified (**Figure 17a**). A standard curve of enzyme activity (ABTS absorbance) upon the concentration of CueO-LPETGGG-eGFP-LCI was generated (**Figure 17b**). CueO-LPETGGG-eGFP-LCI harbors 46.4% activity of CueO-LPETGGGRR. The maximum absorbance value (0.8 AU/h) in the screening assay (**Figure 17b**) correlates to 5.25 pmol (48.1 ng) CueO-LPETGGG-eGFP-LCI in per PP-MTP well. According to the manufacturer´s product data sheet (96 well plate PP-MTP, Greiner Bio-one), the coated surface area of one well is 86 mm2 (flat bottom: 34 mm2; side wall: 52 mm2 (when 100 μL solution incubated)). The CueO-LPETGGG-GFP-LCI has an estimated surface coverage of 0.61 pmol/cm^2, which in agreement to the previous report.[85]
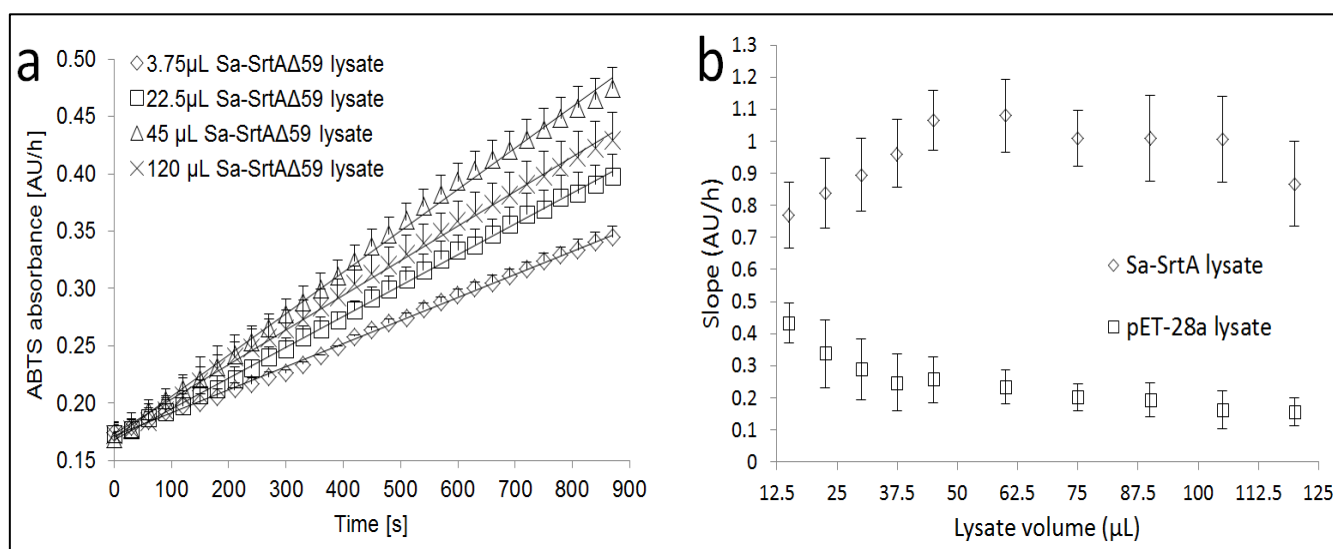
Figure 16. Optimization of Sa-SrtA cell-free lysate in application 1. a) ABTS absorbance with reaction mixture (GGG-eGFP-LCI, CueO-LPETGGGRR, varied amounts of Sa-SrtA employed) in application 1. The constant absorbance determination reveals the linear detection range in ABTS assay. In 15 min, absorbance lies in the linear range (all $R^2 \geq 0.996$). b) Linear detection of Sa-SrtA cell-free lysate in Application 1 (Y-axis shows the slopes of ABTS absorbance (AU/h). X-axis shows the lysate volume used in the assays).

At Sa-SrtA lysate volumes above 105 µL a reduced activity was observed. This phenomenon can likely be caused by reversibility of the reaction (the released product GGGRR competes with substrate GGG-eGFP-LCI to attack the CueO-LPET-Sa-SrtA thioester) which is reported for Sa-SrtA mediated ligations.[35] Furthermore, the generation of fusion protein was visualized by SDS-PAGE and coomassie staining. The formation of CueO-LPPETGG-eGFP-LCI (**Figure 18)** shows an excellent correlation in respect to CueO-LPETGGGRR and GGG-eGFP-LCI consumption and employed ratios under different volumns of Sa-SrtA lysate. Finally, a Sa-SrtA lysate volume of 20 was employed in the directed Sa-SrtA evolution campaign to identify activity-improved variants.
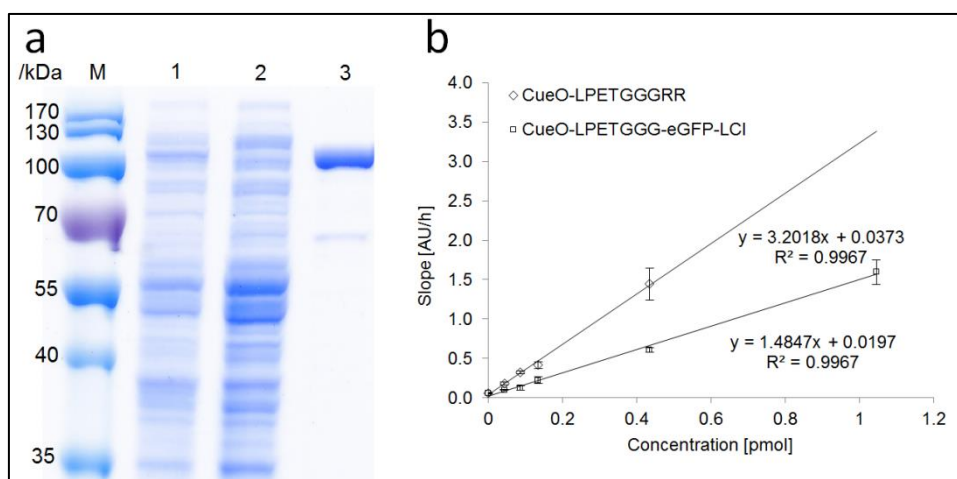
Figure 17. Purification and characterization of CueO-LPETGGG-eGFP-LCI. **(A)** SDS-PAGE gel of CueO-LPETGGG-eGFP-LCI (Molecular weight 91.5 kDa) samples. M: Standard protein ladder; 1: CueO-LPETGGG-eGFP-LCI lysate; 2: Flow through of CueO-LPETGGG-eGFP-LCI after binding with Protino Ni-IDA 2000 packed column; 3: Purified CueO-LPETGGG-eGFP-LCI. **(B)** Correlation of ABTS absorbance slope (Y-axis, AU/h) to CueO-LPETGGG-eGFP-LCI (0.044-1.045 pmol, CueO-LPETGGGRR as a control) concentrations. CueO-LPETGGG-eGFP-LCI /CueO-LPETGGGRR were incubated in PP-MTPs with 3 mM ABTS solution (160 µL, sodium citrate buffer pH 3, 100 mM). Plates were stirred briefly and the absorbance was constantly measured by Tecan Infinite M1000 PRO plate reader ($\varepsilon_{ABTS\cdot+, 420\,nm}$ = 36,000 $M^{-1}cm^{-1}$, room temperature, 15 min).
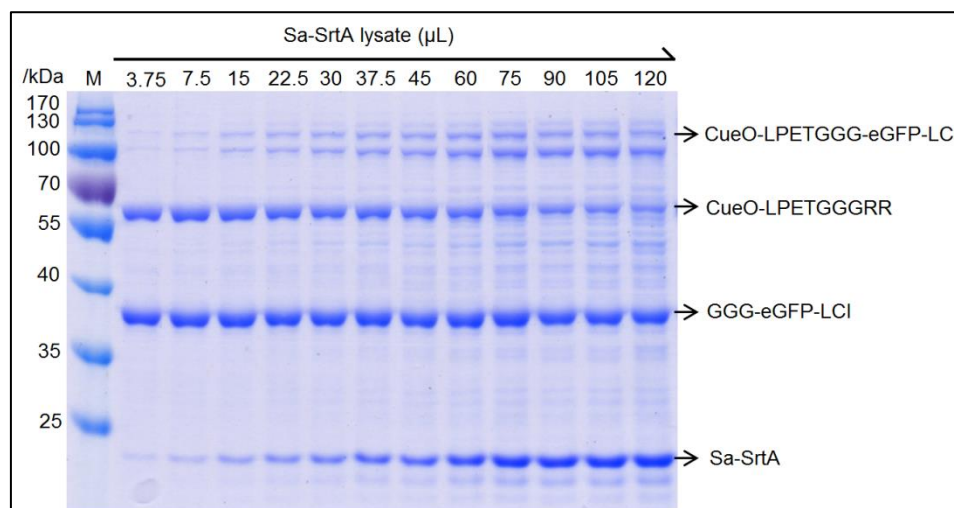
Figure 18. SDS-PAGE gel of the reaction mixture (employed proteins: GGG-eGFP-LCI, CueO-LPETGGGRR, varied volumes of Sa-SrtA lysate) in Application (pET28a: vector without the Sa-SrtA gene).

2.3.3.2 Linear detection range of CueO-LPETGGGRR cell-free lysate in Application 2

Likewise, the linear detection range of CueO-LPETGGGRR was determined by supplementing varied amounts of CueO-LPETGGGRR cell-free lysate to a defined reaction mixture (200 µL, 100 µg/mL GGG-eGFP-LCI, 50 µg/mL Sa-SrtA in buffer A). The slopes (AU/h) were calculated from 16 replications within the determined linear detection range of ABTS absorbance (**Figure 19a**). A linear detection range from 3.75 µL to 60 µL CueO-LPETGGGRR cell-free lysate was determined. Higher volumes did not lead to higher activity of bound CueO laccase. Interestingly, the maximum obtained activity in PP-MTP (absorbance slope≈0.8 AU/h) was comparable with the data in Application 1, which confirms that the PP-MTP surface is the limiting factor for protein anchoring (**Figure 19b**). SDS-PAGE gel of ligated samples with the employed proteins (GGG-eGFP-LCI, varied amounts of CueO-LPETGGGRR, Sa-SrtA)b was also performed. The formation CueO-LPPETGG-eGFP-LCI correlated well in respect to CueO-LPETGGGRR and GGG-eGFP-LCI consumption and employed ratios.
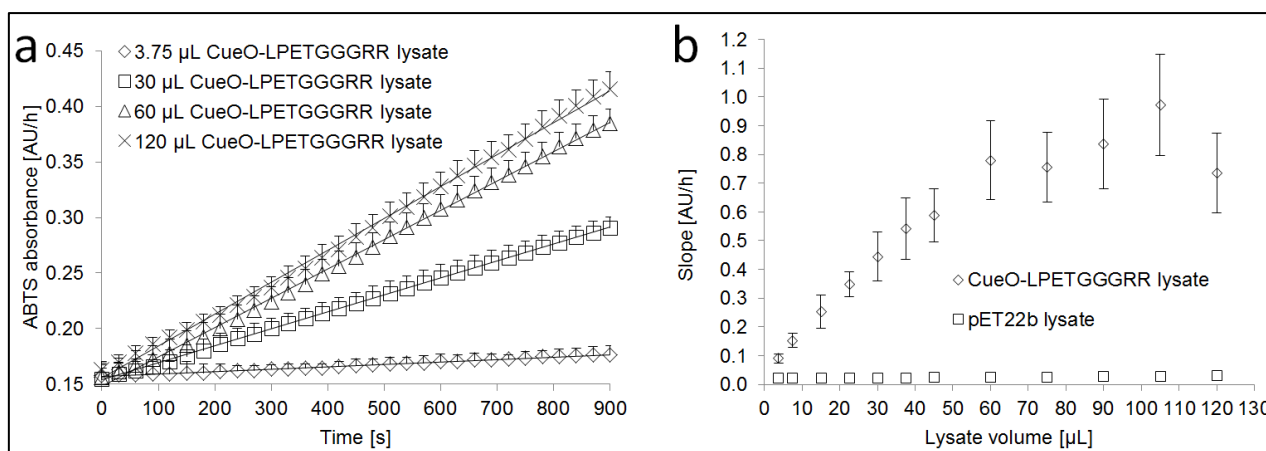
Figure 19. Optimization of CueO-LPETGGGRR cell-free lysate in application 2. a) ABTS absorbance with reaction mixture (GGG-eGFP-LCI, varied amounts of CueO-LPETGGGRR, Sa-SrtA) employed in application 2. The constant absorbance

determination reveals the linear detection range in ABTS assay. In 15 min, absorbance lies in the linear range (all $R^2 \geq 0.996$). b) Linear detection of CueO-LPETGGGRR cell-free lysate in Application 2 (Y-axis shows the slopes of ABTS absorbance (AU/h). X-axis shows the lysate volume used in the assays).

CueO laccase is a housekeeping protein of *E. coli*, which is crucial for copper homeostasis.[87] Therefore, significant background laccase activity was observed in the cell free lysate of pET22b empty vector cells. The volume of 3.75 to 120 µL pET22b lysate was employed in ligation reactions, resulting in a 32-fold increased signal (background noise). In comparison, the ABTS absorbance slope in the developed SortEvolve system increased slightly from 0.021 to 0.031 AU/h (1.48-fold increased signal; background noise). The results show that the background was minimized around 20-fold (32 divided by 1.48) due to the applied semi-purification process.
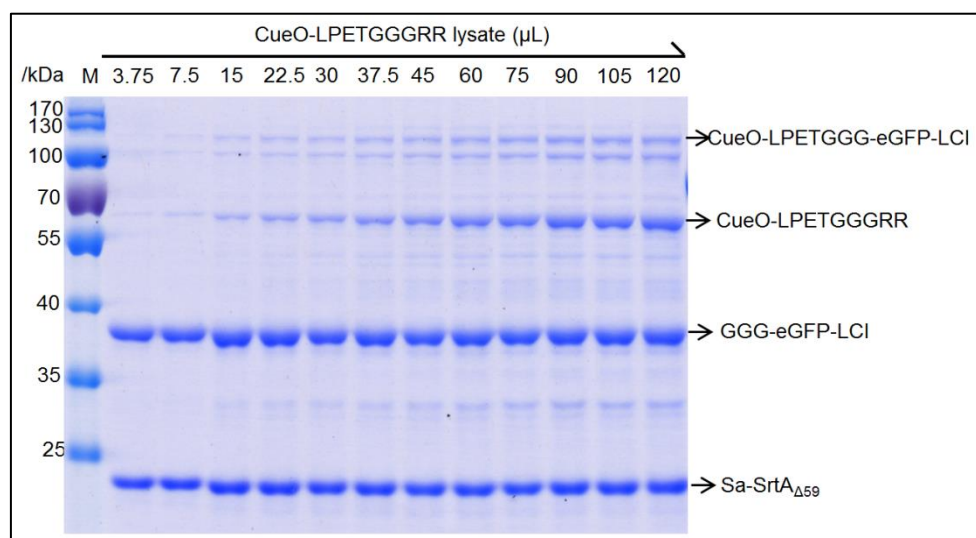
Figure 20. SDS-PAGE gel of the reaction mixture (employed proteins: GGG-eGFP-LCI, varied volumes of CueO-LPETGGGRR lysate, Sa-SrtA) in Application 2 (pET22b: vector without the CueO-LPETGGGRR gene).

2.3.3.3 Determining standard deviations of the SortEvolve platform in 96-well MTP plates

In order to determine the standard deviations of ABTS assays in Application 1 and 2, two 96-well MTPs screens were implemented according to screening protocols in 2.4.6. In order to gain information on background, six wells contained "empty vector" controls and six wells contained the TB-expression media. **Figure 21** show the determined activities in descending order. True coefficient of variations of 18.4 % and 13.2 % were determined for Application 1 (**Figure 21a**) and Application 2 (**Figure 21b**), respectively. Screening assays with standard deviations below 20% are routinely enabled successful directed evolution campaigns.[74-75, 88]
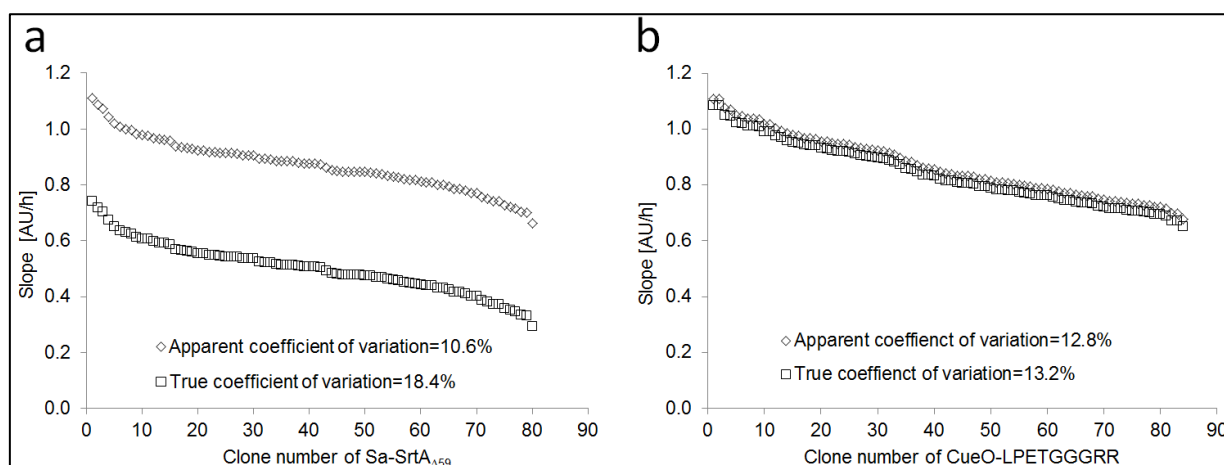
Figure 21. Coefficients of variation to evaluate applicability of SortEvolve screening systems for directed Sa-SrtA evolution (**a**: Application 1) and directed CueO evolution (**b**: Application 2). The apparent coefficient of variation was calculated without subtracting the background and the true coefficient of variation was calculated after background subtraction.

2.3.4. Validation of the SortEvolve screening system for directed Sa-SrtA evolution (Application 1)

Three Sa-SrtA SSM libraries were generated at three previously reported positions (P94, D160 and D165). Each SSM-library was screened individually in one 96-well MTP using the screening protocol (see 2.4.6, **Figure 26a**). Positions P94, D160, and D165 were selected since three Sa-SrtA variants (P94S, D160N and D165A) were reported to improve LPETG-coupling activity (k_{cat}/K_m (LPETG)) by 3.0-fold (P94S, D160N) and 3.5-fold (D165A) when compared to Sa-SrtA WT, respectively.[60] After re-screening, variants with gained activity were identified from corresponding SSM libraries (Table 4). In case of position P94, the Sa-SrtA variant P94S was identified and a comparable improvement of 2.67-fold activity was detected. The most active variant P94T showed a 2.97-fold improved activity when compared to Sa-SrtA WT. In case of position D160, the identical amino acid substitution D160N was identified with a slight reduced (2.37-fold) activity when compared to the reported values (3.0-fold). The amino acid substitution with the highest increase in activity is D160L (2.71-fold) and has not yet been reported. The reported substitution D165A had a 2.55-fold increased activity, slightly lower in comparison with the literature reported improvement (3.5-fold). One possible explanation to this is that D165A caused a significant increase in K_m (GGG-COOH) (WT: 140 µM; D165A: 1000 µM).[60] The most active variant regarding position 165 is D165Q, which was identified with a 2.69-fold enhanced activity in comparison to WT.

Table 4. Activity ratios obtained in the re-screening of Sa-SrtA and CueO-LPETGGGRR SSM libraries. Ratios were calculated with ABTS absorbance slopes of variants (subtracting the background) divided by ABTS absorbance slopes of the corresponding wild-type (subtracting the background).

Application 1	Application 2
Sa-SrtA SSM libraries re-screening results	CueO-LPETGGGRR SSM libraries re-screening

Variant	Variant/WT	results Variant	Variant/WT
SrtA WT	1.00 ± 0.14	CueO WT	1.00 ± 0.09
P94S[a]	2.67 ± 0.41	D439A[b]	2.02 ± 0.32
P94E	2.66 ± 0.46	D439H	2.54 ± 0.18
P94N	2.16 ± 0.45	D439G	1.70 ± 0.27
P94T	2.97 ± 0.44	D439N	3.04 ± 0.61
D160N[a]	2.37 ± 0.28	D439S	2.42 ± 0.44
D160I	2.54 ± 0.53	D439T	2.94 ± 0.48
D160L	2.71 ± 0.46	D439V	3.54 ± 0.64
D160V	2.59 ± 0.64	P444A[b]	2.65 ± 0.30
D165A[a]	2.55 ± 0.43	P444G	3.20 ± 0.36
D165C	2.51 ± 0.42	P444S	2.55 ± 0.32
D165Q	2.69 ± 0.55	P444V	2.95 ± 0.30

[a]*Previously reported Sa-SrtA variants.*[60]

[b]*Previously reported CueO laccase variants.*[82]

To further validate the re-screening results, the reaction mixture (GGG-eGFP-LCI, CueO-LPETGGGRR, Sa-SrtA SSM variants lysate) in **Table 4** were analyzed by SDS-PAGE and coomassie staining. In the SDS-PAGE gels, more CueO-LPETGGG-eGFP-LCI was produced by selected Sa-SrtA variants compared to Sa-SrtA WT (**Figure 22**). These results excellently correlate with the obtained activity data in **Table 4**.
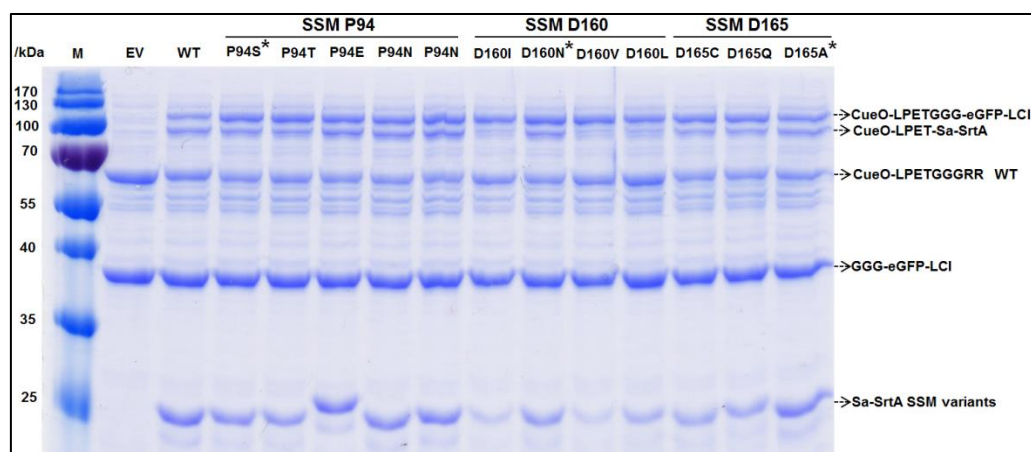
Figure 22. SDS-PAGE gel of reaction mixtures (2.75 µM GGG-eGFP-LCI, 0.89 µM CueO-LPETGGGRR and 20 µL Sa-SrtA lysate) catalyzed by selected Sa-SrtA SSM variants identified from application 1. EV: E. coli BL-21(DE3) harboring empty vector pET28a; WT: Sa-SrtA. Previously reported substitntions of Sa-SrtA are marked with an asterisk.[60]

2.3.5. Validation of the SortEvolve screening system for directed laccase evolution coupled with a semi-purification process (Application 2)

Two CueO-LPETGGGRR SSM libraries were generated at position D439 and P444. Each library was screened independently in one 96-well MTP using screening protocol 2 (see 2.4.6, **Figure 26b**). After screening and subsequent re-screening, CueO variants showing improved activity were isolated from each SSM library (**Table 1**). In position D439, the reported substitution D439A yielded a 2.02-fold activity improvement. Additionally, four additional variants (D439N, D439S D439Tand D439V) were identified

with an activity higher than D439A. The most active variant is D439V which showed 3.54-fold enhanced activity when compared with CueO WT. In case of position P444, the substitution P444A yielded a 2.65-fold increased activity compared to CueO-LPETGGGRR WT. Again, two additional variants (P444G and P444V) with a higher activity than the P444A substitutions were identified (**Table 4**). The SDS-PAGE gel (**Figure 23**) confirmed the re-screening results since highly comparable amounts of CueO(variant)-LPETGGG-eGFP-LCI were generated.
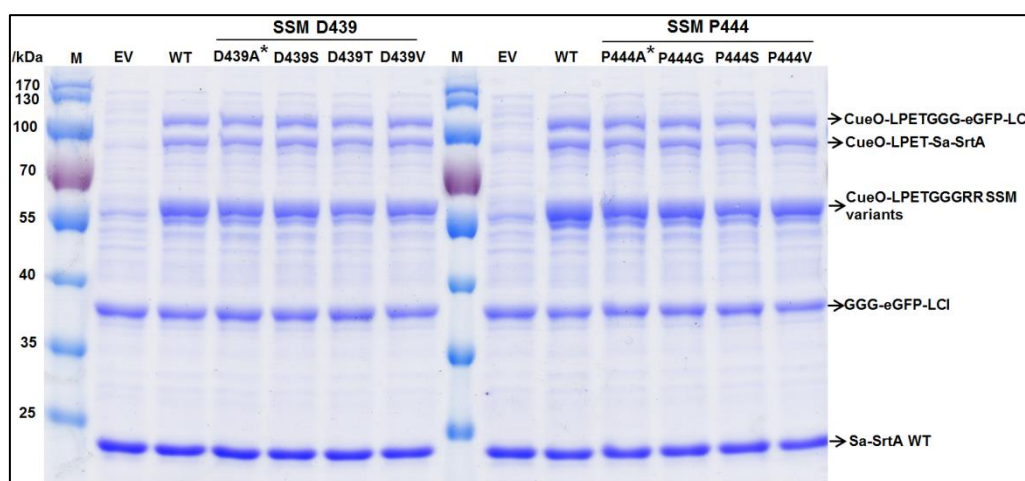
Figure 23. SDS-PAGE gel of reaction mixtures (2.75 µM purified GGG-eGFP-LCI, 100 µL CueO-LPETGGGRR lysate and 2.65 µM purified Sa-SrtA) using identified CueO-LPETGGGRR variants as substrates. EV: E. coli T7 Shuffle express harboring empty vector pET22b; WT: CueO-LPETGGGRR. Previously reported substitntions of CueO laccase are marked with an asterisk.[82]

2.3.6. Characterization of identified Sa-SrtA variants in application 1 and identified CueO-LPETGGGRR variants in application 2

2.3.6.1 Characterization of identified Sa-SrtA variants in application

Characterization of Sa-SrtA WT and evolved variants was carried out with a reported HPLC assay.[76] HPLC trace of ligation product Abz-LPETGGG was showed in **Figure 24**. Activities of Sa-SrtA WT and variants were calculated upon the transpeptidation product Abz-LPETGGG. Plots to determine the K_m $_{(LPETG)}$ and k_{cat} are shown in **Figure 25**. The obtained K_m $_{(LPETG)}$ and k_{cat} for Sa-SrtA WT in **Table 5** well match those reported values.[60] All the selected single mutation variants P94T, D160L and D165Q showed improved turnovers (k_{cat}) and gained coupling ability the LPETG substrate recognition (decreased Km (LPETG) values). Overall, variants P94T, D160L and D165Q had 4.2-fold, 5.1-fold and 3.7-fold catalytic efficiency (k_{cat}/K_m $_{(LPETG)}$) compared with Sa-SrtA WT, respectively (**Table 5**). The recombinant variant P94T/D160L/D165Q was generated and characterized, which harbors 22-fold and 1.4-fold improved k_{cat}/K_m $_{(LPETG)}$ compared with Sa-SrtA WT and the previously reported variant P94S/D160N/D165A, respectively.
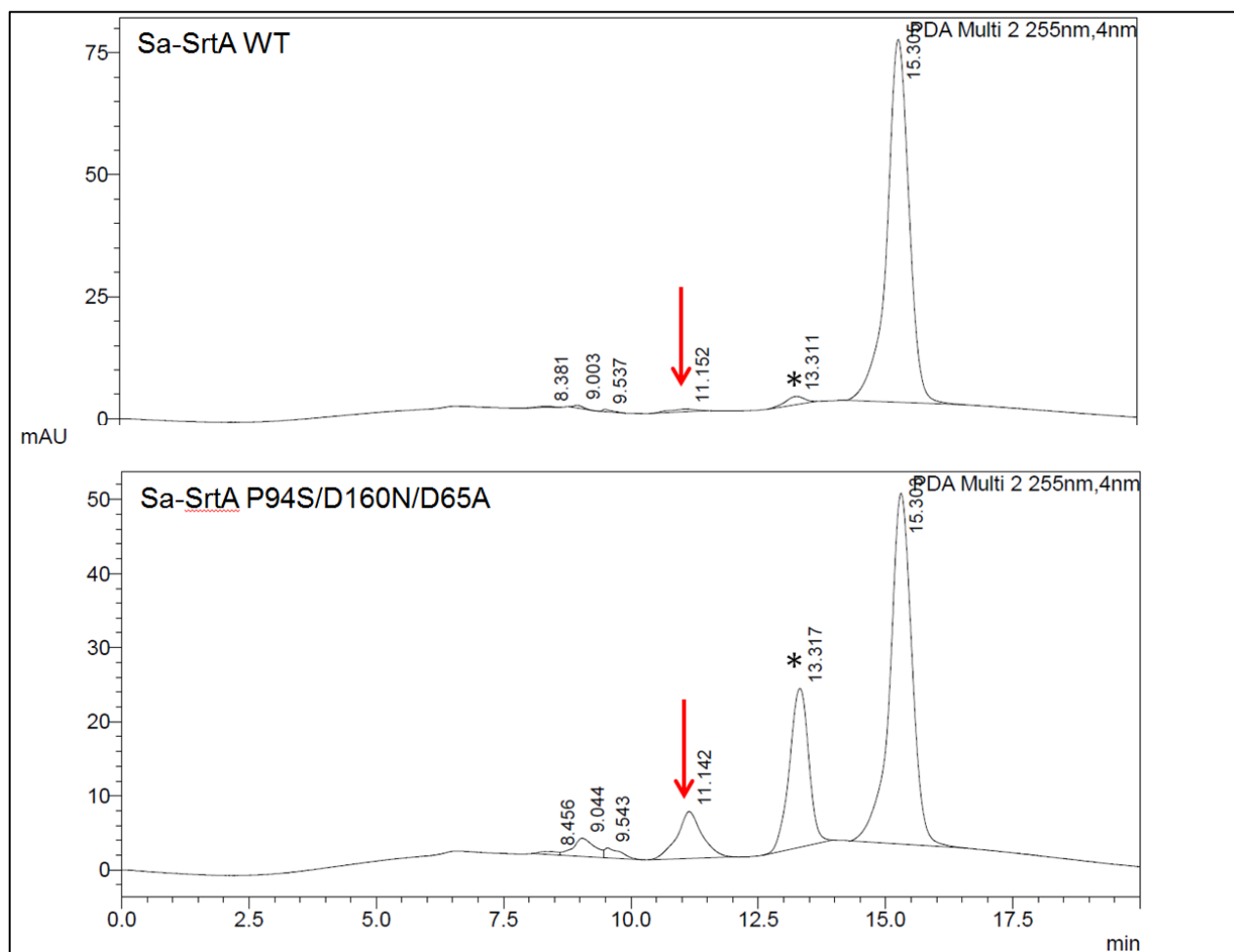
Figure 24. HPLC trace of the sortase-mediated transpeptidase of Abz-LPETGK-Dnp and tri-glycine (concentration of Abz-LPETG-Dnp-NH2 ranged from 0.25 to 6 mM, 9 mM NH2-Gly-Gly-Gly-COOH, 500 nM (9.45 μg/mL) sortase A. Reactions (50 μL) were initiated by adding of enzymes and incubated in room temperature for 5 to 15 min. The red arrow marked the generated tranpeptidase product Abz-LPETGGG. Product GK-Dnp was marked with *. Peak located at 15.3 min is the substrate Abz-LPETGK-Dnp. Details of protocols are described in 2.4.7.

2.3.6.2 Characterization of identified CueO-LPETGGGRR variants in application 2

Characterization of CueO-LPETGGGRR WT and selected variants in each position were performed using an ABTS assay.[82, 89-90] Data are shown in **Table 5.** The observed turnover (k_{cat}) of CueO-LPETGGGRR WT is slightly higher than the reported value.[82] Variant D439A, D439V, P444A and P444V were observed with significant improvements in turnovers (k_{cat}). Catalytic efficiencies ($k_{cat}/K_{m\ (ABTS)}$) of D439A, D439V, P444A and P444V were 10.5, 11.1, 2.70 and 5.67-fold compared with CueO-LPETGGGRR WT, respectively. The improvements in catalytic efficiencies are clearly higher than the obtained ratios in Application 2. One possible reason might be that CueO laccase was immobilized on the PP-MTP surface in Application 2. Furthermore, a recombinant variant CueO-LPETGGGRR D439V/P444V was generated and characterized with 35-fold enhancement in k_{cat} and 3-fold reduced K_m, therefore harboring a 103-fold improved $k_{cat}/K_{m\ (ABTS)}$ compared to WT laccase.

A
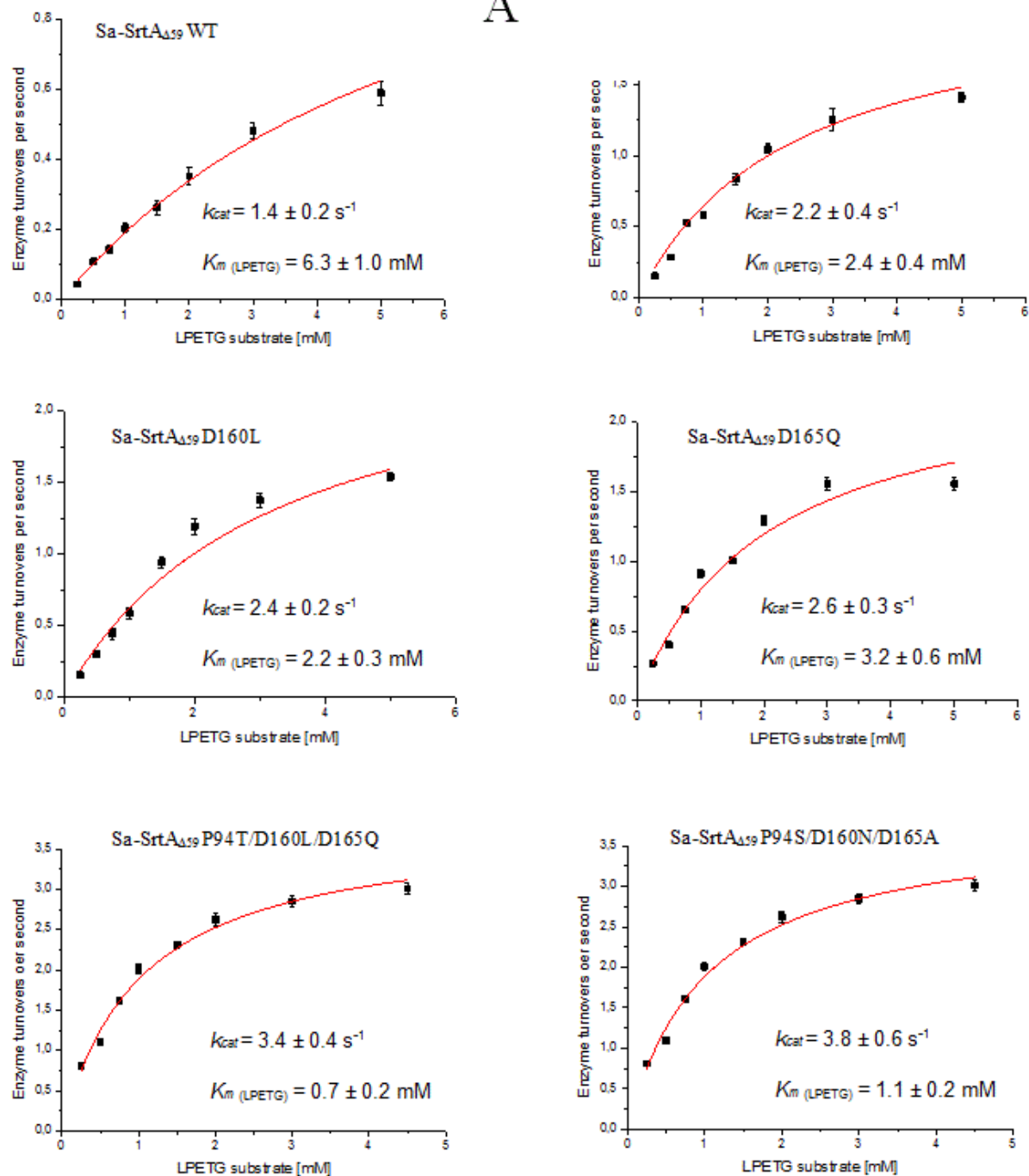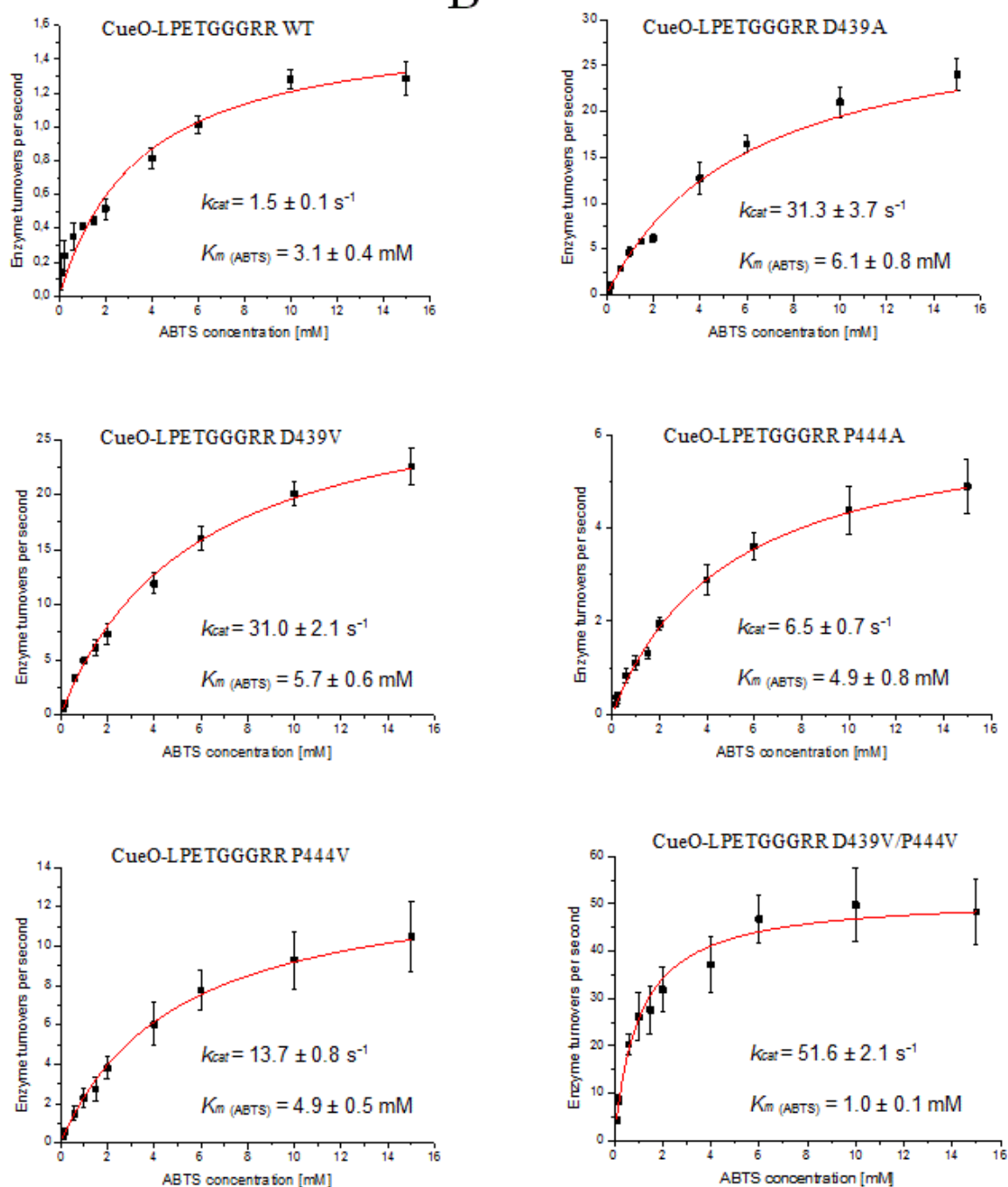
Figure 25. Plots to determine K_m(LPETG) and k_{cat} of Sa-SrtAs (A) and CueO-LPETGGGRRs (B).

Table 5. Kinetic characterization of Sa-SrtA variants in Application 1 and CueO-LPETGGGRR variants in Application 2

Application 1				Application 2			
Selected Sa-SrtA variants				Selected CueO-LPETGGGRR variants			
Variant	k_{cat} (s^{-1})	K_m (mM)	k_{cat}/K_m $(s^{-1}.mM^{-1})$	Variant	k_{cat} (s^{-1})	K_m (mM)	k_{cat}/K_m $(s^{-1}.mM^{-1})$
SrtA WT	1.4 ± 0.2	6.3 ± 1.0	0.22	CueO WT	1.5 ± 0.1	3.1 ± 0.4	0.49
P94T	2.2 ± 0.3	2.4 ± 0.4	0.92	D439A[d]	31.3 ± 3.7	6.1 ± 0.8	5.16
D160L	2.4 ± 0.2	2.2 ± 0.3	1.13	D439V	31.0 ± 2.1	5.7 ± 0.6	5.44

D165Q	2.6 ± 0.3	3.2 ± 0.6	0.82	P444A[d]	6.5 ± 0.7	4.9 ± 0.8	1.32
P94T/D160L/D165Q	3.4 ± 0.4	0.7 ± 0.2	4.86	P444V	13.7 ± 0.8	4.9 ± 0.5	2.78
P94S/D160N/D165A[c]	3.8 ± 0.6	1.1 ± 0.2	3.45	D439V/P444V	51.6 ± 2.1	1.0 ± 0.1	50.54

[a] *The reactions (50 µL, 50 mM Tris-HCl, pH 7.5) contained various concentration of Abz-LPETGK-Dnp-NH$_2$, 9 mM glycine-glycine-glycine nucleophile, 0.5 µM purified Sa-SrtA (WT or variants), 5 mM CaCl$_2$, 150 mM NaCl.*

[b] *The reactions (200 µL, 100 mM sodium acetate buffer, pH 5.5) contained various concentration of ABTS (ε = 36000 M^{-1} cm^{-1}), 5 nM purified CueO-LPETGGGRR laccases (WT or variants).*

In summary, screening of three SSM libraries for Application 1 and two SSM libraries for Application 2 was performed. An array of improved Sa-SrtA variants and CueO laccase variant were identified from screening and subsequent confirmed with kinetic parameters analysis.

2.4. Conclusions

The SortEvolve platform was developed and validated as general screening platform to improve activity of the Sa-SrtA and CueO laccase in directed evolution experiments. Compared with the previously established high throughput sortase screening methods, a main beneficial performance parameter of the SortEvolve screening platform is the implemented purification step through immobilization of the evolved enzymes on PP-MTP plate surface in which comparable enzyme amounts are bound in each well. The purification step minimizes background noise (CueO laccase example) and reduces the common drawback of identifying enzyme variants with higher expression but showing no increased specific activity in directed evolution campaigns. SortEvolve offers a general solution for directed evolution of enzyme classes (e.g. cyclases, glycosyltransferases and phosphorylases) which often have a high background noise from the crude cellular extract. Furthermore, SortEvolve enables the immobilization of enzymes under mild conditions on polypropylene plate and similar surfaces (e.g. beads and particles). It is anticipated that the SortEvolve platform can be expanded to other sortases and other related peptide-peptide bond-forming enzymes (e.g. transglutaminase or butelase 1).

2.5. Materials and Methods

Chemicals with analytical grade purity were obtained from AppliChem (Darmstadt, Germany), Sigma-Aldrich (Hamburg, Germany), Carl Roth (Karlsruhe, Germany), or Invitrogen (Darmstadt, Germany). Chemicals GK-Dnp-NH$_2$, Abz-LPETGK-Dnp-NH$_2$, and Abz-LPETGGG-COOH were purchased from Bachem (Bubendorf, Switzerland). Primers used in polymerase chain reaction (PCR) were purchased from Eurofins MWG Operon. Enzymes were purchased from New England Biolabs (Frankfurt, Germany) or Fermentas (St. Leon-Rot, Germany). Plasmid isolation, PCR purification and His-tag purification kits were purchased from Macherey-Nagel GmbH & Co.KG (Düren, Germany). Flat/V-bottom polystyrene

96-well MTPs and flat-bottom polypropylene 96-well MTPs were purchased from Greiner Bio-One GmbH, (Frickenhausen, Germany).

2.5.1. Cloning of plasmid constructs

2.5.1.1. Cloning of GGG-eGFP, GGG-eGFP-LCI, CueO-LPETGGGRR and CueO-LPETGGG-eGFP-LCI plasmid constructs

Unmodified and phosphorothioate DNA primers used in plasmid gene cloning are shown in **Table 6**. pET28a-eGFP and pET28a-eGFP-LCI, both carrying N-terminal His$_6$-tag were employed as templates to generate pET28a-GGG-eGFP and pET28a-GGG-eGFP-LCI, respectively. In detail, primers *GGG-eGFP Fw* and *GGG-eGFP Rev* were used to generate pET28a-GGG-eGFP. Primers *GGG-eGFP-LCI Fw* and *GGG-eGFP-LCI Rev* (reverse) were employed for the construction PCR of pET28a-GGG-eGFP-LCI. Two PCRs used a same protocol: 98°C for 45 sec (1 cycle); 98°C for 30 sec, 55°C for 30 sec, 72°C for 3 min 30 sec (25 cycles); 72°C for 10 min (1 cycle).

Table 6. List of primers used for the cloning and PLICing. Asterisks mark the positions of phosphorothioate bonds.

Primer Name	Sequence 5'-3'
GGG-eGFP Fw	ATGGGAGGAGGAATGGGCAGCAG
GGG-eGFP Rev	TCCTCCTCCCATGGTATATCTCCTTC
GGG-eGFP-LCI Fw	ATGGGCGGTGGCAGCAGCCATCATCAT
GGG-eGFP-LCI Rev	GCTACCACCGCCCATGGTATATCTCCTTC
CueO-LPETGGGRR Fw	CTACCTGAAACAGGTGGTGGTCGTCGTTAGCGCACTCGAGCACCA
CueO-LPETGGGRR Rev	CTAACGACGACCACCACCTGTTTCAGGTAGCTTTTCGAACTGCGG
GGG-eGFP-LCI insert Fw	G*G*C*G*G*T*G*G*T*A*G*C*AGCCATCATCATC
GGG-eGFP-LCI insert Rev	G*T*G*C*T*C*G*A*G*T*G*C*TTATTTGCGATC
pET22b-CueO-LPET vector Fw	G*C*A*C*T*C*G*A*G*C*A*C*CACCACCACCAC
pET22b-CueO-LPET vector Rev	G*C*T*A*C*C*A*C*C*G*C*C*TGTTTCAGGTAGC

Recombinant plasmid pET22b-CueO (PDB code: 3OD3) with a StrepII-tag sequence in the C-terminus was used as template for construction of pET22b-CueO-LPETGGGRR. PCR was performed by using primers *CueO-LPETGGGRR Fw* and *CueO-LPETGGGRR Rev*. PCR protocol: 98°C for 45 sec (1 cycle); 98°C for 30 sec, 55°C for 30 sec, 72°C for 4 min (25 cycles); 72 °C for 10 min (1 cycle). In order to generated the fusion construct pET22b-CueO-LPETGGG-eGFP-LCI, Phosphorothioate-based ligase independent cloning (PLICing, [86]) was performed. The generated construct pET28a-GGG-eGFP-LCI was employed as the template for the PCR of insert DNA fragment GGG-eGFP-LCI. The generated construct pET22b-CueO-LPETGGGRR was employed as the template for PCR of backbone vector fragment pET22b-CueO-LPET. Primers *GGG-eGFP-LCI insert Fw* and *GGG-eGFP-LCI insert Rev* were used for the amplification of insert DNA fragment GGG-eGFP-LCI. PCR protocol: 98°C for 45 sec (1 cycle); 98°C for 30 sec, 55°C for 30 sec, 72°C for 1 min (25 cycles); 72°C for 10 min (1 cycle). Primers *pET22b-CueO-LPET vector Fw* and *pET22b-CueO-LPET vector Rev* were used for the amplification of

vector backbone DNA fragment pET22b-CueO-LPET. PCR protocol: 98°C for 45 sec (1 cycle); 98°C for 30 sec, 55°C for 30 sec, 72°C for 6 min (25 cycles); 72°C for 10 min (1 cycle). Iodine cleavage and hybridization was performed with 0.08 mM insert and 0.04 mM vector as previously reported [86].

2.5.1.2. Site-saturation mutagenesis

Plasmid pET28a-Sa-SrtA with a His-tag in the N-terminus (PDB code: 2KID) was used as the template to construct Sa-SrtA SSM libraries at literature reported positions P94, D160, and D165.[60] The generated construct pET22b-CueO-LPETGGGRR was used as the template for the generation of CueO-LPETGGGRR SSM libraries at reported position D439 and P444.

Primers used in site-saturation mutagenesis (SSM) are shown in **Table 7**. In detail, primers *Sa-SrtA-P94 SSM Fw* and *Sa-SrtA-P94 SSM Rev* were used to generate Sa-SrtA-P94 SSM library. Primers *Sa-SrtA-D160 SSM Fw* and *Sa-SrtA-D160 SSM Rev* were used for the construction of Sa-SrtA-D160 SSM library. *Sa-SrtA-D165 SSM Fw* and *Sa-SrtA-D165 SSM Rev* were employed for construction of Sa-SrtA-D165 SSM library. Three SSM PCRs used a same protocol: 98°C for 45 sec (1 cycle); 98°C for 30 sec, 58°C for 30 sec, 72°C for 3 min 30 sec (25 cycles); 72°C for 10 min (1 cycle). For generation of CueO-LPETGGGRR D439 SSM library, *CueO-LPETGGGRR D439 SSM Fw* and *CueO-LPETGGGRR D439 SSM Rev* were used. *CueO-LPETGGGRR P444 SSM Fw* and *CueO-LPETGGGRR P444 SSM Rev* were employed for PCR of CueO-LPETGGGRR P444 SSM library. PCRs performed with same protocol: 98°C for 45 sec (1 cycle); 98°C for 30 sec, 55°C for 30 sec, 72°C for 4 min (25 cycles); 72 °C for 10 min (1 cycle).

Table 7. List of primers used in site-saturation mutagenesis. N means G or T and M means A or C.

Primer Name	Sequence 5'-3'
Sa-SrtA-P94 SSM Fw	CCAGGACCAGCAACANNKGAACAATTAAATAGAGGTG
Sa-SrtA-P94 SSM Rev	CACCTCTATTTAATTGTTCMNNTGTTGCTGGTCCTGG
Sa-SrtA-D160 SSM Fw	GACAAGTATAAGANNKGTTAAGCCAACAGATGTAG
Sa-SrtA-D160 SSM Rev	CTACATCTGTTGGCTTAACMNNTCTTATACTTGTC
Sa-SrtA-D165 SSM Fw	GAGATGTTAAGCCAACANNKGTAGAAGTTCTAGATGAAC
Sa-SrtA-D165 SSM Rev	GTTCATCTAGAACTTCTACMNNTGTTGGCTTAACATCTC
CueO-LPETGGGRR D439 SSM Fw	GGCGTGGGCNNKATGATGCTGC
CueO-LPETGGGRR D439 SSM Rev	GCAGCATCATMNNGCCCACGCC
CueO-LPETGGGRR P444 SSM Fw	GATGCTGCATNNKTTCCATATCCAC
CueO-LPETGGGRR P444 SSM Rev	GTGGATATGGAAMNNATGCAGCATC

2.5.1.3. Site-directed mutagenesis (SDM)

Recombinant variant Sa-SrtA P94T/D160L/D165Q, Sa-SrtA P94S/D160N/D165A and CueO-LPETGGGRR D439V/P444V were generated by site-directed mutagenesis (SDM). Primers used in site mutagenesis (SSM) are shown in **Table 8**. The generated plasmid Sa-SrtA P94T was used as the template for the PCR of Sa-SrtA P94T/D160L/D165Q. PCR was performed by using primers *Sa-SrtA-P94T/D160L/D165Q SDM Fw* and *Sa-SrtA- P94T/D160L/D165Q SDM Rev*. The generated plasmid Sa-

SrtA P94S was used as the template for the PCR of Sa-SrtA P94S/D160N/D165A. PCR was performed by using primers *Sa-SrtA-P94S/D160N/D165A SDM Fw* and *Sa-SrtA- P94S/D160N/D165A SDM Rev*. The generated plasmid CueO-LPETGGGRR D439V was employed as template to construct CueO-LPETGGGRR D439V/P444V. PCR was performed by using primers *CueO-LPETGGGRR D439V/P444V SDM Fw* and *CueO-LPETGGGRR D439V/P444V SDM Rev Rev*. The three PCRs used a same protocol: 98°C for 30 sec (1 cycle); 98°C for 15 sec, 55°C for 30 sec, 72°C for 4 min (25 cycles); 72 °C for 10 min (1 cycle).

Table 8. List of primers used in site-directed mutagenesis experiments.

Primer Name	Sequence 5'-3'
Sa-SrtA-P94T/D160L/D165Q SDM Fw	TTGGTTAAGCCAACACAGGTAGAA GTT CTA
Sa-SrtA- P94T/D160L/D165Q SDM Rev	CTGTGTTGGCTTAACCAATCTTATACT TGT
Sa-SrtA-P94S/D160N/D165A SDM Fw	TCTGTTAAGCCAACAGCGGTAGAA GTT CTA
Sa-SrtA- P94T/D160N/D165A SDM Rev	CGCTGTTGGCTTAACAGATCTTATACT TGT
CueO-LPETGGGRR D439V/P444V SDM Fw	GTTATGATGCTGCATGTTTTCCATATC CAC
CueO-LPETGGGRR D439V/P444V SDM Rev	AACATGCAGCATCATAACGCCCAC GCCAGA

All PCR solutions (50 μL) for amplification consist of 2.5 U PfuS DNA polymerase, 10 mM dNTP mix, 20 ng plasmid template and 25 uM of each primer (forward primer and reverse primer). All PCR products were digested by Dpn I (5 U, 37°C, overnight) and subsequently conducted by heat inactivation (80°C for 20 min). The Dpn I digested samples were purified. Clean-up PCR products were then transformed into corresponding competent cells.

2.5.2. Protein expression and purification

The expression of Sa-SrtAs (WT and selected variants in Table 2), GGG-eGFP and GGG-eGFP-LCI in flask were conducted as previously described.[91] Expression of CueO-LPETGGGRR (WT and selected variants in Table 2) and CueO-LPETGGG-eGFP-LCI were performed in flask. In detail, Pre-cultures of *E. coli* Shuffle T7 express harboring pET22b-CueO-LPETGGGRR plasmids (5 mL TB media, 100 μg/mL ampicillin) were inoculated from a glycerol stock and incubated in Multitron II Infors shaker overnight (250 rpm, 16 h, 37°C, 70% humidity). The main culture (1 L flask, 200 mL TB media, 100 μg/mL ampicillin) was inoculated with 1 mL pre-culture in Multitron II Infors shaker for ~2 h (250 rpm, 37°C, 70% humidity). At an OD_{600} of ~1 the main culture was induced with 0.2 mM IPTG and 1.5 mM $CuSO_4$ followed with incubation in the same shaker (200 rpm, 16 h, 30°C, 70% humidity). The expressed cells were harvested by centrifugation (Eppendorf centrifuge 5810 R, 3220 g, 30 min, 4°C). The preparation of pre-culture and main culture of CueO-LPETGGG-eGFP-LCI used the same protocol as CueO-LPETGGGRR. At an OD_{600} of ~1 the main culture of CueO-LPETGGG-eGFP-LCI was induced with 0.2 mM IPTG and 1.5 mM $CuSO_4$, subsequently incubated in the same shaker (200 rpm, 48 h, 20°C, 70% humidity). The expressed cells harvested by centrifugation (Eppendorf centrifuge 5810 R, 3220 g, 30 min, 4°C).

Chapter II: A sortase-mediated high throughput screening platform for directed enzyme evolution

Expressions of Sa-SrtA and CueO-LPETGGGRR SSM libraries were conducted in 96-well MTPs. Colonies of Sa-SrtA SSM libraries and CueO-LPETGGGRR SSM libraries were picked from solid LB plates (supplemented with 50 μg/mL kanamycin and 100 μg/mL Ampicillin, respectively) into V-bottom 96-well polystyrene (PS) MTP (150 μL/well TB media, 50 μg/mL kanamycin for Sa-SrtA SSM libraries and 100 μg/mL ampicillin for CueO-LPETGGGRR SSM libraries). After cultivation (900 rpm, 24 h, 37°C, and 70% humidity; Multitron Pro, Infors HT, Bottmingen, Switzerland), 5 μL pre-culture was inoculated into another 96-well V-type MTP with 150 μL TB main culture with corresponding antibiotics. When OD_{600} reached around 0.8, Sa-SrtA SSM libraries were induced by adding 1 mM IPTG followed with further overnight cultivation (900 rpm, 16 h, 30°C, and 70% humidity; Multitron Pro, Infors HT). CueO-LPETGGGRR SSM libraries are induced by adding 0.2 mM IPTG and 1.5 mM $CuSO_4$ at OD_{600} around 1 and subsequently with overnight cultivation (900 rpm, 16 h, 30°C, and 70% humidity; Multitron Pro, Infors HT). Induced cells were harvested by centrifugation (3220 g, 30 min, 4°C). Cell pellets were kept at -20°C until use.

The expressed cell pellets were employed to produce cell lysate. In detail, cell pellets from flasks were first re-suspended with Tris-HCl buffer (pH 7.5, 50 mM) and then sonicated on ice (60% amplitude, 12 cycles, 15 seconds per cycle, intervals 15 seconds). After centrifugation (Eppendorf centrifuge 5810 R, 3220 g, 1 h, 4°C) the supernatant was used for SDS-PAGE analysis. Cell pellets from MTP culture were incubated with 150 μL 0.8 mg/mL lysozyme in Tris-HCl buffer (pH 7.5, 50 mM, 45 min, 37°C and 900 rpm). After centrifugation (Eppendorf centrifuge 5810 R, 3220 g, 45 min, 4°C) the clear supernatant was analyzed by SDS-PAGE and used in the screening assay. SDS-PAGE samples were prepared by mixing 30 μL lysate supernatant and 10 μL 4x SDS loading buffer. The mixture was heated at 95°C for 5 min. Eight microliters of the samples were loaded and analyzed on 10 % acrylamide gels.

The clear supernatants of GGG-eGFP-LCI, GGG-eGFP, Sa-SrtA, CueO-LPETGGGRR and CueO-LPETGGG-eGFP-LCI were employed to produce the corresponding purified proteins. Clear supernatants of Sa-SrtA SSM libraries and CueO-LPETGGGRR SSM libraries were used in the SortEvolve Application 1 and 2.

Protino Ni-IDA 2000 packed columns (Macherey-Nagel GmbH & Co. KG, Düren, Germany) were employed to purify the overexpressed protein GGG-eGFP-LCI, GGG-eGFP, Sa-SrtA and CueO-LPETGGG-eGFP-LCI. Regarding purification of CueO-LPETGGGRR, Strep-Tactin Superflow Plus cartridge (Qiagen, Venlo, Germany) was used. Purification process was performed according to the manufacturer´s protocol. Purified samples were firstly checked by SDS-PAGE and then dialyzed overnight in Tris-HCl buffer (at 4°C; pH 7.5, 50 mM) by Spectra/Por dialysis tubing (Spectrum

Laboratories, Inc., CA, USA). Amicon ultra-15 centrifugal filter units with 10 kDa cut-off (Merck Millipore Ltd, Tullagreen, IRL) were used for preparation of concentrated protein samples.

2.5.3. Anchoring test of purified GGG-eGFP-LCI to PP-MTP

Anchoring test of GGG-eGFP-LCI to PP-MTP was performed in three steps used the similar protocol as previously reported [83]. First, 100 µL mixture containing purified GGG-eGFP-LCI (range from 0.069 µM (2.5 µg/mL) to 5.51 µM (200 µg/mL), GGG-eGFP as control) and 400 µg/mL bovine serum albumin (BSA; in Tris-HCl buffer, pH 7.5, 50 mM) were incubated in polypropylene (PP)-MTP (600 rpm, room temperature, 10 min; MTP shaker, TiMix5, Edmund Bühler GmbH, Hechingen, Germany). Then the liquid was removed by decanting. Washing steps were performed using Tris-HCl (200 µL, pH 7.5, 50 mM), followed by an incubation step (600 rpm, room temperature, 5 min). Fluorescence of immobilized eGFPs was determined by Tecan infinite 1000 plate reader (λ_{exc} = 488 nm; λ_{em} = 509 nm, gain = 100; Tecan Group AG, Männedorf, Switzerland).

2.5.4. Activity assay of purified CueO-LPETGGGRR

Activity determination of CueO-LPETGGGRR laccase was performed according the standard 2,2'-azino-bis(3-ethylbenzothiazoline-6-sulphonic acid assay.[92] In detail, ABTS (3 mM) was dissolved in sodium citrate buffer (pH 3, 100 mM). Purified CueO-LPETGGGRR (range from 0.044 pmol to 1.045 pmol, CueO as control) was incubated in 160 µL prepared ABTS solution. Plates were stirred briefly and the absorbance was continuously measured by Tecan Infinite M1000 PRO plate reader (($\varepsilon_{ABTS\cdot+ \ 420 \ nm}$= 36,000 $M^{-1}cm^{-1}$), room temperature).

2.5.5. Screening protocol for Application 1: Directed Sa-SrtA evolution

Screening protocol for directed Sa-SrtA evolution (Application 1: screening protocol 1) was showed in **Figure 26a**. In *Step1*, Sa-SrtA libraries were expressed in V-bottom 96-well polystyrene MTP (PS-MTP) as mentioned in Supplementary Information. The cell pellets from -20°C were thawed and cells lysed by lysozyme (150 µL, 0.8 mg/mL, 50 mM Tris-HCl, pH 7.5) and incubated (600 rpm, 1 h, 37°C). Clear supernatant was obtained by centrifugation (3220 g, 30 min, 4°C). An aliquot from each well (20 µL) was transferred into the corresponding well in F-bottom 96-well PS-MTP. In *Step2*, Conjugation of CueO-LPETGGGRR and GGG-eGFP-LCI was catalyzed by 20 µl Sa-SrtA variant lysate in F-bottom 96-well PS-MTP (reaction mixture: 200 µL, 2.75 µM (100 µg/mL) purified GGG-eGFP-LCI, 0.89 µM (50 µg/mL) purified CueO-LPETGGGRR, in buffer A) followed by an incubation (800 rpm, 3 h, room temperature). In *Step3*, binding of generated CueO-LPETGGG-eGFP-LCI in PP-MTP was performed by adding 50 µL reacted solution (from *Step2*) with 50 µL BSA solution (800 µg/mL, Tris-HCl buffer, pH 7.5 50 mM) and incubation (10 min, 600 rpm, room temperature). BSA was reported to effectively reduce

unspecific protein binding in previous study.[85] After incubation, the liquid is removed by decanting. In *Step4*, two identical washing processes were carried to ensure complete removal unspecific and weak binding proteins. Each washing process employed Tris-HCl buffer (200 µl, pH 7.5, 50 mM) and intensive shaking (5 min, 600 rpm, room temperature). Washing solution was removed by decanting. In *Step5*, activity of Sa-SrtA variant was determined by measuring the activity of the reporter enzyme laccase CueO (CueO-LPETGGG-eGFP-LCI). CueO activity was determined with the ABTS assay under standard conditions (160 µL; 3 mM ABTS, sodium citrate buffer (pH 3.0, 100 mM), room temperature). A green-blueish color formation of the ABTS-radical cation quantifies the CueO activity within the determined linear detection range (**Figure 16**).

2.5.6. Screening protocol for Application 2: Directed CueO laccase evolution

 Figure 26b shows the screening protocol of directed CueO laccase evolution (Application 2: screening protocol 2). In *Step1*, CueO-LPETGGGRR libraries were expressed in V-bottom 96-well PS-MTP and frozen as mentioned above. Supernatants of cell-free lysate were obtained using the same protocol as in screening protocol 1. An aliquot from each well (100 µL) was transferred into the corresponding well in F-bottom 96-well PS-MTPs. In *Step2*, Conjugation of CueO (variant)-LPETGGGRR lysate and GGG-eGFP-LCI catalyzes by Sa-SrtA WT in F-bottom 96-well PS-MTP (200 µL, 2.75 µM (100 µg/mL) purified GGG-eGFP-LCI, 2.65 µM (50 µg/mL) purified Sa-SrtA WT, in buffer A) followed by incubation (800 rpm, 3 h, room temperature). *Step3*, *Step4,* and *Step5* were performed similar as described in screening protocol 1.

Chapter II: A sortase-mediated high throughput screening platform for directed enzyme evolution

A **Application 1 : Directed Sa-SrtA$_{\Delta59}$ evolution**

Step1: **Production** of Sa-SrtA$_{\Delta59}$ variants in *E. coli* BL-21 (DE3)
- V-bottom PS-MTP
- Preculture (TB medium, 150 μL, 37°C, 900 rpm, 16 h)
- Cultivation (TB medium, 150 μL, 30°C, 900 rpm, 16 h)

Cells are lysed by lysozyme and 20 μL clear supernatant is transferred

Step2: **Conjugation** of CueO-LPETGGGRR and GGG eGFP-LCI ligated by **Sa-SrtA$_{\Delta59}$ variants**
- F-bottom PS-MTP
- **20 μL Sa-SrtA$_{\Delta59}$ variant lysate**
- **50 μg/mL CueO-LPETGGGRR WT**
- 100 μg/mL GGG-eGFP-LCI
- Ligation (200 μL, 800 rpm, 3 h , RT, Tris-HCl pH 7.5)

50 μL reacted solution is transferred to **PP-MTP**

Step3: **Anchoring** of generated CueO-LPETGGG-eGFP-LCI in **PP-MTP**
- **F-bottom PP-MTP**
- 50 μL reacted solution from *Step2*
- 50 μL 800 μg/mL BSA
- Anchoring (100 μL, 600 rpm, 10 min, RT, Tris-HCl pH 7.5)

Liquid is decanted and unbound proteins are removed

Step4: **Washing** of PP-MTPs
- **F-bottom PP-MTP**
- 2 times washing
- Washing (200 μL, 600 rpm, 5 min, RT, Tris-HCl pH 7.5)

Liquid is decanted and ABTS is supplemented

Step5: **Activity determination** of Sa-SrtA$_{\Delta59}$ through immobilized CueO-LPETGGG-eGFP-LCI via **ABTS**
- **F-bottom PP-MTP**
- ABTS assay (160 μL,15 min, RT, sodium citrate, pH 3.0)
- Absorbance determination

B Application 2 : Directed CueO laccase evolution

Step1: Production of CueO-LPETGGGRR variants in *E.coli* T7 shuffle express
- V-bottom PS-MTP
- Preculture (TB medium, 150 μL, 37°C, 900 rpm, 16 h)
- Cultivation (TB medium, 150 μL, 30°C, 900 rpm, 16 h)

Cells are lysed by lysozyme and 100 μL clear supernatant is transferred

Step2: Conjugation of CueO-LPETGGGRR variants and GGG-eGFP-LCI ligated by Sa-SrtA$_{\Delta59}$ WT
- F-bottom PS-MTP
- **100 μL CueO-LPETGGGRR variant lysate**
- **50 μg/mL Sa-SrtA$_{\Delta59}$ WT**
- 100 μg/mL GGG-eGFP-LCI
- Ligation (200 μL, 800 rpm, 3 h, RT, Tris-HCl pH 7.5)

50 μL reacted solution is transferred to PP-MTP

Step3: Anchoring of generated CueO (variant)-LPETGGG-eGFP-LCI in PP-MTP
- **F-bottom PP-MTP**
- 50 μL reacted solution from *Step2*
- 50 μL 800 μg/mL BSA
- Anchoring (100 μL, 600 rpm, 10 min, RT, Tris-HCl pH 7.5)

Liquid is decanted and unbound proteins are removed

Step4: Washing of PP-MTP
- **F-bottom PP-MTP**
- 2 times washing
- Washing (200 μL, 600 rpm, 5 min, RT, Tris-HCl pH 7.5)

Liquid is decanted and ABTS is supplemented

Step5: Activity determination of immobilized CueO (variant)-LPETGGG-eGFP-LCI via **ABTS**
- **F-bottom PP-MTP**
- ABTS assay (160 μL,15 min, RT, sodium citrate, pH 3.0)
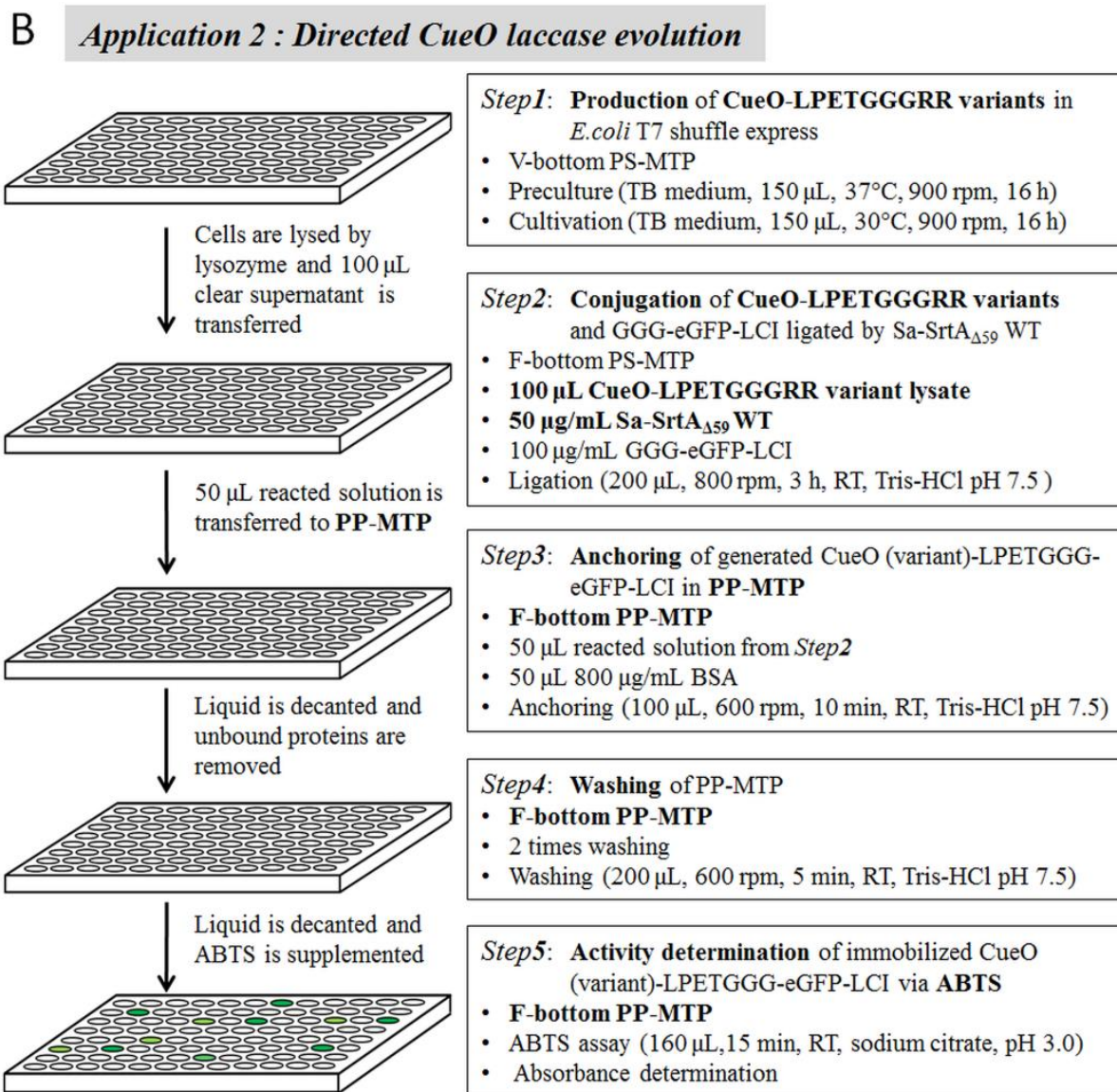- Absorbance determination

Figure 26. Schemes of the directed Sa-SrtA evolution (Application 1) and directed CueO-LPETGGGRR laccase evolution (Application 2) in two Five-Step protocols. **A**: Scheme of the directed Sa-SrtA evolution (Application 1). **B**: Scheme of the directed CueO laccase evolution (Application 2).

2.5.7. Characterization of evolved Sa-SrtA variants

Characterization of Sa-SrtA WT and variants were implemented via a HPLC assay as previously described.[60] Assays were performed in buffer A with 9mM NH$_2$-Gly-Gly-Gly-COOH and 5% DMSO (buffer A: 5 mM CaCl2, 150 mM NaCl, 50mM Tris-HCl buffer pH 7.5). Concentration of Abz-LPETG-Dnp-NH$_2$ ranged from 0.25 to 6 mM and Sa-SrtA concentration fixed at 500 nM (9.45 μg/mL). Reactions (50 μL) were initiated by adding of enzymes and incubated in room temperature for 5 to 15 min before quenching with 25 μL 1 M HCl. Five μL quenched samples were injected into the reversed-phase C18 HPLC column (4.6x150 mM, 5 μM (Macherey-Nagel, Düren, Germany). A gradient of 10 to 40% acetonitrile/0.1% TFA (0 to 7 min) and constant 40% acetonitrile/0.1% TFA (7 to 20 min) was used as

the chromatograph condition. Retention times for Abz-LPETG-Dnp-NH$_2$, GK-Dnp-NH$_2$ and Abz-LPETGGG-COOH were 15.2, 13.2 and 11.1 min, respectively. Absorbance of Dnp containing peaks were detected at 355 nM and Abz containing peaks were detected at 255 nM (220 nM was not used as the interference peak from DMSO). The yield of product Abz-LPETGGG-COOH was calculated by integrating the area under HPLC trace. To obtain the kinetics, calculated reaction rates were fit to the Michaelis-Menten equation using software Originpro 8.6.

2.5.8. Characterization of evolved CueO-LPETGGGRR variants

Characterization of CueO-LPETGGGRR WT and variants was performed by using an ABTS based assay. CueO-LPETGGGRR WT and selected variants were expressed and purified as mentioned above. After purification, 10 μM (559 μg/mL) purified proteins were incubated with 1 mM CuSO$_4$ for overnight. ABTS assays were performed in sodium acetate buffer (0.1M, pH 5.5) in 96-well polystyrene MTP with 200 μL volume of solution. Concentration of ABTS ranged from 0.05 to 15 mM and enzyme concentration fixed at 5 nM (280 ng/mL). Plates were stirred briefly and the absorbance changes of ABTS was constantly measured by Tecan Infinite M1000 PRO plate reader (420 nm ($\varepsilon_{ABTS\cdot+} = 36{,}000$ M^{-1}cm^{-1}), room temperature). Kinetic was determined by fitting the calculated reaction rates to the Michaelis-Menten equation using software Originpro 8.6.

3. Chapter III: Directed sortase A evolution for efficient site-specific bioconjugations in organic co-solvents

3.1. Declaration

Parts of this chapter have been published in the journal ''chemical communications'' and are adapted to this thesis with the permission of Royal Chemical Society Copyright Clearance Center.

3.2. Site-specific bioconjugation: challenges and scientific importance

Bioconjugation enables modification of polypeptides with diverse functionalities.[93] Chemical approaches for the modification of polypeptides such as coupling of lysine (NH_2 group), cysteine (SH group), or tyrosine (OH) residues have been developed.[94-95] A main challenges remains for biocomjugation is to achieve a high specificity in which only desired positions on the surface protein can be modified in order to avoid inactivation.[96,97] Enzyme-mediated conjugations are versatile tools in protein bioconjugation due to their high site-specificity and mild reaction conditions.[98] In the last decade, sortase-mediated ligation (SML) are emerging as a powerful approach if selective functionalization of polymer building blocks or proteins are required.[35, 99]

Among the numerous applications of SML, a general problem is the poor water solubility of hydrophobic substrates. Organic solvents (e.g. DMSO, DMF) are commonly used to improve solubility of a broad variety of compounds.[39] However, the low conjugated efficiency and instability of enzyme in organic co-solvents limits the further applications of SML. Reengineering of Sa-SrtA for enhanced activity, Ca^{2+} independence, altered specificity in water conditions were discussed above. Protein engineering of Sa-SrtA with enhanced resistance or specific activity in organic co-solvents and understanding of influence of organic solvents on the structure and dynamics of Sa-SrtA or any other sortase class has not been reported yet.

In the current work, we performed a first directed Sa-SrtA evolution campaign towards DMSO co-solvent. Sa-SrtA variant with improved resistance or activity were identified. Structure-function relationships of Sa-SrtA and selected variants in water or in DMSO co-solvent were further investigated by computational analysis. Lastly, sortase-mediated ligation was expanded in organic solvents with hydrophobic compounds substrates.

3.3. Results and discussions

The work described here was done in four sections. In the first section, SortEvolve assay was optimized in DMSO co-solvent (3.3.1). In the second section, a directed Sa-SrtA evolution campaign (KnowVolution, 3.3.2) was performed in DMSO co-solvent using the optimized SortEvolve assay. In detail, KnowVolution of Sa-SrtA towards DMSO co-solvents includes: a) Optimization of SortEvolve system in DMSO co-solvent (3.3.2.1-3.3.2.4); b) Evolution of Sa-SrtA towards DMSO co-solvents (3.3.2.5-3.3.2.8); c) Characterization of identified Sa-SrtA variants (3.3.2.9); d) Activity measurements of Sa-SrtA in different organic co-solvents (3.3.2.10). In the third section, computational studies were performed. Molecular dynamic simulations of Sa-SrtAs (WT and selected variants) in DMSO co-solvent were carried out (3.3.3). The interactions between Sa-SrtA WT and water/DMSO (3.3.3.1), Sa-SrtA M1 and water/DMSO (3.3.3.2), Sa-SrtA M3 and water/DMSO (3.3.3.3) were individually investigated. In the last section, application of evolved Sa-SrtA variants was exploited to conjugate hydrophobic peptides in organic co-solvents (3.4.3) which including sortase-mediated peptide-peptide ligation in DMSO/DMF co-solvents (3.4.3.1) and peptide-amines ligation in DMSO co-solvent.

3.3.1. Optimization of SortEvolve in DMSO co-solvent

The developed SortEvolve screening system in Chapter II was optimized in DMSO co-solvent. Main experiments included: evaluating GGG-eGFP-LCI and CueO-LPETGGGRR stabilities in DMSO co-solvent, optimizing the DMSO concentration in SortEvole assay, determining the coefficient of variations of SorEvolve assay in DMSO co-solvent.

3.3.1.1. GGG-eGFP-LCI stability in DMSO co-solvent

Stability of GGG-eGFP-LCI in different concentrations of DMSO co-solvent was studied. We assumed that the structure stability GGG-eGFP-LCI relates to its fluorescence. The residual fluorescence of GGG-eGFP-LCI in gradient DMSO concentrations is given in **Figure 27a**. GGG-eGFP-LCI was structural stable (retained full fluorescence) when incubated in 60% (v/v) or lower concentration of DMSO. GGG-eGFP-LCI is denatured (fluorescence is completely demolished) when 70% (v/v) or higher concentration of DMSO is employed.

3.3.1.2. CueO-LPETGGGRR stability in DMSO co-solvent

Stability of CueO-LPETGGGRR in different concentrations of DMSO co-solvent was studied. CueO was incubated in different concentrations of DMSO co-solvent. After incubation, activity of CueO-LPETGGGRR was monitored via ABTS assay. As the data shown in **Figure 27b**, CueO-LPETGGGRR was stable (retained full activity) when incubated in 60% (v/v) or lower concentration of DMSO. CueO-

LPETGGGRR was denatured (activity is completely demolished) when 70% (v/v) or higher concentration of DMSO is used.
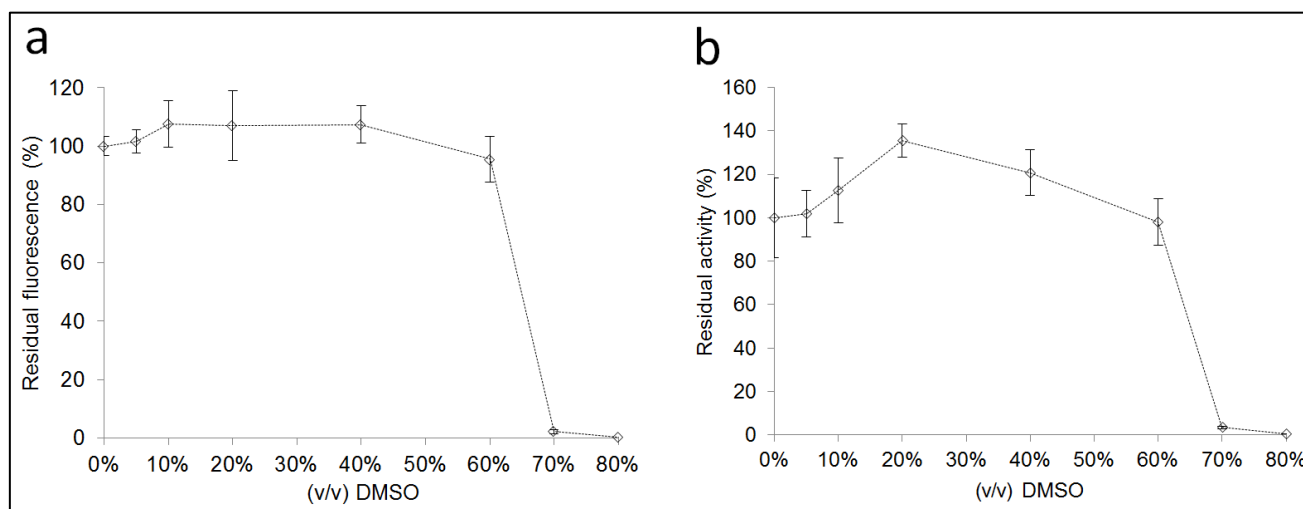

Figure 27. Stability of protein substrates in DMSO co-solvent. a) Stability of GGG-eGFP-LCI in gradient concentration of DMSO. Fluorescence was recorded after incubation in DMSO co-solvent. Residual activity was calculated as the ratio (percentage) of detected fluorescence divided the fluorescence in absence of DMSO. b) Stability of CueO-LPETGGGRR in gradient concentration of DMSO. Activity of CueO-LPETGGGRR (ABTS was used as substrate) was measured after incubation in DMSO co-solvent. Residual activity was calculated as the ratio (percentage) of measured activity divided the activity in absence of DMSO.

3.3.1.3. Optimization of DMSO concentration in the SortEvolve screening assay

Sortase-mediated conjugation of GGG-eGFP-LCI and CueO-LPETGGGRR was performed in different concentration of DMSO. After reaction, the generated conjugate was bound to the PP-MTP and amount of bound protein was evaluated by ABTS assay. Activities in SortEvolve decreased when 35% (v/v) or higher DMSO concentrations were used (see **Figure 28a**). No visible activity was detected when 55% (v/v) or higher concentrations of DMSO was employed. Finally, the concentration of 45% (v/v) DMSO was selected as screening pressure for the SortEvolve assay to improve the specific activity and resistance of Sa-SrtA towards DMSO (~40% residual activity).

3.3.1.4. Coefficient of variation of SortEvolve assay in 45% (v/v) DMSO co-solvent

Coefficient of variations (CV) of SortEvolve assay was determined. One 96-well MTP contains 84 Sa-SrtA WT clonies (in order to gain information on background, six wells contained an "empty vector" control and six wells contained the TB-expression media) was screened by SortEvolve assay according to screening protocols which decribed in 3.5.2.4. **Figure 28b** shows the determined activities in descending order. True coefficients of variations of SortEvolve in absence and in presence of 45% (v/v) DMSO are 12.9% and 14.5%, respectively. Screening systems with standard deviations below 15 % are routinely applied in directed evolution campaigns.[74-75]
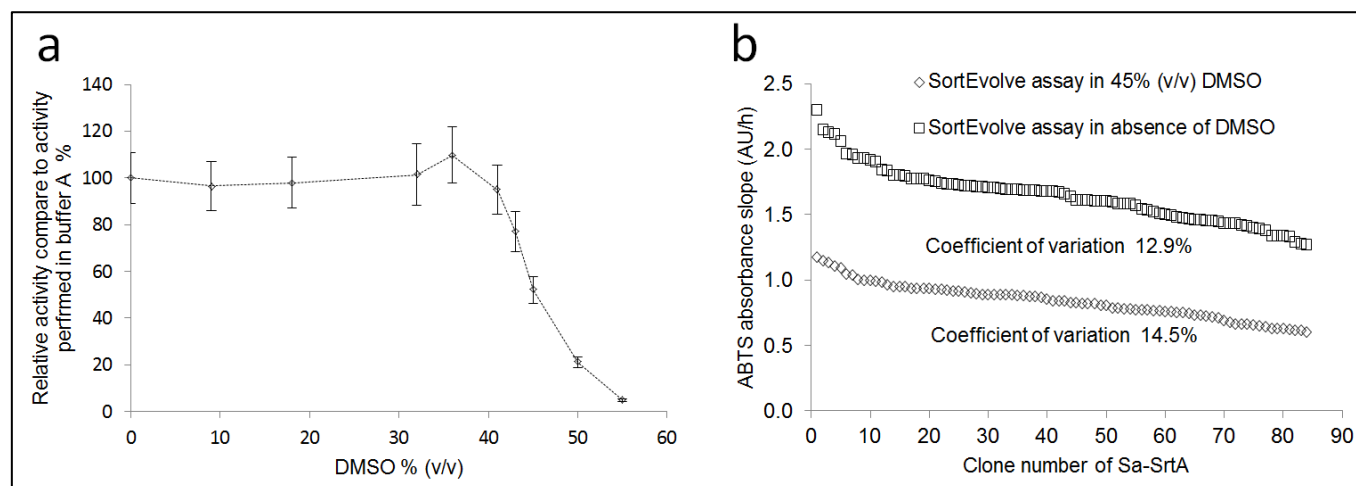
56

Figure 28. Optimization of DMSO concentration in SortEvolve assay. a) Residual activity of SortEvolve assay performed in gradient concentration of DMSO (a control using pET-28a empty vector lysate instead of Sa-SrtA WT lysate was substrate in all cases, see detail in 3.5.2.3); b) Coefficient of variations of SortEvolve assay in absence and in presence 45% (v/v) DMSO.

3.3.2 KnowVolution of Sa-SrtA for DMSO co-solvent

3.3.2.1. Diversity generation of Sa-SrtA library

A sequence saturation mutagenesis (SeSaM) library of Sa-SrtA lacking the N-terminal 59 residues (PDB code: 2KID) was generated to achieve a high chemical diversity. Templates for individual steps were generated (**Figure. 29a**). Phosphorothioate deoxynucleotides (dATPαS and dGTPαS) concentrations were used: A-forward library-35% (**Figure. 29b**), A-reverse library-35% (Figure. 29c), G-forward library-40% (**Figure. 29d**), and G-reverse library-40% (**Figure. 29e**). The final Sa-SrtA-SeSaM library was generated using 200 ng PCR products of each library (**Figure. 29f**) and cloned into pET28a(+) vector via phosphorothioate-based ligase-independent gene cloning (PLICing).[86]

The PLICing product of Sa-SrtA-SeSaM was transformed into chemically competent E. coli BL21 Gold (DE3). Colonies (on agar plate after transformation) from the generated SeSaM library were randomly selected for sequencing (**Figure 30**). Four Sa-SrtA wide-types were found among 13 selected colonies. Eleven mutations were found in nine variants. Transition and transversion frequency of mutations were calculated as 55% and 45%, respectively. The transversion frequency in typical epPCR libraries was reported as around 25%.[100] A 1.8-fold enrichment in transversion frequency was observed in SeSaM libraries when compared to epPCR libraries.
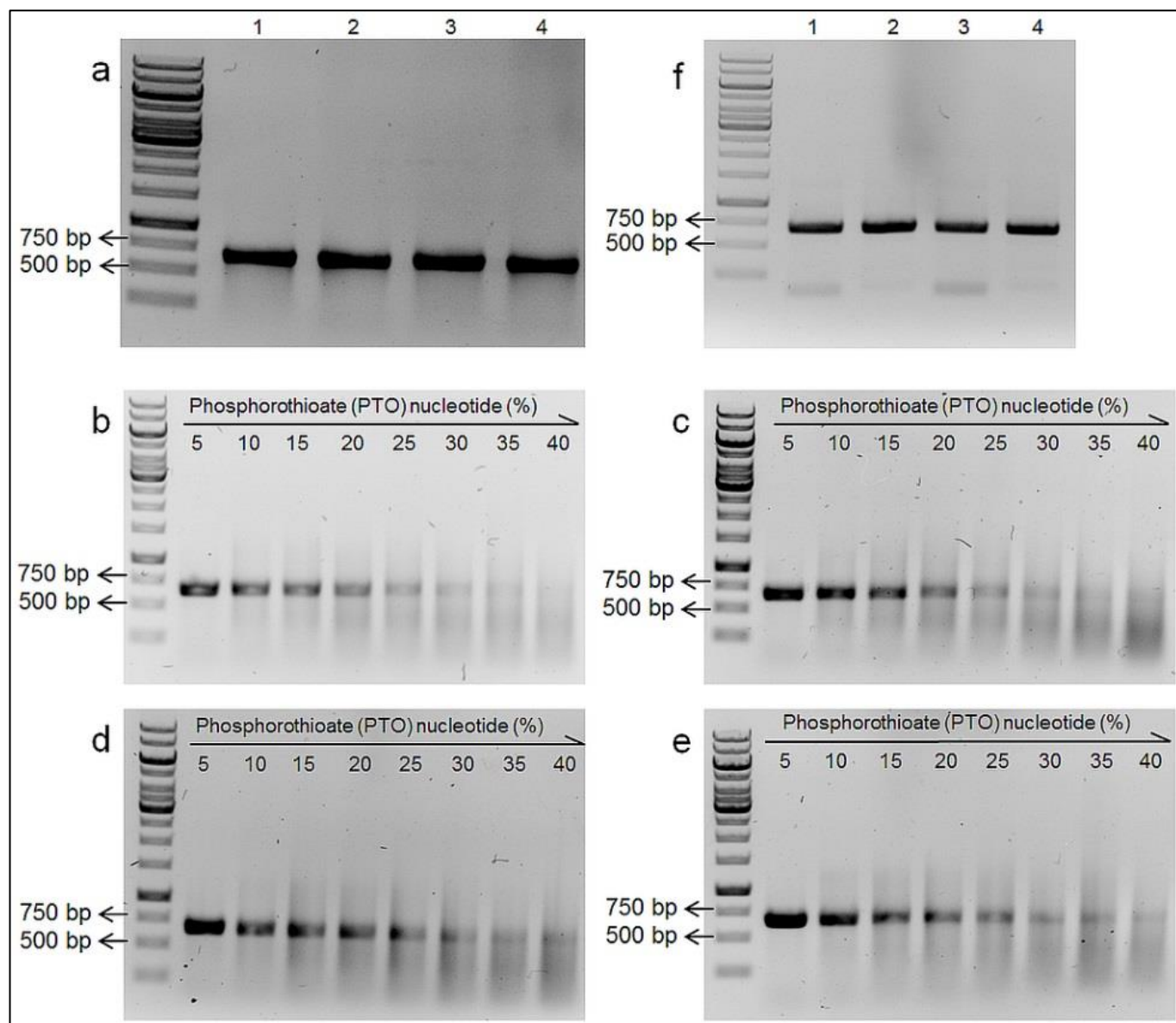
Figure 29. Agarose gel electrophoretic analysis of SeSaM steps during construction of Sa-SrtA library. Steps were performed as described.[101] a) Preliminary step 1: amplification PCR to generate template for step 1 and step 3 (expected band size: 0.55 kb). 1: Step 1 forward library template, 2: Step 1 reverse library template, 3: Step 3 forward library template, 4: Step 3 reverse library template. b) – e) Optimization of phosphorothioate deoxynucleotides percentage using gradient concentrations of dATPαS or dGTPαS for A-forward library (b), A-reverse library (c), G-forward library (d), G-reverse library (e). f) Final A and G libraries.
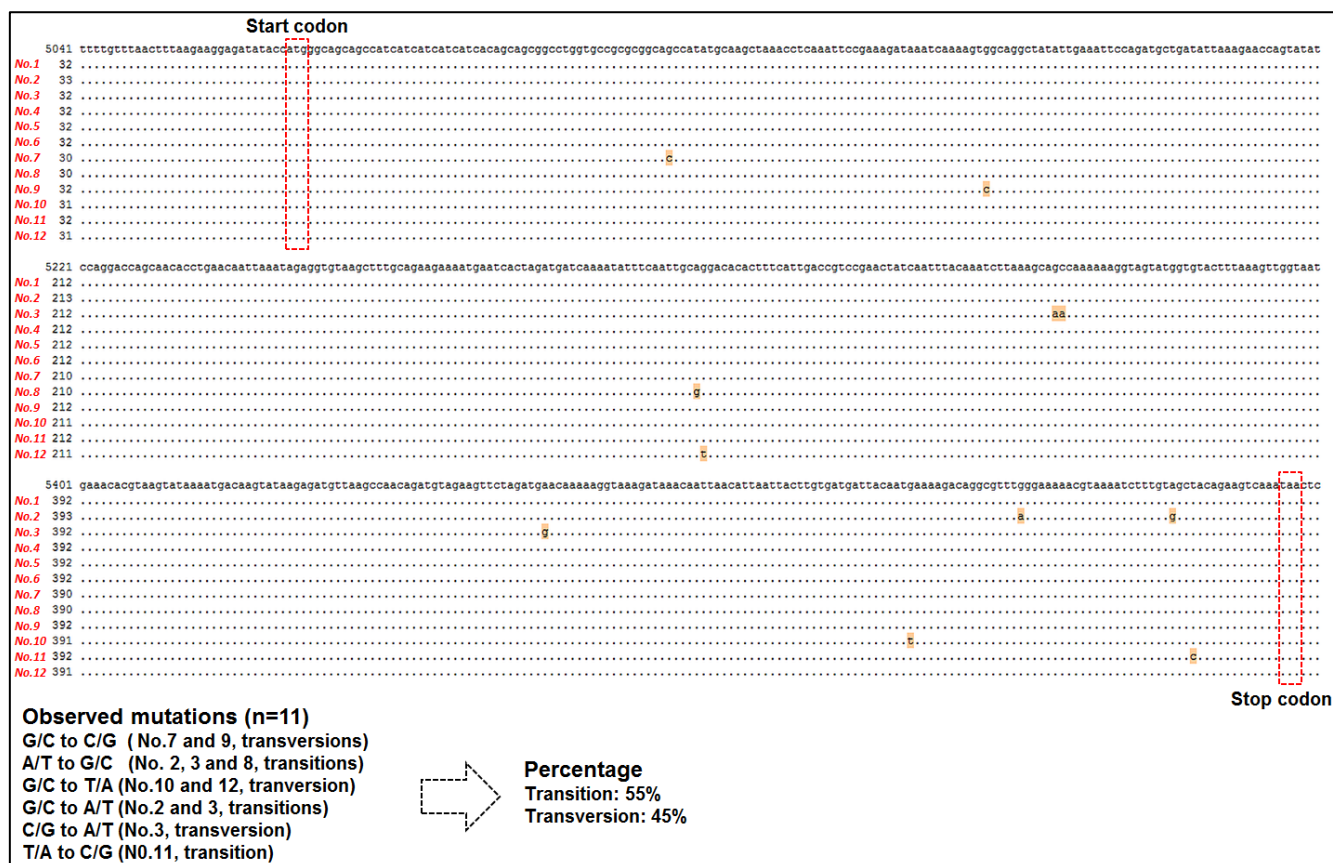
Figure 30. Sequencing results analysis of randomly selected colonies in Sa-SrtA SeSaM library.

3.3.2.2. KnowVolution Phase I: Screening of SeSaM library in DMSO co-solvent

The generated library (1680 colonies) was transferred in 96-well polystyrene microtiter plates (V-bottom, one clone per well). Each plate contained six wells with negative control (cells containing empty vector pET-28 instead of Sa-SrtA). For the library screening in DMSO co-solvent, each plate was screened with the optimized SortEvolve protocols (**3.5.3.2**). The activity values from negative controls were averaged as the background and subtracted in all cases. Variants with 1.16-fold or higher improved activity (compared to Sa-SrtA WT) were selected for subsequent rescreening. Rescreening results of the SeSaM library variants (variants which showed 1.2-fold or higher activity in DMSO co-solvents in comparison to Sa-SrtA WT) are showed **Figure 31**. Plasmids of the twelve colonies were obtained and subsequently sequenced.
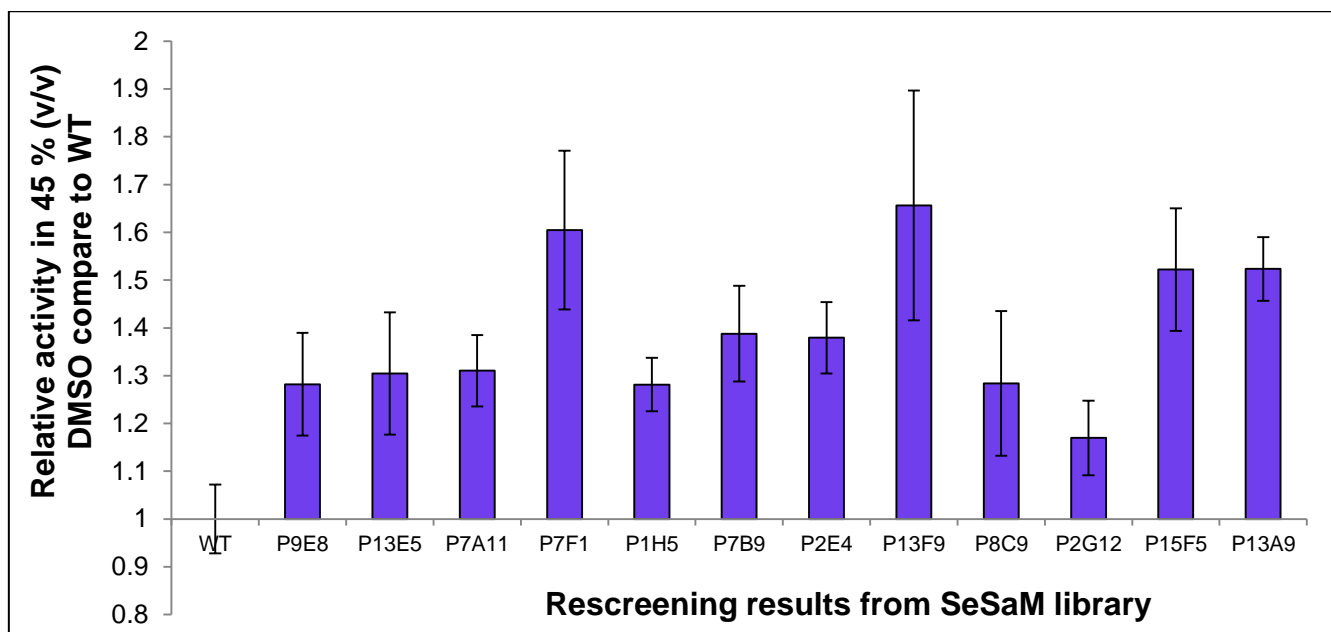
Figure 31. Re-screening results from random mutagenesis SeSaM library in 45% (v/v) DMSO co-solvent. Data is shown by ratios of Sa-SrtA variant activity (background subtracted) divided Sa-SrtA WT activity (background subtracted). Twelve variants which showed 1.2-fold or higher activity in DMSO co-solvents in comparison to Sa-SrtA WT were selected.

3.3.2.3. KnowVolution Phase II: generation and screening of site-saturation mutagenesis

The sequencing results of identified variants in *KnowVolution Phase I* reveal that most of the identified positions are in a close proximity of Sa-SrtA LPxTG substrates binding pocket (e.g P94H (P7F1), R159G (P13F9), A61D/D160N (P9E8), and D165S (P2E4)), calcium binding region (e.g. K84R/D170G (P7A11) and Q172R (P2G12)) or the active sites C184 (e.g. D186N (P15F5)), R197 (e.g. R159G (P13F9) and K196E (P13A9) (**Figure 32**).
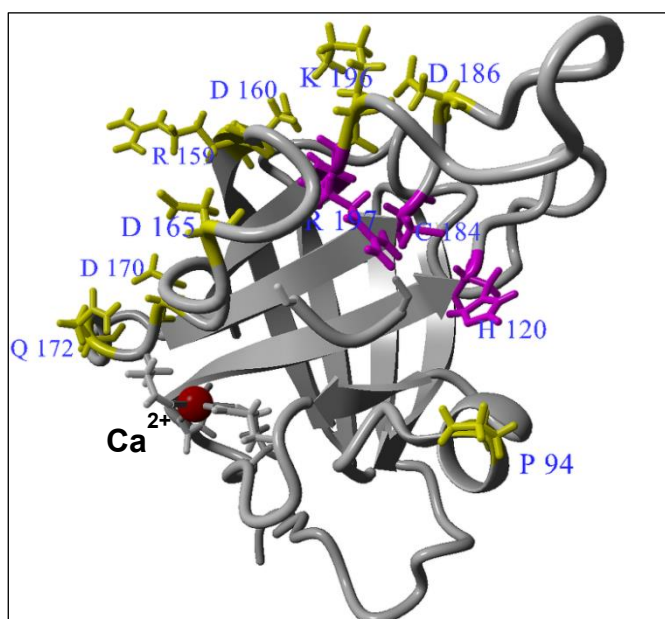
Figure 32. Visualization of the identified positions in structure of Sa-SrtA (PDB 2KID), identified positions (yellow), active sites (magenta) and calcium ion (red) are shown.

Figure 33. Rescreening results from single-site SSM libraries both in absence and in 45% (v/v) DMSO co-solvent. Relative activities are shown by ratio of Sa-SrtA variant activities (background subtracted) divided Sa-SrtA WT activity (background subtracted). Residual activity in 45% (v/v) DMSO is shown by ratio of activity in 45% (v/v) DMSO divided activity in absence of DMSO.

Table 9 Sequencing results of identified variants in Sa-SrtA SSM libraries.

Library	Number in MTP	Substitution (DNA codon)	Substitution (amino acid)
SSM P94	P1F1	CCT/CAT	Pro94His (P94H)
	P1F7	CCT/ACT	Pro94Thr (P94T)
	P1B2	CCT/ACT	Pro94Thr (P94T)
SSM R159	P1F1	AGA/GGG	Arg159Gly (R159G)
	P2B10	AGA/ACT	Arg159Gly (R159T)
	P2E12	AGA/ACG	Arg159Gly (R159T)
SSM D160	P1D9	GAT/AAT	Asp160Asn (D160N)
	P1E10	GAT/AAT	Asp160Asn (D160N)
	P1E11	GAT/AAT	Asp160Asn (D160N)
SSM D165	P1B10	GAT/CAG	Asp165Gln (D165Q)
	P1C11	GAT/CAG	Asp165Gln (D165Q)
	P1H7	GAT/GCG	Asp165Ala (D165A)
SSM D170	P1B8	GAT/TGG	Asp170Trp (D170W)
	P2D5	GAT/TGG	Asp170Trp (D170W)
	P2F3	GAT/GAT	Wild-type
SSM Q172	P2C6	CAA/CAA	Wild-type
	P2E2	CAA/TGG	Gln172Trp (Q172W)
	P2H1	CAA/CTA	Gln172Leu (Q172L)
SSM D186	P1C11	GAT/GGG	Asp186Gly (D186G)
	P1E8	GAT/GGT	Asp186Gly (D186G)
	P2A7	GAT/GGG	Asp186Gly (D186G)

SSM K196	P1C1	AAA/GTG	Lys196Val (K196V)
	P1D9	AAA/GTG	Lys196Val (K196V)
	P2F12	AAA/GTG	Lys196Val (K196V)

Eight site saturation mutagenesis libraries at positions 94, 159, 160,165, 170, 172, 186, and 196 were generated. One hundred and sixty-eight clones of each SSM library were screened with the optimized SortEvolve protocols (**see 3.5.3.2**) in absence and in presence of 45% (v/v) DMSO individually. Rescreening results of the identified variants from all single-site SSM libraries are summarized in **Figure 33**. Sequencing results of the identified variants are summarized in **Table 9**. A general trend was observed that the four most active Sa-SrtA variants (R159T, D165Q, D170W, and D186G) in 45% (v/v) DMSO are not the most resistant ones (**Figure 33**). D186G showed the highest activity (2.3-fold) and R159G (M1) presented the highest resistance (2.2-fold) in 45% DMSO. In summary, seven positions (94, 159, 160, 165, 170, 186, and 196) that improved activity and two positions (159 and 172) that improved DMSO resistance were identified.

3.3.2.4. KnowVolution Phase IV: recombination

Structural analysis of the identified SSM substitutions was performed based on the obtained results in single-site SSM screening (3.4.1.7). The two substitutions D186G and K196V are not only in close proximity to each other, but also in close proximity to the active sites cysteine 184 and arginine 197. In order to maximize activity in 45% (v/v) DMSO, a simultaneous SSM library (SSM-D186/K196) was generated and 504 colonies were screened with the optimized SortEvolve protocols. After screening, eight variants were selected for further rescreening. Three variants with 2.5-fold or higher specific activities (compared to Sa-SrtA WT) in 45% (v/v) DMSO were identified in rescreening. Results are given in **Figure 34**. Interestingly, the substitution of D186G was found in all selected variants (D186G/K196Y, D186G/K196L, and D186G/K196V (M2)) and substitution in position 196 is more likely to be hydrophobic amino acid residue (K196Y, K196L or K196V). The variant D186G/K196V (M2) showed the best specific activity (3.5-fold compared to Sa-SrtA) and DMSO resistance (highest residual activity in 45% (v/v) DMSO) among the three variants and was selected as starting variant for further recombination.
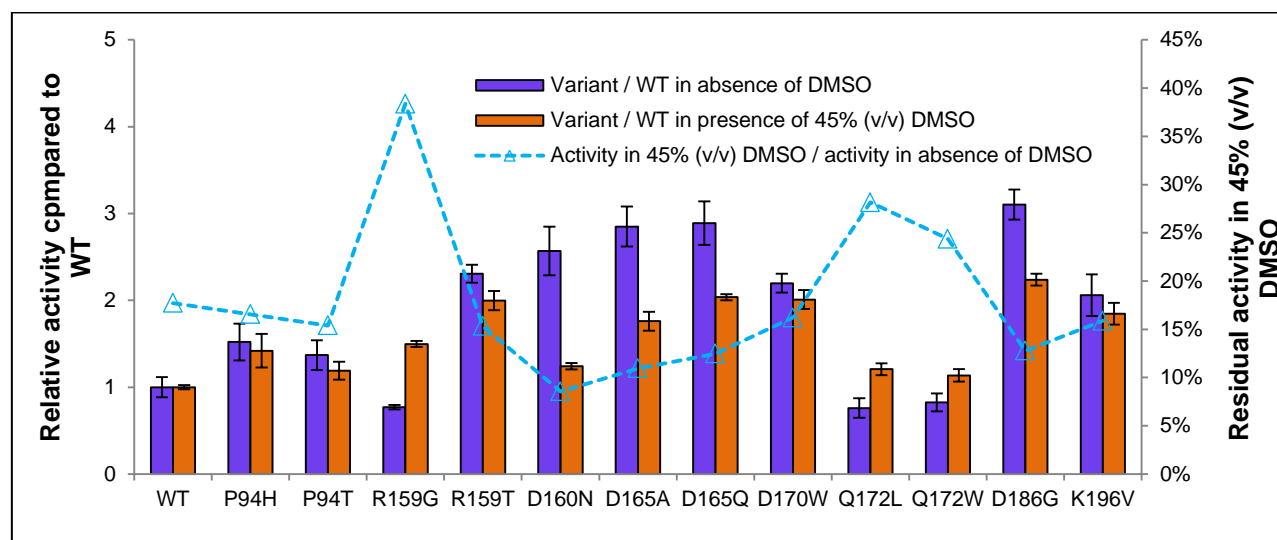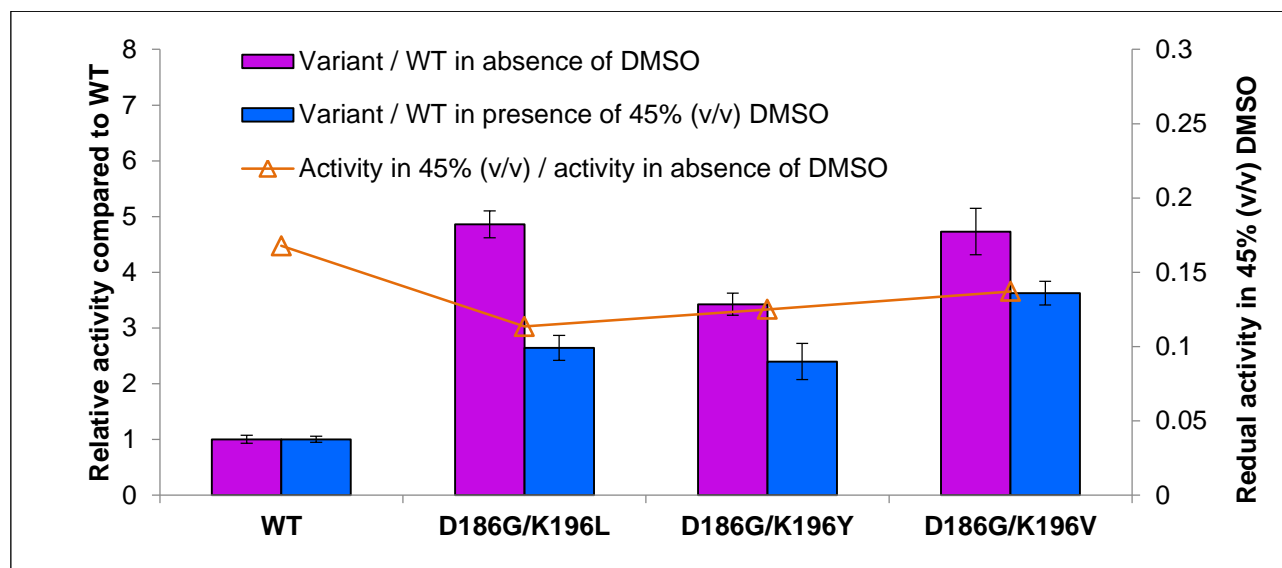
Figure 34. Rescreening results from D186/K196 simultaneous SSM library in absence and in 45% (v/v) DMSO co-solvent. Relative activities are shown by ratio of Sa-SrtA variant activities (background subtracted) divided Sa-SrtA WT activity (background subtracted). Residual activity in 45% (v/v) DMSO is shown by ratio of activity in 45% (v/v) DMSO divided activity in absence of DMSO.

The identified substitutions R159G, R159T, D165A, D165Q, and D170W in 3.4.1.8 were individually incorporated into variant M2 (D186G/K196V) by site-directed mutagenesis (SDM). Moreover, a reported variant P94S/D160N/D165A/K196T (rM4) showing a 140-fold activity[60] compared to Sa-SrtA WT was generated and used as the reference. Variants were individually expressed in flask and purified using the protocols as described (2.5.2.). Samples were analyzed by SDS-PAGE and results were showed in **Figure 35**.
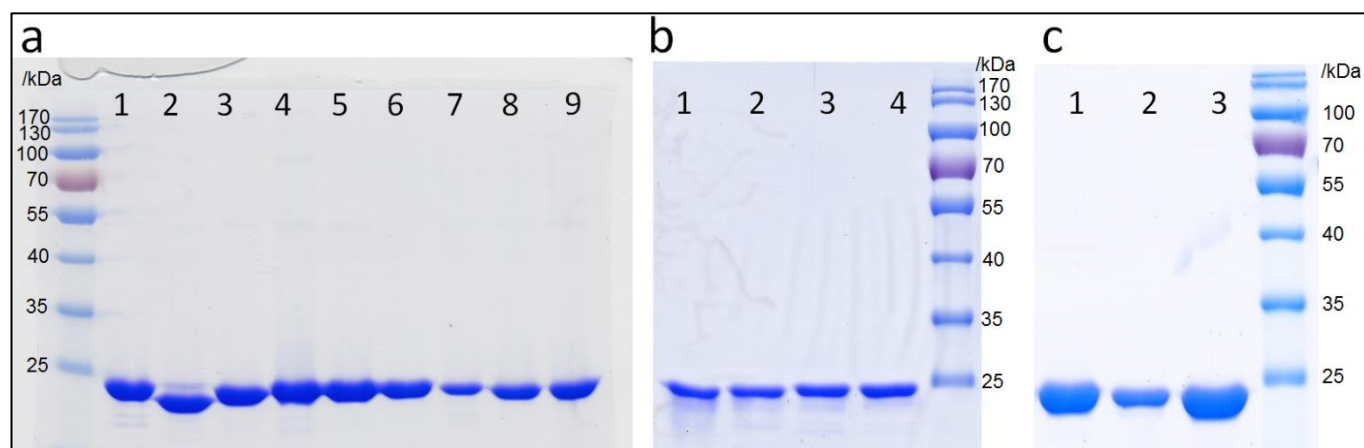
Figure 35. SDS-PAGE of purified Sa-SrtAs: a) Purified Sa-SrtA WT and recombined variants, Sa-SrtA WT (line 1), Sa-SrtA D186G/K196V (line 2), Sa-SrtA P94H/D186G/K196V (line 3), Sa-SrtA R159G/D186G/K196V (line 4) Sa-SrtA R159T/D186G/K196V (line 5) Sa-SrtA D165A/D186G/K196V (line 6) Sa-SrtA D165Q/D186G/K196V (line 7) Sa-SrtA D170W/D186G/K196V (line 8), and Sa-SrtA P94S/D160N/D165A/K196T (line 9)); b) Purified single site variants identified in *KnowVolution Phase II,* Sa-SrtA R159G (line 1) Sa-SrtA R159T (line 2) Sa-SrtA D170W (line 3) and Sa-SrtA Q172L (line

# Chapter III: Directed sortase A evolution for efficient site-specific bioconjugations in organic co-solvents

4); c) Purified Sa-SrtA WT and single site variants identified in *KnowVolution Phase II,* Sa-SrtA K196V (line 1) Sa-SrtA D186G (line 2), and Sa-SrtA WT (line 3).

Activity of the purified Sa-SrtAs (WT and variants) in absence and presence DMSO co-solvent were monitored using a fluorescence resonance energy transfer (FRET) assay as aforementioned.[102] The specific activities of Sa-SrtAs were obtained. Relative activities of variants in respect to Sa-SrtA WT and resistance towards DMSO were calculated. Data was summarized and shown in **Table 10**. All selected variants represented improved activities in 45% (v/v) DMSO when compared with Sa-SrtA WT. Especially, three variants R159G, D170W and Q172L showed improved resistance in comparison with WT, this data is in well agreement with the data obtained in SortEvolve (**Figure 33**). All the recombined variants (based on M2) showed improved (2-fold or higher) activities but reduced resistance in in 45% (v/v) DMSO when compared to Sa-SrtA WT. Variant R159G/D186G/K196V (Sa-SrtA M5) showed increased resistance (1.9-fold) but decreased activity when compared with Sa-SrtA M2. This finding indicates the substitution of R159G plays a crucial role for improving the resistance but leads to reduced activity of Sa-SrtA. Impressively, variant D165Q/D186G/K196V (Sa-SrtA M3) showed a 5.5-fold improved activity in 45% (v/v) DMSO and a 17-fold increased specific activity in absence of DMSO when compared to Sa-SrtA WT. As a comparison, the Sa-SrtA variant P94S/D160N/D165A/K196T (Sa-SrtA rM4) showed a 79.5-fold increased activity in absence DMSO and a 1.84-fold improved activity in 45% (v/v) DMSO, when compared to Sa-SrtA WT. The latter demonstrates that the developed co-solvent resistant screening system based on the SortEvolve protocol (reference) selects Sa-SrtA variants with improved co-solvent resistance.

Table 10. Activity of Sa-SrtA variants in absence and presence of DMSO using FRET assay.[102] Reactions (100 μL, 0.05 mM Abz-LPETGK-Dnp, 5 mM glycine-glycine-glycine (tri-glycine) in buffer A (buffer A: 5 mM CaCl2, 150 mM NaCl, 50 mM Tris-HCl, pH 7.5)) were initiated by adding 1.5 μM Sa-SrtA (WT or variants). The variants selected for further characterization are marked in red**.

Sa-SrtA WT/variants	Specific activity in absence of DMSO (slope/s)	Relative activity in absence of DMSO (variant/WT)[a]	Specific activity in 45% (v/v) DMSO (slope/s)	Relative activity in 45% (v/v) DMSO (variant /WT)[b]	Resistance (%) in 45% (v/v) DMSO[c]
WT	3.34±0.08	1.00	0.55±0.06	1.00	16.39
M1 (R159G)	2.15±0.03	0.64	0.83±0.04	1.52	38.6
R159T	7.23±0.17	2.16	1.11±0.11	2.02	15.35
D170W	6.88±0.11	2.06	1.16±0.03	2.10	16.86
Q172L	2.80±0.22	0.84	0.67±0.07	1.22	23.93
D186G	10.36±0.48	3.10	1.23±0.09	2.24	11.87
K196V	6.46±0.24	1.90	1.02±0.13	1.85	16.1

M2 (D186G/K196V)	19.31±0.48	5.78	1.66±0.09	3.02	8.61
M4 (P94H/D186G/K196V)	18.72±0.57	5.60	1.47±0.11	2.68	7.85
M5 (R159G/D186G/K196V)	7.76±0.54	2.33	1.21±0.12	2.22	15.62
M6 (R159T/D186G/K196V)	31.32±0.68	9.38	1.68±0.14	3.07	5.42
M7 (D165A/D186G/K196V)	59.72±1.39	17.80	2.53±0.12	4.63	4.23
M3 (D165Q/D186G/K196V)	56.76±1.32	17.01	2.99±0.13	5.46	5.26
M8 (D170W/D186G/K196V)	15.88±0.27	4.76	1.13±0.07	2.06	7.10
rM4 (P94S/D160N/D165A/K196T)	265.39±3.27	79.46	1.01±0.04	1.84	0.37

[a] Relative activity was calculated the ratio of specific activity of Sa-SrtA variants in absence of DMSO divided specific activity of Sa-SrtA WT in absence of DMSO

[b] Relative activity was calculated the ratio of specific activity of Sa-SrtA variants in 45% (v/v) DMSO divided specific activity of Sa-SrtA WT in 45% (v/v) DMSO

[c] Resistance in 45% (v/v) DMSO was calculated as the ratio (percentage) of specific activity in 45% (v/v) DMSO divided specific activity in absence of DMSO.

3.3.2.5. Characterization of Sa-SrtA variants in water and DMSO co-solvent

Characterizations of Sa-SrtA M1, M3, and rM4 in absence and presence of 45% (v/v) DMSO were performed by using an HPLC analytics with previously described.[76, 102] Details of protocol are described in 3.5.5. Plots of Sa-SrtA turnovers in respect to Abz-LPETGK-Dnp substrates concentration were generated **(Figure 36).** Kinetics of Sa-SrtAs in absence and presence of 45% (v/v) DMSO are listed in **Table 11**. k_{cat} value of Sa-SrtA M1 is slightly lower (94%) in absence of DMSO and 2.2-fold higher in 45% (v/v) DMSO when compared to Sa-SrtA WT. The catalytic efficiency of Sa-SrtA M1 (k_{cat}/K_m) was decreased (0.6-fold) in absence of DMSO but increased (2.1-fold) in 45% (v/v) DMSO. Sa-SrtA M3 showed an impressive 4.8-fold and 3.8-fold higher k_{cat} in absence and presence of 45% (v/v) DMSO when compared with WT, respectively. Sa-SrtA M3 gained 11.6- and 6.3-fold catalytic efficiency in in absence and presence of 45% (v/v) DMSO in when compared with WT, respectively. The k_{cat} value of Sa-SrtA rM4 in absence of DMSO is reproduced as previously studies[60, 68] A notable 30-fold reduction of k_{cat} was observed for rM4 in 45% (v/v) DMSO in compassion to water.

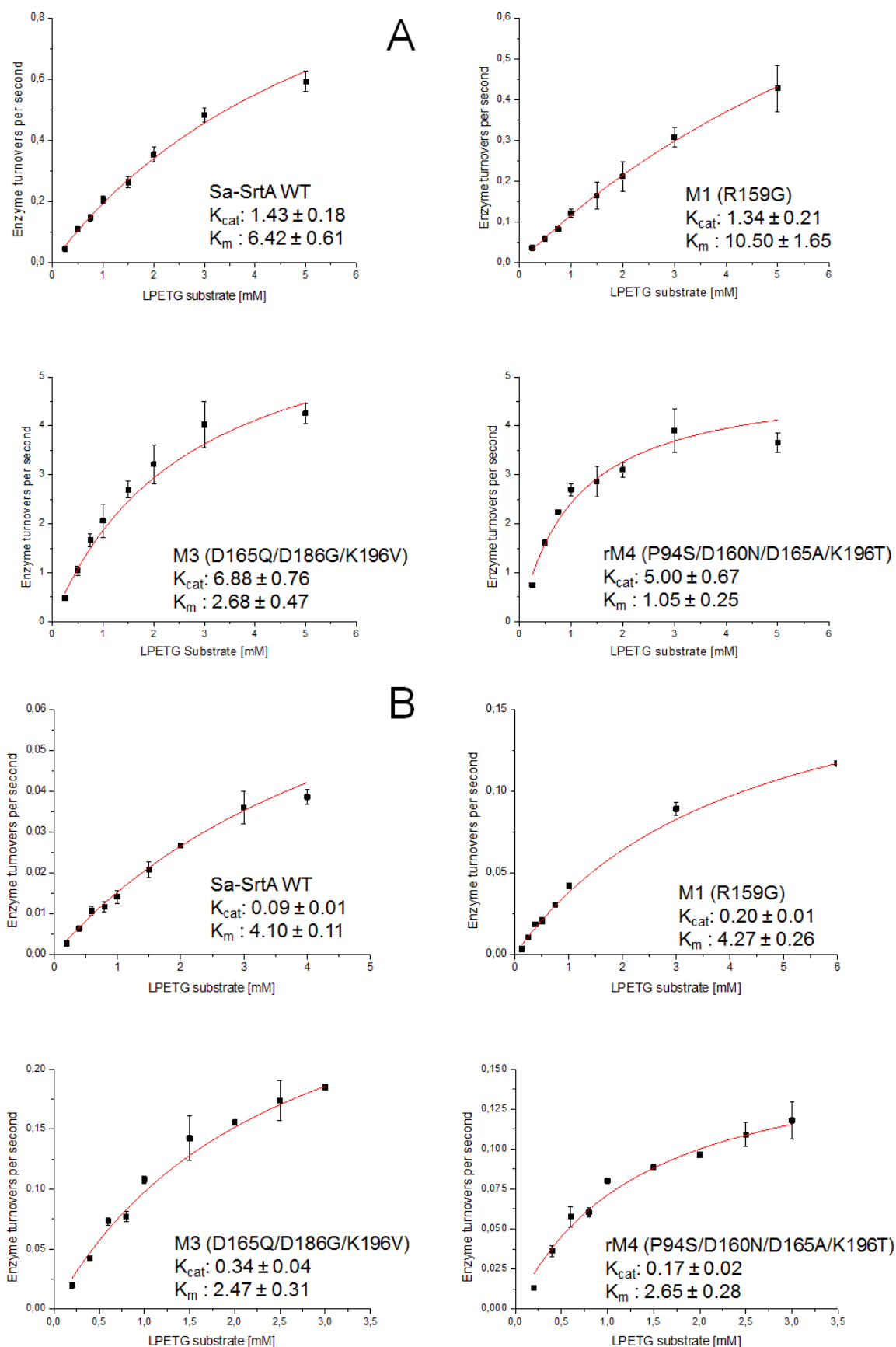**Figure 36.** plots to determine $K_{m\,(LPETG)}$ and k_{cat} of Sa-SrtAs in absence (A) and in presence of 45% (v/v) DMSO (B).

Table 11. Kinetics of Sa-SrtAs in transpeptidation of Abz-LPETGK-Dnp and tri-glycine in absence and presence of 45% (v/v) DMSO.

Sa-SrtA	k_{cat} in absence of DMSO (s^{-1})	k_{cat} in 45% (v/v) DMSO (s^{-1})	$K_{m(LPETG)}$ in absence of (mM)	$K_{m(LPETG)}$ in 45% (v/v) DMSO (mM)	$k_{cat}/K_{m(LPETG)}$ in absence of $(s^{-1} \cdot mM^{-1})$	$k_{cat}/K_{m(LPETG)}$ in 45% (v/v) DMSO $(s^{-1} \cdot mM^{-1})$
WT	1.43±0.18	0.09±0.01	6.42±0.61	4.10±0.11	0.22	0.022
M1 (R159G)	1.34±0.21	0.20±0.01	10.50±1.65	4.27±0.26	0.13	0.047
M3 (D165Q/D186G/K196V)	6.88±0.76	0.34±0.04	2.68±0.47	2.47±0.31	2.56	0.138
rM4 (P94S/D160N/D165Q/K196T)	5.00±0.67	0.17±0.02	1.05±0.25	2.65±0.28	4.76	0.064

3.3.2.6. Circular dichroism spectrum of Sa-SrtA variants

Circular dichroism spectrums (CD-spectrum) of Sa-SrtAs in buffer A were recorded (**Figure 37).** Spectra of Sa-SrtA WT showed as a typical β-sheet structure which in well agreement with the previous study.[27] CD-spectrums of variants M3 and rM4 represented similar as WT, indicate there is not significant changes in the secondary structure of these two variants. Interestingly, CD spectrum of M1 showed a remarkable difference of absorbance at 202 nm. The changes might be cause by the introducing of new α helix in the β6/β7 loop and improves the solvent resistance of M1. CD-spectrum of Sa-SrtA in 45% (v/v) DMSO was unable to record since signal of protein sample was strongly interfered by DMSO (data is not shown).
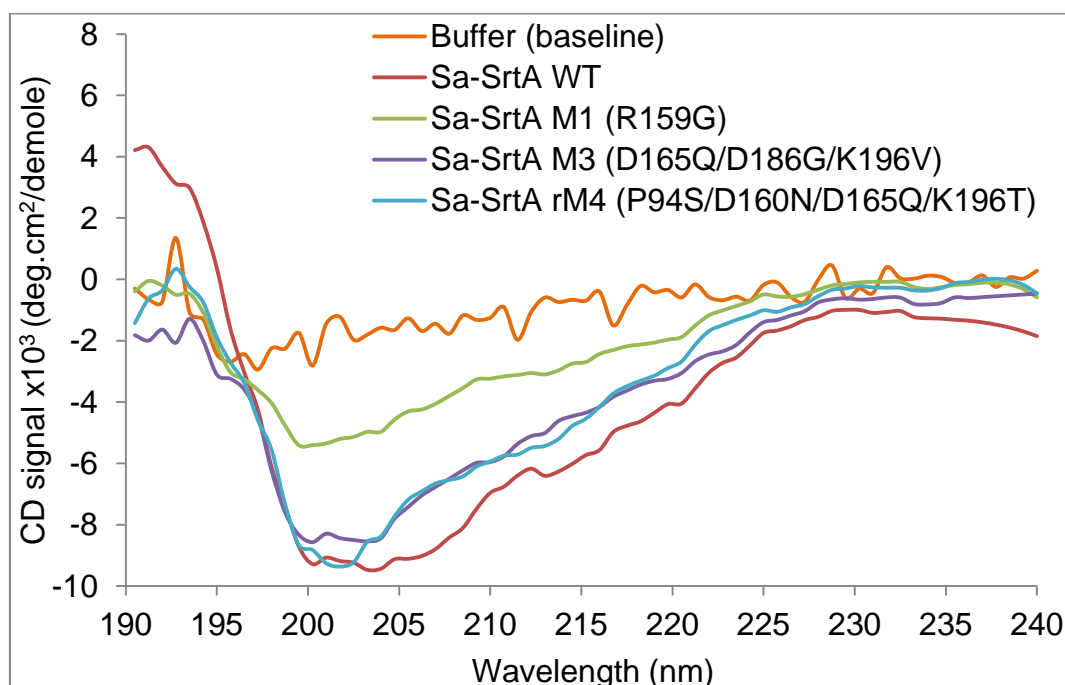

Figure 37. Circular dichroism spectra of Sa-SrtA WT and variants in buffer A. Wavelength scan spectra from 240 to 190 nm were recorded in triplets and averaged.

3.3.2.7. Activity profiles of Sa-SrtA in different organic co-solvents

Activity profiles of Sa-SrtA WT, M1, M3, and rM4 in varied concentrations of DMSO co-solvent were studied. Sa-SrtA M1 showed the best resistance among Sa-SrtA WT, M1, M3, and rM4 under different concentrations of DMSO. Sa-SrtA rM4 lost more than 80% activity when incubated in 15 % (v/v) or higher concentrations of DMSO. The half minimal inhibitory concentrations (IC50) of DMSO for Sa-SrtAs were calculated. IC50 of DMSO for Sa-SrtA WT, M1, M3, and rM4 are 36% v/v, 44% v/v, 23% v/v, and 11% v/v (**Figure 38**), respectively.
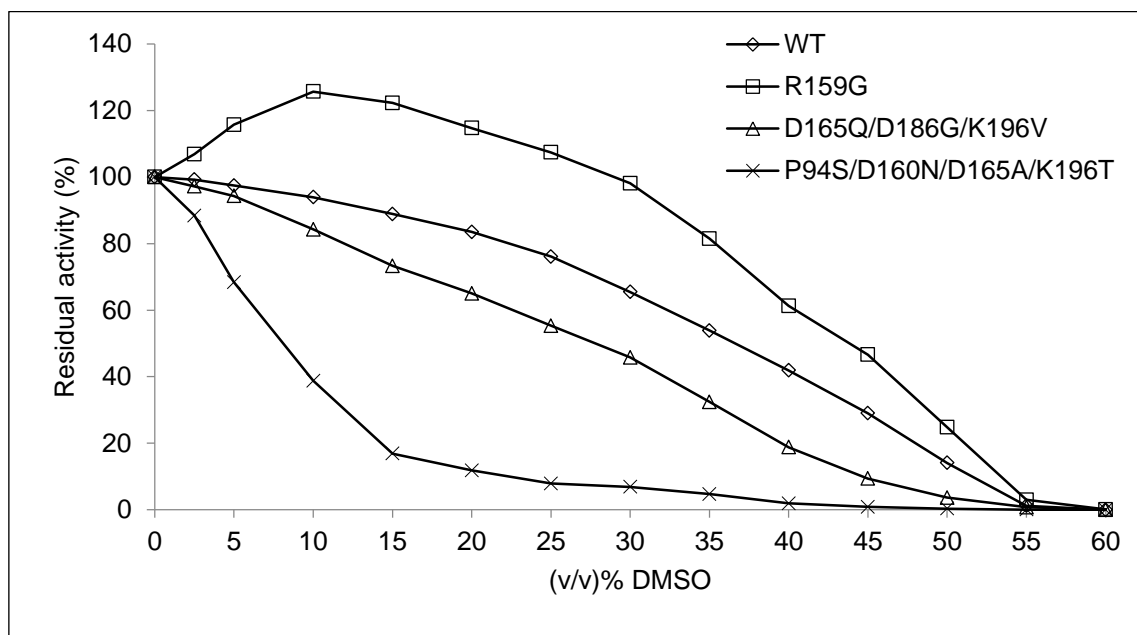
Figure 38. Activity profiles of Sa-SrtAs in different concentrations of DMSO co-solvent. Sa-SrtA WT and variants R159G (M1), D165Q/D186G/K196V (M3) and P94S/D160N/D165A/K196T were selected for the analysis.

Directed enzyme evolutions toward DMSO, yielded often variants with improved resistance towards multiple co-solvents.[90, 103] Activity profiles of Sa-SrtAs were further investigated in DMF, ethanol, methanol and acetonitrile (**Figure 39**) using the FRET assay as aforementioned.[76, 102] Sa-SrtA M1 showed the best resistance in in DMF, ethanol and methanol co-solvent. A similar performance of resistance of Sa-SrtA M1 was observed in acetonitrile co-solvent when compared to Sa-SrtA WT. M1 showed the best resistance profiles in DMF and methanol when compared to Sa-SrtA WT, M3, and rM4. Sa-SrtA WT retained best resistance in ethanol and acetonitrile when compared to when compared to Sa-SrtA M1, M3, and rM4. Compared to the resistance in DMSO co-solvent, IC50 concentrations of Sa-SrtA WT, M1, M3, and rM4 towards DMF, methanol, ethanol and acetonitrile were significantly lower (Figure 4.4.1.10). IC50 concentrations of Sa-SrtA WT, M1, M3, and rM4 in DMF are 6% (v/v), 8% (v/v), 6% (v/v), and 4.5% (v/v). IC50 concentrations of Sa-SrtA WT, M1, M3, and rM4 in methanol are 16% (v/v), 24% (v/v), 11% (v/v), and 7% (v/v). IC50 concentrations of Sa-SrtA WT, M1, M3, and rM4 in ethanol are 12% (v/v), 9%

(v/v), 8% (v/v), and 3.5% (v/v). IC50 concentrations of Sa-SrtA WT, M1, M3, and rM4 in acetonitrile are 9.5% (v/v), 9% (v/v), 9% (v/v), and 4% (v/v). Comparable results of solvent resistance of Sa-SrtA WT were reported.[104]
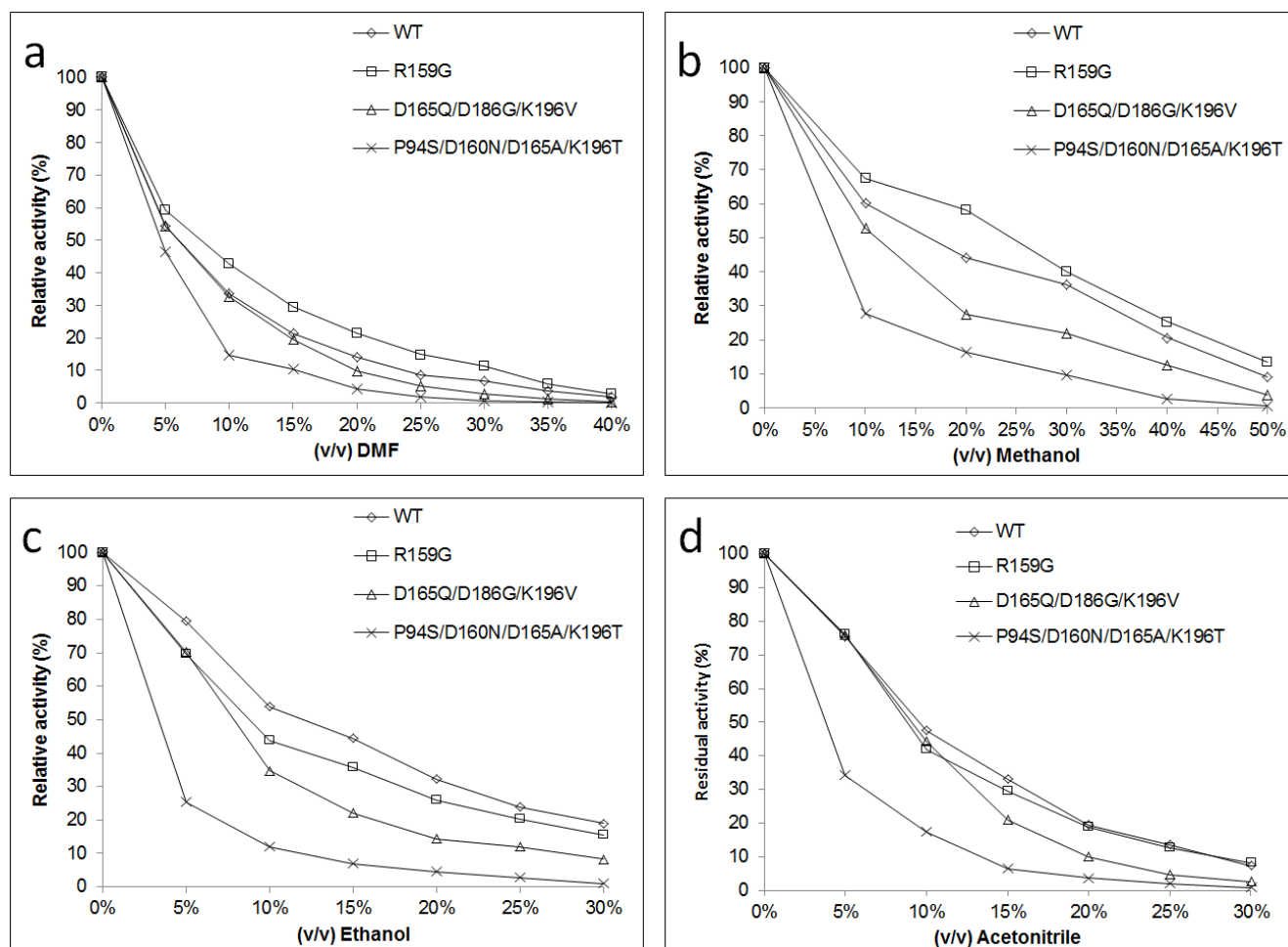
Figure 39. Activity profiles of Sa-SrtAs in different co-solvents. Activity is recorded by a standard FRET assay using Abz-LPETGK-Dnp as substrate. Residual activity was calculated as the ratio of activity in presence of solvent divided activity in absence of solvent. a) gradient concentration of DMF; b) gradient concentration of methanol; c) gradient concentration of ethanol; d) gradient concentration of acetonitrile. Sa-SrtA WT and variants R159G (M1), D165Q/D186G/K196V (M3) and P94S/D160N/D165A/K196T were selected for the analysis.

Relative activities of variants in different co-solvents were calculated. Notably, variant M3 showed a remarkable enhanced specific activity in 30% (v/v) DMF, 30% (v/v) ethanol, 50% (v/v) methanol and 25% (v/v) acetonitrile when compared to Sa-SrtA WT (**Table 12**). Sa-SrtA rM4 showed higher activity than WT in all the selected co-solvents, but was only observed in 25% (v/v) acetonitrile co-solvent that was more active than M3 (**Table 12**).

Table 12. Relative activity of Sa-SrtAs in 45% (v/v) DMSO, 30% (v/v) DMF, 30% (v/v) ethanol, 50% (v/v) methanol and 25% acetonitrile. Relative activity was calculated as the ratio of variant's activity in presence of a certain concentration of co-solvent divided by Sa-SrtA WT's activity in presence of corresponding concentration of co-solvent.

Sa-SrtAΔ59 variant	Relative activity in 45% (v/v) DMSO	Relative activity in 30% (v/v) DMF	Relative activity in 30% (v/v) Ethanol	Relative activity in 50% (v/v) Methanol	Relative activity in 25% (v/v) Acetonitrile
WT	1.00±0.11	1.00±0.14	1.00±0.07	1.00±0.10	1.00±0.17
M1 (R159G)	1.52±0.05	1.21±0.07	0.94±0.10	1.07±0.14	0.94±0.26
M3 (D165Q/D186G/K196G)	5.46±0.04	8.58±0.21	5.99±0.16	5.37±0.14	6.81±0.36
rM4 (P94S/D160N/D165A/K196T)	1.84±0.04	6.74±0.17	4.00±0.12	5.77±0.10	8.89±0.56

3.3.2.8 Sortase-mediated protein-protein ligation in organic co-solvent

A further validation that M3 can efficiently perform protein-protein fusions in organic solvents was performed on the example of the fusion of laccase CueO-LPETGGGRR and the adhesion peptide GGG-eGFP-LCI (the two protein substrates in SortEvolve assay). Purified Sa-SrtAs, CueO-LPETGGGRR and GGG-eGFP-LCI employed and conjugations were carried out in 45% (v/v) DMSO as well as in 30% (v/v) ethanol co-solvents (protocols are described in 3.5.7). As expected, highest yields of fusion protein (CueO-LPETGGG-eGFP-LCI) were achieved by Sa-SrtA M3 in both 45% (v/v) DMSO and 30% (v/v) ethanol co-solvents (**Figure 40**).
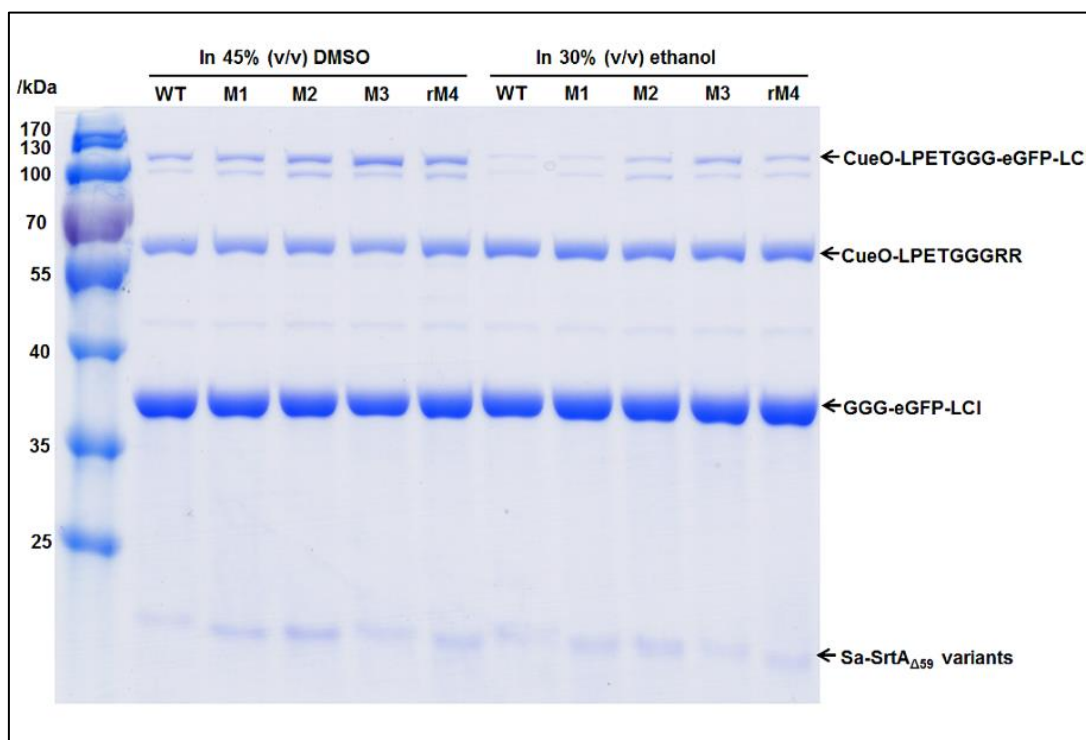
Figure 40. SDS-PAGE of sortase-mediated protein-protein ligations in 45% (v/v) DMSO or 30% (v/v) ethanol. Reaction mixture contains (500 μL, 500 μg/mL purified GGG-eGFP-LCI, 250 μg/mL purified CueO-LPETGGGRR, 30 μg/mL purified Sa-SrtA, 45% (v/v) DMSO or 30% (v/v) ethanol). Reactions were performed at room temperature for 14 h.

In summary, activity profiles of Sa-SrtA WT, M1, M3, and rM4 were investigated in different organic co-solvents (DMSO, DMF, methanol, ethanol and acetonitrile) with different concentrations. Sa-SrtA M1

represented the best resistance in DMSO, DMF and methanol co-solvents and Sa-SrtA M3 showed the best relative ligation activity in DMSO, DMF and methanol co-solvents when compared to Sa-SrtA. The gained ligation activities of variants were not only proved by the FRET assay for short peptide ligation but also confirmed in protein-protein ligation experiments.

3.3.3. Computational studies of Sa-SrtA in DMSO co-solvent

3.3.3.1. In silico generation of sortase variants

Stabilization energy ($\Delta\Delta G$) upon substitution of amino acid residues in unfolded and folded states compared to Sa-SrtA WT is analyzed. $\Delta\Delta G$ was computed with FoldX version 3.0 Beta[105] using standard settings. Results are shown in **Figure 41**. The substitution R159G (M1) showed a slight destabilizing effect (values less than cutoff 1.0 kcal/mol is considered as the stable substitutions). In contrast, the substitutions (D165Q/D186G/K196V) in Sa-SrtA M3 showed a stabilizing effect ($\Delta\Delta G$ <0 kcal/mol). Computational structures of the most stable variants (run 1 for M1 and run 3 for M3) were employed for further molecular dynamics (MD) simulation studies.

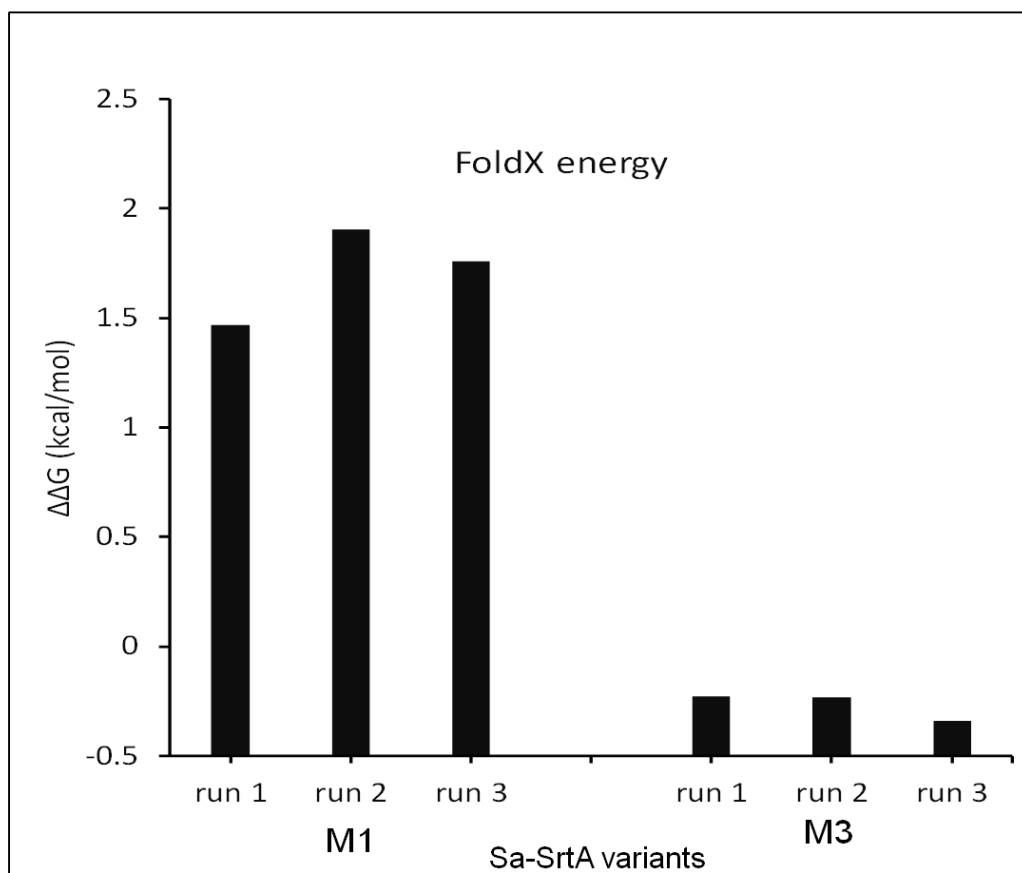**Figure 41.** Calculated stabilization energies ($\Delta\Delta G$) in kcal/mol for 3 independent runs of Sa-SrtA variants (M1 and M3) with respect to Sa-SrtA WT by using the FoldX method; $\Delta\Delta G=\Delta G(variant) \Delta G(WT)$.

3.3.3.2. MD simulations of Sa-SrtA WT in water and DMSO co-solvent

Destabilization effects of DMSO molecules on proteins are determined by relative exposure of polar and nonpolar residues of a protein, the DMSO concentration, and the mode of action of DMSO on targeted proteins.[106] MD simulations of Sa-SrtA WT were performed in water and 45% (v/v) DMSO co-solvent. Solvation mechanism of Sa-SrtA WT was analyzed by a spatial distribution function (SDF) of water or the co-solvent DMSO. **Figure 42** shows that DMSO partially strips off bound water molecules from molecule surface of Sa-SrtA WT. DMSO and polar organic solvents strip off essential water molecules from the protein surface has been reported.[107] The removal of essential water molecules from Sa-SrtA WT surface is more evident in the substrate binding pocket (**Figure 42**). Interestingly, identified beneficial positions in *KnowVolution Phase II* are located in the same regions that were identified to bind DMSO (3.3.2.3).
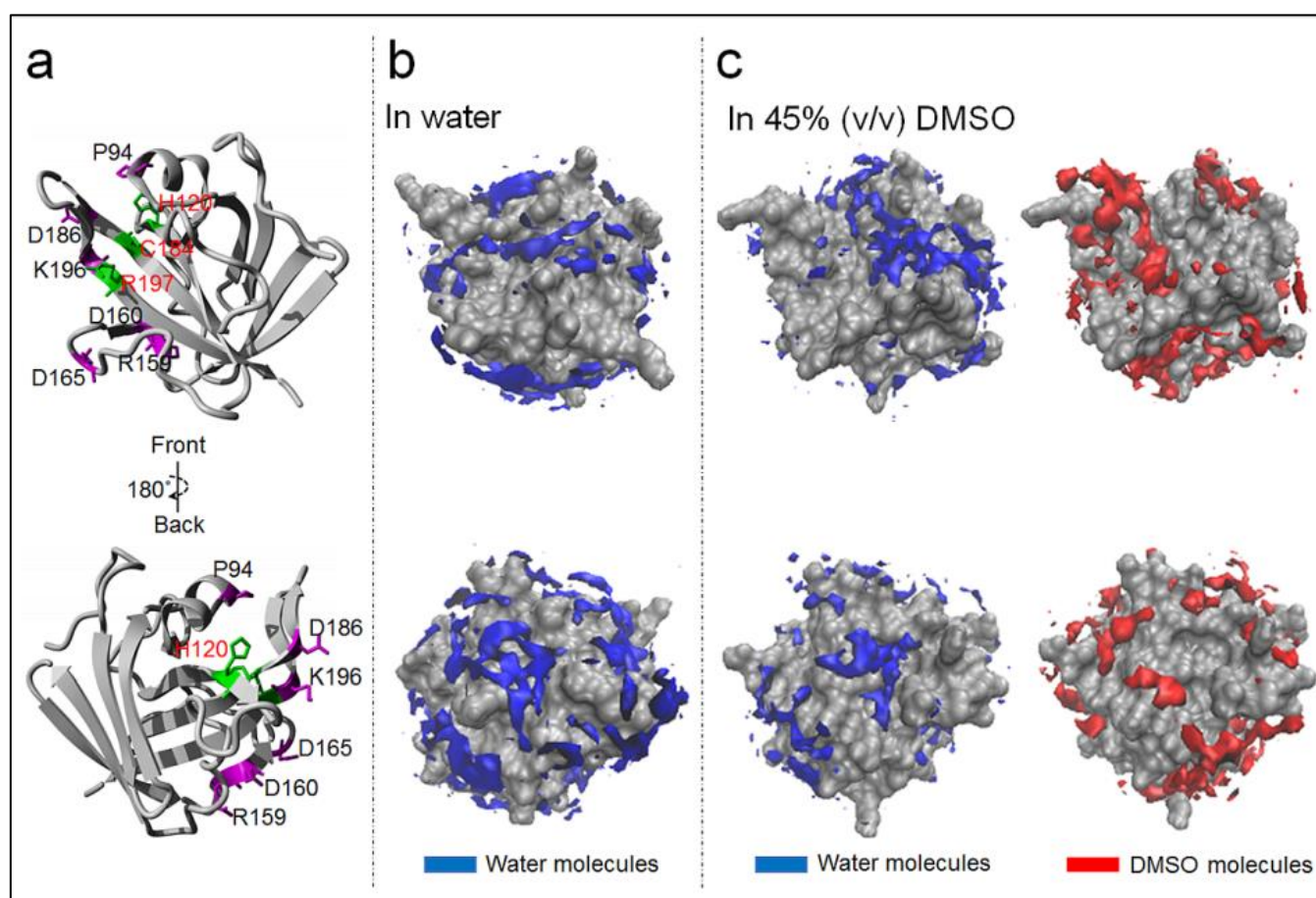
Figure 42. (a) Structures of Sa-SrtA WT (PDB ID: 1T2P, resolution: 2 Å). Catalytic residues (H120, C184 and R197) are shown in green. The residues coloured in magenta represent positions that were substituted. (b) Spatial distribution function (SDF) depicting the solvation mechanism of Sa-SrtA WT in water (b) and 45% DMSO (c). Density distribution of water molecules are shown in blue (c1) and of DMSO molecules in red (c2). The molecular surface corresponds to the average structure of Sa-SrtA from a 50 ns trajectory (for each solvation system). Two sides of the Sa-SrtA are shown. Each view in (b) and (c) of the Sa-SrtA has the same orientation as in (a).

Chapter III: Directed sortase A evolution for efficient site-specific bioconjugations in organic co-solvents

Root mean square deviation (RMSD) of Sa-SrtA WT backbone atoms was calculated in water and 45% (v/v) DMSO co-solvent. A clearly decreased RMSD value was observed in 45% (v/v) DMSO co-solvent when compared to water. This observation revealed that conformational mobility of Sa-SrtA WT in DMSO co-solvent is decreased in comparison to water (**Figure 43a**). Analysis of solvent accessible surface area (SASA) and the radius of gyration (Rg) of Sa-SrtA WT showed increased protein size and larger solvent exposure in 45% (v/v) DMSO co-solvent when compared to water. Both SASA and Rg indicated that size of Sa-SrtA WT was swelled in 45% (v/v) DMSO co-solvent (**Figure 43b/c**).

Likewise, analysis of simulation trajectories of Sa-SrtA WT in 45% (v/v) DMSO showed that interactions of DMSO and enzyme result in alteration of H-bonds between surface residues and water molecules (decrease of radial distribution function (RDF) of water in presence of the DMSO co-solvent and decrease in average number of H-bonds between Sa-SrtA and water molecules(**Figure 43d**). From root mean square fluctuations (RMSF) per residue it is found that substrate binding residues show less flexibility in presence of the co-solvent DMSO than in water **(Figure 47a).** The latter could lead to a reduced enzymatic activity.
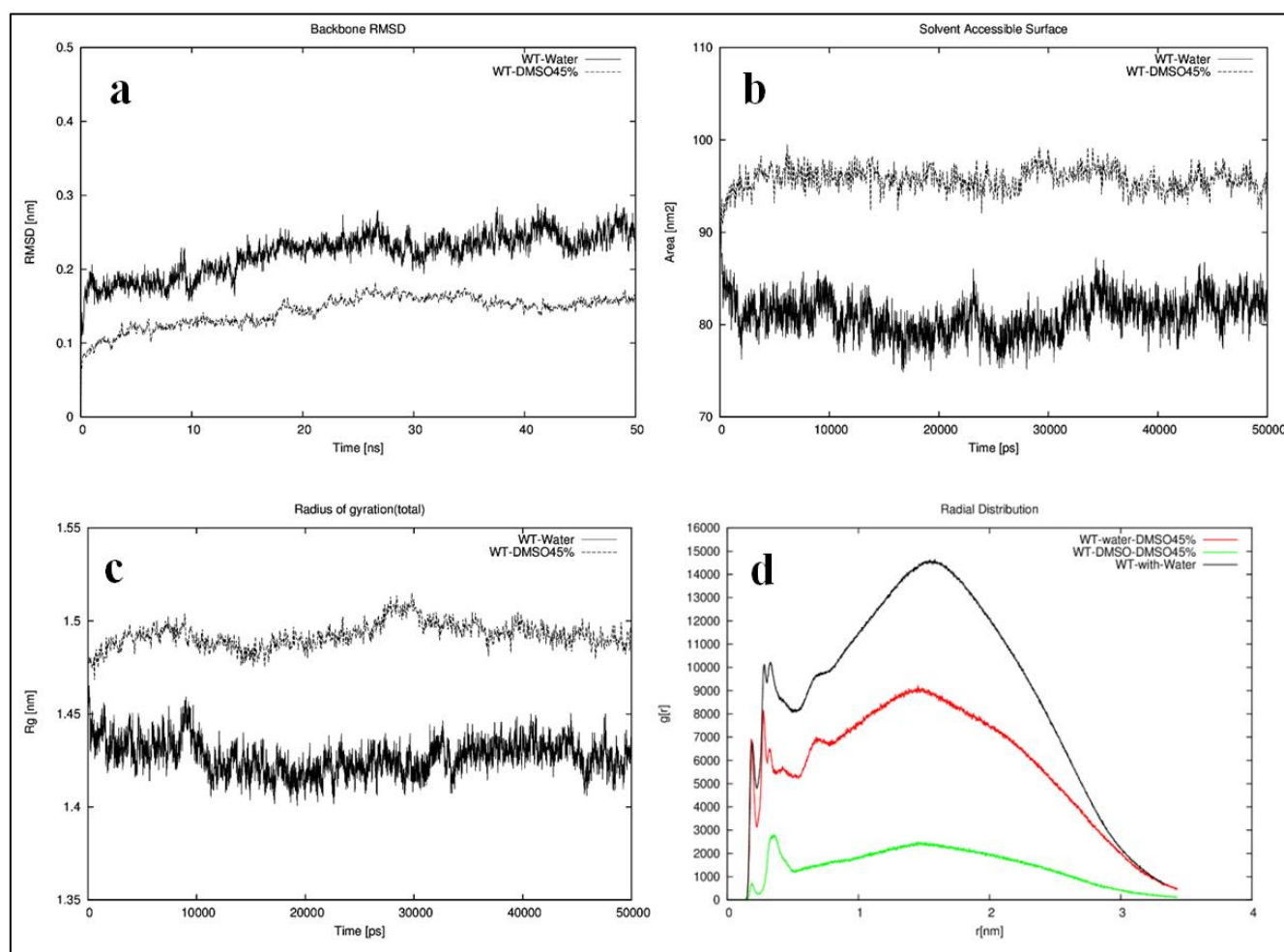
Figure 43. Analysis of Sa-SrtA WT MD simulation trajectory in water and DMSO co-solvent; (a) RMSD of back bone atoms; (b) Solvent accessible surface area (SASA); (c) radius of gyration (Rg) of sortase; (d) radial distribution functions (RDF) of water and DMSO molecules in the surface of Sa-SrtA WT.

3.3.3.3. MD simulations of Sa-SrtA M1and M3 in water and DMSO co-solvent

Solvation mechanism of variants M1 and M3 (**Figure 44**) were compared to Sa-SrtA WT. Results revealed that amino acid substitutions in close proximity of the LPxTG binding pocket can partially retain essential water molecules in 45% (v/v) DMSO. Variant M1 has more H-bond interactions with DMSO molecules (**Figure 45a**), which leads to increased surface interactions in 45% (v/v) DMSO (increased SASA and Rg, **Figure 46 b/c**). In addition, variant M1 showed a higher conformational mobility (higher RMSD values **Figure 46a**) and a more flexible active site (higher RMSF for active site residues, **Figure 47b**) in 45% (v/v) DMSO in comparison to Sa-SrtA WT. Similarly, analysis of variant M3 showed increased conformational mobility (higher RMSD values, **Figure 46d**) and a more flexible active site (higher RMSF, **Figure 47c**) in water and in 45% (v/v) DMSO compared to Sa-SrtA WT. To sum up, the larger conformational mobility and higher active site flexibility leads to higher activity and consequently higher resistance of M1 and M3 compared to Sa-SrtA WT.
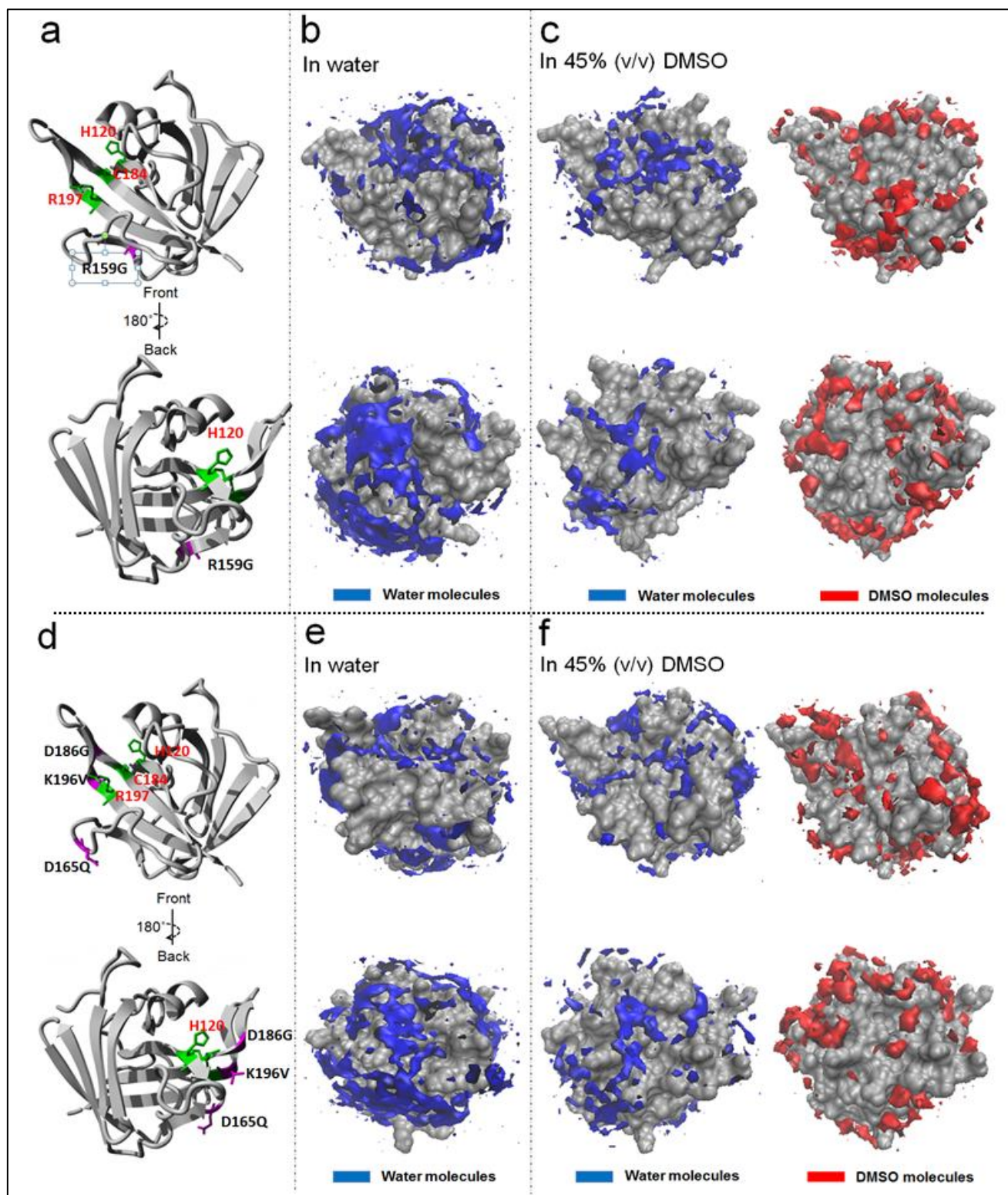
Figure 44. (a) Model of Sa-SrtA variant M1 (R159G: a, b, and c) and M3 (D165Q/D186G/K196V: d, e, and f); Spatial distribution function (SDF) depicting the solvation mechanism of Sa-SrtA from front and back view in (M1: b, e) water and (M3: c, f) in 45% (v/v) DMSO co-solvent. Density distribution of water molecules are shown in blue and DMSO molecules in red. The molecular surface corresponds to the average structure of Sa-SrtA M1 from the 50 ns trajectory, for each solvation system. Two sides of the Sa-SrtA M1 and M3 are shown in order to provide a complete view of the surface. Each view has the same orientation in (a or d).
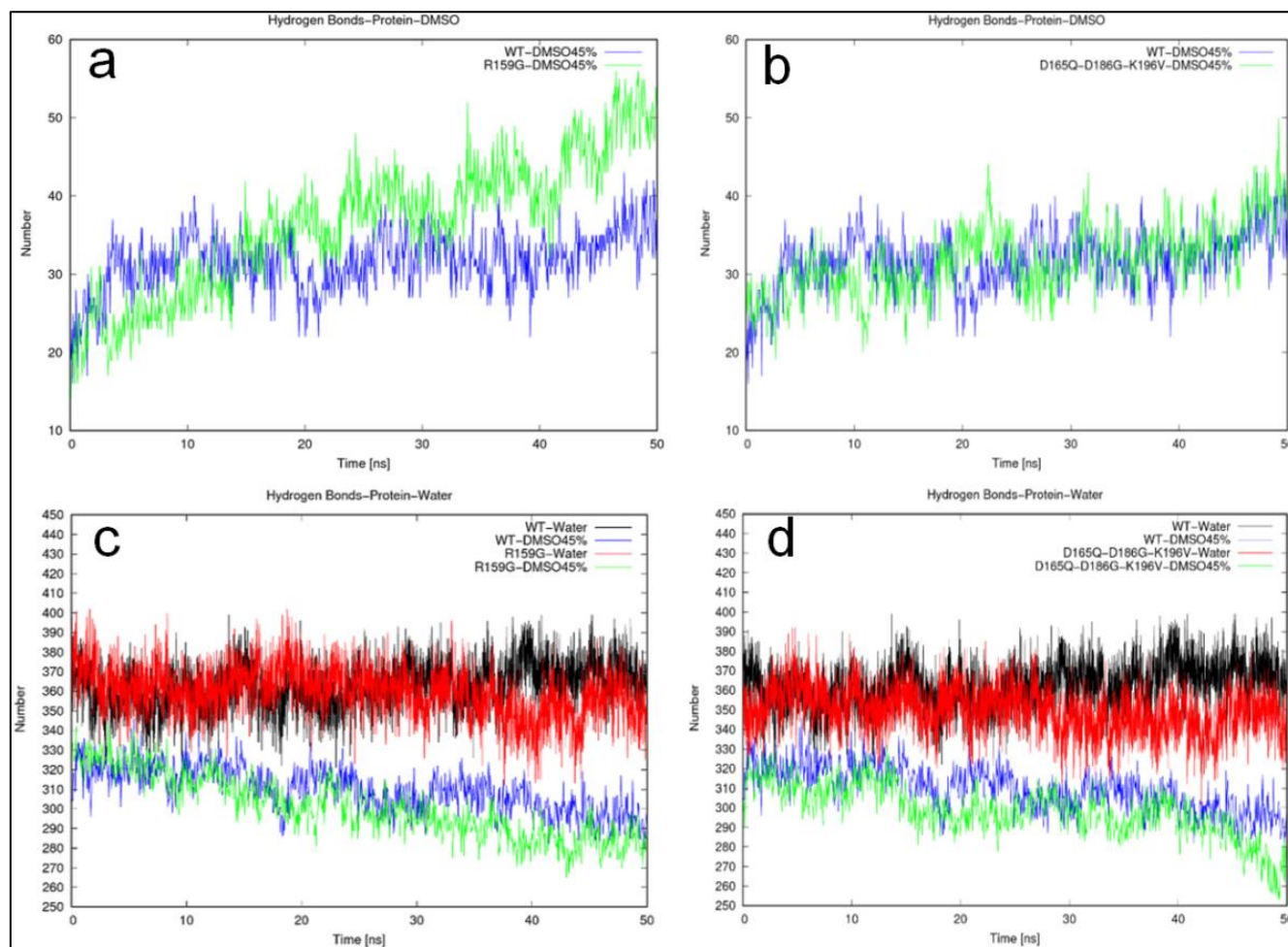
Figure 45. Analysis of Sa-SrtA M1 (R159G) and M3 (D165Q/D186G/K196V) MD simulation trajectory; (**a**) number of hydrogen bond between M1 and DMSO, (**b**) number of hydrogen bond between M3 and DMSO, (**c**) number of hydrogen bond between M1 and water (**d**) number of hydrogen bond between M3 and water. Sa-SrtA WT was employed as a control in each analysis.
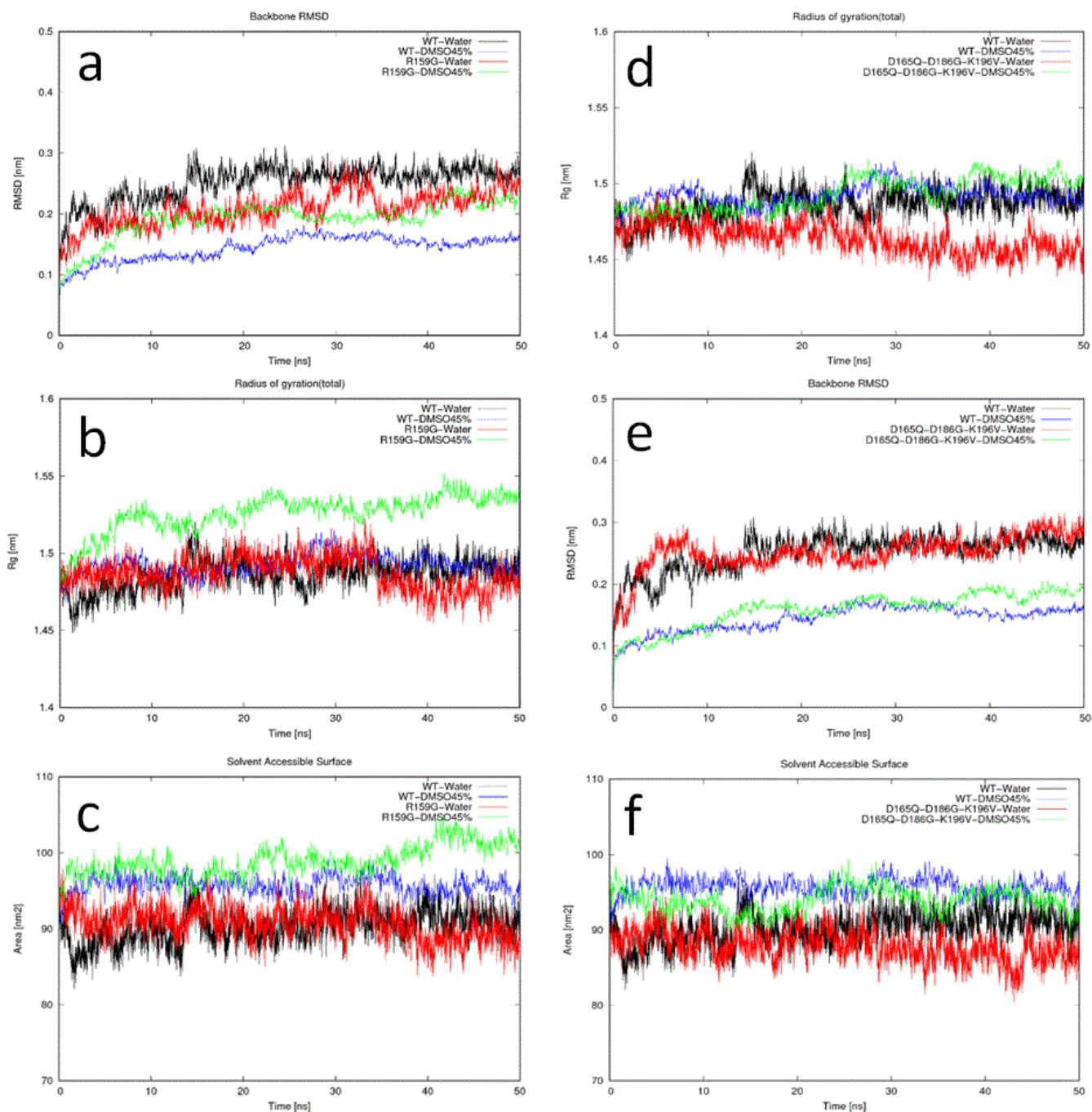
Figure 46. Analysis of Sa-SrtA M1 (R159G) and M3 (D165Q/D186G/K196V simulation trajectory; (**a, d**) RMSD of back bone atoms for Sa-SrtAs; (**b, e**) radius of gyration of Sa-SrtAs (**c, f**) Solvent accessible surface area (SASA) of Sa-SrtAs.
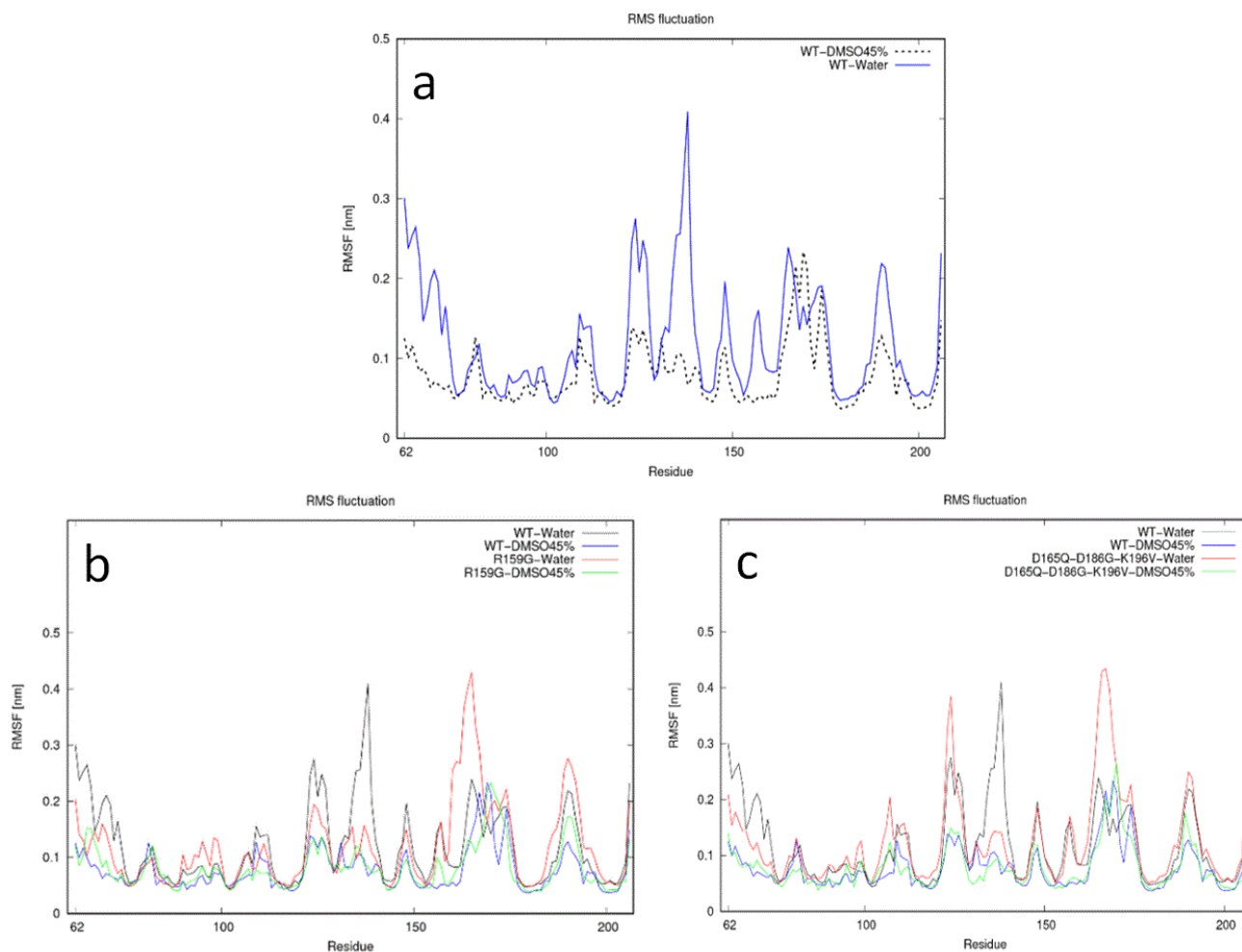
Figure 47. Root mean square fluctuation (RMSF) per residues of Sa-SrtA WT (a), M1 (R159G, (b)) and M3 (D165Q/D186G/K196V, (c)), Red arrow highlights the substrate binding site region.

3.3.4. Applications of sortase-mediated site-specific conjugation in organic co-solvents

3.3.4.1 Sortase-mediated ligation of primary amines and Abz-LPETG-Dnp peptide in organic co-solvents

Organic solvents (e.g. DMSO and DMF) dissolve polar and nonpolar compounds. They are commonly employed as solvents to increase the solubility of substrates in chemical synthesis. Sa-SrtA have been reported to ligate many molecules (e.g. primary amines) to peptides.[51] To investigate whether the evolved Sa-SrtA M3 variant could be employed for the conjugation of hydrophobic peptide and amines in co-solvents, SML in 45% (v/v) DMSO/30% (v/v) DMF were performed (**Figure. 48a**). Hydrophobic peptide Abz-LPETGK-Dnp (solubility in pure water <5 mM) was employed as constant donor of LPxTG. Hydrophobic peptide AVP 0683 (amino acid sequence: GGHRRYFTFGGGYVYF[108]), tyramine, 4-(Trifluoromethyl)-benzylamine (4-TFB amine) and O-(2-Aminoethyl) polyethylene glycol (PEG amine,

78

M_P=5000 da) with unbranched primary amines were used as nucleophiles (**Figure 48b** and **Table 13**). Similar as the FRET reaction aforementioned,[102] upon the transpeptidation, the Abz (fluorophore) gets separated from Dnp (quencher) and subsequently ligates to corresponding primary amine. A fluorescent signal is generated and recorded (**Figure 48a**).
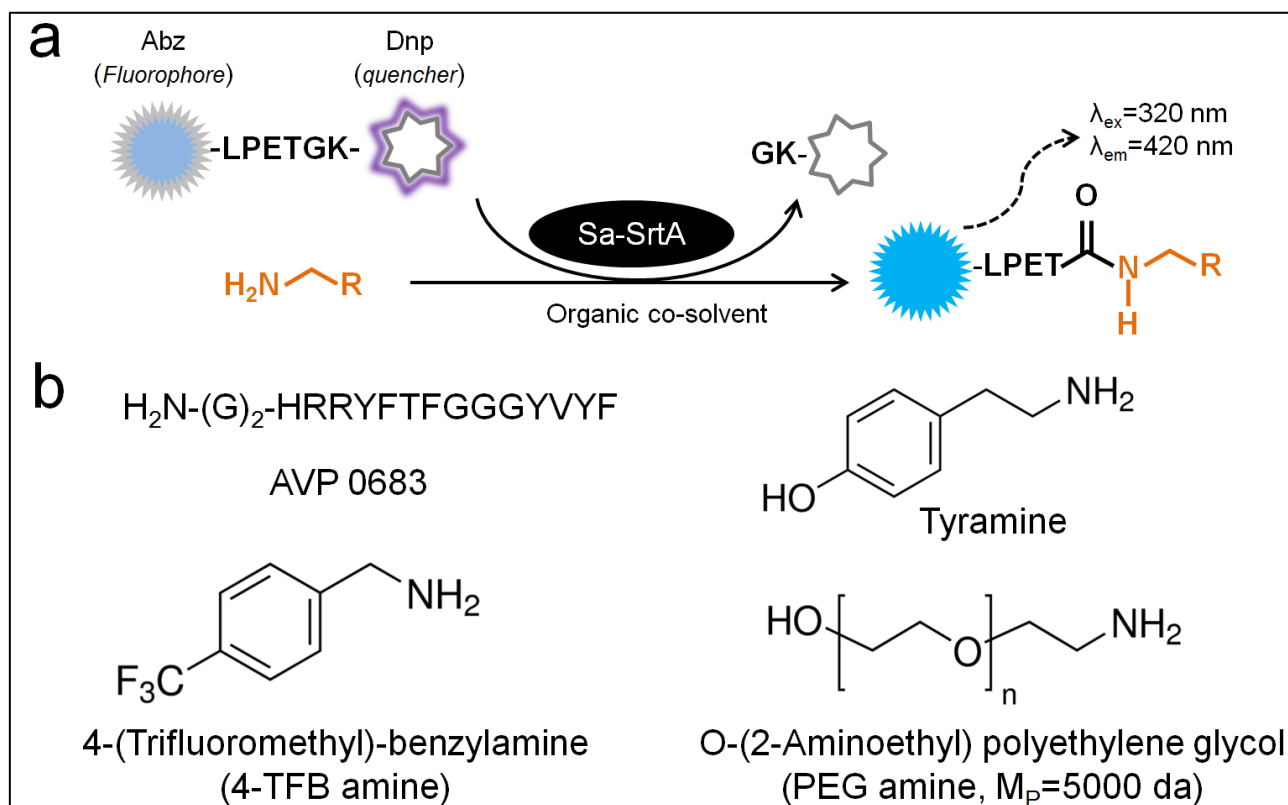
Figure 48. Sortase-mediated ligation of hydrophobic peptide/amine in organic co-solvent. (a) Schematic representation of sortase A-mediated FRET assay in presence of co-solvents with Abz-LPETGK-Dnp and the unbranched primary amines as substrates. (b) Chemical structures of the selected unbranched primary amines.

Table 13. Molecular weight and solubility of peptide and unbranched primary amines donors in this study

Primary amine donor	Molecular weight (da)	Solubility in pure water (mM)	Conjugate with Abz-LPETGK-dNP	Theoretical molecular weight of conjugate (da)
AVP 0683	1884.7	< 0.3	Abz-LPET-AVP 0683	2446.6
Tyramine	137.18	< 50	Abz-LPET-tyramine	697.38
4-TFB amine	175.15	< 5	Abz-LPET-4-TFB	736.32
PEG-amine	≈ 5000 (mean value)	soluble	Abz-LPET-PEG	≈ 5545 (mean value)

M3 showed up to 4.7-fold improved activities in ligation of AVP0683 and LPxTG peptides in 45% (v/v) DMSO or 30 % (v/v) DMF (**Figure 49a**). Sa-SrtAs are able to conjugate all the selected unbranched primary amines to the Abz-LPETG peptide in 45 % (v/v) DMSO (**Figure 49b**). Impressively, Sa-SrtA

Chapter III: Directed sortase A evolution for efficient site-specific bioconjugations in organic co-solvents

M3 showed highest activities in ligation of the three sleeted amines when compared to Sa-SrtA WT and Sa-SrtA rM4. The latter demonstrated the versatility of M3 in efficient site-specific conjugation of not only peptide but also non-peptide related chemical compounds in co-solvents. In summary, Sa-SrtA M3 showed up to 3.8-fold activity for the ligation of unbranched primary amines to LPxTG peptide in 45% (v/v) DMSO when compared with Sa-SrtA WT. In comparison to the native glycine amine donors, the relative activities of Sa-SrtA M3 towards non-native primary amine donors are reduced in 45% (v/v) DMSO. These findings indicate further potentials to Sa-SrtA with enhanced activity towards non-native amine substrates.
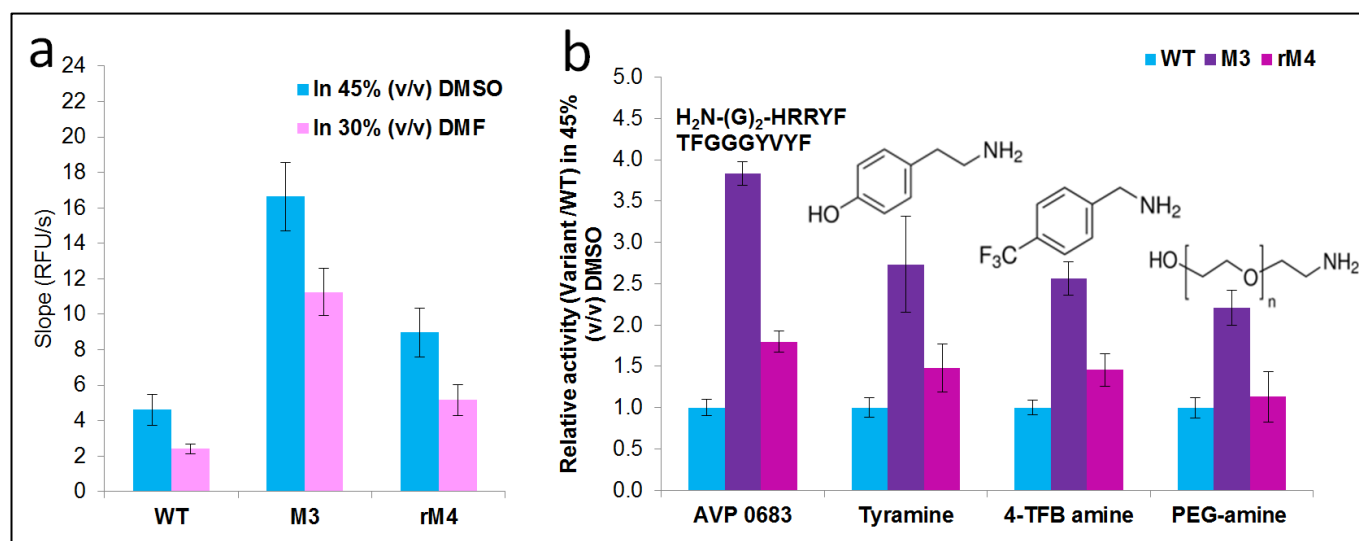
Figure 49. Relative activities of Sa-SrtAs (WT, M3, and rM4) in the ligation of different primary amines to Abz-LPETG peptide in 45% (v/v) DMSO. Relative activity was calculated as the ration of Sa-SrtA variant activity divided Sa-SrtA WT activity in FRET assay.

Conversions of Abz-LPETGK-Dnp to conjugated products were calculated. M3 showed an up to 3.2-fold in yield of conjugated product when compared to Sa-SrtA WT in DMSO co-solvent (**Figure 50**). Notably, up to 94% percent of 4-TFB was converted to conjugated product in 30 min. The high yield indicates that the generated Abz-LPET-4-TFB might be not recognizing by the Sa-SrtA. Similar results were also reported in previously when primary amines were used as substrates in SML.[51]

80
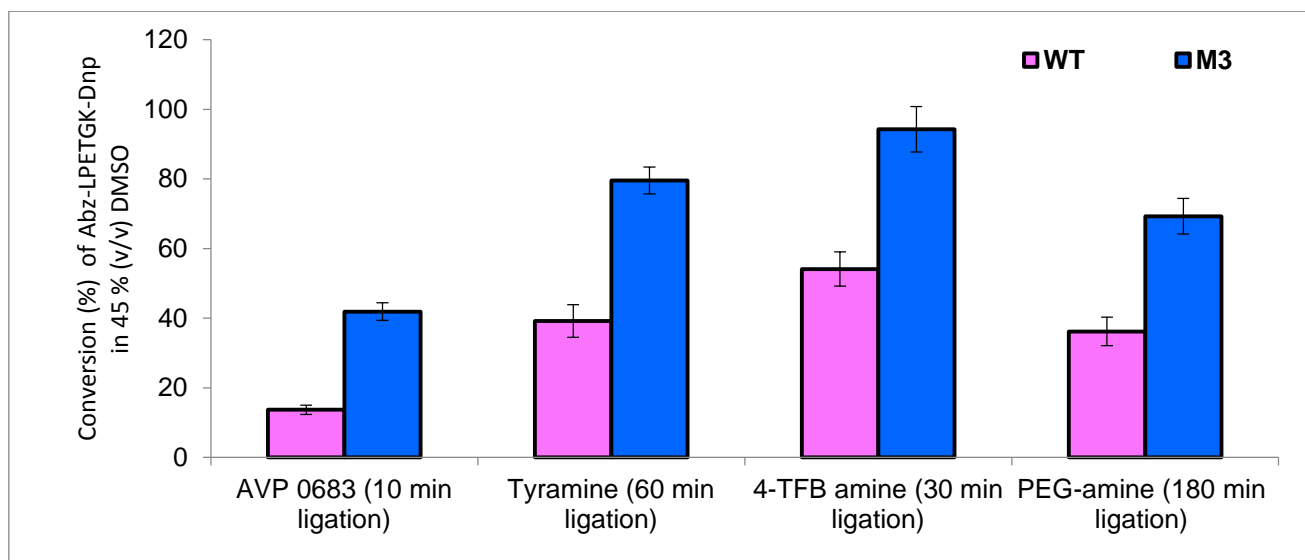
Figure 50. Conversion of Abz-LPETGK-Dnp to corresponding conjugated products in SMLs in 45% (v/v) DMSO which catalysed by Sa-SrtA WT or M3.

3.3.4.2 Detection and quantification of bioconjugate Abz-LPET-AVP0683

The generation of conjugates Abz-LPET-AVP0683 was visualized by tricine sodium dodecyl sulfate-polyacrylamide gel electrophoresis (SDS-PAGE, **Figure 51a**). In comparison with Sa-SrtA WT, high yields of Abz-LPET-AVP0683 were achieved by Sa-SrtA M3 both in 45% (v/v) DMSO (10 min) and 30% (v/v) DMF (30 min) which is in well agreement with the activity data showed in **Figure 49a.** A further confirmation of Abz-LPET-AVP0683 (theoretical molecular weight is 2446.6 Dalton) was performed by using matrix-assisted lasers desorption/ionization mass spectrum (MALDI-MS). Molecule peaks at 2449.3 Dalton (synthesized in 45% (v/v) DMSO, **Figure 51b**) and 2451.2 Dalton (synthesized in 30% (v/v) DMF, **Figure 51c**) were detected.
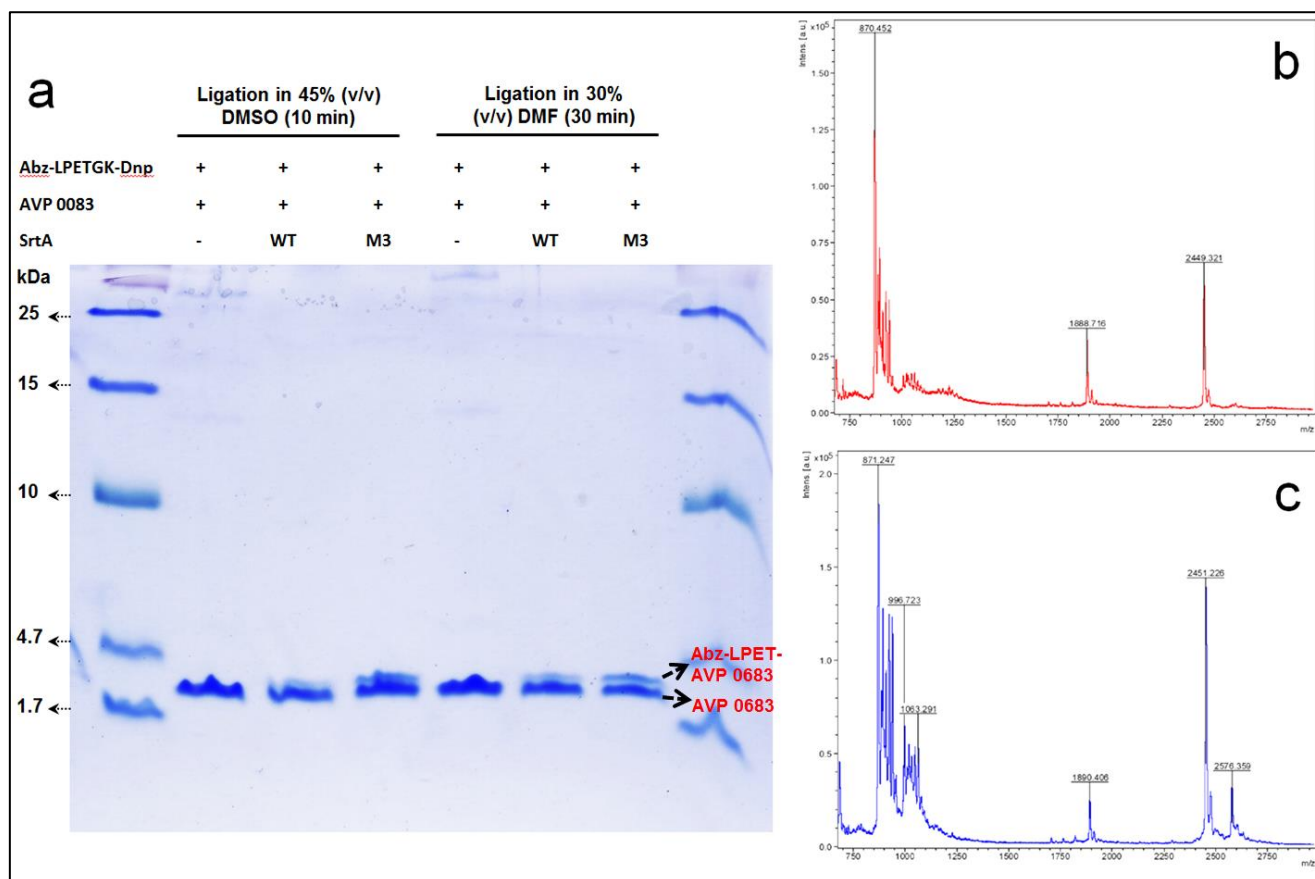
Figure 51. a) Tricine SDS-PAGE of hydrophobic peptide samples (1 mM Abz-LPETGK-Dnp, 3 mM peptide AVP0683 and 10 μM purified Sa-SrtA (WT or M3)) after sortase-mediated ligation in 45% (v/v) DMSO or 30% (v/v) DMF co-solvents. b) MALDI-TOF MS of reaction mixture catalyzed by Sa-SrtA M3 (10 min) in (a) in 45% (v/v) DMSO. c) MALDI-TOF MS of reaction mixture catalyzed by Sa-SrtA M3 (30 min) in (a) in 30% (v/v) DMF. The theoretical molecular weight of AVP0683 is 1884.7 Da (Dalton) and the theoretical molecular weight of Abz-LPET-AVP0683 is 2446.6 Da (Dalton).

HPLC was employed to determine the conversion of Abz-LPETGK-Dnp to Abz-LPET-AVP0683. Protocols of HPLC were described in 4.4.1.9. The HPLC trace of Abz-LPETGK-Dnp and GK-Dnp is shown in **Figure 52**. Conversions of Abz-LPETGK-Dnp to Abz-LPET-AVP0683 in 45% (v/v) DMSO are 13.7% (Sa-SrtA WT, 10 min) and 41.9% (Sa-SrtA M3, 10 min). Conversions of Abz-LPETGK-Dnp to Abz-LPET-AVP0683 in 30% (v/v) DMF are 13.3% (Sa-SrtA WT, 30 min) and 61.8% (Sa-SrtA M3, 30 min). In comparison to Sa-SrtA WT, around 3.1- and 4.6-fold of yield Abz-LPET-AVP0683 was achieved by Sa-SrtA M3 in 45% (v/v) DMSO and 30% (v/v) DMF, respectively.
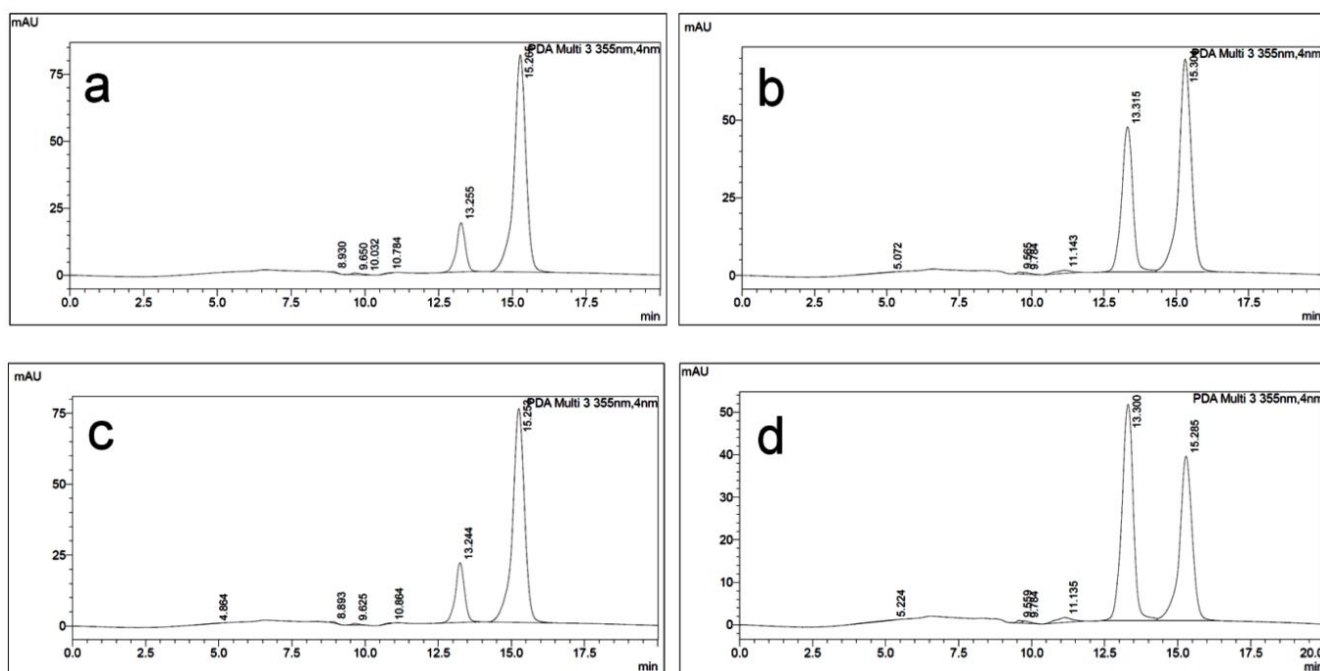
Figure 52. HPLC trace of reaction mixtures: a) Reaction mixture (100 μL, 1 mM Abz-LPETGK-Dnp, 3 mM peptide AVP0683, 45% (v/v) DMSO, 10μM Sa-SrtA WT); b) Reaction mixture (100 μL, 1 mM Abz-LPETGK-Dnp, 3 mM peptide AVP0683, 45% (v/v) DMSO, 10μM Sa-SrtA M3); c) Reaction mixture (100 μL, 1 mM Abz-LPETGK-Dnp, 3 mM peptide AVP0683, 30% (v/v) DMF, 10μM Sa-SrtA WT); Reaction mixture (100 μL, 1 mM Abz-LPETGK-Dnp, 3 mM peptide AVP0683, 30% (v/v) DMF, 10μM Sa-SrtA M3). Absorbance peak at around 13.3 and 15.3 min are generated product GK-Dnp and substrate Abz-LPETGK-Dnp, respectively. Conversions of Abz-LPETGK-Dnp to Abz-LPETG-AVP0683 in (a), (b), (c), and (d) are 13.7 %, 41.9%, 13.3% and 61.8%, respectively.

3.3.4.3 Detection and quantification of bioconjugates Abz-LPET-tyramine and Abz-LPET-4-TFB

The generated conjugate of Abz-LPET-tyramine was confirmed by Ultra-Performance Liquid Chromatography-Mass Spectrum (UPLC-MS). The expected molecular weight of Abz-LPET-tyramine is 697.32 da. The detected molecular weight of Abz-LPET-tyramine were 697.29 (conjugation catalyzed by Sa-SrtA WT) and 697.36 da (conjugation catalyzed by Sa-SrtA M3). Yields of Abz-LPET-tyramine were calculated by integrating the absorbance curve of Abz-LPETGK-Dnp and generated product GK-Dnp which recorded at 355 nm. The conversions of Abz-LPETGK-Dnp to Abz-LPET-tyramine in DMSO co-solvent are 39.2 (catalyzed by Sa-SrtA WT) and 79.6% (conjugation catalyzed by Sa-SrtA M3) respectively. A 2.0-fold improved yield of Abz-LPET-tyramine catalyzed by Sa-SrtA M3 within 1 h when compared to Sa-SrtA WT. The results are in good agreement with the data which obtained in FRET assay (**Figure 53**).

83
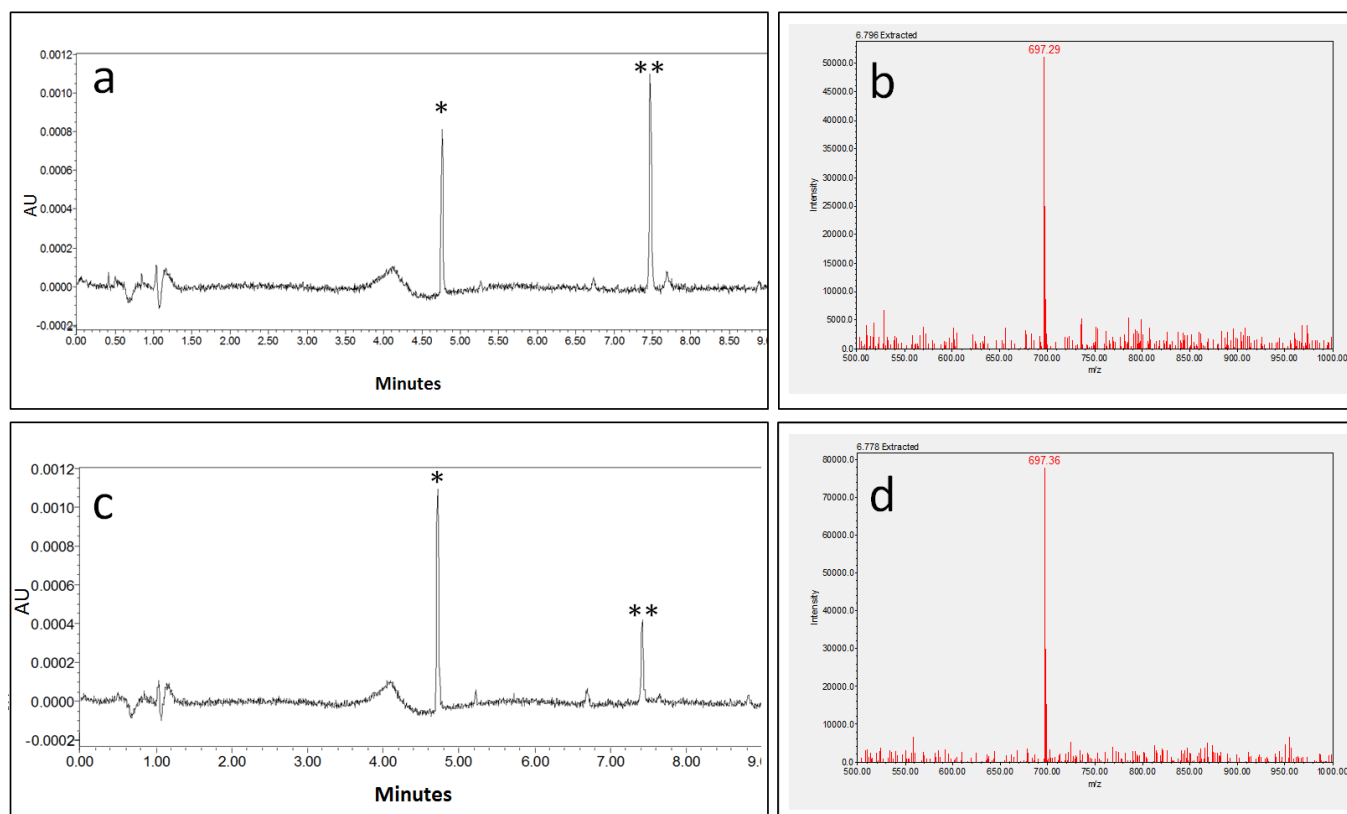
Figure 53. UPLC-MS of sortase-mediated ligation of tyramine and Abz-LPETGK-Dnp: a) UPLC trace ligation mixture (100 µL, 1 mM Abz-LPETGK-Dnp, 10 mM tyramine, 45% (v/v) DMSO, 20µM Sa-SrtA WT); b) Mass spectrum of ligation mixture in (a). The theoretical molecular weight of conjugate (Abz-LPET-tyramine) is 697.38 da. c) UPLC trace ligation mixture (100 µL, 1 mM Abz-LPETGK-Dnp, 10 mM tyramine, 45% (v/v) DMSO, 20µM Sa-SrtA M3); d) Mass spectrum of ligation mixture in (c). Absorbance was monitored at 355 nm. Peak* is the generated product GK-Dnp. Peak** is the substrate Abz-LPETGK-Dnp.

The generated conjugate of Abz-LPET-4-TFB was confirmed by UPLC-MS. The expected molecular weight of Abz-LPET-tyramine is 735.38 da. The detected molecular weight of Abz-LPET-4-TFB were 735.35 (conjugation catalyzed by Sa-SrtA WT) and 935.30 da (conjugation catalyzed by Sa-SrtA M3). Yields of Abz-LPET-TFB were calculated as aforementioned. The conversions of Abz-LPETGK-Dnp to Abz-LPET-4-TFB in DMSO co-solvent are 54.1 (catalyzed by Sa-SrtA WT) and 94.3% (conjugation catalyzed by Sa-SrtA M3) respectively. A 1.74-fold improved yield of Abz-LPET-4-TFB catalyzed Sa-SrtA M3 within 30 min when compared to Sa-SrtA WT (**Figure 54 a/c**).

84
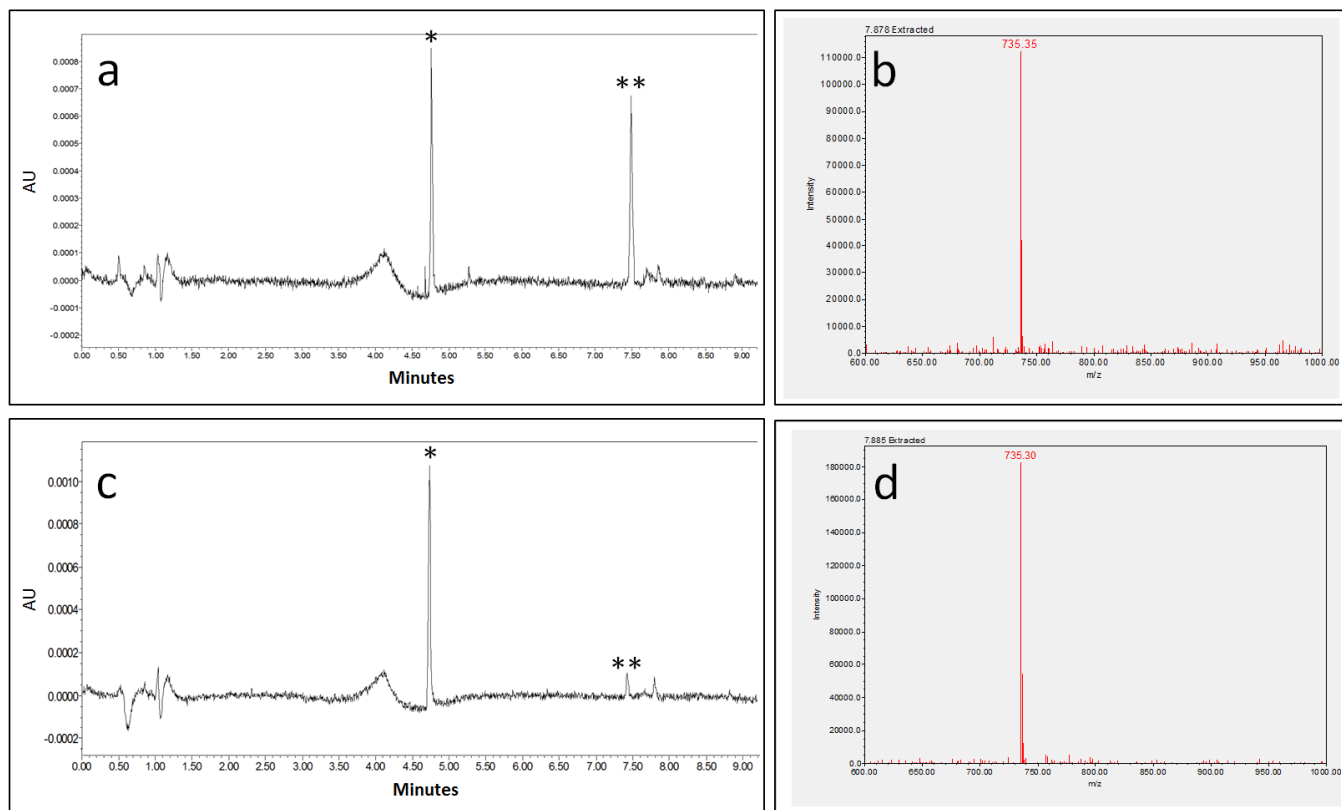
Figure 54. UPLC-MS of sortase-mediated ligation of tyramine and Abz-LPETGK-Dnp: a) UPLC trace ligation mixture (100 µL, 1 mM Abz-LPETGK-Dnp, 10 mM 4-(Trifluoromethyl)-benzylamine (4-TFB amine, 45% (v/v) DMSO, 20µM Sa-SrtA WT); b) Mass spectrum of ligation mixture in (a). The theoretical molecular weight of conjugate (Abz-LPET-4-TFB amine) is 735.32 da. c) UPLC trace ligation mixture (100 µL, 1 mM Abz-LPETGK-Dnp, 4-TFB amine, 45% (v/v) DMSO, 20µM Sa-SrtA M3); d) Mass spectrum of ligation mixture in (c). Absorbance was monitored at 355 nm. Peak* is the generated product GK-Dnp. Peak** is the substrate Abz-LPETGK-Dnp.

3.3.4.4 Detection and quantification of bioconjugates Abz-LPET-PEG

The generation of Abz-LPET-PEG was detected my MALDI-TOF MS. The PEG-amine substrate has an average molecular weight at 5000 da which is approved in mass spectrum in **Figure 55a**. The expected average molecular weight of Abz-LPET-PEG is at 5545 da. After 5 h conjugation (100 µL, 1 mM Abz-LPETGK-Dnp, 10 mM PEG amine, 45% (v/v) DMSO, 20µM Sa-SrtA), reaction mixtures were analyzed by MALDI-TOF MS. Data is given in **Figure 55b**. A shift of molecular weight (appropriately from 5100 to 5600 da) of PEG molecules was observed (low part). The gained molecular (500 da) is comparable to the molecular weight of Abz-LPET group. In the reaction, ten times PEG-amine (10 mM) compared with Abz-LPETGK-Dnp peptide (1 mM), therefore most of PEG molecules retained the molecule size at 5100 da. Conversion of Abz-LPETGK-Dnp to Abz-LPET-PEG was determined by UPLC **Figure 56**. The conversions of Abz-LPETGK-Dnp to Abz-LPET-PEG in DMSO co-solvent are 36.2 (catalyzed by Sa-SrtA WT) and 69.3% (conjugation catalyzed by Sa-SrtA M3) respectively. A 1.9-fold improved yield of Abz-LPET-PEG catalyzed Sa-SrtA M3 within 180 min when compared to Sa-SrtA WT (**Figure 56).**
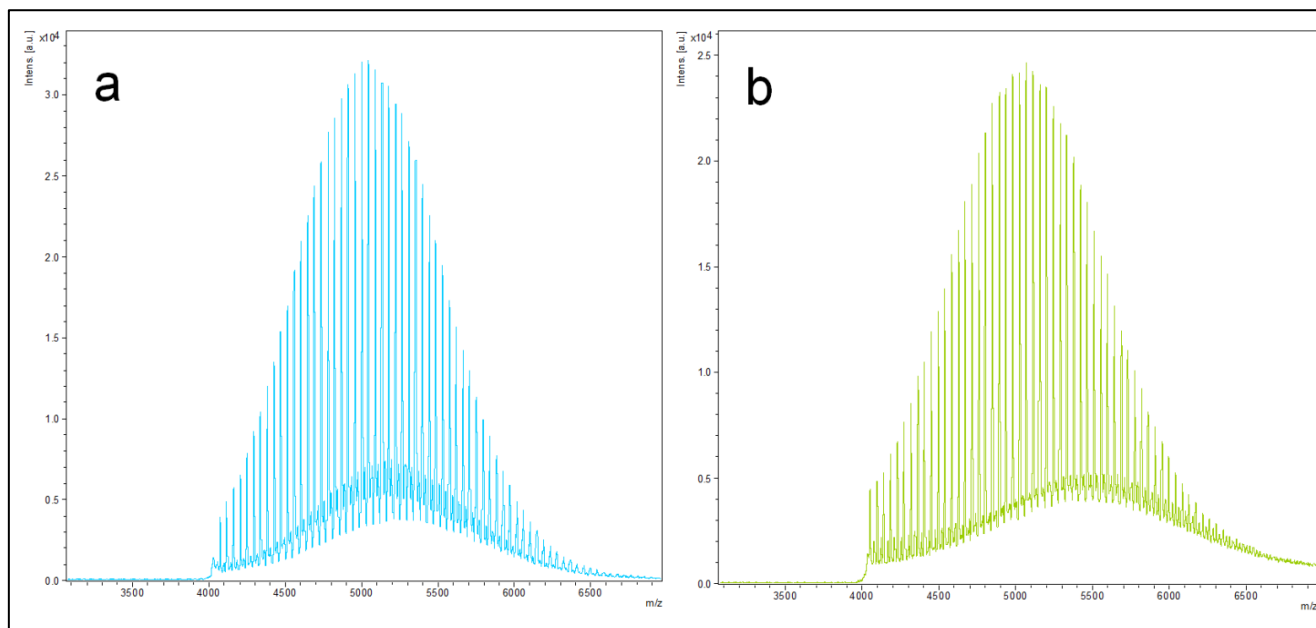
Figure 55. MALDI-TOF MS of (a) PEG-amine and (b) reaction mixture catalyzed by Sa-SrtA M3 (after 5 h conjugation) in 45% (v/v) DMSO. The average molecular weight of PEG amine is 5000 Da (Dalton) and the average molecular weight of Abz-LPET-PEG is 5545 Da. A shift of molecular weight (5100 to 5600 da) of PEG was observed in (b).
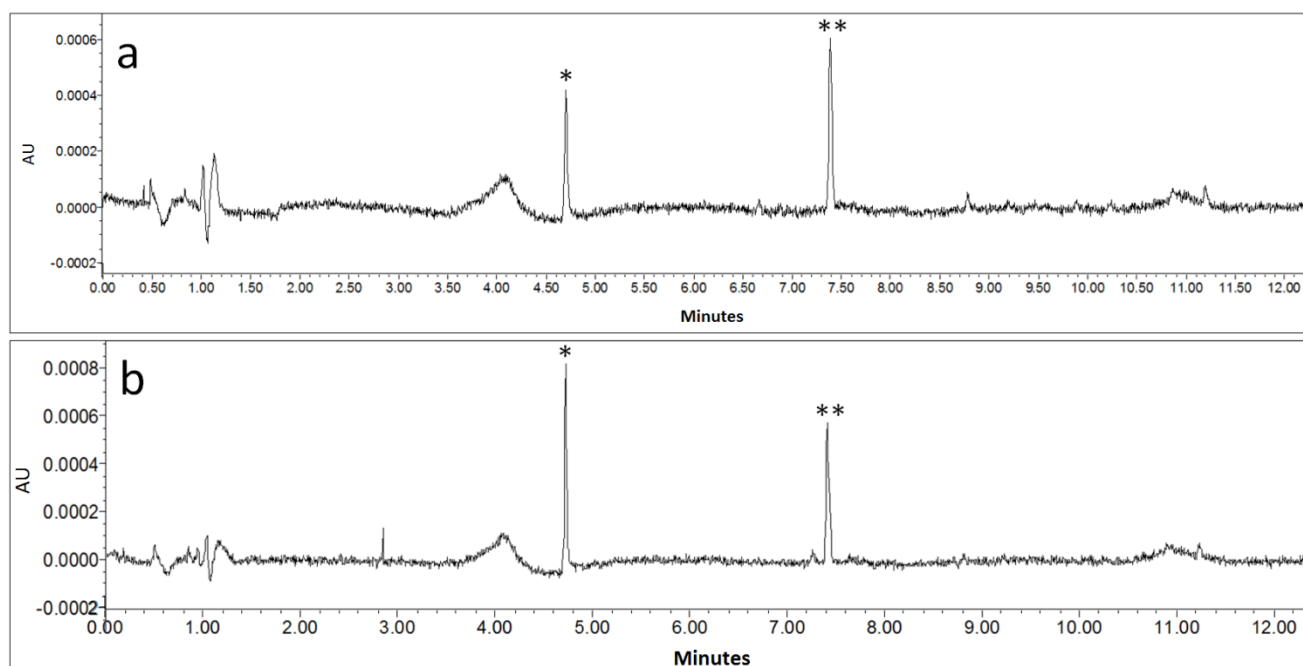
Figure 56. UPLC of sortase-mediated ligation of O-(2-Aminoethyl) polyethylene glycol (PEG amine, M_P=5000 da) and Abz-LPETGK-Dnp: a) UPLC trace of ligation mixture (100 μL, 1 mM Abz-LPETGK-Dnp, 10 mM PEG amine, 45% (v/v) DMSO, 20μM Sa-SrtA WT); b) UPLC trace ligation mixture (100 μL, 1 mM Abz-LPETGK-Dnp, 10 mM PEG amine, 45% (v/v) DMSO, 20μM Sa-SrtA M3). Absorbance was monitored at 355 nm. Peak* is the generated product GK-Dnp. Peak** is the substrate Abz-LPETGK-Dnp.

3.4. Conclusion

Despite diverse applications of sortase-mediated site-specific conjugation reported in the past decade, few examples have implemented those conjugations under non-aqueous conditions. The latter is mainly limited by the poor resistance and low activity of sortase in non-aqueous solutions. Being able to perform

sortase-mediated conjugation in organic co-solvents not only improves the solubility of hydrophobic substrates (e.g. hydrophobic peptides, hydrophobic amines, water insoluble polymers) but also reduces the workload to separate solvents from substrates during their synthesis (e.g. remove DMF solvent after solid phase peptide synthesis (SPPS). The results we achieved prove that it is feasible to improve sortase resistance and activity in organic co-solvents by directed evolution. MD simulation studies revealed that variants M1 and M3 have increased conformational mobility and active site flexibility in 45 % (v/v) DMSO compared to the Sa-SrtA WT leading to improve sortase activity and resistance in DMSO co-solvent. Moreover, we performed sortase-mediated conjugations using millimolar concentrations of hydrophobic substrates (hydrophobic peptide and hydrophobic amines) in organic co-solvents, a process that is not feasible in aqueous media. The methodology proved its versatility in peptide-peptide ligation, peptide-amine ligation, peptide PEGylation. Based on these results, this toolbox can be implemented in polymer-protein conjugation, polymer PEGylation, and polymer functionalization. These "hybrid" polymers are needed to construct materials with integrated biological functionalities (e.g. biocompatibility, biocatalytic activity, antiviral/antimicrobial activity, ion selectivity membranes). The availability of such materials will pave the way for their utilization in various applications including medical devices, green chemistry, biosensors, water desalination, and battery technology. A prerequisite for these application potentials is an efficient introduction of biological functionalities in standard polymer synthesis routes or an efficient polymer functionalization after synthesis. In both cases, highly organic solvent resistant sortases are required for site-specific conjugations.

3.5. Materials and Methods

3.5.1 Materials

Chemical reagents and solvents with analytical grade or higher purity were purchased from Sigma-Aldrich (Hamburg, Germany), Carl Roth (Karlsruhe, Germany), and AppliChem (Darmstadt, Germany). Organic solvents, Dimethylsulfoxide (DMSO, 99.5%, AppliChem), dimethylformamide (DMF, 99.5%, AppliChem), methanol (99.8%, Sigma-Aldrich), ethanol (99.8%, Sigma-Aldrich), acetonitrile (99.8%, Sigma-Aldrich) were purchased accordingly. Peptides (or peptide derivatives) Abz-LPETGK-Dnp-NH2 (97.8%), Abz-LPETGGG-COOH (97.2%), antiviral peptide 1 and antiviral peptide 2 were purchased from Bachem (Bubendorf, Switzerland). Enzymes were all purchased from New England Biolabs (Frankfurt, Germany) or Fermentas (St. Leon-Rot, Germany). Primers used in polymerase chain reactions (PCR) were purchased from Eurofins MWG Operon. V/flat-bottom polystyrene 96-well microtiter plates and flat-bottom polypropylene 96-well microtiter plates were purchased from Greiner Bio-One GmbH, (Frickenhausen, Germany).

3.5.2. Optimization of SortEvolve screening assay in DMSO co-solvent

3.5.2.1. Determination of GGG-eGFP-LCI stability in DMSO co-solvents

GGG-eGFP-LCI was expressed and purified as reported.[109] Stabilities of GGG-eGFP-LCI in DMSO co-solvents was measured by the fluorescence intensity of eGFP in presence of different DMSO concentrations. In detail, purified GGG-eGFP-LCI was incubated (3 h, 600 rpm, room temperature, MTP shaker, TiMix5, Edmund Bühler GmbH, Hechingen, Germany) in gradient concentrations of DMSO (0 to 80% (v/v)) in buffer A (100 µL, 5 mM CaCl$_2$, 150 mM NaCl, 50 mM Tris-HCl, pH 7.5) in polypropylene microtiter plates (PP-MTP). Subsequently eGFP fluorescence was determined (Tecan infinite 1000Pro plate reader, λ_{exc} = 488 nm; λ_{em} = 509 nm, gain = 100; Tecan Group AG, Männedorf, Switzerland).

3.5.2.2. Determination of CueO-LPETGGGRR stability in DMSO co-solvent

CueO-LPETGGGRR was produced as reported.[109] Resistance of CueO-LPETGGGRR against DMSO co-solvents was evaluated by a standard 2,2'-azino-bis(3-ethylbenzothiazoline-6-sulphonic acid (ABTS, ε = 36000 M^{-1} cm^{-1}) assay. In detail, purified GueO-LPETGGGRR (50 µg/mL)) was incubated (3 h, 600 rpm, room temperature, MTP shaker, TiMix5) with gradient concentration of DMSO (0 to 80% (v/v)) in 100 µL buffer A in polypropylene microtiter plates (PP-MTP). Ten microliter liquid was transferred into 190 µL buffer B (100 mM, pH 3.0, sodium citrate) with 3 mM ABTS. Plates were stirred for 5 seconds and the absorbance was determined (420 nm (εABTS·+, 420 nm = 36,000 M^{-1}cm^{-1}), room temperature, Tecan Infinite 1000 Pro plate reader).

3.5.2.3 Optimization of DMSO concentration in the SortEvolve screening assay

SortEvolve was performed in different concentrations of DMSO with a modified protocol based on Application 1[109]. A Five-step process is included. In *Step1*, Sa-SrtA WT was expressed in MTP and clear supernatant of cell lysates were obtained as previously described.[109] Sa-SrtA containing cell-free lysates (30 µL per well) were transferred into F-bottom 96-well PS-MTPs. In *Step2*, conjugation of CueO-LPETGGGRR and GGG-eGFP-LCI was performed in F-bottom 96-well PS-MTPs (reaction mixture: 200 µL, 100 µg/mL purified GGG-eGFP-LCI, 50 µg/mL purified CueO-LPETGGGRR, different concentrations of DMSO (range from 0 to 55% (v/v) in buffer A) followed by an incubation (800 rpm, 3 h, room temperature). *Step3*, *4* and *5* were performed as aforementioned (2.5.5).[109]

3.5.2.4 Determination of coefficient of variation of SortEvolve assay in 45% (v/v) DMSO co-solvent

In order to determine the coefficient of variation of SortEvolve assay in buffer and in presence of 45% (v/v) DMSO, two 96-well MTPs containing Sa-SrtA WT were screened (in order to gain information on background, six wells contained an "empty vector" control and six wells contained the TB-expression media). Slopes of ABTS absorbance over time were analyzed. The overall activity of SortEvolve in 45% (v/v) DMSO was 60% decreased compared to activity in buffer. Coefficient of variation of SortEvolve assay in absence and presence of 45% (v/v) DMSO were calculated.

3.5.3 *KnowVolution* of Sa-SrtA towards organic solvents

The directed Sa-SrtA evolution for organic solvents was performed with a standard *KnowVolution* strategy.[73]

3.5.3.1. Diversity generation of Sa-SrtA library

A sequence saturation mutagenesis (SeSaM) library of Sa-SrtA lacking the N-terminal 59 residues (PDB code: 2KID) was generated.[110] Unless otherwise stated, the standard PCRs and the related primers in PCRs during the generation of SeSaM library were performed as reported.[101] Templates for individual steps were generated (**Figure 29a**).[111] The following phosphorothioate deoxynucleotides (dATPαS and dGTPαS) concentrations were used: A-forward library-35% (**Figure 29b**), A-reverse library-35% (**Figure 29c**), G-forward library-40% (**Figure 29d**), and G-reverse library-40% (**Figure 29e**). The final Sa-SrtA-SeSaM library was generated using 200 ng PCR products of each library (**Figure 29f**) and cloned into pET28a(+) vector via phosphorothioate-based ligase-independent gene cloning (PLICing).[86] The PCR conditions for amplification of vector backbone for PLICing were 98°C for 60 sec, 98°C for 45 sec, 55°C for 30 sec, 72°C for 3 min (25 cycles); 72°C for 10 min (one cycle). The PCR conditions for amplification of insert (Sa-SrtA-SeSaM library) for PLICing were 98°C for 60 sec, 98°C for 45 sec, 55°C for 30 sec, 72°C for 45 sec (25 cycles); 72°C for 5 min (1 cycle). Primers for PCRs are listed in Table. S1. The PLICing product of Sa-SrtA-SeSaM was transformed into chemically competent E. coli BL21 Gold (DE3). Colonies (on agar plate after transformation) from the generated SeSaM library were randomly selected for sequencing. Four Sa-SrtA wide-types were found among 13 selected colonies. Eleven mutations were found in 9 variants. Transition and transversion rates of mutations were calculated as 55% and 45%, respectively.

Table 14. List of primers for Sa-SrtA-SeSaM library generation.

Primer name	Sequence (5'-3')
F1	CGACTCACTATAGGGGAATTGTGAGCGGA

R3	CGGGCTTTGTTAGCAGCCGGATCTCAG
SeSaM_F	CACACTACCGCACTCCGTCG
SeSaM_R	GTGTGATGGCGTGAGGCAGC
SeSaM_F1	CACACTACCGCACTCCGTCGCGACTCACTATAGGGGAATTGTGAGCGGA
SeSaM_R3	GTGTGATGGCGTGAGGCAGCCGGGCTTTGTTAGCAGCCGGATCTCAG
F1_up	CGCCTGTCACCGACTCACTATAGGGGAATTGTGAGCGGA
R3_dn	GCGGACAGTGCGGGCTTTGTTAGCAGCCGGATCTCAG
Bio_SeSaM_F	[Biotin]CACACTACCGCACTCCGTCG
Bio_SeSaM_R	[Biotin]GTGTGATGGCGTGAGGCAGC
V-F_PLIC	catccgcagttcGAAAAGTAGCGTC
V-R_PLIC	ctatagtgagtcgTATTAATTTCGCGGGATCG
SaSrtA_F_PLIC	cgactcactatagGGGAATTGTGAGCGGATAAC
SaSrtA _R_PLIC	gaactgcggatgGCTCCATGC

(F: forward primer; R: reverse primer; small letters indicate phosphorothioate deoxynucleotides)

3.5.3.2. Phase I: Screening of SeSaM library in DMSO co-solvent

The generated library (1680 colonies) was transferred in 96-well polystyrene microtiter plates (V-bottom, one clone per well). Each plate contained additionally six wells with negative control (cells containing empty vector pET-28 instead of Sa-SrtA). Protein was expressed and lysate was produced as previously described.[109] For the library screening in DMSO co-solvent, each plate was screened with the optimized protocol. In brief, a five-step work flow was followed. *Step1,* an aliquot (30 μL) of library lysate from each well was transferred into in 96-well polystyrene microtiter plates (F-bottom). *Step2* Conjugation of CueO-LPETGGGRR and GGG-eGFP-LCI was performed in 96-well polystyrene microtiter plates (F-bottom, reaction mixture: 200 μL, 100 μg/mL purified GGG-eGFP-LCI, 50 μg/mL purified CueO-LPETGGGRR, 45% (v/v) of DMSO, in buffer A) followed by incubation (800 rpm, 3 h, room temperature). *Step3*, *4* and *5* were performed as previously described.[109] The activity values from negative controls were averaged as the background and subtracted in all cases. Variants with 1.16-fold or higher improved activity (compared to Sa-SrtA WT) were selected for subsequent re-screening. Rescreening was performed with six replicates per clone using the aforementioned screening protocol.

3.5.3.3. Phase II: generation and screening of site-saturation mutagenesis

SSM libraries at positions P94 and D165 were generated as previously described.[109] Primers used in new generated SSM libraries are shown in **Table 15**. *Fw SSM* and *Rev SSM* primers were used to generate Sa-SrtA at the corresponding positions. *Fw SSM D186/K196* and *Rev SSM D186/K196* were used to saturate simultaneously two sites in Sa-SrtA. To generate all SSM PCRs, the following protocol was used: 98°C for 45 sec (1 cycle); 98°C for 45 sec, 58°C for 30 sec, 72°C for 3 min 30 sec (25 cycles); 72°C for 10 min (1 cycle). PCR solutions (50 μL) for amplification consist of plasmid template (15 ng), dNTP mix (10 mM), PfuS DNA polymerase (2.5 U), and forward and reverse primer (50 μM each). Parental DNA was digested by *Dpn* I (5 U, 37°C, overnight). DpnI was heat inactivated (80°C for 20 min). PCR products were purified (PCR clean-up kit, Macherey-Nagel™, Düren, Germany) subsequently transformed into

E.coli BL-21(DE3) competent cells. One hundred and sixty-eight clones of each single-site SSM library were transferred into two 96-well polystyrene microtiter plates (V-bottom) and 504 clones of double-site SSM-D186/K196 were transferred in to six 96-well polystyrene microtiter plates (V-bottom). Cells were cultivated and lysate containing Sa-SrtA was produced using the methods described above. The aforementioned protocol for screening of SeSaM library was employed for the screening and rescreening of all the SSM libraries.

Table 15. List of primers used for the generation of site-saturation mutagenesis libraries (N includes G or T and M includes A or C)**.**

Primer Name	Sequence 5'-3'
Fw SSM R159	GACAAGTATA**NNK**GATGTTAAGCC
Rev SSM R159	GGCTTAACATC**MNN**TATACTT GTC
Fw SSM D170	GTAGAAGTTCTA**NNK**GAACAAAAGG
Rev SSM D170	CCTTTTTGTTC**MNN**TAGAACTTCTAC
Fw SSM Q172	GTTCTAGATGAA**NNK**AAAGGTAAAG
Rev SSM Q172	CTTTACCTTT**MNN**TTCATCTAGAAC
Fw SSM D186	CATTAATTACTTGTGAT**NNK**TACAATGAAAAGACAG
Rev SSM D186	CTGTCTTTTCATTGTA**MNN**ATCACAAGTAATTAATG
Fw SSM K196	GGCGTTTGGGAA**NNK**CGTAAAATCTTTG
Rev SSM K196	CAAAGATTTTACG**MNN**TTCCCAAACGCC
Fw SSM D186/K196	TTACTTGTGAT**NNK**TACAATGAAAAGACAGGCGTTTGGGAA**NNK**CGTAAAA
Rev SSM D186/K196	AAGATTTTACG**MNN**TTCCCAAACGCCTGTCTTTTCATTGTA**MNN**ATCACAAGTAA

3.5.3.4 Phase IV: recombination

Recombination of identified amino acid substitutions was conducted via site-directed mutagenesis (SDM). Primers used in SDM are listed in **Table 16**. In detail, the isolated variant Sa-SrtA D186G/K196V (M2) was used as the template to generated variants Sa-SrtA R159G/D186G/K196V (primers *Fw SDM R159G* and *Rev SDM R159G* were employed), Sa-SrtA R159T/D186G/K196V (primers *Fw SDM R159T* and *Rev SDM R159T* were employed), Sa-SrtA D165A/D186G/K196V (primers *Fw SDM D165A* and *Rev SDM D165A* were employed), Sa-SrtA D165Q/D186G/K196V (primers *Fw SDM D165Q* and *Rev SDM D165Q* were employed), Sa-SrtA D170W/D186G/K196V (primers *Fw SDM D170W* and *Rev SDM D170W* were employed) and Sa-SrtA P94S/D160N/D165A/K196T (rM4)[60] (primers *Fw SDM D160N/D165A*, *Rev SDM D160N/D165A*, *Fw SDM K196T* and *Rev SDM K196T* were employed first step)were employed). The PCR and subsequent PCR product purification were performed as described above. PCR products were purified (PCR clean-up kit, Macherey-Nagel) and subsequently transformed into *E.coli* BL-21(DE3) competent cells.

Table 16. List of primers used in the site-directed mutagenesis (N means G or T and M means A or C).

Primer Name	Sequence 5'-3'
Fw SDM R159G	GACAAGTATAGGAGATGTTAAGCCAAC
Rev SDM R159G	GTTGGCTTAACATCTCCTATACTTGTC
Fw SDM R159T	GACAAGTATAACGGATGTTAAGCCAAC

Rev SDM R159T	GTTGGCTTAACATCCGTTATACTTGTC
Fw SDM D165A	GTTAAGCCAACAGCTGTAGAAGTTCTAGATG
Rev SDM D165A	CATCTAGAACTTCTACAGCTGTTGGCTT AAC
Fw SDM D165Q	GTTAAGCCAACACAGGTAGAAGTTCTAGATG
Rev SDM D165Q	CATCTAGAACTTCTACCTGTGTTGGCTTAAC
Fw SDM D170W	GTAGAAGTTCTATGGGAACAAAAAGG
Rev SDM D170W	CCTTTTTGTTCCCATAGAACTTCTAC
Fw SDM K196T	GACAGGCGTTTGGGAAACACGTAAAATCTTTGTAG
Rev SDM K196T	CTACAAAGATTTTACGTGTTTCCCAAACGCCTGTC
Fw SDM D160N/D165A	GACAAGTATAAGAAATGTTAAGCCAACAGCTGTAGAAGTTCTAGATGAAC
Rev SDM D160N/D165A	GTTCATCTAGAACTTCTACAGCTGTTGGCTTAACATTTCTTATACTTGTC

3.5.4. FRET assay of recombined Sa-SrtA variants

Recombined variants were expressed in flask and cell-free lysate containing Sa-SrtAs were produced as previously described.[109] A fluorometric assay was employed to determine Sa-SrtA activity.[102] In short, reactions (reaction mix: 100 µL, 0.05 mM Abz-LPETGK-Dnp, 5 mM glycine-glycine-glycine (tri-glycine) in buffer A (buffer A: 5 mM $CaCl_2$, 150 mM NaCl, 50 mM Tris-HCl, pH 7.5)) were initiated by adding 1.5 µM Sa-SrtA (WT or variants). The increase in fluorescence was continuously detected (λ_{exc} = 320 nm; λ_{em} = 420 nm, gain = 100, Tecan infinite 1000Pro plate reader).

3.5.5 Characterization of Sa-SrtA WT and variants in absence/presence of 45% (v/v) DMSO

Kinetics of Sa-SrtAs was evaluated via a HPLC assay which was previously described.[60] Reactions (50 µL) were performed with 9 mM NH_2-Gly-Gly-Gly-COOH, varied concentrations of Abz-LPETG-Dnp-NH_2 (0.25 to 5 mM) and 2 µM Sa-SrtAs in buffer A (5 mM $CaCl_2$, 150 mM NaCl, 50 mM Tris-HCl buffer, pH 7.5), or 45% (v/v) DMSO co-solvent (22.5 µL DMSO, 5 mM $CaCl_2$, 150 mM NaCl, 50 mM Tris-HCl buffer pH 7.5). Reactions were performed in room temperature for 5 to 60 min before quenching with 25 µL HCl (1 M). The quenched reaction mixture was then diluted 5-times (final volume: 375 µL) with pure water. Twenty microliter of the diluted sample was injected into a reversed-phase C18 HPLC column (4.6x150 mM, 5 µM, Macherey-Nagel, Düren, Germany) and chromatographed using a gradient of 10 to 40% acetonitrile with 0. 1% TFA (trifluoroacetic acid) in 0.1% aqueous TFA over 20 minutes. Retention times for Abz-LPETG-Dnp-NH2, GK-Dnp-NH2 and Abz-LPETGGG-COOH were 15.2, 13.2 and 11.1 min, respectively. Dnp containing peaks were detected at 355 nm and Abz containing peaks were detected at 255 nm. The yield of product Abz-LPETGGG-COOH was calculated by integrating the area under HPLC trace. K_m and *kcat* were calculated using Originpro 8.6 (OriginLab, Northampton, USA).

3.5.6 Activity profiles of Sa-SrtA in diverse organic co-solvents

A fluorometric assay[102] was employed to detect Sa-SrtAs activity in DMSO, DMF, ethanol and methanol co-solvents. In short, reactions (100 μL, 0.1 mM Abz-LPETGK-Dnp, 5 mM tri-glycine in buffer A (buffer A: 5 mM $CaCl_2$, 150 mM NaCl, 50 mM Tris-HCl, pH 7.5)) with gradient concentration of DMSO, DMF, ethanol or methanol co-solvents were initiated by supplementing 1.6 μM purified Sa-SrtA enzyme (WT or variants). The fluorescence of the reaction liquid was constantly determined (λ_{exc} = 320 nm; λ_{em} = 420 nm, gain = 100; Tecan infinite 1000Pro plate). The residual activity of Sa-SrtAs in co-solvents was calculated as the ratio of activity in presence of solvent divided by activity in absence of solvent. The relative activity in co-solvent was calculated as the ratio of Sa-SrtA variant's activity divided by Sa-SrtA WT's activity.

3.5.7 Sortase-mediated protein-protein ligation in DMSO or ethanol co-solvents

The ligation of CueO-LPETGGGRR and GGG-eGFP-LCI catalyzed by Sa-SrtAs was performed in 45% (v/v) DMSO and 30% (v/v) ethanol. In short, the reaction mixture (500 μL, purified GGG-eGFP-LCI (500 μg/mL), CueO-LPETGGGRR (500 μg/mL), purified Sa-SrtA (30 μg/mL), 45% (v/v) DMSO) was incubated 14 h (room temperature, 800rpm). After ligation, an aliquot (15 μL) of reaction mixture was first diluted with 60 μL pure water and subsequently mixed with 25 μL 4x SDS loading buffer. The mixture was immediately incubated at 95°C for 5 min. Ten microliters of the samples were loaded and analyzed on 10% acrylamide gels. Similarly, reaction mixture (500 μL, purified GGG-eGFP-LCI 500 μg/mL, 250 μg/mL purified CueO-LPETGGGRR, 30 μg/mL purified Sa-SrtA, 30% (v/v) ethanol) was incubated (room temperature, 800 rpm, 14 h). An aliquot (15 μL) of reaction mixture was first diluted to 75 μL with pure water and immediately mixed with 25 μL 4x SDS loading buffer. The mixture was heated at 95°C for 5 min. Ten microliters of the samples were loaded and analyzed on 10% acrylamide gels.

3.5.8. *In silico* generation of sortase variants

Structural models of the sortase variants were designed in YASARA Structure version 13.9.8.[112-113] using the YASARA-FoldX plugin.[113] and by employing the FoldX method.[105] The starting coordinates for the FoldX [105] *in silico* mutagenesis were taken from the X-ray structure of the Sa-SrtA WT, chain A (PDB ID: 1T2P for wild type, resolution: 2 Å[114]). A FoldX mutation run including rotamer search, exploring alternative conformations (3 independent runs) were performed during the FoldX energy minimization. Stabilization energy calculation were computed with FoldX version 3.0 Beta[105] using standard settings. Calculated stabilization energy (ΔΔG) corresponds to the Gibbs free energy changes upon substitution of amino acids in unfolded and folded states compared to Sa-SrtA WT.

3.5.9. Molecular dynamics (MD) simulations

Molecular dynamics (MD) simulations were used to derive statistical properties of the water and/or co-solvents and analyze the sortase-co-solvent interactions leading to stabilization or destabilization. The main factors in MD simulation studies for describing sortase activity or resistance in DMSO/water mixtures were: (a) DMSO co-solvent-sortase interactions; (b) conformational changes of the sortase structure. We have elucidated the important properties that can differentiate the resistant and more active sortase variants (M1 and M3) from wild-type (WT) based on MD simulation results. MD simulations and analysis were performed using GROMACS 5.1.2 software.[115-119] The GROMOS96 (53a6) force field [120] was used for the simulations of sortase in water as single solvent system and co-solvent with 45% (v/v) DMSO. Chain A of crystal structures (PDB ID: 1T2P for wild type, resolution: 2 Å[114]) were taken as starting structure for simulations. The protonation states were determined with pKa estimation using PROPKA method using the PDB2PQR server.[121-123] Hydrogen atoms were added by assuming conventional protonation states of the polar side chains: Lys and Arg, positively charged; Glu and Asp, negatively charged. The *his* side chains were protonated following the analysis of their environments. The Gln and Asn amide-group rotamers were verified by an inspection of their local interactions. Structures were solvated into a cubic box of SPCE[124] water molecules using periodic boundary. Simulation box with volume of 326 nm^3 was used. The simulation box was filled with around 9886 water molecules in water system, 1185 DMSO molecules and 6343 water molecules in 45% DMSO system.

Furthermore, in order to neutralize the system, Na+ or Cl$^-$ ions were added into simulation box. Prior to simulations, energy minimization of the whole system was performed individually using steepest descent minimization algorithm until the maximum force reached to 1000.0 kJ mol^{-1} nm^{-1}. The electrostatic interactions were calculated by applying the particle mesh Ewald (PME) method.[125-126] Short-range electrostatic interactions (rcoulomb) and Van der Waals (rvdw) were calculated using a cut-off value 1.0 respectively. Subsequently, system equilibration was performed under an NVT ensemble and NPT ensemble. First, NVT equilibration was conducted at constant temperature of 300 K for 100 ps with time step of 0.002 ps. Initial random velocities were assigned to the atoms of the molecules according to the Maxwell–Boltzmann algorithm at same temperature. Second, NPT equilibration was conducted at constant temperature of 300 K for 100 ps with time step of 2 fs, respectively. The Berendsen thermostat and Parrinello–Rahman pressure coupling were used to keep the system at 300 K, time constant (τ_T) of 0.1 ps and 1 bar pressure, time constant (τ_P) of 2 ps. The production run was carried out in triplicate (run1, run2, run3) using NPT ensemble for 50 ns with time step of 2 fs at constant temperature of 300 K. The coordinates were saved every 200 ps from MD trajectories. All bonds between hydrogen and heavy atoms were constrained with the LINCS algorithm.[127]

For analyzing the different properties of our system, combined global and local sortase properties analysis was a suitable solution to achieve a deep understanding of molecular interaction between sortase and DMSO co-solvents during MD simulations. Analyses were including root mean square deviation (RMSD) of backbone atoms of the protein with respect to minimized crystal structure,[128] root mean square fluctuations (RMSF) per residues,[129] radius of gyration (Rg),[130] hydrogen-bonding,[131] secondary structure change [132], spatial distribution function (SDF),[133] solvent accessible surface areas (SASA) [134] of protein. MD trajectories and the structures were analyzed and visualized by using GROMACS analysis tools[135] and VMD 1.9.1 software.[136]

3.5.10. Sostase-mediated ligation of hydrophobic antiviral peptide AVP 0683 and Abz-LPETGK-Dnp in DMSO or DMF co-solvent

The ligation of Abz-LPETGK-Dnp and peptide AVP0683 catalyzed by Sa-SrtAs in 45% (v/v) DMSO and 30% (v/v) DMF was performed. In short, reaction solution 1 (100 μL, 1 mM Abz-LPETGK-Dnp, 3 mM peptide AVP0683, 45% (v/v) DMSO) and reaction solution 2 (100 μL, 1 mM Abz-LPETGK-Dnp, 3 mM peptide AVP0683, 30% (v/v) DMF) were incubated in black F-bottom 96-well PS-MTP. Reactions were initiated by adding 10 μM purified Sa-SrtA. Fluorescence was constantly recorded (λ_{exc} = 320 nm; λ_{em} = 420 nm, gain = 100, Tecan infinite 1000Pro plate reader). After measurement, samples from MTP was subsequently heated at 90°C for 10 min. Samples were stored in 4°C either for subsequently SDS-PAGE, HPLC or MALDI-TOF MS analysis (matrix-assisted laser desorption ionization time-of-flight mass spectroscopy). Three microliter was added into 57 μL water (20-fold dilution) and subsequently mixed with 20 μL 4x SDS loading buffer. The mixture was heated at 95°C for 5 min. Three microliters of the samples were loaded for SDS-PAGE analysis. In order to separate the fusion product Abz-LPETG-AVP0683 (theoretical molecular weight 2446.6 Dalton) from the peptide substrate AVP0683 (molecular weight 1884.7 Dalton), a modified 25% tricine acrylamide gels[137] was used. Electrophoresis was performed with a constant current at 6 mA for 18 h. HPLC of the reaction mixture was performed based on the protocol as aforementioned. In brief, 20 μL reaction mixture was then diluted 5-times (final volume: 100 μL) with pure water. Twenty microliter of the diluted sample was injected into a reversed-phase C18 HPLC column (4.6x150 mM, 5 μM, Macherey-Nagel, Düren, Germany) and chromatographed using a gradient of 10 to 40% acetonitrile with 0. 1% TFA (trifluoroacetic acid) in 0.1% aqueous TFA over 20 minutes. Dnp containing peaks were detected at 355 nm.

3.5.11. Sortase-mediated ligation of hydrophobic amines (tyramine or 4-(Trifluoromethyl)-benzylamine) and Abz-LPETGK-Dnp in DMSO co-solvent

The ligation of Abz-LPETGK-Dnp and tyramine catalyzed by Sa-SrtA WT or M3 in 45% (v/v) DMSO was performed. In short, reaction 1 (100 µL, 10 mM tyramine (M_w = 137.18 da, solubility in pure water $\cong$ 50 mM), 1 mM Abz-LPETGK-Dnp, 20 µM Sa-SrtA, 45% (v/v) DMSO) and reaction 2 (100 µL, 10 mM 4-(Trifluoromethyl)-benzylamine (4-TFB amine, M_W=175.15 da, solubility in pure water $\cong$ 5 mM), 1 mM Abz-LPETGK-Dnp, 20 µM Sa-SrtA, 45% (v/v) DMSO) were performed. Fluorescence was constantly recorded (λ_{exc} = 320 nm; λ_{em} = 420 nm, gain = 100, Tecan infinite 1000Pro plate reader). Reaction was subsequently quenched with HCl (100µL, 500 mM). Quenched sample (2 µL) was analyzed by ultra-performance liquid chromatography mass spectrum (UPLC-MS, Waters ACQUITY UPLC*). Samples were chromatographed using a gradient of 10 to 90% acetonitrile with 0. 1% TFA (trifluoroacetic acid) in 0.1% aqueous TFA over 15 minutes. Absorbance of samples was monitored, due to the optimized absorbance of Dnp group at 355 nm. The theoretical molecular weight of generated conjugates Abz-LPET-tyramine and Abz-LPET-4-TFB are 697.38 and 735.32 da, respectively.

3.5.12. Sortase-mediated PEGylation of hydrophobic peptide Abz-LPETGK-Dnp in DMSO co-solvent

The ligation of Abz-LPETGK-Dnp and O-(2-Aminoethyl) polyethylene glycol (PEG amine, M_P=5000 da) catalyzed by Sa-SrtA WT and M3 in 45% (v/v) DMSO was performed. In short, reaction (100 µL, 10 mM PEG amine (M_P=5000 da), 1 mM Abz-LPETGK-Dnp, 20 µM Sa-SrtA, 45% (v/v) DMSO) was performed. Fluorescence was constantly recorded (λ_{exc} = 320 nm; λ_{em} = 420 nm, gain = 100, Tecan infinite 1000Pro plate reader). Reaction was quenched with HCl (100µL, 500 mM) and aliquots (2 µL) were analyzed by UPLC as aforementioned.

4. Chapter IV: A platform for covalent enzyme immobilization on surface of stimuli microgels via sortase-mediated ligation

4.1. Declaration

The work described in this chapter was performed in cooperation with PhD fellow Elisabeth Gau from the group of Prof. Dr. Andrij Pich group. Microgel synthesis, microgel characterizations were done by Elisabeth Gau from Prof. Dr. Andrij Pich group. Enzymes production, sortase-mediated enzyme immobilization on surface of microgel, activity profiles of immobilized enzymes (e.g kinetics, solvent resistance, pH dependent profile, storage/thermo stabilities and reusability studies) and application of immobilized enzyme in decolourization of dyes were done by me.

4.2. Enzyme immobilization: challenges and applications

Enzymes are known as the sustainable, green and high selective biocatalysts which have been widely used in biotechnological industries.[138] However, due to the complex molecular structure of enzymes, maintenance of their catalytic performances (e.g. activity, shelf life and reusability) during biochemical reactions *in vitro* is highly challenging.[139-140] Immobilizations of enzymes enable easy handing, enhanced activity/stability, facile separation, and continuous usability in biological reactions which well suit for the demands in industrial applications.[138, 141]

When an immobilization of enzyme is panned, two basic decisions should be considered: The selection of the carrier and the method of attachment. Selection of an appropriate carrier is governed by properties both from the enzyme and the carrier. Materials such as silica, acrylic/exchange resins, membranes and polymers are used as carriers for immobilization.[140] An appropriate carrier should have minimized interfere with the native structure of the enzyme and offer an aqueous environment for enzyme to survive. Microgels, the cross-linked "smart" particles (hydrogels range in micrometer size) are employed as carriers for enzymes due to their stimulus-responsive (e.g. temperature, pH, light and ionic strength)[142-143] and high water holding capacity (around 99% (w/w)) properties.[144] *N*-Vinylcaprolactam (N-VCL) has a low critical solution temperature (LCST) (at 32 °C in aqueous phase) and high biocompatible properties which is commonly used as a monomer for the synthesis of microgel particles (Poly (*N*-vinylcaprolactam) (PVCL)).[145-146] On the basis of these facts, an array of applications including drug delivery[147-149], biomolecules purification[150], enzyme immobilization,[151] tissue engineering[152] have been reported based on PVCL microgels. Among those applications, drugs and biomolecules are generally entrapped in the

Chapter IV: A platform for covalent enzyme immobilization on surface of stimuli microgels via sortase-mediated ligation

PVCL microgels with non-covalent attachment. Few examples have reported which covalently and site-specifically attached the target cargos on the surfaces of PVCL microgel.

Four methods namely, physical adsorption, entrapment, cross-linking and covalent bonding are used for the attachment of enzyme to carrier.[138, 153-155] None of these methods is applicable for all enzymes and carriers. Decisions of attachment are usually made after considering many factors (e.g. the properties of enzyme, the availability of carriers and the operability in applications).[141] Covalent binding is widely used since the covalent bond prevents less leaching of enzyme and allows more reusable cycles than other immobilization methods.[141] In general, bond-forming reactions between enzyme and carrier usually achieved via the side chain groups (e.g. ε-amino group from lysine residue, thiol group from cysteine residue, and carboxylic group from aspartic/glutamic acids residue).[140] As aforementioned, the main challenge remains is the low site-specificity when high number of side chain groups within the target enzyme. The undesired ligations might change the structure or orientation of enzyme, and subsequently lose its activity.[96] Enzyme-mediated ligation provides ideal solutions when high site-specific ligations are required.[93] In the past decade, sortase-mediated ligation (SML) has emerged as a powerful site-specific tool-box to attach proteins (e.g. enzyme, antibody) to different supports.[44, 156-158]

We have previously reported the covalent functionalization of LPETG tagged PVCL/GMA (PVCL/GMA-LPETG) surface with N-terminal GGG tagged enhanced green fluorescent protein (GGG-eGFP) via sortase-mediated ligation (SML).[159] Those positive results have motivated us to further explore the SML in enzymes immobilization on surface of PVCL/GMA microgels. In order to establish a general platform for immobilization of enzymes by using SML tool-box, developing more flexible ligation strategies (e.g. C- or N-terminus ligation), providing more versatilities (e.g. as many as enzyme species to be immobilized) and performing a higher grafting efficiency (cell-free lysate instead of purified protein as substrates) are prerequisite.

In this work, we reported two strategies to graft enzymes to PVCL/GMA either at N- or C-terminus (**Figure 57**). GGG tagged PVCL/GMA (GGG-PVCL/GMA) was synthesized, in addition to PVCL/GMA-LPETG as previously reported.[159] C-terminus ligation of enzymes has performed by ligation of LPETG tagged enzymes to GGG-PVCL/GMA (**Figure 57,** upper) microgel and N-terminus ligation of enzymes has performed by ligation of GGG tagged enzymes to PVCL/GMA-LPETG microgel (**Figure 57,** bottom). The versatility of the immobilization platform have been demonstrated by grafting five different enzymes (*Bacillus subtilis* lipase A (BSLA[100]), *Yersinia mollaretii* phytase (Ym phytase[79]), *E.coli* CueO laccase,[87] cellulase A2 M2[160] and monooxygenase P450 BM3 (F87A) from *Bacillus megaterium*[161]) which have varied molecule sizes (molecular weight range from 20 to 120 kDa) and

catalytic properties on PVCL/GMA microgel. GGG or LPETG tagged enzymes in cell-free lysate instead of purified enzymes were employed and site-specifically immobilized on PVCL/GMA microgels by a highly active sortase A variant rM4 (P94S/D160N/D165A/K196T) with a 80-fold improved catalytic efficiency compared to sortase A wild-type.[60] After immobilization, generated CueO-LPETGGG-PVCL/GMA and PVCL/GMA-LPETGGG-his-P450 BM3 F87A conjugates were subjected to kinetics, solvent resistance, pH dependent profile, storage/thermo stabilities and reusability studies. Furthermore, the CueO-LPETGGG-PVCL/GMA was employed in decolourization of aromatic dyes (e.g. Indigo Carmine and Methyl Orange) which showed potential applications in waste water treatment.
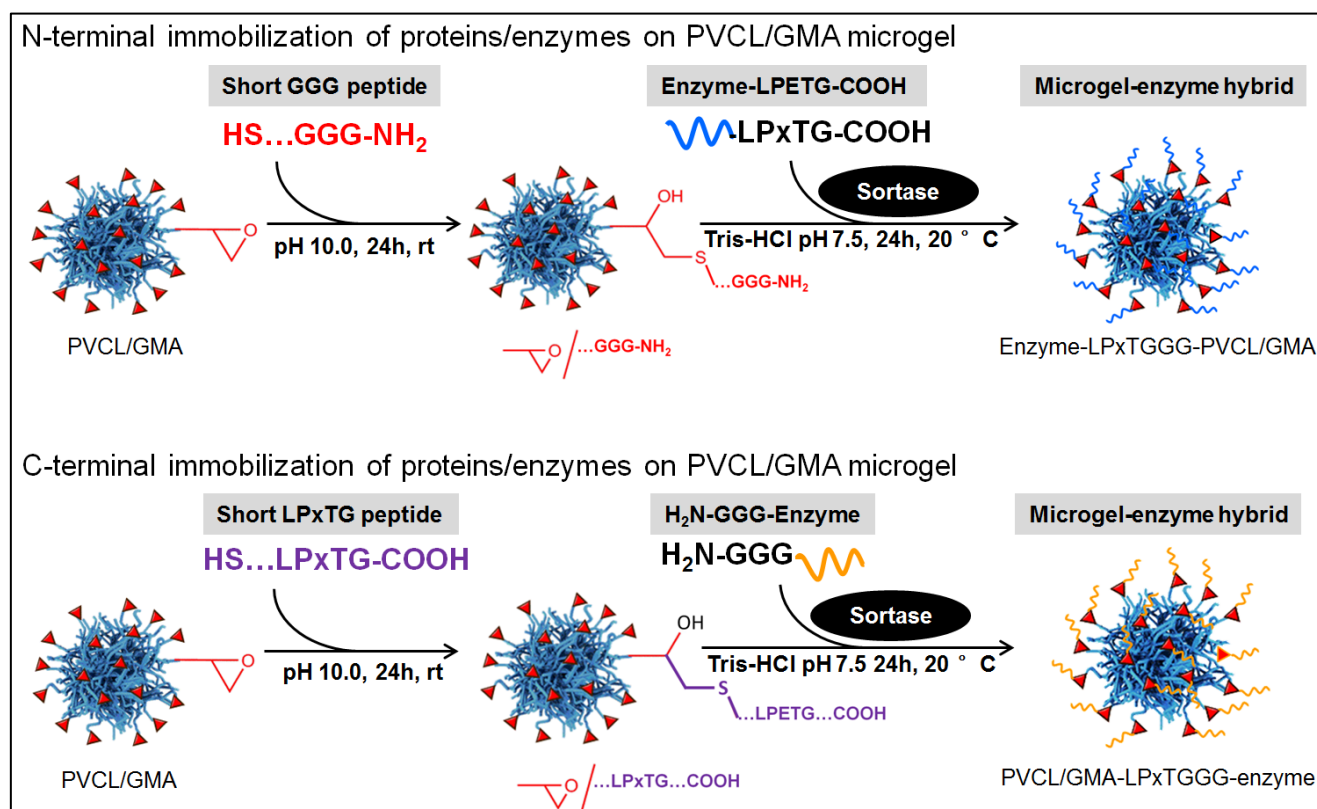
Figure 57. Schematic representation of sortase-mediated immobilization of enzymes at C-terminus (upper) or N-terminus (bottom) on surface of microgel particles.

4.3. Results and discussions

The work was carried out in four main sections. In the first section, proteins and microgels with sortase recognized motifs were produced (4.3.1-4.3.2). In the second section, sortase-mediated immobilizations of enzymes on surface of microgel were performed (4.3.3). Activity kinetics of immobilized CueO laccase and P450 BM3 monooxygenase were characterized (4.3.4). In the third section, activity profiles of immobilized CueO laccase and P450 BM3 monooxygenase were investigated in organic co-solvent (4.3.5) and different pH (4.3.6). Meanwhile, thermostabiliy (4.3.7), storage stability (4.3.8) and

reusability (4.3.9) were measured. In the last section, application of immobilized CueO laccase in decolourization of synthetic dyes was implemented (4.3.10).

4.3.1. Production of GGG and LPETG-tagged enzymes

Incorporation of GGG and LPETGGGRR coded DNA sequence in the N- or C-terminus of enzyme genes was performed by overlapping PCR (see 4.4.1). Plasmids containing the target genes were transformed into corresponding *E.coli* competent cells.

GGG-his-BSLA, GGG-Ym-phytase, CueO-LPETGGGRR, GGG-CelA2 M2, GGG-his-P450 BM3 F87A and P450 BM3-LPETGGGRR F87A were successfully expressed (**Figure 58**). Furthermore, GGG-CelA2 M2, CueO-LPETGGGRR and GGG-his-P450 BM3 F87A were purified (**Figure 58 c/d/e**). No visible expression of GGG-CueO was observed (data is not shown).
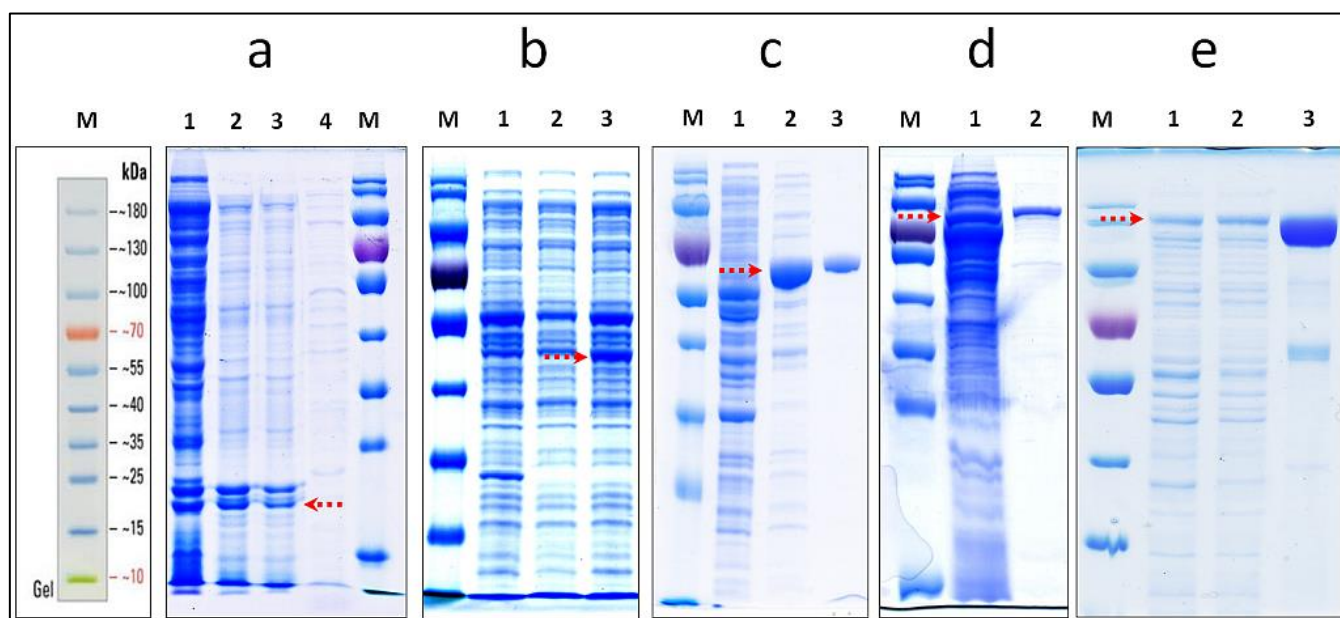
Figure 58. Expression of GGG- and LPETG-tagged enzymes. a) Expression of GGG-his-BSLA. Line 1: supernatant of GGG-his-BSLA cell lysate; line 2-4, elution fragments of GGG-his-BSLA during his-tag based purification. Expected size of GGG-his-BSLA is 20.7 kDa. b) Expression of GGG-Ym-phytase. Line 1: cell lysate of *E.coli* harboring pET-22b empty vector; line 2: pellet of Ym-phytase lysate; line 3: supernatant of GGG-Ym-phytase lysate. Expected size of GGG-Ym-phytase is 47.5 kDa. c) Expression of CueO-LPETGGGRR. Line 1: cell lysate of *E.coli* harboring pET-22b empty vector; line 2: supernatant of CueO-LPETGGGRR cell lysate; line 3: purified CueO-LPETGGGRR after Strep-tag based purification. Expected size of CueO-LPETGGGRR is 55.9 kDa. d) Expression of GGG-CelA2 M2. Line 1: supernatant of GGG-CelA2 M2 cell-free lysate; line 2: purified GGG-CelA2 M2. Expected size of GGG-CelA2 M2 is 71.5 kDa. e) Expression of GGG-his-P450 BM3 F87A and P450 BM3-LPETGGGRR F87A. Line 1: supernatant of GGG-his-P450 F87A cell-free lysate; line 2: supernatant of P450 BM3-LPETGGGRR F87A cell-free lysate; line 3: purified GGG-his-P450 BM3 F87A. Expected sizes of GGG-his-P450 BM3 F87A and P450 BM3-LPETGGGRR F87A are 118.9 and 119.6 kDa, respectively.

Enzymatic activities of GGG- and LPETG-tagged enzymes in cell-free lysate were determined (**Figure. 59**). GGG-his-BSLA, GGG-Ym-Phytase, GGG-CelA2 (M2), CueO-LPETGGGRR (see **figure 14** in chapter II) and GGG-his-P450-BM3 F87A) showed comparable activity ($\geq$ 80%) when compared to the corresponding "parent" enzyme. An exception is found for P450 BM3-LPETGGGRR F87A in which the

incorporation of LPETGGGRR in the C-terminus had significantly decreased the activity (only 30% activity retained, **Figure 59d**). The reason might be that the fused LPETGGGRR at C-terminus blocks the binding of NADPH (cofactor of P450 BM3) since it is in a close proximity to the binding site.[162] Information regarding the molecular weight (Mw), isoelectric point (pI) and Zeta potential (in 50 mM, pH 7.5, Tris-HCl buffer) of GGG- and LPETG- tagged enzymes are summarized in **Table 17**.
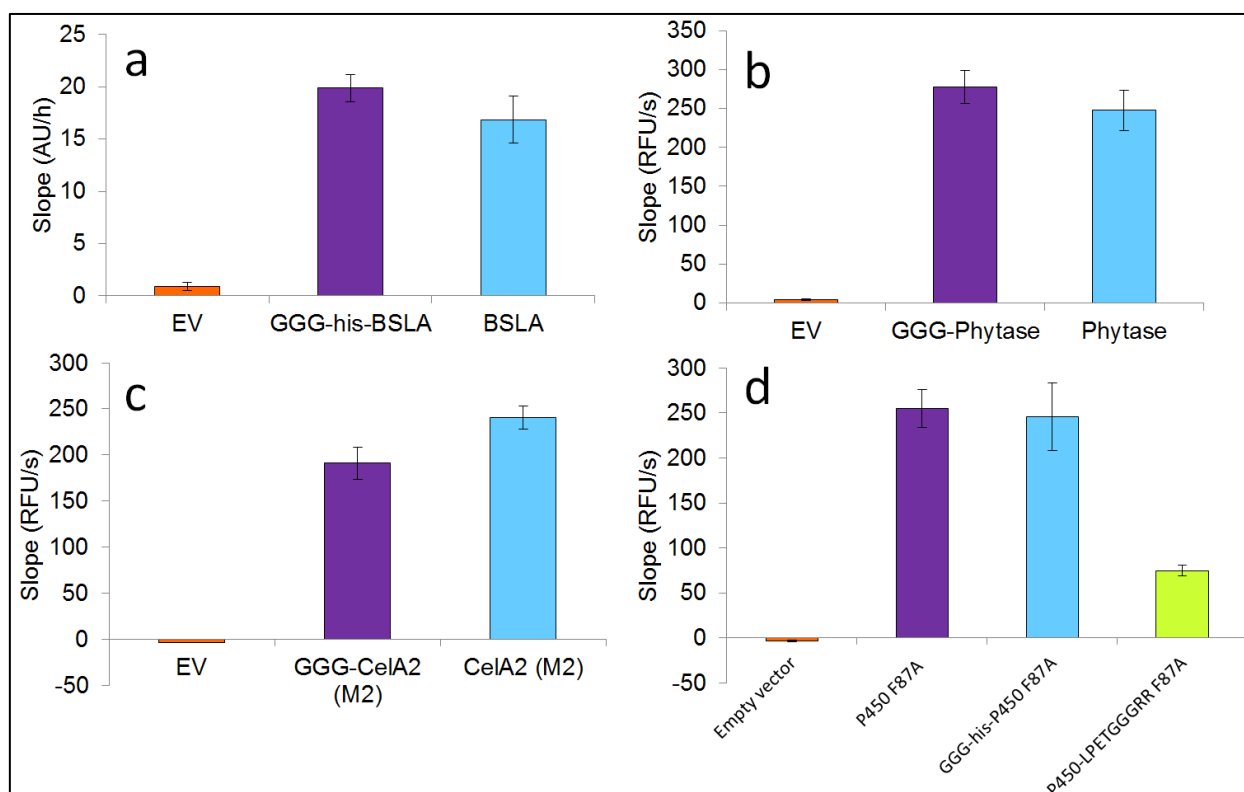
Figure 59. Activity of GGG- and LPETG-tagged enzymes. a): Activity measurements of *Bacillus subtilis* lipase A (BSLA) with pNPB as substrate; b) Activity measurements of *Yersinia mollaretii* phytase with 4-MUP as substrate; c): Activity measurements of cellulase A2 M2 variant (CelA2 (M2)) with 4-MUP as substrate; d) Activity measurements of monooxygenase P450-BM3 F87A with BCCE as substrate. All assays were performed with enzymes in cell-free lysate as catalyst. Protocols are described as aforementioned.

Table 17. Theoretical molecular weight (Mw), isoelectric point (pI) and detected Zeta potential (in 50 mM, pH 7.5, Tris-HCl buffer) of GGG- and LPETG- tagged enzymes

Enzymes	Molecular weight (kDa)	Isoelectric point (pH)	ζ-potential (mV)
GGG-his-BSLA	20.7	9.05	/
GGG-Ym-phytase	47.5	6.59	/
CueO-LPETGGGRR	55.9	6.1	-18.80 ± 4.56
GGG-CelA2 M2	71.7	4.45	-11.31 ± 2.78
GGG-his-P450 BM3 F87A	118.8	5.34	-7.83 ± 2.21
P450 BM3-LPETGGGRR F87A	119.6	5.37	/

4.3.2. Synthesis of pVCL/GMA-LPETG and GGG-pVCL/GMA microgels

PVCL/GMA microgel containing 5 mol % GMA in the microgel shell and thus carrying accessible epoxy groups for post modification reactions on the microgel surface were synthesized and characterized like described earlier.[159] The epoxy groups were used in the next step for the coupling of the LPETG and GGG-peptide sequence via thiol-epoxy reaction between a cysteine residue in the peptide sequence and the GMA in the microgel shell (**Figure 60a**). Due to the pK_a of the thiol group in the cysteine being 8.3, the reaction is performed in basic media (Tris-HCl buffer 50 mM, pH 10.0). The synthesis of pVCL/GMA-LPETG was performed as previously described.[159]
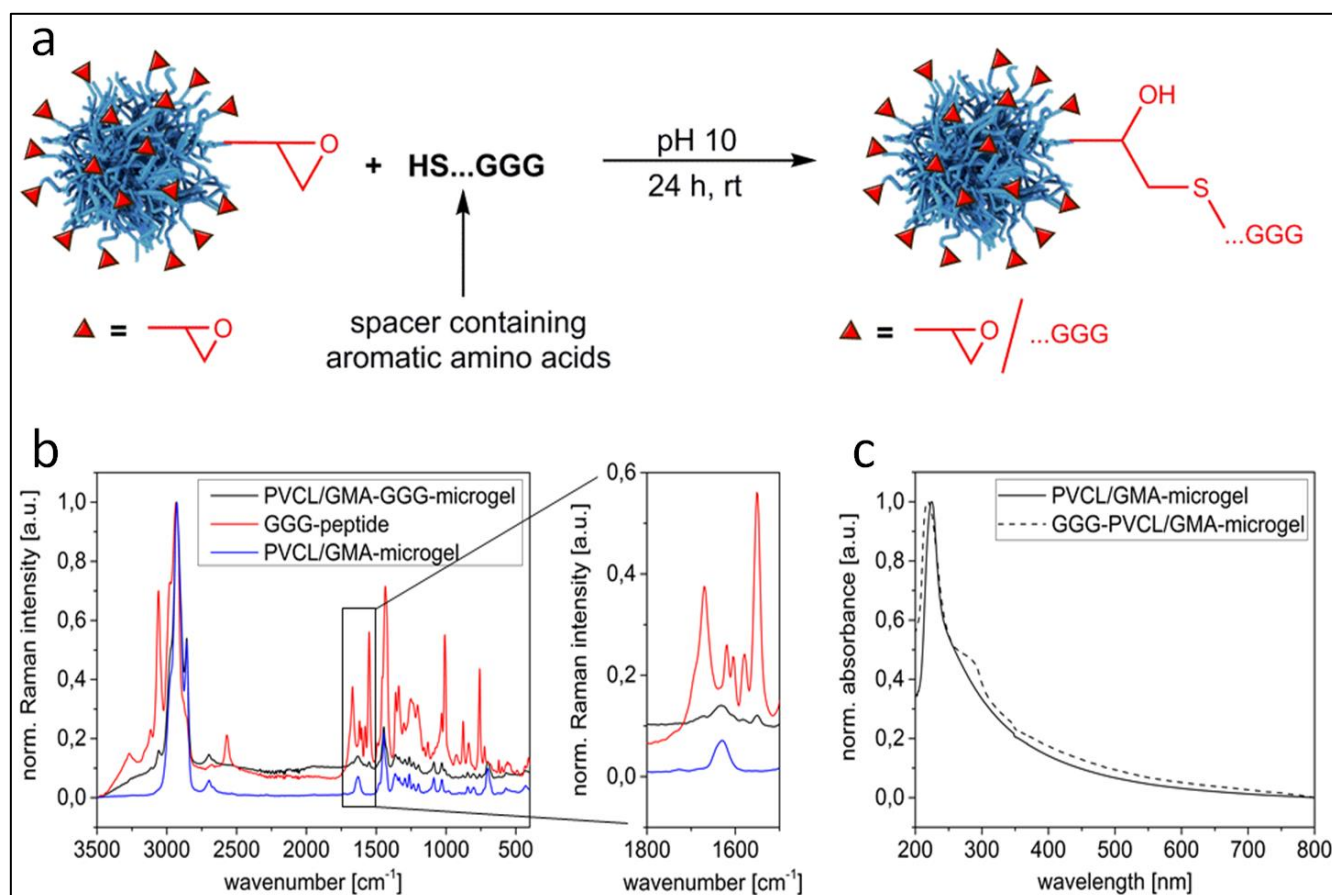
Figure 60. a) Coupling of the GGG peptide sequence to the PVCL/GMA microgel. b) Raman spectra of the GGG-PVCL/GMA microgel-peptide construct, the GGG-peptide sequence and the pure PVCL/GMA microgel (left) and UV/Vis spectra of the GGG-PVCL/GMA and the pure PVCL/GMA microgel (right).

UV/Vis and Raman spectroscopy were employed to detect the coupling of the GGG-peptide (full amino acid sequence: GGGRPWFWGMHC-OH) and PVCL/GMA microgel. Regarding Raman spectroscopy (**Figure 60b**) the spectrum for the GGG-PVCL/GMA microgel construct (black line) shows the characteristic bands for phenylalanine and tryptophan in the region from $\nu = 1666$ cm^{-1} to 1578 cm^{-1}. Besides, the band for the thiol group from the cysteine residue being present in the spectrum of the peptide sequence (red line) at $\nu = 2569$ cm^{-1} is disappeared in the spectrum of the microgel-peptide

construct, indicating successful coupling of the epoxy to the thiol groups. The successful synthesis of GGG-PVCL/GMA microgel was also monitored by UV/Vis spectroscopy (**Figure 60c**). The spectrum for the pure microgel shows only one single peak at a wavelength of ca. 220 nm, while the spectrum for the GGG-tagged PVCL/GMA exhibits a clearly visible shoulder at 280 nm. This band is characteristic for aromatic compounds and belongs to the phenylalanine and tryptophan residues being present in the peptide sequence spacer.

Furthermore, hydrodynamic radius of GGG-PVCL/GMA conjugate was measured by dynamic light scattering (DLS). The hydrodynamic radius (Rh) of the microgel GGG-PVCL/GMA is increased to 308.7 ± 13.1 nm (PDI =0.453, 20 °C) when compared to 273.8 ±0.5nm (PDI = 0.067, 20 °C) of PVCL/GMA. A 50 nm enlargement in partial size was achieved through the conjugation of the GGG-peptide sequence on the surface (**Table 18**).

Table 18. Hydrodynamic radii, PDI values and Zeta-Potential of the PVCL/GMA and the PVCL/GMA-LPETG tagged microgels

	PVCL/GMA	PVCL/GMA-LPETGGRR	GGG-PVCL/GMA
hydrodynamic radius (nm)	273.80 ± 0.50 (253.80 ± 4.11)*	276.5 ± 1.09*	308.7 ± 13.1
PDI	0.067 (0.038)*	0.061*	0.453
ζ-potential (pH 7.5) [mV]	-2.82 ± 1.12	9.70 ± 3.01*	*-0.82*

4.3.3. Sortase-mediated enzyme immobilizations on surface of PVCL/GMA microgels

Two strategies have been designed to immobilize enzymes (in cell-free lysate) either at the N- or C-terminus via sortase-mediated ligation (Figure 57). C-terminal immobilization of enzymes was implemented by grafting LPETGGGRR tagged enzymes (CueO-LPETGGGRR and P450 BM3-LPETGGGRR F87A) to GGG-PVCL/GMA. N-terminal immobilization of enzymes was implemented by conjugate GGG tagged enzymes (GGG-his-BSLA, GGG-Ym-phytase, GGG-CelA2 M2, GGG-his-P450 BM3 F87A) to PVCL/GMA-LPETGGRR. Activity of enzyme immobilized PVCL/GMA-LPETGGRR and GGG-PVCL/GMA were measured with corresponding protocols (see 4.4.4). Results are given in Figure 61 and 62. In all cases, activities were observed in negative controls. The reason might be explained that the cross-linking structure of gel particles enables the unspecific entrapment of enzymes. Nevertheless, highest activities were generally (except the BSLA experiments) observed in ligation samples when compared to controls. The results indicate that sortase A can specifically recognize the GGG or LPETG substrates in cell-free lysate and fused them to corresponding microgels. Interestingly, activities in control 2 (which no sortase employed) are always higher those in control 1 (which non tagged

PVCL/GMA was employed). The higher activity in control 2 might be achieved by the charge interactions between the target enzymes (negative charged in pH 7.5, **Table 17**) and the PVCL/GMA-LPETGGRR (positive charged, zeta potential = 9.70 ± 3.01 (mV), **Table 18**). Another finding is that the activity enhancement in sortase-mediated immobilization samples (compared to the controls) is highly dependent on the molecular size of the immobilized enzyme. Higher enhancements in activity were obtained when large size enzyme was immobilized (**Figure 61**). These results indicate that small size enzymes are more easily entrapped by cross-linking PVCL/GMA particles which lead more unspecific binding besides the sortase-mediated covalent binding. To emphasize the sortase-mediated covalent binding rather than the unspecific entrapment, immobilizations with highest enhancements (immobilization of GGG-his-P450 BM3 F87A to PVCL/GMA-LPETGGRR (**Figure 60d**), immobilization of CueO-LPETGGGRR to GGG-PVCL/GMA) were selected for further investigation. (**Figure 61a**)
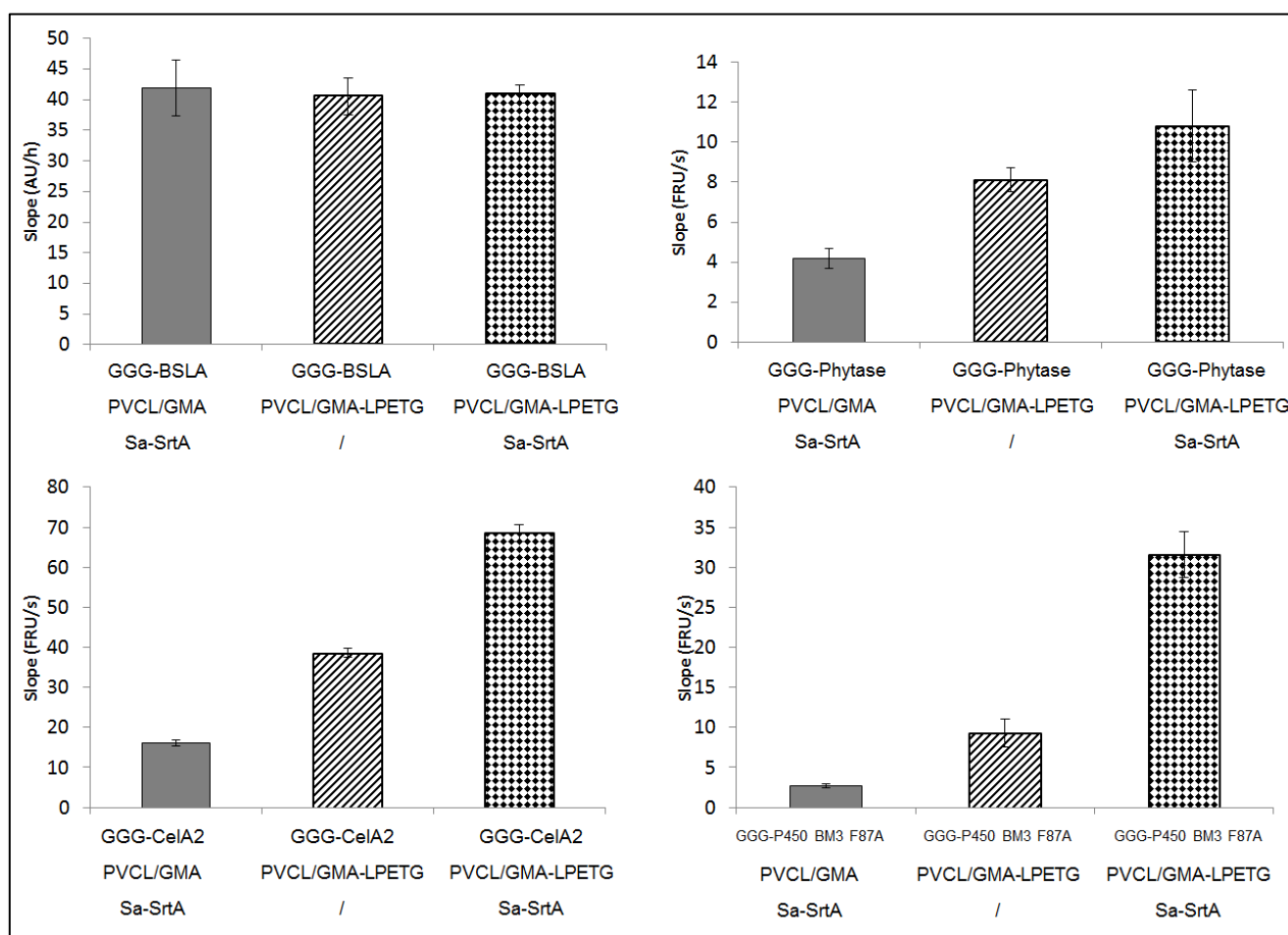
Figure 61. Enzymatic assays of N-terminal immobilized enzymes on PVCL/GMA microgels. Two controls were performed for each experiment. In first control, non-LPETG tagged PVCL/GMA was used; in the second control, no sortase was used. Enzymatic assays were performed as described in 4.4.6.
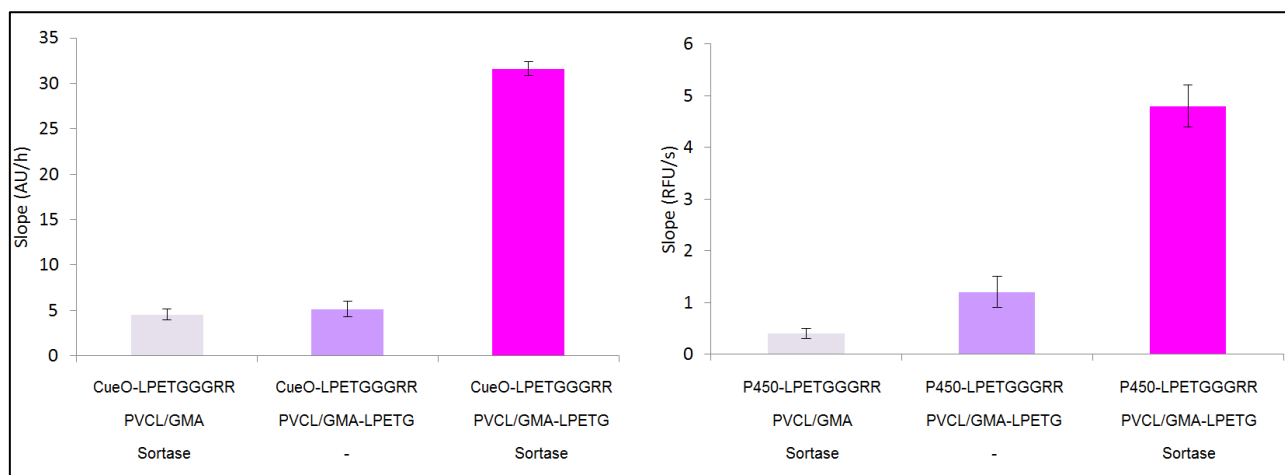
Figure 62. Enzymatic assays of C-terminal immobilized enzymes on PVCL/GMA microgels. Two controls were performed for each experiment. In first control, non-GGG tagged PVCL/GMA was used; in the second control, no sortase was used. Enzymatic assays were performed as described in 4.4.6.

4.3.4. Characterization of immobilized enzymes

Purified GGG-his-P450 BM3 F87A and CueO-LPETGGGRR were immobilized to PVCL/GMA-LPETGGRR and GGG-PVCL/GMA respectively (see protocol in **4.4.7**) in order to minimize the unspecific entrapment /absorption of unknown protein. The latter may interference the concentration measurement of target enzymes.

Immobilized amount of enzyme on microgels was detected using BCA assay. Absorbance curves of bovine serum albumin (BSA) supplemented with GGG-PVCL/GMA (**Figure 63a**) or PVCL/GMA-LPETGGGRR (**Figure 63b**) were generated and used as the standards for calculating the amount of immobilized proteins. The immobilized amount of CueO-LPETGGG on per milligram of GGG-PVCL/GMA is 1.6 μg. The immobilized amount of GGG-his-P450 F87A on per milligram of PVCL/GMA-LPETG is 2.2 μg (details are shown in 4.4.7).
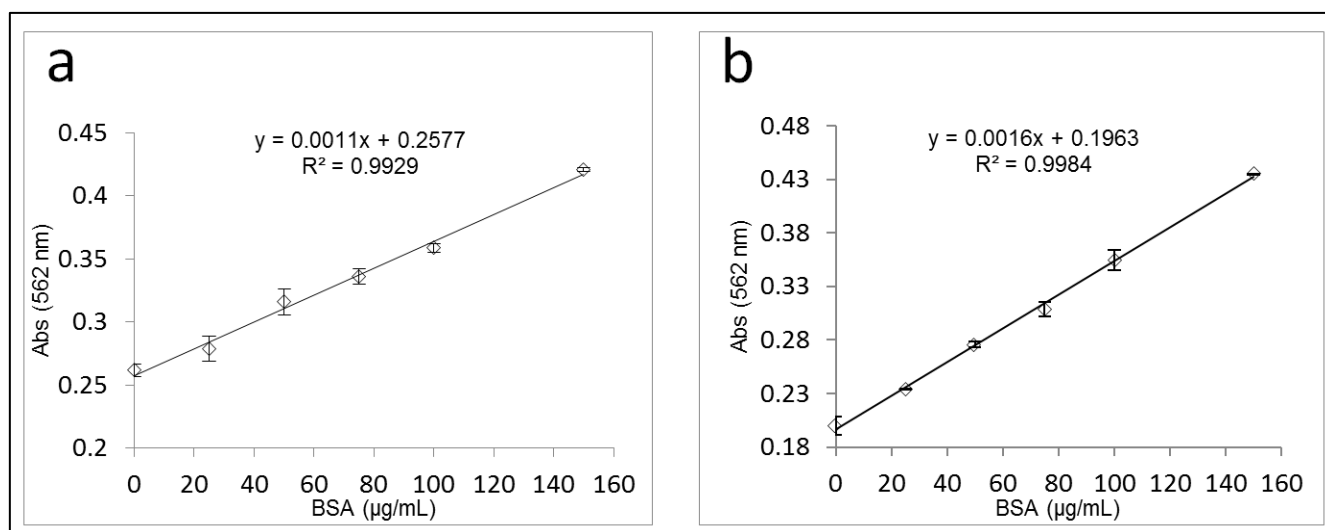
105

Chapter IV: A platform for covalent enzyme immobilization on surface of stimuli microgels via sortase-mediated ligation

Figure 63. Standard curves of BSA in microgel solutions. a) BSA was incubated with GGG-PVCL/GMA; b) BSA was incubated with PVCL/GMA-LPETGGGRR. BCA assays were perfomed accroding to the manufacture's protocol. The OD_{600} of microgels were set at 1.0

Characterizations of CueO-LPETGGGRR and CueO-LPETGGG-PVCL/GMA were performed with gradient concentrations of ABTS as substrate. In comparison to CueO-LPETGGGRR, the Michaelis constant (K_m) of CueO-LPETGGG-PVCL/GMA is increased (**Figure 64, Table 19**). The higher K_m indicates a lower affinity of enzyme towards substrate after immobilization. It is supposed that the immobilized enzymes have restricted flexibility/substrate accessibility to the active site which therefore leads to low affinity.[163] Interestingly, the k_{cat} (turnover numbers) for CueO-LPETGGG-PVCL/GMA gained 1.26-fold (**Table 19**) with respected to the CueO-LPETGGGRR. The superior activity of CueO-LPETGGG-PVCL/GMA may be attributed to the stabilization of enzyme structure through the covalent binding as well as the corrected alignment of enzymes.[164] Immobilized enzyme with improved activity were previously reported.[165] Overall, CueO-LPETGGG-PVCL/GMA represented 45% catalytic efficiency (k_{cat}/K_m) when compared to the free enzyme CueO-LPETGGGRR.
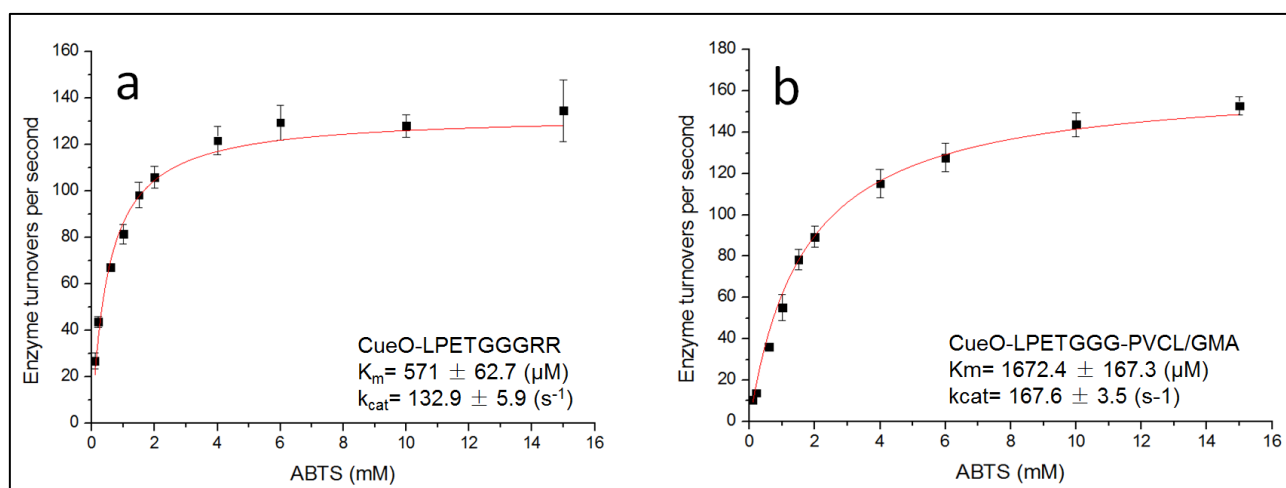

Figure 64. Plots to determine the kinetics (K_m and k_{cat}) of free (a) and immobilized CueO (b).

Kinetics of GGG-his-P450 BM3 F87A, PVCL/GMA-LPETGGG-his-P450 BM3 F87A was investigated. In the BCCE based FRET assay, a fluorescence product 3-CCE was produced (**Figure 65a**).[81] Firstly, a standard curve of 3-CCE regarding the fluorescence upon its concentration is generated (**Figure 65b**). Based on standard curve and the obtained fluorescence slope of the free and immobilized P450 BM3 F87A in BCCE assay, K_m and k_{cat} were calculated. A comparable k_{cat} of free P450 BM3 F87A was obtained in comparison to previously study (**Table 19**, **Figure 65c**).[81] However, the k_{cat} of immobilized GGG-his-P450 BM3 F87A is 5.0-fold decrease (**Table 19, Figure 65d**) when compared to free enzyme. One reason is that GGG-his-P450 BM3 F87A lost activity during the immobilization (20°C, 24h, **Table 21**). Storage stability (see **Figure 69b**) proved that of GGG-his-P450 BM3 F87A lost activity during incubation. The full-length P450 BM3 consists of an N-terminal heme domain and a C-terminal reductase

domain which are connected with a flexible linker region.[166] The heme domain has reported with multiple conformations which contribute to the highly efficient catalysis for the enzyme.[166] Another reason for significant decrement of k_{cat} likely to be the immobilization by heme domain reduced its conformational flexibility and lead to the loss of activity P450 BM3.[167] Few examples have reported for immobilization of P450 BM3 with high activity due to its complex structure.[168] Overall, the GGG-his-P450 BM3 F87A retained 35% catalytic efficiency (k_{cat}/K_m) after immobilization on PVCL/GMA-LPETGGRR microgel.
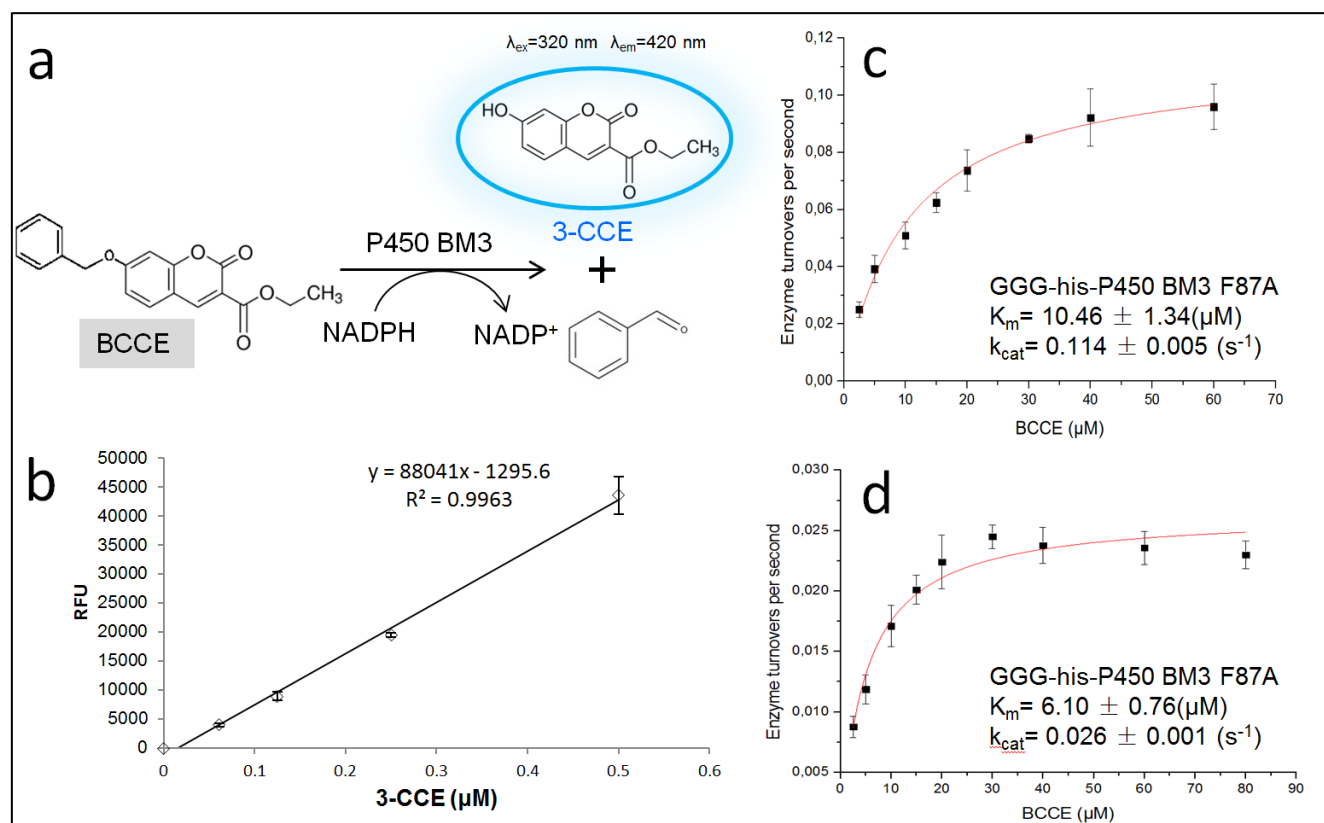
Figure 65. Kinetics measurements for GGG-P450 BM3 (F87A) monooxygenase. a) Scheme of P450 BM3 catalyzed FRET assay using BCCE as substrate, b) Standard curve of 3-CCE (the generated fluorescent product in P450 BCCE assay) between concentrations and relative fluorescence. Plots to determine the kinetics (K_m and k_{cat}) of free (c) and immobilized GGG-P450 BM3 (F87A) (d).

Table 19. Kinetic parameters of free and immobilized enzymes (CueO laccase and P450 BM3 monooxygenase).

Enzyme	K_m (µM)	k_{cat} (s^{-1})	k_{cat}/K_m (s^{-1}· µM^{-1})
CueO-LPETGGGRR (free)	571 ± 62.7	132.9 ± 5.9	0.233
CueO-LPETGGG-PVCL/GMA (immobilized)	1672.4 ± 167.3	167.6 ± 3.5	0.101
GGG-his-P450 BM3 F87A (free)	10.46 ± 1.34	0.114 ± 0.005	0.0109
PVCL/GMA-LPETGGG-his-P450-BM3 F87A (immobilized)	7.10 ± 0.76	0.026 ± 0.001	0.0037

4.3.5. Activity profiles of immobilized enzymes in DMSO co-solvent

Effect of organic solvent towards free and immobilized enzymes was studied. Activity profiles of CueO-LPETGGGRR and CueO-LPETGGG-PVCL/GMA were investigated under a broad DMSO concentration

range (0-70 % (v/v)). CueO-LPETGGG-PVCL/GMA (immobilized CueO) showed higher residual activity (resistance) compared the free enzyme CueO-LPETGGGRR in presence of DMSO co-solvent (**Figure 66a**). More than 3-fold improved resistances of immobilized CueO were observed (versus free enzyme) when 55% or higher concentrations of DMSO were used. Likewise, PVCL/GMA-LPETGGG-his-P450 BM3 F87A presented higher resistance compared the GGG-his-P450 BM3 F87A (free enzyme) in DMSO co-solvent (0-25 % (v/v), **Figure 66b**). Impressively, up to 4-fold improved resistances were observed when 15% or higher concentrations of DMSO were used. The replacements of DMSO molecules instead of the essential water molecules on the enzyme surface or active sites lead to the structure changes and loss of activity.[169] Especially, our previous studies revealed that DMSO molecule was in competition with the active-site water molecule. The ability of the DMSO molecule to coordinate the haem iron decreases the activity of P450 BM3 F87A.[170] When enzyme is immobilized on microgel surface, lower accessibility of DMSO is supposed and therefore higher resistance is expected. The gained resistances in organic co-solvents offer potential applications of immobilized laccase/P450 BM3 in chemical synthesis of compounds when co-solvent is involved.
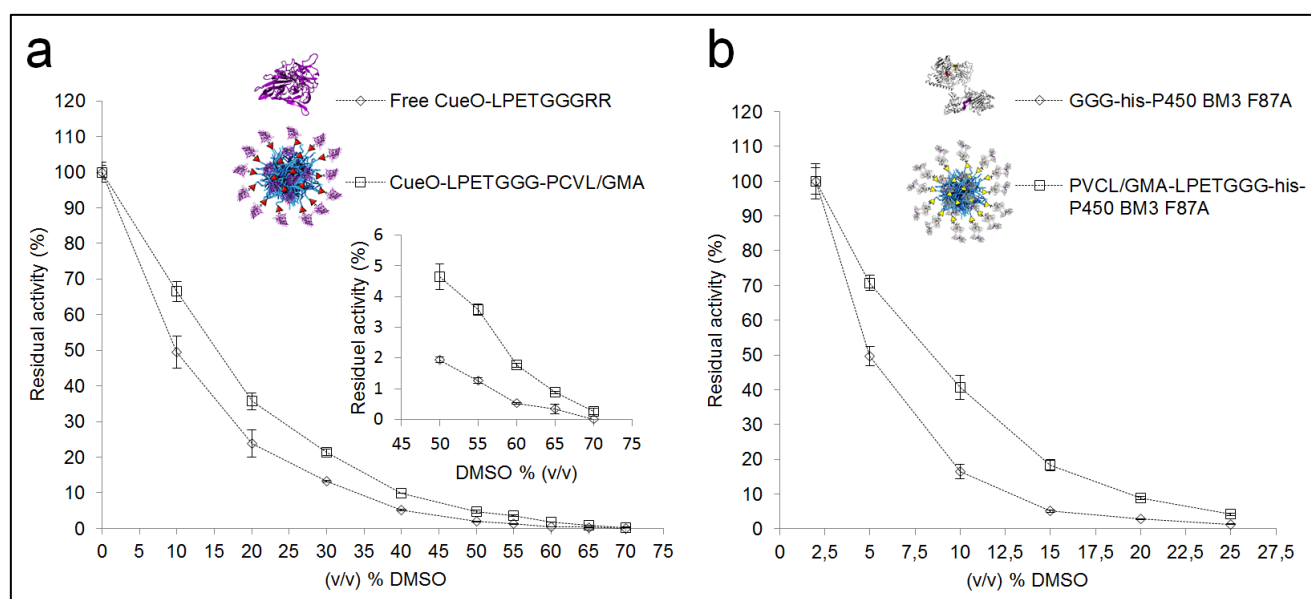
Figure 66. Activity profiles of free and immobilized (a) CueO laccase and (b) P450 BM3 F87A in different concentrations of DMSO co-solvent. Residual activities are calculated as the percentage of retained activity with respect to the maximum activity.

4.3.6. Activity profiles of immobilized enzymes in different pH

The free and immobilized enzymes were subjected to pH dependent studies. Activity profiles of CueO laccase was investigated in a pH range 2.6-5.0 (**Figure 67a**). The maximum activities of CueO-LPETGGGRR and CueO-LPETGGG-PVCL/GMA in ABTS assay were observed at pH 2.8 which in agreement with previously study.[171] No visible shift of pH profiles was found between free and immobilized CueO. The maximum activities of free enzyme GGG-his-P450 BM3 F87A and

PVCL/GMA-LPETGGG-his-P450-BM3 F87A were observed at pH 8.0 and 8.3, respectively (**Figure 67b**). Upon the immobilization, activity profile has slightly shift (pH≈0.3) towards lower pH. Improved resistance of immobilized P450 BM3 was found in under 5.7 < pH < 8.0 when compared to free counterpart. However, the gained resistance is minimized when pH is lower than 5.7. It has reported the changes in pH of immobilized enzymes are caused by Donnan partition effects. New microenvironments around enzymes might be formed when the charged polymers (e.g. positive charged PVCL/GMA-LPETGGRR, **Table 17**) are presented in solution. The unequal displaying of H^+ and OH^- ions affects the accessibility of substrates towards the enzymes and thus changes the optimized pH.[172]
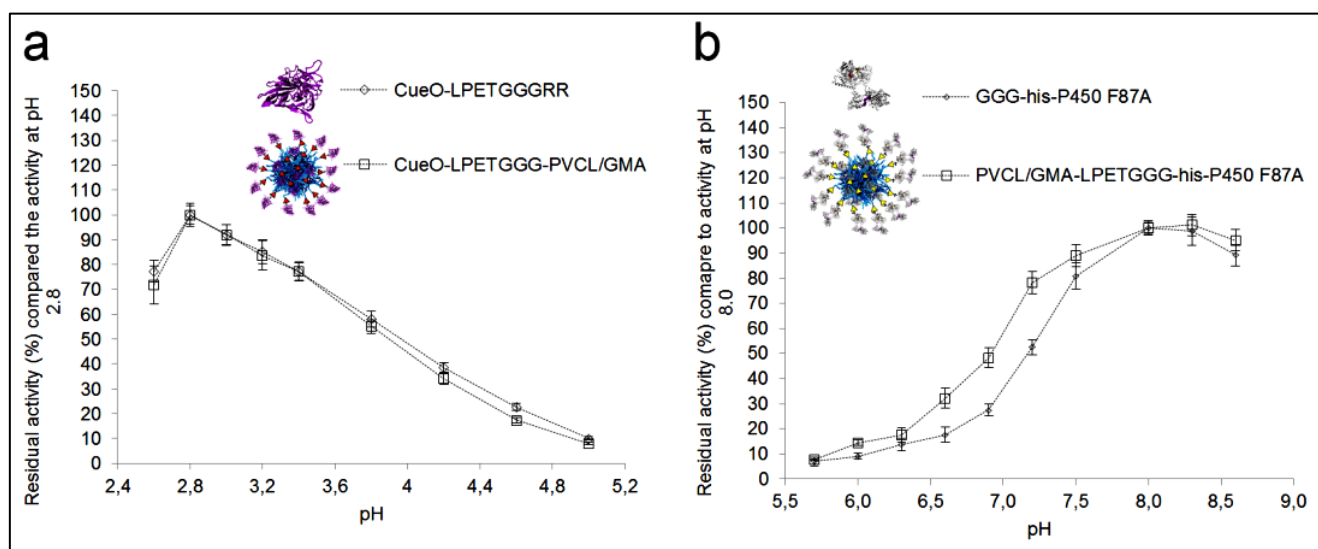
Figure 67. Activity profiles of free and immobilized (a) CueO laccase and (b) P450 BM3 F87A under different pH. Residual activities are calculated as the percentage of remaining activity with respect to the maximum activity under optimized pH.

4.3.7. Thermo-stability of immobilized enzymes

CueO is a thermo-stable enzyme and shows maximum activity at 55°C.[171] Thermo-stabilities of free and immobilized CueO-LPETGGGRR were investigated. At 60°C, PVCL/GMA clearly became turbidity since this temperature is far much higher than the detected LCST (29.3°C).[159] Microgels were dispersed by cooling down to room temperature before activity measurements. Surprisingly, CueO-LPETGGGRR retained more than 50% activity after 1h incubation at 60°C whereas CueO-LPETGGG PVCL/GMA only retained 23% activity (**Figure 68a**). The precipitation of microgel reduced the stability of CueO rather than providing the protection. Likewise, thermo-stabilities of free and immobilized GGG-his-P450 BM3 F87A were investigated at 35°C. Lower stability of PVCL/GMA-LPETGGG-his-P450-BM3 F87A was determined in comparison to the free enzyme GGG-his-P450 BM3 F87A. A sharp decrement was observed in the first 20 min of PVCL/GMA-LPETGGG-his-P450-BM3 F87A (**Figure 68b**).

Similar trends for decreased thermal stabilities of enzymes at temperatures higher than LCST were observed. We therefore assumed that the transition of PVCL/GMA from expansion (temperature $\leq$ 29.3°C) to rigidity (temperature $\geq$ 29.3°C) narrows the space and has irreversibly changed the conformational structure of the immobilized enzymes. It is reasonable this effect is even more obvious for immobilized P450 BM3 F87A, since it has a big molecule size and dimeric form for functional catalysis.[167, 173]
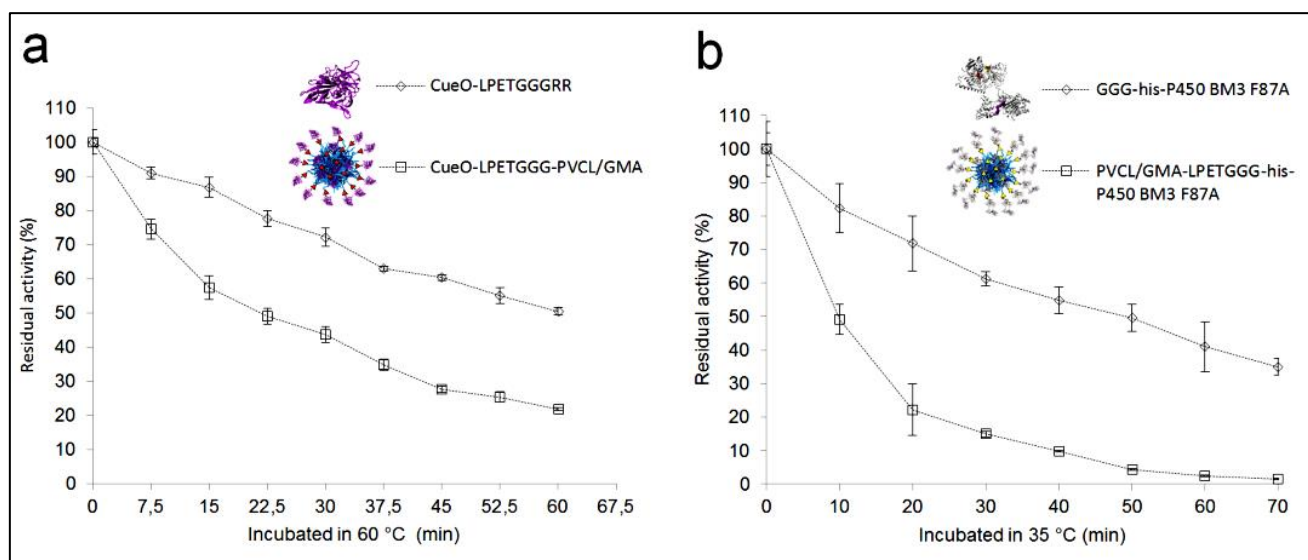
Figure 68. Thermo-stability of CueO-LPETGGG PVCL/GMA at 60°C (a) and PVCL/GMA-LPETGGG-his-P450 BM3-F87A (b) at 35°C.

4.3.8. Storage stability of immobilized enzymes

Enzymes have highly conformational structures. It is believed that immobilization of enzymes would gain the conformational stability and therefore an elongated shelf life is expected. The storage stabilities of immobilized enzymes at 4°C were studied. The CueO-LPETGGG PVCL/GMA possessed more than 75% initial activity after 2 months incubation at 4°C (**Figure 69a**). As a comparable control, free enzyme CueO-LPETGGGRR retained 55% initial activity. The results are in good agreement with the expectation as aforementioned. Surprisingly, a slight decreased stability of PVCL/GMA-LPETGGG-his-P450-BM3 F87A was found when compared with its free counterpart (**Figure 69b**).
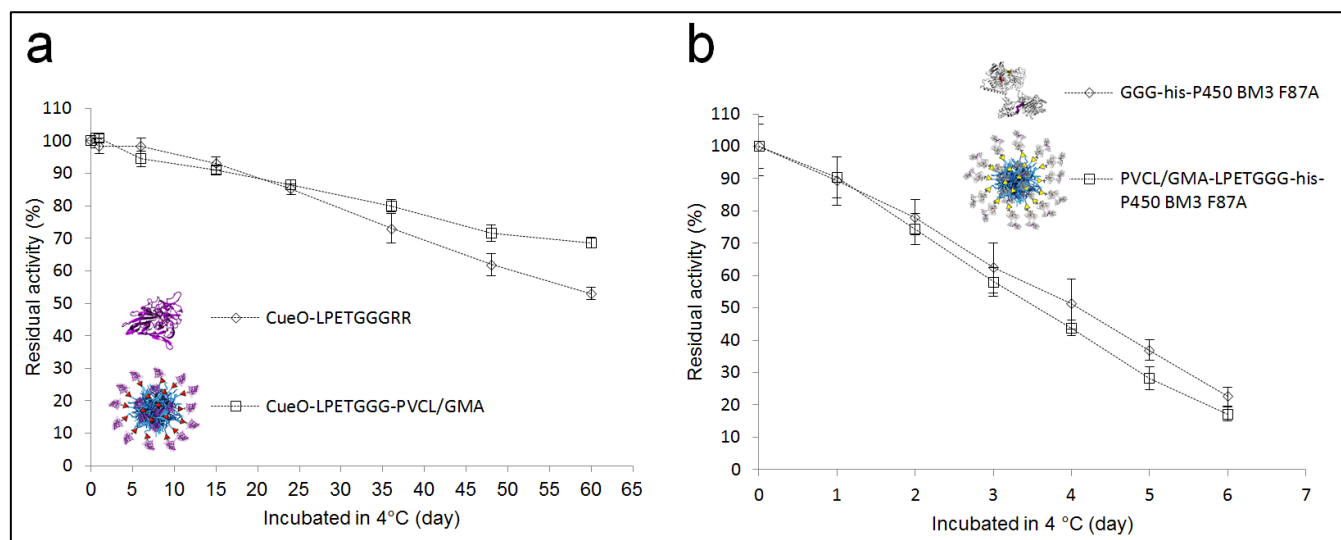
Figure 69. Storage stability of CueO-LPETGGG PVCL/GMA (a) and PVCL/GMA-LPETGGG-his-P450 BM3-F87A (b) at 4°C.

4.3.9. Reusability of immobilized enzymes

The immobilization of enzyme on solid support facilitates the isolation of enzyme from the reaction mixture. Being able to reuse the enzymes is one of main advantages for immobilization techniques. The latter well meets demands of industrial applications. The reusability of CueO-LPETGGG-PVCL/GMA and PVCL/GMA-LPETGGG-his-P450 BM3-F87A were investigated. **Figure 70** shows the reusability of CueO-LPETGGG-PVCL/GMA and PVCL/GMA-LPETGGG-his-P450 BM3-F87A. CueO-LPETGGG-PVCL/GMA retained 55% activity after ten consecutive reactions when using ABTS as substrate (**Figure 70a**). PVCL/GMA-LPETGGG-his-P450 BM3-F87A retained 52% activity after six consecutive reactions in which BCCE was used as substrate (**Figure 70b**). CueO presents better reusability than P450 BM3. Two reasons can be explained. Firstly, CueO laccase is far more stable than P450 BM3. P450 BM3 lost more activity during the operating processes. This difference of stability is evident from the thermo-stability experiment. Secondly, the CueO-LPETGGG-PVCL/GMA conjugate has better recovery yield of pellet after centrifugation in comparison to PVCL/GMA-LPETGGRR. The neutral zeta potential (**Table 18**) of GGG-PVCL/GMA enables easy aggregation of CueO-LPETGGG-PVCL/GMA during centrifugation, while the clearly positive charged (**Table 18**) PVCL/GMA-LPETGGRR showed a strong repulsion to each other. Nevertheless, the overall studies suggested that the immobilized CueO and P450 BM3 showed a good reusable availability and could be potentially used in industrial applications.
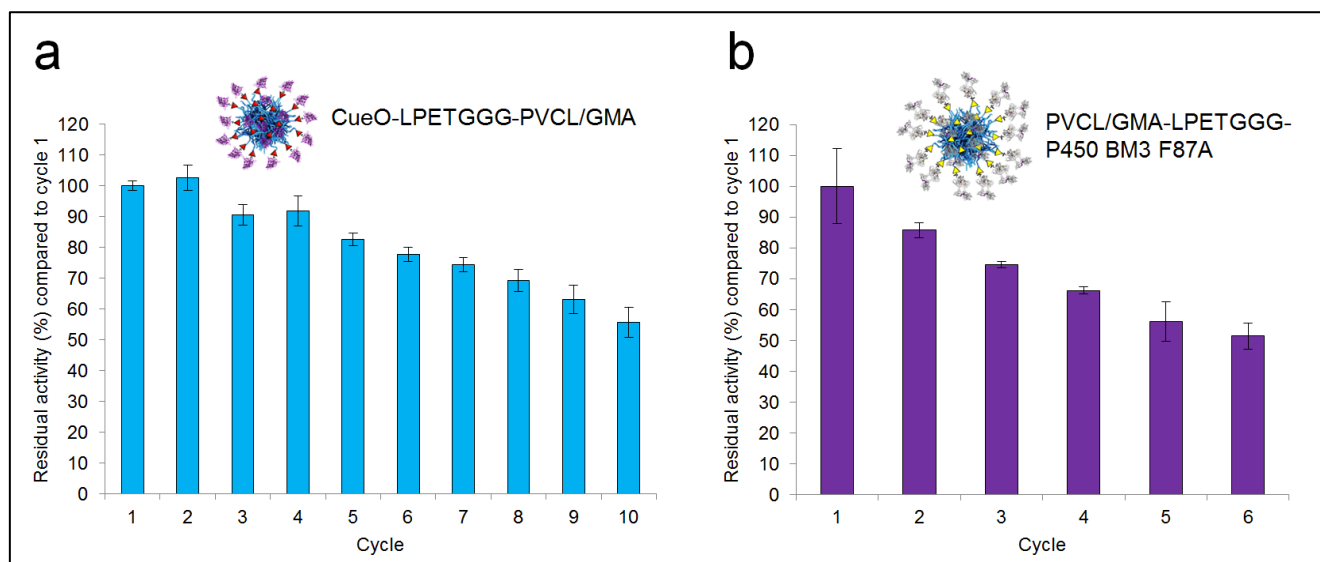
Figure 70. Reusability of immobilized CueO-LPETGGG-PVCL/GMA in consecutive ABTS assay (a) and PVCL/GMA-LPETGGG-his-P450 BM3-F87A in consecutive BCCE assay (b).

4.3.10. Application of immobilized CueO laccase in decolourization of synthetic dyes

Synthetic dyes are widely used in textile and printing industries. The stable chemical structures of synthetic dyes are often not uniformly susceptible to typical microbial attack in conventional coloured effluents treatments which remains as a challenge for environmental friendly manufacturing.[174] Laccase-based oxidation have emerged as a powerful tool in decolourization of textile dyes and degradation of micropollutants.[175]

In this work, five synthetic dyes Azure B, Coomassie Brilliant blue R250, Indigo carmine, Methyl Orange, and Reactive black were selected as the model substrates for decolourization of CueO laccase (structure of these dyes are shown in **Figure 71a**). The decolourization efficiencies for five dyes were firstly studied using free CueO laccase as catalyst. Results are given in **Figure 71b**. Under the defined condition, more than 50% Indigo carmine, Methyl Orange, and Reactive Black were decolorized after 180 h. Slight (≤ 10%) decolourization was found for Azure B, Coomassie Brilliant blue R250.
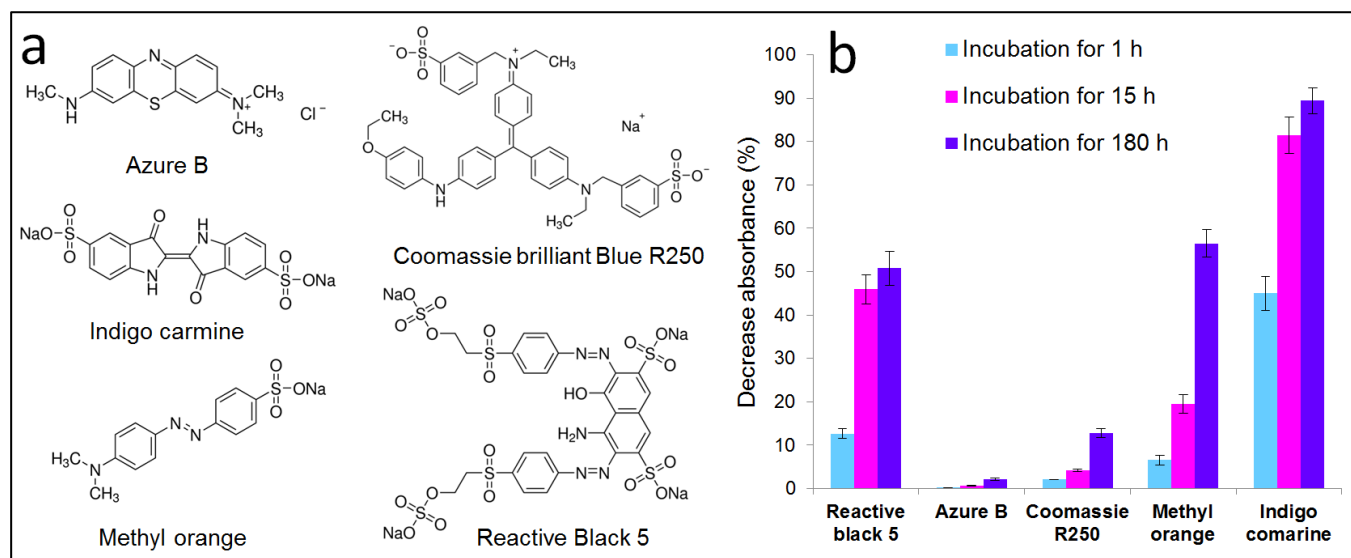
Figure 71. Chemical structures of selected synthetic dyes in this study. Decolourization of synthetic dyes using CueO laccase as the catalyst. Azure B, Coomassie Brilliant blue R250, Indigo carmine, Methyl Orange, or Reactive Black 5 was incubated with CueO laccase (6 μM CueO-LPETGGGRR). Absorbance (Azure B (at 647 nm), Coomassie Brilliant blue R250 (at 555 nm), Indigo carmine (at 608 nm), Methyl Orange (at 465 nm), or Reactive Black 5(at 597 nm)) was recorded after 1, 16 and 180 hours incubation. Blank controls containing concentration of dye but no CueO enzyme were performed in parallel. Data is shown as percentage of decreased absorbance with respect to the blank control.

Time-dependent decolourization studies of CueO-LPETGGG-PVCL/GMA were performed using Indigo carmine, Methyl orange as substrates. Results are shown in **Figure 72**. Absorbance of Indigo carmine and Methyl orange both immediately decreased ($\geq$ 50%) when just incubated with GGG-PVCL/GMA or CueO-LPETGGG-PVCL/GMA. These results indicates dyes were absorbed/entrapped by PVCL/GMA microgels due to their cross linking structures. On the basis of the facts, GGG-PVCL/GMA or CueO-LPETGGG-PVCL/GMA showed clear higher efficiencies in decolourization of Indigo carmine within 2 h ($\geq$ 80%, **Figure 72a)** and in decolourization of Methyl orange with 16 h (($\geq$ 75%, **Figure 72b**) when compared to CueO-LPETGGGRR. The highest decolourzation efficiencies were observed for CueO-LPETGGG-PVCL/GMA in decolourization of two dyes when compared to GGG-PVCL/GMA and CueO-LPETGGGRR.
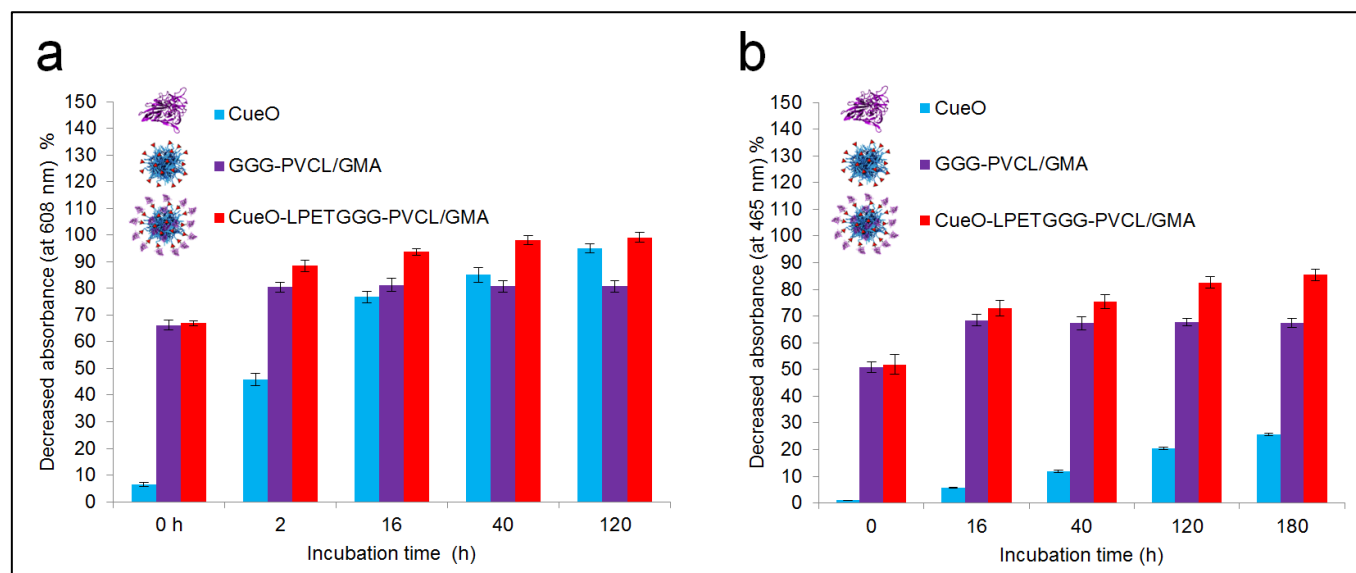
Figure 72. Decolourization of synthetic dyes by using CueO-LPETGGG-PVCL/GMA. a) Time dependent decolouriaztion of Indigo carmine; b) Time dependent decolouriaztion of Methyl orange. CueO-LPETGGGRR and GGG-PVCL/GMA were used as controls.

Reusability of GGG-PVCL/GMA or CueO-LPETGGG-PVCL/GMA in dye decolourization was investigated. Within the increase in recycle numbers, the decolourization efficiency of GGG-PVCL/GMA towards Indigo carmine was remarkable decreased while CueO-LPETGGG-PVCL/GMA kept the majority of its efficiency (**Figure 73a**). After eight consecutive reusing cycles, 80 and 17% residual efficiency were observed for CueO-LPETGGG-PVCL/GMA and CueO-LPETGGGRR, respectively. Regarding reusability in decolourization of Methyl orange, CueO-LPETGGG-PVCL/GMA and GGG-PVCL/GMA retained 52% and 27% after six consecutive reusing cycles, respectively (**Figure 73b**). Pictures of recycled CueO-LPETGGG-PVCL/GMA (**Figure 74**) confirmed that dyes inside gel particle were also decolorized by surface immobilized CueO. A possible explanation is that CueO-LPETGGG-PVCL/GMA aggregated the dyes inside itself via absorption/entrapment. Upon the aggregation, a micro-environment with higher concentration of dyes was formed and a high efficient decolourization was therefore achieved by the surface attached enzymes.
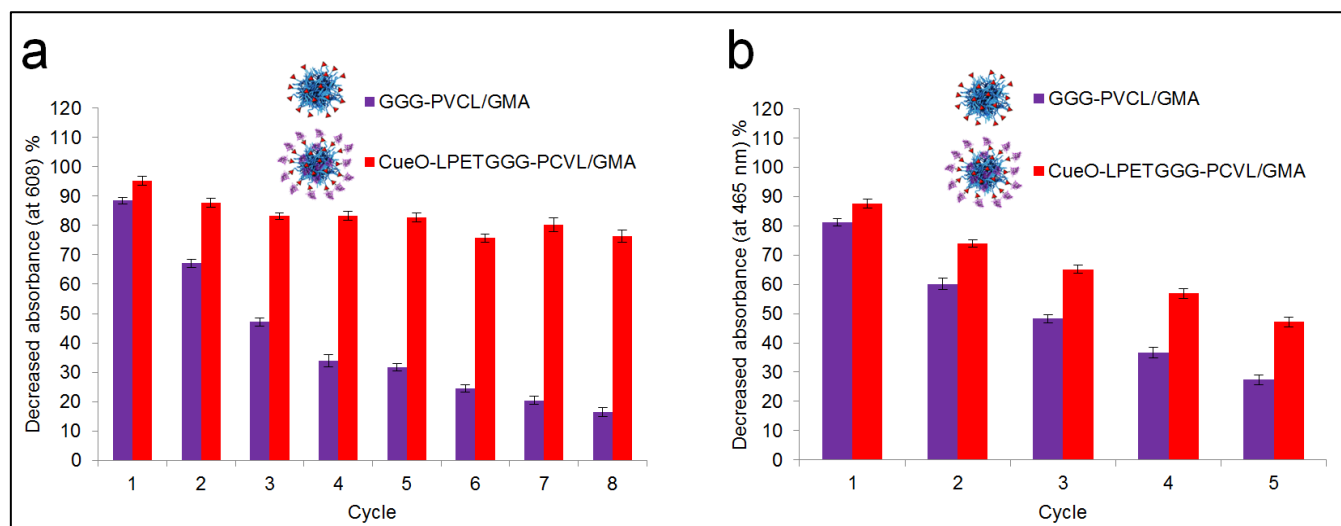
Figure 73. Reusability of CueO-LPETGGG-PVCL/GMA in decolourization of synthetic dyes. a) Reusability of CueO-LPETGGG-PVCL/GMA in decolourization of Indigo carmine; b) Reusability of CueO-LPETGGG-PVCL/GMA in decolourization of Methyl orange. In both experiments, GGG-PVCL/GMA was used as a control.
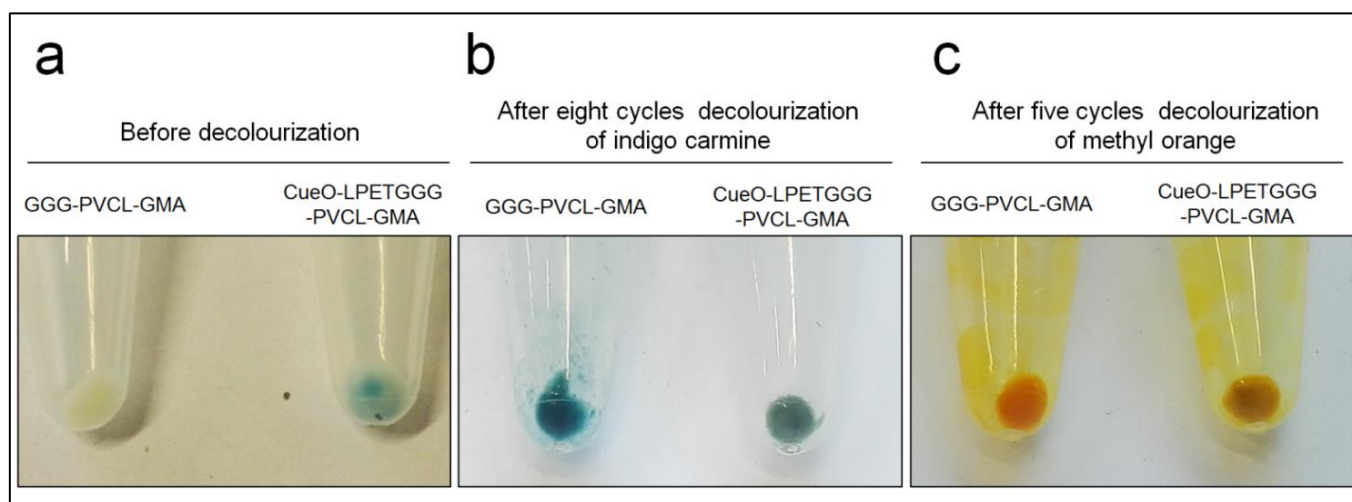
Figure 74. Photos of obtained GGG-PVCL/GMA microgel after consecutive decolourization cycles. a) Photo of microgels before used in dye decolourization; b) Photo of microgels after eight consective cycles in decolourization of indigo carmine; c) Photo of microgels after five consective cycles in decolourization of methyl orange.

4.5. Conclusion

Design and development of powerful enzyme immobilization techniques are hot topics in biotechnology In this study, we established a platform for the site-specific immobilization of enzymes on the surface of stimuli-responsive microgel particles by means of sortase-mediated ligation. The broad applicability of the platform was demonstrated by immobilizing five different enzymes from the cell-free lysate either at C- or N-terminus. Catalytic profile of the immobilized enzymes in regards of solvent/pH resistance, thermos/storage stability, and reusability were investigated. Despite of diverse methods have been developed for enzyme immobilization. There are few studies reported a general site-specific strategy for enzyme immobilization on surface of soft matter (e.g. hydrogel). In comparison to non-specific immobilization approaches, the sortase-mediated immobilization enables high possibility of proper orientation of enzymes on the surface of supports which generally retained more activities. Application of immobilized laccase have implemented in decolourization of several synthetic dyes. The immobilization of CueO laccases in a simple protocol using the sortase-mediated ligation offered the possibility for their use in multiple cycles for the decolourization of dyes. Enzymes are expensive catalysts, the high reusability of immobilized enzymes facilitate their practical usage in industry.

In summary, our work expanded the methods for immobilization of biomolecules on surface of soft materials. The versatility and site-specificity of sortase-mediated conjugation enables multi-modification (e.g. fluorination, PEGylation, biotinylation) of polymer surface with diverse functionalities (e.g. super hydrophobicity, biocompatibility and biometrics). The latter will open up numerous potential applications such as water-proof materials, trigger released medicines and biosensors.

4.4. Materials and Methods

4.4.1. Materials

Peptides NH$_2$-GGGRPWFWGMH-COOH and NH$_2$-CRPWFWGMHLPETGGRR-COOH (purity ≥ 90%) were purchased from BIOTREND (Köln, Germany). *N*-Vinylcaprolactam (VCL, Sigma-Aldrich, 98%) and glycidyl methacrylate (GMA, Sigma-Aldrich, 97%) were distilled before usage. VCL was recrystallized from hexane after distillation. The crosslinker *N,N'*-methylenebis(acrylamide) (BIS, Sigma-Aldrich, 99%) and the initiator *2,2'*-azobis(2-methylpropionamidine) dihydrochloride (AMPA, Sigma-Aldrich, 97%) were used as received. Azure B, indigo carmine, and methyl orange were purchased from Sigma-Aldrich (Hamburg, Germany). Coomassie brilliant blue R250 was obtained from AppliChem (Darmstadt, Germany). Reactive black five was purchased from Santa Cruze Biotechnology (Heidelberg

Germany). Enzymes for gene cloning were all purchased from New England Biolabs (Frankfurt, Germany). Primers used in polymerase chain reactions (PCR) were obtained from Eurofins MWG Operon. Microtiter plates were purchased from Greiner Bio-One GmbH, (Frickenhausen, Germany).

4.4.2 Gene constraction of GGG or LPETGGGRR tagged enzyme

All PCR solutions (25 μL) for amplification consist of 1.25 U PfuS DNA polymerase, 10 mM dNTP mix, 10 ng plasmid template and 25 uM of each primer (forward primer and reverse primer). PCR products were digested by Dpn I (5 U, 37°C, overnight) and subsequently treated by heat inactivation (80 °C for 20 min). The digested samples were then purified. Clean-up PCR products were transformed into corresponding competent cells.

Primers for the polymerase chain reactions (PCR) are list in Table S1. The pET22b(+)-*bsla* of *Bacillus subtilis* lipase A (BSLA, [100]) was used as template to generated GGG-his-BSLA. *Fw-ggg-bsla* and *Fw-ggg-bsla* were used to make construction of GGG-his-BSLA. A two-step PCR protocol was performed: 98°C for 30 sec (1 cycle); 98°C for 30 sec, 55°C for 30 sec , 72°C for 3 min 30 sec (5 cycles); 72°C for 10 min (1 cycle); 8°C for holding and mixing the forward and reverse fragments; 98°C for 30 sec, 55°C for 30 sec, 72°C for 3 min 30 sec (25 cycles); 72°C for 10 min (1 cycle). The amplified plasmids encoded GGG-his-BSLA was transformed into *E. coli* BL-21 (DE3) strain.

Plasmid pET-22b CueO-StrepII was used to generated GGG-CueO and CueO-LPETGGGRR. Construction of CueO-LPETGGGRR was performed as previously described.[109] Primer *Fw ggg-cueo* and *Rev ggg-cueo* were employed for amplification of GGG-CueO. PCRs protocol: 98°C for 45 sec (1 cycle); 98°C for 45 sec, 55°C for 30 sec, 72°C for 4 min 30 sec (25 cycles); 72°C for 10 min (1 cycle). The amplified plasmid encoded GGG-CueO was transformed into *E. coli* Shuffle T7.

Plasmid of cellulase A2 variant M2 (Cel A2) in previously work[160] was used as template to generated GGG-CelA2. Primers *Fw ggg-cel-a2* and *Rev ggg-ce-a2* were used. PCRs protocol: 98°C for 30 sec (1 cycle); 98°C for 30 sec, 57°C for 30 sec, 72°C for 3 min 30 sec (25 cycles); 72°C for 10 min (1 cycle). The amplified plasmid encoded GGG-CelA2 was transformed into *E. coli* BL-21 and (DE3).

Plasmid containing the gene of P450 BM3 (F87A)[161] was used as template to generated GGG-his-P450 BM3 (F87A) and P450 BM3-LPETGGGRR (F87A). *Fw ggg-his-p450* and *Rev ggg-his-p450* were used to construct of GGG-his-P450 BM3 (F87A). A two-step PCR was performed: 98°C for 30 sec (1 cycle); 98°C for 30 sec, 58°C for 30 sec, 72°C for 3 min 30 sec (5 cycles); 72°C for 10 min (1 cycle). The PCR tubes were holding in 8°C and the forward and reverse fragments were mixed. A followed step was

117

performed by protocol: 98°C for 30 sec, 58°C for 30 sec, 72°C for 3 min 30 sec (20 cycles); 72°C for 10 min (1 cycle). *Fw p450 lpetgggrr and Rev p450 lpetgggrr* were used to construct P450 BM3-LPETGGGRR (F87A). A same PCR protocol was used as described for cloning of GGG-his-P450. Plasmids encoded P450 BM3 genes were transformed into *E. coli* BL-21 (DE3) Lac[IQ] strain.

Table 20. List of primers used for the gene construction of N-terminal GGG and C-terminal LPETGGGRR enzymes

Primer Name	Sequence 5'-3'
Fw ggg-his-bsla	GGTGGAGGACATCATCATCATCATCATGATATAGCTGAAC
Rev ggg-his-bsla	ATGATGATGATGATGATGTCCTCCACCGGCCATCGCCGG
Fw ggg-phytase	GGAGGAGGACGATTAACTGCACTGGGCTTAAT
Rev ggg-phytase	TCCTCCTCCCATATGTATATCTCCTTCTTAAA
Fw ggg-cueo	ATGGGTGGCGGGGCAGAACGCCCA
Rev ggg-cueo	CCCGCCACCCATATGTATATCTCC
Fw ggg-cel-a2	ACCATGGGTGGTGGTAGCAGCCATCACCAC
Rev ggg-cel-a2	ACCACCACCCATGGTATATCTCCTTCTTAA
Fw ggg-his-p450	GGAGGAGGACATCATCATCATCATCATACAATTAAAGAAATG
Rev ggg-his-p450	ATGATGATGATGATGATGTCCTCCTCCCATGCTGCCCAGGGT
Fw p450 lpetgggrr	CTACCTGAAACAGGTGGTGGTCGTCGTTAAGCTAACAAAGCCCGA
Fw p450 lpetgggrr	ACGACGACCACCACCTGTTTCAGGTAGCCCAGCCCACACGTC

4.4.3 Production of N-terminal GGG and C-terminal LPETGGGRR enzymes

Expression and purification Sa-SrtA rM4, and CueO-LPETGGGRR were implemented with same protocols as previously reported.[109] The expression of GGG-his-BSLA was performed based on previously described.[176] In shortly, pre-cultures (5 mL LB media, 100 μg/mL ampicillin) were inoculated from a glycerol stock and incubated (16h, 250 rpm, 137°C, 70% humidity). The main culture (200 mL auto-induction media, 100 μg/mL ampicillin) in 1 L flask was inoculated with 1 mL pre-culture (18h, 250 rpm, 37°C, 70% humidity). GGG-Ym-Phytase was expressed in TB medium. Main culture (200 mL TB medium, 50 μg/mL ampicillin) in 1 L flask was inoculated with pre-culture with an initial OD_{600} at 0.05 and incubated (250 rpm, 37°C, 70% humidity). When OD_{600} reached 1.0, IPTG (200μL, 1M) was added and main culture was subsequently cultivated (16h, 250 rpm, 30°C, 70% humidity). GGG-CelA2 (M2) was also expressed in TB medium. In shortly, main culture (200 mL TB medium, 50 μg/mL kanamycin) in 1 L flask was inoculated with pre-culture with an initial OD_{600} at 0.05 and cultivated (250 rpm, 37°C, 70% humidity) until OD_{600} reached 0.8 . Cells were induced by adding IPTG (200μL, 1M) and

subsequently incubated (16 h, 250 rpm, 30°C, 70% humidity). GGG-his-P450 BM3 (F87A) and P450 BM3-LPETGGGRR (F87A) were expressed based on the protocol as previously implemented.[161] In shortly, main culture (200 mL TB medium, 50 μg/mL kanamycin, 200 μL 1M trace elements) in 1 L flask was inoculated with pre-culture with an initial OD_{600} at 0.05. Cultures were firstly incubated in Multitron II Infors shaker for around 3 h (250 rpm, 30°C, 70% humidity) until OD_{600} reached 0.8 . Cultures were induced by adding IPTG (200 μL, 100 mM), δ-aminolevulinic acid anhydride (ALA, 200 μL, 500 mM) subsequently cultivated (24 h, 250 rpm, 25°C, 70% humidity).

All the cultivated cells were harvested by centrifugation (30 min, 3220 g, 4°C, Eppendorf centrifuge 5810 R,). The obtained cell pellets were firstly frozen (- 20°C, 24h) and then dispersed with a ratio 1 g cell pellet in 10 mL buffer (pH 7.5, 50 mM, Tris-HCl). Cell-free lysate was produced by sonication (60% amplitude, 12 cycles, 15 seconds per cycle, intervals 15 seconds, performed on ice). After centrifugation (1 h, 3220 g, 4°C, Eppendorf centrifuge 5810 R) the supernatant of cell lysate was used for SDS-PAGE analysis (Fig. S1).

Purification of GGG-CelA2 and P450 BM3s was performed by using Ni SepharoseTM 6 Fast Flow purification kits (GE Healthcare, Freiburg, Germany). Procedures were implemented according to the manufacturer´s protocol. Elution fragments were firstly checked by SDS-PAGE. The pure fragments were pooled and dialyzed overnight at 4°C (pH 7.5, 50 mM, Tris-HCl buffer) by using Spectra/Por dialysis tubing (Spectrum Laboratories, Inc., CA, USA). Amicon ultra-15 centrifugal filter units with 10 kDa cut-off (Merck Millipore Ltd, Tullagreen, IRL) were used for preparation of concentrated protein samples. Copper ions (CuCl2, 2 mM) was added and incubated with purified CueO-LPETGGGRR for at least 24 h before using.

4.4.4. Activity measurements of GGG and LPETG tagged enzyme in cell-free lysates

The activity of BSLAs was measured with colormetric assay of p-nitrophenol (absorbance detected at 410 nm).[176] In detail, p-nitrophenyl butyrate (pNPB, 10 μL, 10 mM in DMSO) was pipetted into a 96-well MTP (transparent, flat bottom, GreinerBio-one, Frickenhausen, Germany) and incubated with buffer (185 μL, pH 7.5, 50 mM, Tris-HCl). The reaction was initiated by adding of 5 μL supernatant of BSLA cell-free lysates. Plates were stirred briefly and the absorbance was continuously measured (410 nm, room temperature, Tecan Infinite M1000 PRO plate reader, Tecan Group AG, Männedorf, Switzerland).

Activity measurement of *Yersinia mollaretii* phytase (Ym-Phytase) was performed based on a 4-methylumbelliferylphosphate (4-MUP) assay.[79] Firstly, cell-free lysate (10 μL) was pipetted into 96-well MTP (black, flat bottom, GreinerBio-one). In the next step, buffer (40 μL, 100 mM, pH 5.5, sodium

acetate) was added. Reaction was initialed by mixing with MUP solution (50 μL, 1 mM MUP dissolved in 100 mM, pH 5.5, sodium acetate). Fluorescence was continuously recorded (λ_{exc} = 360 nm; λ_{em} = 465 nm, room temperature, gain = 100, Tecan infinite 1000 PRO plate reader).

Activity measurement of CueO laccase cell-free lysates were performed based on a 2,2'-azino-bis(3-ethylbenzothiazoline-6-sulphonic acid (ABTS) assay as previously described.[109] In shortly, ABTS (3 mM) was dissolved in 96-well MTP (transparent, flat bottom, GreinerBio-one) with buffer (198 μL, pH 3, 100 mM, sodium citrate). Reaction was initiated by adding cell-free lysate (2 μL). Absorbance was recorded (420 nm, room temperature, Tecan Infinite M1000 PRO plate reader)

Activity of CelA2 (M2) cell-free lysates were recorded based on a 4-methylumbelliferyl-β-D-cellobioside (4-MUC) assay.[160] In shortly, cell-free lysate (3 μL) was incubated in buffer (47 μL, pH 7.2, 200 mM, phosphate buffer). Reaction was initiated by adding MUC solution (50 μL, 1 mM 4-MUC). Plates were stirred briefly (5 seconds) and the florescence was continuously recorded (λ_{exc} = 330 nm; λ_{em} = 450 nm, room temperature, gain = 100, Tecan infinite 1000 PRO plate reader). Activity of Cel-A2 and GGG-CelA2 were calculated and data is shown in **Fig. S2c**.

7-benzoxy-3-carboxycoumarin ethyl ester (BCCE) was used as the substrate to determine the activity of P450 BM3.[81] In detail, cell-free lysate (5 μL) lysate was firstly incubated in buffer (88 μL, pH 8.0, 50 mM Tris-HCl) in 96-well MTP ((black, flat bottom GreinerBio-one). Two microliter of BCCE (2 mM in DMSO) was subsequently pipetted into the MTP and subsequently incubated (5 min, 700 rpm, room temperature). Reaction was initiated by addition NADPH (5 μL, 10 mM). The fluorescence was constantly recorded (λ_{exc}: 400 nm, λ_{em}: 440 nm room temperature, gain=120, Tecan Infinite M1000 PRO microtiter plate reader).

4.4.5. Synthesis of pVCL/GMA-LPETG and GGG-pVCL/GMA microgels

The PVCL/GMA microgel containing 5 mol % GMA in the microgel shell was synthesized by a modified procedure based on the work of Häntzschel at al.[177] as published by our groups elsewhere.[159] To reach a microgel structure with a VCL rich core and a GMA rich shell and thus the localization of epoxy groups on the microgel surface, the GMA was added three minutes after the polymerization initiation.[159] The obtained microgel was purified by dialysis for three days against distilled water (regenerated cellulose tube MWCO 12-14 kDa). Afterwards, the dispersant was changed from water to 50 mM Tris HCl buffer pH 10.0 via centrifugation (10 min, 25°C, 10000 rpm) to perform the coupling of the peptide sequences.

The covalent coupling reaction of the peptide sequences to the microgels via thiol-epoxy coupling reaction was performed as reported by our groups earlier.[159] Basically, 1.34 µmol of the respective peptide (2.8 mg of the LPETGGRR-peptide or 1.8 mg of the GGG-peptide) was solved in 1 mL buffer (50 mM, pH 7.5, Tris HCl) and added to 1.0 mL of microgel dispersion containing 1.34 µmol GMA in buffer (50 mM, pH 7.5, Tris HCl). The mixture was stirred over night at room temperature and purified afterwards by centrifugation. For the following up sortase-mediated ligation, the peptide-tagged microgels were re-dispersed in storage buffer (50 mM, pH 7.5, Tris HCl).[159]

UV/Vis Spectroscopy was employed to proof the coupling of the peptide sequences to the PVCL/GMA microgels. The hydrodynamic radius of the microgel samples as well as the particle size distributions were investigated with dynamic light scattering (DLS). Raman spectroscopy was used to proof the successful coupling of the peptide sequences to the PVCL/GMA microgels.

4.4.6. Sortase-mediated enzyme immobilizations on surface of PVCL/GMA microgels

4.4.5.1.N-terminal GGG-tagged enzymes immobilization on PVCL/GMA-LPETGGRR microgel

Immobilization of GGG-tagged enzymes on PVCL/GMA-LPETGGRR microgel was performed based on previous report.[159] Compounds and reactions conditions are summated in **Table 21**. In a 1.5 mL Eppendorf reaction tube, PVCL/GMA-LPETGGRR microgel (4 mg) was dispersed in buffer (200 µL, 50 mM, pH 7.5, Tris HCl). The supernatant (150 µL) of GGG-his-BSLA, GGG-Ym-phytase, GGG-CelA2 (M2), or GGG-his-P450 BM3 F87A was pipetted into the PVCL/GMA-LPETGGRR microgel solution. CaCl₂ (20 µL, 100 mM), NaCl (20 µL, 3000 mM) and SrtA 4M (10 µL, 50 µM) were subsequently added in reaction containing of GGG-his-BSLA, GGG-phytase or GGG-CelA2 (M2). Regarding GGG-his-P450 F87A, only SrtA 4M (50 µL, 40 µM) was subsequently added. Two negative controls were performed in parallel for each immobilization experiment. In the negative control, PVCL/GMA (4 mg) was dispersed instead of PVCL/GMA-LPETGGRR. In negative control 2, buffer (50 mM, pH 7.5, Tris-HCl) was added instead of SrtA-4M. The reaction mixtures were incubated (20 °C, 16 h, 800 rpm) for immobilization of GGG-his-BSLA, GGG-phytase or GGG-CelA2 (M2) or (20 °C, 24 h, 800 rpm) for immobilization of GGG-his-P450 BM3 F87A. After sortase-mediated immobilization, samples were centrifuged (15 °C, 10 min, 10000 rpm). The supernatant was pipetted out and pellet was dispersed (400 µL, pure water) and followed with incubation (600 rpm, 5 min, room temperature). The same procedure was repeated one more cycle. The microgel pellet was obtained again by centrifugation (15 °C, 10 min, 10000 rpm). The

pellets of microgel with immobilized enzymes was re-dispersed (200 μL pure water, concentration of microgel in water is 20 mg/mL) and used to evaluate the immobilized enzyme activity.

Table 21. Summary of compounds and conditions for sortase-mediated N- or C-terminus immobilization of proteins on PVCL/GMA microgels

Enzyme	Lysate (μL)	GGG-PVCL/GMA (mg/mL)	PVCL/GMA-LPETGGRR (mg/mL)	CaCl2 (mM)	NaCl (mM)	SrtA M4 (μM)	T (°C)	Time (h)
GGG-BSLA	150		10	5	150	1.25	20	16
GGG-phytase	150		10	5	150	1.25	20	16
GGG-CelA2	150		10	5	150	1.25	20	16
GGG-his-P450 BM3 F87A	150		10			5	20	24
CueO-LPETGGGRR	150	10		5	150	1.25	20	16
P450 BM3-LPETGGGRR F87A	150	10				5	20	24

Re-dispersed PVCL/GMA-LPETGGRR which immobilized with GGG-his-BSLA (10 μL in pure water) in was mix with buffer (180 μL, 50 mM, pH 7.5, Tris-HCl) in a 96-well MTP (transparent, flat bottom GreinerBio-one). Reaction was initialed by adding pNPB substrate (10 μL, 10 mM). Plates were stirred (5 seconds) and the absorbance was continuously recorded (410 nm, room temperature, Tecan Infinite M1000 PRO plate reader).

Re-dispersed PVCL/GMA-LPETGGRR which immobilized with GGG-Ym-phytase (50 μL in pure water) was pipetted into 96-well MTP (black, flat bottom, GreinerBio-one). Reaction was initialed by adding MUP solution (50 μL, 1 mM MUP). Fluorescence was continuously recorded (λ_{exc} = 360 nm; λ_{em} = 465 nm, room temperature, gain = 100, room temperature, Tecan infinite 1000 PRO plate reader).

Re-dispersed PVCL/GMA-LPETGGRR which immobilized with GGG-CelA2 M2 (50 μL in pure water) was pipetted into 96-well MTP (black, flat bottom, GreinerBio-one). Reaction was initialed by adding MUC solution (50 μL, 1 mM MUP). Florescence was continuously recorded (λ_{exc} = 330 nm; λ_{em} = 450 nm, gain = 100, room temperature, Tecan infinite 1000 PRO plate reader).

Likewise, re-dispersed PVCL/GMA-LPETGGRR which immobilized with GGG-his-P450 BM3 F87A (50 μL in pure water) was pipetted into 96-well MTP (black, flat bottom, GreinerBio-one). Buffer (43 μL, 50 mM, pH 8.0, Tris-HCl) was added and followed with an addition of BCCE (2 μL, 2 mM in DMSO). MTP plate was incubated (5 min, 700 rpm, room temperature) and the reaction was initiated by supplement of NADPH (5 μL, 10 mM). Fluorescence was constantly recorded (λ_{exc}: 400 nm, λ_{em}: 440 nm room temperature, gain=120, Tecan Infinite M1000 PRO microtiter plate reader).

4.4.5.2 C-terminal LPETG-tagged enzymes immobilization on GGG-PVCL/GMA microgel

The immobilization of LPETG-tagged enzymes on GGG-PVCL/GMA microgel was performed similarly as mentioned above (see N-terminal GGG-tagged enzymes immobilization on PVCL/GMA-LPETGGRR microgel). GGG-PVCL/GMA-LPETGGRR (4 mg) microgel was dispersed in 200 μL buffer (50 mM, pH 7.5, Tris HCl) in a 1.5 mL Eppendorf reaction tube. The supernatant (150 μL) of CueO-LPETGGGRR, was pipetted into the GGG-PVCL/GMA microgel solution. CaCl$_2$ (20 μL, 100 mM), NaCl (20 μL, 3000 mM) and SrtA 4M (10 μL, 50 μM) were added in reaction mixture of CueO-LPETGGGRR. Regarding P450 BM3-LPETGGGRR F87A reaction mixture, only SrtA 4M (50 μL, 40 μM) was added. Two negative controls were performed in parallel for each immobilization experiment. In the negative control 1, PVCL/GMA (4 mg) was dispersed instead of GGG-PVCL/GMA. In negative control 2, buffer (50 mM, pH 7.5, Tris-HCl) was added instead of SrtA-4M. The reaction mixtures were incubated (20 °C, 16 h, 800 rpm) for immobilization of CueO-LPETGGGRR or (20 °C, 16 h, 800 rpm) for immobilization of P450 BM3-LPETGGGRR F87A. After immobilization, GGG-PVCL/GMA microgels were washed and obtained as aforementioned.

Activity of immobilized CueO-LPETGGGRR on GGG-PVCL/GMA micrgel was measured by ABTS assay. Re-dispersed GGG-PVCL/GMA which immobilized with CueO-LPETGGGRR (25 μL in pure water) was transferred into a 96-well MTP (transparent, flat bottom, GreinerBio-one). Reaction was initialed by adding 175 μL ABTS solution (3.4 mM, pH 3.0, 100 mM, sodium citrate buffer). Plates were stirred (5 seconds) and the absorbance was continuously recorded (420 nm, room temperature, Tecan Infinite M1000 PRO plate reader).Method for the BCCE assay was performed same as aforementioned (see N-terminal GGG-P450 BM3 experiments).

4.4.7. Quantification of enzymes amount on PVCL/GMA microgel surface

Purified CueO-LPETGGGRR and GGG-his-P450 BM3 F87A were immobilized on GGG-PVCL/GMA and PVCL/GMA-LPETGGRR, respectively. Conditions and compounds for the immobilizations are list in **Table 22.** The GGG-PVCL/GMA (4 mg) was dispersed in buffer (200 μL, 50 mM, pH 7.5, Tris HCl) in a 1.5 mL Eppendorf reaction tube. The purified CueO-LPETGGGRR (134 mM, 50 mM, pH 7.5, Tris HCl) was pipetted into the GGG-PVCL/GMA solution. CaCl$_2$ (20 μL, 100 mM), NaCl (20 μL, 3000 mM) and SrtA 4M (10 μL, 50 μM) were added subsequently. The sortase-mediated immobilization was performed by incubation (20 °C, 16 h, 800 rpm).

Likewise, the PVCL/GMA-LPETGGRR (4 mg) microgel was dispersed in buffer (200 μL, 50 mM, pH 8.0, Tris HCl) in a 1.5 mL Eppendorf reaction tube. The purified GGG-his-P450 F87A (134 mM, in 50

mM, pH 8.0, Tris HCl) was pipetted into the PVCL/GMA-LPETGGRR solution. SrtA 4M (50 μL, 20 μM) was subsequently added. The sortase-mediated immobilization was performed by incubation (20 °C, 24 h, 800 rpm).

After ligation, samples were centrifuged (15 °C, 10 min, 10000 rpm) and washed as aforementioned (see experiments of N-terminal GGG-tagged enzymes immobilization on PVCL/GMA-LPETGGRR microgel). The pellet of PVCL/GMA microgels with immobilized enzyme was re-dispersed (200 μL pure water, concentration of microgel in water is 20 mg/mL).

The amount of immobilized enzymes on microgels was quantified by BCA assay (BCA Protein Assay Kit, Novagen®, Merck Millipore, Darmstadt, Germany). The standard curve of bovine berum blbumin (BSA) was implemented by mixing different concentrations of BSA (200 μL) with GGG-PVCL/GMA (25 μL, 20 mg/mL) or PVCL/GMA-LPETGGRR (25 μL, 20 mg/mL). The other procedures were performed according to manufactures protocol (BCA Protein Assay Kit, Novagen®, Merck Millipore). CueO-LPETGGG-PVCL/GMA (25 μL, 20 mg/mL) or PVCL/GMA-LPETGGG-his-P450 BM3 F87A (25 μL, 20 mg/mL) was used for BCA assay according to manufactures protocol (BCA Protein Assay Kit, Novagen®, Merck Millipore). Absorbance was measured and immobilized protein concentrations were calculated by fitting the obtained absorbance to the generated standard curves, respectively. The immobilized amount of CueO-LPETGGG on per milligram of GGG-PVCL/GMA is 1.6 μg. The immobilized amount of GGG-his-P450 F87A on per milligram of PVCL/GMA-LPETG is 2.2 μg.

Table 22. Reaction settings of sortase-mediated immobilization using purified enzymes as substrate

	Enzyme concentration (μM)	GGG-PVCL/GMA (mg/mL)	PVCL/GMA-LPETGGRR (mg/mL)	CaCl₂ (mM)	NaCl (mM)	SrtA M4 (μM)	T (°C)	Time for reaction (h)
CueO-LPETGGGRR	50	10		5	150	1.25	20	16
GGG-his-P450 F87A	50		10			2.5	20	24

4.4.8. Characterization of immobilized enzymes

Characterization of CueO-LPETGGG-PVCL/GMA (Immobilized CueO) and CueO-LPETGGGRR (free CueO) was performed by using an ABTS based assay. ABTS assays were performed in sodium citrate buffer (0.1M, pH 3.0) in 96-well polystyrene MTP with 200 μL volume of solution. Concentration of ABTS ranged from 0.05 to 15 mM and immobilized/free CueO concentration fixed at 17.8 nM. Plates were stirred for 5 seconds and the absorbance of ABTS was constantly measured (420 nm ($\varepsilon_{ABTS\cdot+}$ = 36,000 M⁻¹cm⁻¹), room temperature, Tecan Infinite M1000 PRO plate reader). Activity was calculated and

kinetics was obtained by fitting activity data to the Michaelis-Menten equation (software Origin pro 8.6, OriginLab, Massachusetts, USA).

Characterization of PVCL/GMA-LPETGGG-his-P450 F87A (immobilized P450 BM3 F87A) and GGG-his-P450 F87A (free P450 BM3 F87A) was performed by using the BCCE assay. A standard curve of fluorescence of the 3-carboxycoumarin ethyl ester (3-CCE) was generated (**Figure S7**). BCCE assay was performed in black 96-well polystyrene MTP (100 μL, 0.05 M, pH 8.0, Tris-HCl buffer). Concentrations of BCCE are ranged from 5 μM to 200 μM and immobilized/free GGG-his-P450 BM3 F87A concentrations were fixed at 200 nM (24 μg/mL). BCCE (2 μL, 2 mM in DMSO) was subsequently pipetted into MTP and incubated (5 min, 700 rpm, room temperature). Reaction was initiated by addition of NADPH (1 μL, 10 mM). The fluorescent signal was constantly recorded (λ_{exc}: 400 nm, λ_{em}: 440 nm gain=120, room temperature, Tecan Infinite M1000 PRO microtiter plate reader). Activity was calculated based on the 3-CCE standard curve and kinetics was obtained by fitting the activity data to software Origin pro 8.6.

4.4.9. Activity profiles of immobilized enzymes in organic co-solvent

Activity of free and immobilized CueO in different concentration of DMSO (range from 0 to 50%) was investigated. ABTS assay was employed for activity measurement. The concentration of free or immobilized CueO was settled at 17.8 nM (1 μg/mL). Except the addition of DMSO instead of equal volumes of sodium citrate buffer (0.1 M, pH 3.0) as well as the settled ABTS concentration (3 mM), protocol of ABTS assays were performed same as aforementioned (see CueO characterization experiment).

Activity profiles of immobilized PVCL/GMA-LPETGGG-his-P450 BM3 F87A and GGG-his-P450 BM3 F87A in gradient DMSO were carried out by using the BCCE assay. The concentrations of DMSO were implemented from 0 to 25% (v/v) with 200 nM (24 μg/mL) free or immobilized GGG-his-P450 BM3 F87A in BCCE solution (100 μL, 40 nM, pH 8.0, Tris-HCl) and followed with an incubation (5 min, 700 rpm, room temperature). The reaction was initiated by addition of NADPH (1 μL 10 mM). Fluorescence was constantly recorded (λ_{exc}: 400 nm, λ_{em}: 440 nm gain=120, Tecan Infinite M1000 PRO microtiter plate reader).

4.4.10. Activity profiles of immobilized enzymes in different pH

Sodium citrate buffer (pH range from 2.6 to 5.0) was employed as the buffer for pH profiles of CueO laccase. In detail, 36.6 nM CueO-LPETGGG or CueO-LPETGGG-PVCL/GMA was incubated in ABTS solution (200 μL, 3 mM ABTS, 100 mM, sodium citrate buffer) with different pH in MTP (transparent, flat bottom). MTPs were briefly stirred (5 seconds). The absorbance was continuously recorded (420 nm, room temperature, Tecan Infinite M1000 PRO microtiter plate reader).

The activity profile of P450 BM3 F87A in gradient pH was measured by BCCE assay. In detail, 0.2 μM free or immobilized GGG-his-P450 BM3 F87A (PVCL/GMA-LPETGGG-his-P450 BM3 F87A) was incubated in 97 μL BCCE solution (44.5 nM BCCE, 100 mM, potassium phosphate) with different pH (range from 5.7 to 8.6) in MTP (black, flat bottom). Sample was incubated (5 min, 700 rpm, room temperature). The reaction was initiated by adding NADPH (1μL, 10 mM). Fluorescence was constantly recorded (5 min, room temperature, λ_{exc}: 400 nm, λ_{em}: 440 nm gain=120, Tecan Infinite M1000 PRO microtiter plate reader).

4.4.11. Thermo-stability of immobilized enzymes

Thermo-stability of immobilized CueO (CueO-LPETGGG-PVCL/GMA) and CueO-LPETGGGRR was performed by incubation at 60°C. Firstly, 1.25 nM (70 μg/mL) free or immobilized CueO was incubated (20 μL, 60°C, 1000 rpm, 50 mM, pH 7.5 Tris-HCl). Samples were first cooled down (standing on ice for 3 min) and 3 μL sample was pipetted into ABTS solution (200 μL, 3 mM ABTS, 100 mM, pH 3.0, sodium citrate) in MTP (transparent, flat bottom). The absorbance was continuously recorded (420 nm, room temperature, 5 min, Tecan Infinite M1000 PRO microtiter plate reader).

Thermo-stability of PVCL/GMA-LPETGGG-his-P450 F87A was performed by incubation at 35°C. Firstly, free or immobilized GGG-his-P450 BM3 F87A was incubated (30 μL, 35°C, 1000 rpm, 50 mM, pH 8.0, Tris-HCl). Samples were first cooled down (standing on ice for 3 min) and 10 μL aliquot was transferred into 90 μL BCCE solution (44.5 nM BCCE, 50 mM, pH 8.0, Tris-HCl) in MTP (black, flat bottom). Sample was incubated (5 min, 700 rpm, room temperature). The reaction was initiated by adding NADPH (1μL, 10 mM). Fluorescence was constantly recorded (5 min, room temperature, λ_{exc}: 400 nm, λ_{em}: 440 nm gain=120, Tecan Infinite M1000 PRO microtiter plate reader).

4.4.12. Reusability of immobilized enzymes

Reusability of CueO-LPETGGG-PVCL/GMA was performed. CueO-LPETGGG-PVCL/GMA (4 mg) was dispersed and incubated (2 min, 800 rpm, room temperature) in ABTS solution (200 μL, 3 mM ABTS in 100 mM, pH 5.5 sodium acetate) in a 1.5 mL Eppendorf reaction tube. Sample was then

centrifuged (3 min, 10000 rpm, 15°C). All the supernatant was immediately transferred in MTP (transparent, flat bottom) and the absorbance was recoded (420 nm, room temperature, Tecan Infinite M1000 PRO microtiter plate reader). The CueO-LPETGGG-PVCL/GMA pellet was re-dispersed and incubated (2 min, 800 rpm, room temperature) in ABTS solution (200 µL, 3 mM ABTS in 100 mM, pH 5.5 sodium acetate) for cycle 2. Ten consecutive cycles were performed with a same protocol as aforementioned (see cycle 1).

Reusability of PVCL/GMA-LPETGGG-his-P450 F87A was carried out by dispersing PVCL/GMA-LPETGGG-his-P450 F87A (10 mg) in BCCE solution (100 µL, 80 µM BCCE, 50 mM, pH 8.0, Tris-HCl) in MTP (black, flat bottom). Sample was firstly incubated (5 min, 700 rpm, room temperature) and then reaction was initiated by adding NADPH (1µL, 20 mM). Fluorescence was constantly recorded (4 min, room temperature, λ_{exc}: 400 nm, λ_{em}: 440 nm gain=80, Tecan Infinite M1000 PRO microtiter plate reader). In the second cycle, the MTP plate containing PVCL/GMA-LPETGGG-his-P450 F87A was centrifuged (Eppendorf centrifuge 5810 R, 3220 g, 30 min, 4°C). The supernatant was pipetted out. Fresh BCCE solution (40 µM BCCE in 50 mM, pH 8.0, Tris-HCl) was added and pellet was dispersed. The followed procedures were performed same as above (cycle 1). Six consecutive cycles were implemented.

4.4.13. Storage stability of immobilized enzymes

The storage stability of CueO-LPETGGG-PVCL/GMA or PVCL/GMA-LPETGGG-his-P450 F87A was implemented by monitoring their activity when stored at 4°C (0.05 M, pH 7.5, Tris-HCl buffer). Free and immobilized CueO (CueO-LPETGGG-PVCL/GMA) were incubated (1.25 nM CueO, 4°C, 50 mM, pH 7.5, Tris-HCl buffer). Aliquots (5 µL) were pipetted for activity measurement during the incubation. In detail, 5 µL CueO-LPETGGG-PVCL/GMA or CueO-LPETGGGRR was pipetted into ABTS solution (195 µL, 3 mM ABTS, sodium citrate buffer, pH 3.0). Absorbance of ABTS was measured as aforementioned.

Free and immobilized GGG-his-P450 BM3 F87A (PVCL/GMA-LPETGGG-his-P450 BM3 F87A) were incubated (2 µM P450 BM3 F87A, 4°C, 0.05 M, pH 8.0, Tris-HCl buffer). Aliquot (10 µL) of PVCL/GMA-LPETGGG-his-P450 F87A or GGG-his-P450 F87A was pipetted into 83 µL BCCE solution (48.2 µM BCCE, 50 mM, pH 8.0, Tris-HCL) in MTP (black, flat). After incubation (5 min, 700 rpm, room temperature) reaction was initiated by addition of NADPH (1 µL, 10 mM). The fluorescence was constantly recorded (λexc: 400 nm, λem: 440 nm, room temperature, gain=120, Tecan Infinite M1000 PRO reader).

4.4.14. Application of immobilized CueO laccase in decolourization of synthetic dyes

Five synthetic dyes (Azure B, Coomassie Brilliant blue R250, Indigo carmine, Methyl Orange, and Reactive Black 5) were selected as substrates to perform laccase-mediated decolourization in this study. The efficiencies of decolourization of CueO laccase (free enzyme) towards the dyes were firstly investigated. In detail, 0.1 mM dye, 1.5 mM $CuSO_4$, and 6 μM CueO-LPETGGGRR were incubated (1000 rpm, room temperature) in buffer (200 μL, 0.1 M, pH 5.5, sodium acetate) in 1.5 mL Eppendorf reaction tube. Absorbance (Azure B (at 647 nm), Coomassie Brilliant blue R250 (at 555 nm), Indigo carmine (at 608 nm), Methyl Orange (at 465 nm), or Reactive Black 5(at 597 nm)) was recorded (room temperature, Tecan Infinite M1000 PRO plate reader) after 1, 16 and 180 hours incubation. Blank controls containing buffer instead of CueO-LPETGGGRR were performed in parallel. Results are shown as percentage of decreased absorbance with respect to the blank control.

The two dyes (Indigo carmine, Methyl Orange) were selected for further decolourization using immobilized CueO (CueO-LPETGGG-PVCL/GMA). In shortly, 0.25 mM dye (Indigo carmine or Methyl Orange), 1.5 mM $CuSO_4$, and CueO–LPETGGG-PVCL/GMA (10.5 mg, containing 17 μg CueO laccase) were incubated (1000 rpm, room temperature) in buffer (200 μL, 0.1 M, pH 5.5, sodium acetate) in 1.5 mL Eppendorf reaction tube. Three controls were performed in parallel. In the decolonization control 1, GGG-PVCL/GMA (10.5 mg) was added instead of CueO-LPETGGG-PVCL/GMA. In decolourization control 2, 17 μg free Cue-LPETGGGRR laccase was added instead of CueO-LPETGGG-PVCL/GMA. In decolourization control 3, no CueO-LPETGGG-PVCL/GMA was added. Sample was centrifuged (10 min, 10000 rpm, 15°C). Supernatant was transferred into transparent 96-well MTP well. Absorbance of supernatant of indigo carmine (at 608 nm) or methyl orange (at 465 nm), was recorded after 1, 16, 40, 120 and 180 hours incubation. Data is shown as percentage of decreased color absorbance with respect to the absorbance in DC3. The decolourization of Indigo carmine and Methyl Orange catalyzed by immobilized CueO-LPETGGG-PVCL/GMA was showed in Figure S13a and S13b.

Reusability of CueO-LPETGGG-PVCL/GMA in decolourization of indigo carmine was implemented based on the previous protocol (see reusability experiment of CueO-LPETGGG-PVCL/GMA). In short, 0.25 mM indigo carmine, 1.5 mM $CuSO_4$, and CueO-LPETGGG-PVCL/GMA (16 mg, containing 26 μg CueO laccase) were incubated (1000 rpm, room 20°C) in buffer (200 μL, 0.1 M, pH 5.5, sodium acetate) in 1.5 mL Eppendorf reaction tube. After 24 h, sample was centrifuged (3 min, 10000 rpm, 15°C). Supernatant was transferred into MTP (transparent, flat bottom) and absorbance was recorded. The pellet of CueO-LPETGGG-PVCL/GMA in reaction tube was dispersed again with fresh dye solution (200 μL, 0.25 mM indigo carmine, 1.5 mM CuSO4, 0.1 M, pH 5.5, sodium acetate) in cycle 2. Same protocol was

used in each reused cycle. One control of reusability was performed in parallel in which GGG-PVCL/GMA (16 mg) instead of CueO-LPETGGG-PVCL/GMA was added. Reusability of CueO-LPETGGG-PVCL/GMA in methyl orange was performed similarly as the protocol in decolourization of indigo carmine. Two changes were made: 0.25 mM methyl orange instead of indigo carmine was used; the incubation time for each cycle was performed 72 h instead of 24 h.

5. Lessons learned from directed sortase evolution and sortase-mediated polymer functionalization

In 2018, the Nobel Prize of Chemistry has been awarded to three scientists (Frances Arnold, George Smith, and Gregory Winter) who have innovated techniques of directed protein/enzyme evolution. The power of evolution is revealed through the diversity of life in the world. By means of directed evolution, we harness the power of evolution for purposes that bring the greatest benefit to the society.

In this thesis, we developed a polypropylene surface based screening platform for directed evolution of enzymes (e.g. sortase and laccase). By means of SML, enzymes with a minimal LPxTG modification in the C-terminal are conjugated to a polypropylene binding peptide LCI. The conjugates specifically attach to PP-MTP surface and a semi-purification of enzyme is achieved. A main advantage of the screening platform is that background noise can be minimized in screening of enzymes. This platform provides a simple approach to overcome the common risk of the high interferences from cell-free lysate in HTS assays. Furthermore, we learned that Sa-SrtA enables a controlled surface coating by bioactive molecules. The latter might promote the *in situ* regeneration of biofilms or biomembranes on polymer surfaces.

We engineered Sa-SrtA for improved activity/resistance in organic co-solvents using a KnowVolution strategy, an optimized directed protein evolution strategy from our group.[52] By using the standard four phases in KnowVolution (see 3.3.2), Sa-SrtA variants with desirable resistance/activity were obtained after a single round of screening within three months. KnowVolution has significantly reduces the time requirements in protein engineering when compared to the traditional directed evolution campaign (in general one to two year are need). The advancement of KnowVolution brings enzyme engineering a step closer to the process developments.

Sa-SrtA has relaxed specificity for the diverse substrates (e.g. primary amines, hydrazines) in addition to the canonical oligo glycine peptides. Organic solvents dissolve many compounds which are low-/non-soluble in water. We proved sortase-mediated peptide-amine ligations are able to perform in high concentration of organic solvents (≤ 45 % (v/v)) with high yields (up to 94%) using the evolved Sa-SrtA variants. The latter expands SML application when hydrophobic substrates are involved. Moreover, by using of amine/hydrazine substrates, the generated conjugate lacks the LPxTG and does not recognizes by Sa-SrtA. The latter prevents the back reaction and product hydrolysis in SML and therefore a high yield of product can be achieved.

Lessons learned from directed sortase evolution and sortase-mediated polymer functionalization

We exploited SML for the enzymatic functionalization of soft polymer surface (Poly (*N*-vinylcaprolactam microgel surface). Sa-SrtA shows its versatilities in different enzyme-microgel bioconjugations either at N- or C-terminus. Notably, protein purification and immobilization can be combined in a single step using SML. Hereby, we saw the high site specificity of SML toolbox facilitates the protein engineering and process engineering. Immobilized enzymes (CueO laccase) showed comparable catalytic efficiency after eight consecutive reused rounds in indigo decolourization by using a single step of sortase-mediated ligation. The results reveal the main advantage of site-specific covalent immobilization of enzymes.

6. Summary and conclusions

Sortase-mediated ligation has endowed scientists with a powerful tool in protein engineering and materials science when site-specific bioconjugation are required. In this thesis, we achieved progresses in tailoring sortase A properties (e.g. activity, solvents resistance) by directed evolution. We gained the knowledge for stabilizing sortase A in organic co-solvents. We developed sortase-mediated methodologies to efficiently functionalize polymer surface and microgel.

In chapter II, a sortase-mediated screening platform (SortEvolve) in 96-well PP-MTP was established. Employing SortEvolve in directed enzyme evolution was demonstrated using two applications. In the first application, directed sortase evolution for improved ligation efficiencies (Application 1) was demonstrated. In the second application, sortase was used to mediate directed laccase evolution for enhanced oxidation activity coupled with a semi-purification process (application 2). Applications of the sortase-based screening were successfully validated by screening three Sa-SrtA SSM libraries and two CueO laccase SSM libraries, respectively. Notably, background noise in SortEvolve (application 2) was minimized by 20-fold. The latter offers a general solution for screening of enzymes when high background noise is observed using the crude cellular extract. Furthermore, SortEvolve enables site-specific immobilization of biomolecules on polypropylene and other similar surfaces under mild conditions. The latter could potentially open new methodologies for chemo-selective and controlled surface functionalization.

In chapter III, directed Sa-SrtA evolution campaign to improve its resistance towards organic solvents was performed. Sa-SrtA variants with up to 2.2-fold improved resistance (Sa-SrtA M1) and 6.3-fold (Sa-SrtA M3) catalytic efficiency in 45% (v/v) DMSO were identified. Impressively, M3 not only gained remarkable activity (5.5-fold) in DMSO co-solvent but also in other co-solvents (e.g. DMF, ethanol, methanol, ACN). Computational studies of Sa-SrtA WT and variants were initially investigated in water and DMSO co-solvent. Analysis of molecular dynamic simulations addressed the importance of conformation mobility for the resistance and activity performance in DMSO co-solvent. The gained knowledge in simulations might offer a new guideline to further engineer Sa-SrtA for higher resistance/activity in organic co-solvents. Finally, sortase-mediated toolbox has been expanded to site-specifically conjugate hydrophobic substrates in organic co-solvents. Notably, evolved variants M3 showed enhanced conjugation activities for peptide as well as commercially available amines. These results will likely expand availability of sortase-mediated toolbox to use hydrophobic amine based compounds as substrates or synthesize hydrophobic products. The latter will facilitate more applications in hybrid peptide and biomaterials synthesis.

Summary and conclusions

In Chapter IV, a general enzyme immobilization methodology was demonstrated by covalently and site-specifically grafting enzymes on the surface of stimuli-responsive PVCL microgel. A series of enzymes were successfully immobilized on microgel by simply using the cell-free lysate, combining protein purification and immobilization in a single step. Performance of immobilized enzymes regarding, kinetics, solvent/pH/thermos/storage stability, and reusability were studied. Finally, immobilized CueO laccase was successfully exploited in decolorizing synthetic dyes. In summary, this study provides a versatile approach to functionalize polymers with desired bio-functionalities as well as to rapidly and cost-effectively generate immobilized biocatalysts.

7. References

1.   Scott, J. R.; Barnett, T. C., Surface proteins of gram-positive bacteria and how they get there. *Annu Rev Microbiol* **2006,** *60*, 397-423.

2.   Spirig, T.; Weiner, E. M.; Clubb, R. T., Sortase enzymes in Gram-positive bacteria. *Mol Microbiol* **2011,** *82* (5), 1044-1059.

3.   Scott, J. R.; Zahner, D., Pili with strong attachments: Gram-positive bacteria do it differently. *Mol Microbiol* **2006,** *62* (2), 320-330.

4.   Mazmanian, S. K.; Liu, G.; Hung, T. T.; Schneewind, O., *Staphylococcus aureus* sortase, an enzyme that anchors surface proteins to the cell wall. *Science* **1999,** *285* (5428), 760-763.

5.   Bradshaw, W. J.; Davies, A. H.; Chambers, C. J.; Roberts, A. K.; Shone, C. C.; Acharya, K. R., Molecular features of the sortase enzyme family. *Febs J* **2015,** *282* (11), 2097-2114.

6.   Paterson, G. K.; Mitchell, T. J., The biology of Gram-positive sortase enzymes. *Trends Microbiol* **2004,** *12* (2), 89-95.

7.   Maresso, A. W.; Schneewind, O., Sortase as a target of anti-infective therapy. *Pharmacol Rev* **2008,** *60* (1), 128-141.

8.   Cossart, P.; Jonquieres, R., Sortase, a universal target for therapeutic agents against Gram-positive bacteria? *P Natl Acad Sci USA* **2000,** *97* (10), 5013-5015.

9.   Guimaraes, C. P.; Witte, M. D.; Theile, C. S.; Bozkurt, G.; Kundrat, L.; Blom, A. E. M.; Ploegh, H. L., Site-specific C-terminal and internal loop labeling of proteins using sortase-mediated reactions. *Nat. Protocols* **2013,** *8* (9), 1787-1799.

10.   Suree, N.; Liew, C. K.; Villareal, V. A.; Thieu, W.; Fadeev, E. A.; Clemens, J. J.; Jung, M. E.; Clubb, R. T., The Structure of the *Staphylococcus aureus* Sortase-Substrate Complex Reveals How the Universally Conserved LPXTG Sorting Signal Is Recognized. *J Biol Chem* **2009,** *284* (36), 24465-24477.

11.   Clancy, K. W.; Melvin, J. A.; McCafferty, D. G., Sortase Transpeptidases: Insights Into Mechanism, Substrate Specificity, and Inhibition (vol 94, pg 385, 2010). *Biopolymers* **2010,** *94* (5), 681-681.

12.   Huang, X. Y.; Aulabaugh, A.; Ding, W. D.; Kapoor, B.; Alksne, L.; Tabei, K.; Ellestad, G., Kinetic mechanism of Staphylococcus aureus sortase SrtA. *Biochemistry* **2003,** *42* (38), 11307-11315.

13.   Ilangovan, U.; Ton-That, H.; Iwahara, J.; Schneewind, O.; Clubb, R. T., Structure of sortase, the transpeptidase that anchors proteins to the cell wall of Staphylococcus aureus. *P Natl Acad Sci USA* **2001,** *98* (11), 6056-6061.

14.   Naik, M. T.; Suree, N.; Ilangovan, U.; Liew, C. K.; Thieu, W.; Campbell, D. O.; Clemens, J. J.; Jung, M. E.; Clubb, R. T., *Staphylococcus aureus* Sortase A transpeptidase - Calcium promotes sorting signal binding by altering the mobility and structure of an active site loop. *J Biol Chem* **2006,** *281* (3), 1817-1826.

15.   Race, P. R.; Bentley, M. L.; Melvin, J. A.; Crow, A.; Hughes, R. K.; Smith, W. D.; Sessions, R. B.; Kehoe, M. A.; McCafferty, D. G.; Banfield, M. J., Crystal Structure of Streptococcus pyogenes Sortase A IMPLICATIONS FOR SORTASE MECHANISM. *J Biol Chem* **2009,** *284* (11), 6924-6933.

16.   Kang, H. J.; Coulibaly, F.; Proft, T.; Baker, E. N., Crystal Structure of Spy0129, a Streptococcus pyogenes Class B Sortase Involved in Pilus Assembly. *Plos One* **2011,** *6* (1).

17.   Kruger, R. G.; Otvos, B.; Frankel, B. A.; Bentley, M.; Dostal, P.; McCafferty, D. G., Analysis of the substrate specificity of the Staphylococcus aureus sortase transpeptidase SrtA. *Biochemistry* **2004,** *43* (6), 1541-1551.

18.   Dorr, B. M.; Ham, H. O.; An, C. H.; Chaikof, E. L.; Liu, D. R., Reprogramming the specificity of sortase enzymes. *P Natl Acad Sci USA* **2014,** *111* (37), 13343-13348.

19.   Schmohl, L.; Bierlmeier, J.; von Kugelgen, N.; Kurz, L.; Reis, P.; Barthels, F.; Mach, P.; Schutkowski, M.; Freund, C.; Schwarzer, D., Identification of sortase substrates by specificity profiling. *Bioorgan Med Chem* **2017,** *25* (18), 5002-5007.

References

20.   Popp, M. W.; Dougan, S. K.; Chuang, T. Y.; Spooner, E.; Ploegh, H. L., Sortase-catalyzed transformations that improve the properties of cytokines. *P Natl Acad Sci USA* **2011,** *108* (8), 3169-3174.

21.   Nikghalb, K. D.; Horvath, N. M.; Prelesnik, J. L.; Banks, O. G. B.; Filipov, P. A.; Row, R. D.; Roark, T. J.; Antos, J. M., Expanding the Scope of Sortase-Mediated Ligations by Using Sortase Homologues. *Chembiochem* **2018,** *19* (2), 185-195.

22.   Mazmanian, S. K.; Ton-That, H.; Su, K.; Schneewind, O., An iron-regulated sortase anchors a class of surface protein during Staphylococcus aureus pathogenesis. *P Natl Acad Sci USA* **2002,** *99* (4), 2293-2298.

23.   Mazmanian, S. K.; Skaar, E. P.; Gaspar, A. H.; Humayun, M.; Gornicki, P.; Jelenska, J.; Joachmiak, A.; Missiakas, D. M.; Schneewind, O., Passage of heme-iron across the envelope of Staphylococcus aureus. *Science* **2003,** *299* (5608), 906-909.

24.   Maresso, A. W.; Chapa, T. J.; Schneewind, O., Surface protein IsdC and sortase B are required for heme-iron scavenging of Bacillus anthracis. *J Bacteriol* **2006,** *188* (23), 8145-8152.

25.   Perry, A. M.; Ton-That, H.; Mazmanian, S. K.; Schneewind, O., Anchoring of surface proteins to the cell wall of Staphylococcus aureus. III. Lipid II is an in vivo peptidoglycan substrate for sortase-catalyzed surface protein anchoring. *J Biol Chem* **2002,** *277* (18), 16241-8.

26.   Jacobitz, A. W.; Wereszczynski, J.; Yi, S. W.; Amer, B. R.; Huang, G. L.; Nguyen, A. V.; Sawaya, M. R.; Jung, M. E.; McCammon, J. A.; Clubb, R. T., Structural and Computational Studies of the Staphylococcus Aureus Sortase B-Substrate Complex Provide New Insight into the Mechanism of Sortase Transpeptidases. *Biophys J* **2014,** *106* (2), 677a-677a.

27.   Bentley, M. L.; Gaweska, H.; Kielec, J. M.; McCafferty, D. G., Engineering the substrate specificity of Staphylococcus aureus Sortase A. The beta6/beta7 loop from SrtB confers NPQTN recognition to SrtA. *J Biol Chem* **2007,** *282* (9), 6571-81.

28.   Neiers, F.; Madhurantakam, C.; Falker, S.; Manzano, C.; Dessen, A.; Normark, S.; Henriques-Normark, B.; Achour, A., Two Crystal Structures of Pneumococcal Pilus Sortase C Provide Novel Insights into Catalysis and Substrate Specificity. *J Mol Biol* **2009,** *393* (3), 704-716.

29.   Barnett, T. C.; Patel, A. R.; Scott, J. R., A novel sortase, SrtC2, from Streptococcus pyogenes anchors a surface protein containing a QVPTGV motif to the cell wall. *J Bacteriol* **2004,** *186* (17), 5865-5875.

30.   Marraffini, L. A.; Schneewind, O., Sortase C-mediated anchoring of BasI to the cell wall envelope of Bacillus anthracis. *J Bacteriol* **2007,** *189* (17), 6425-6436.

31.   Marraffini, L. A.; Schneewind, O., Targeting proteins to the cell wall of sporulating Bacillus anthracis. *Mol Microbiol* **2006,** *62* (5), 1402-1417.

32.   Gaspar, A. H.; Ton-That, H., Assembly of distinct pilus structures on the surface of Corynebacterium diphtheriae. *J Bacteriol* **2006,** *188* (4), 1526-1533.

33.   Comfort, D.; Clubb, R. T., A comparative genome analysis identifies distinct sorting pathways in gram-positive bacteria. *Infect Immun* **2004,** *72* (5), 2710-22.

34.   Mao, H. Y.; Hart, S. A.; Schink, A.; Pollok, B. A., Sortase-mediated protein ligation: A new method for protein engineering. *J Am Chem Soc* **2004,** *126* (9), 2670-2671.

35.   Schmohl, L.; Schwarzer, D., Sortase-mediated ligations for the site-specific modification of proteins. *Curr Opin Chem Biol* **2014,** *22*, 122-128.

36.   Tsukiji, S.; Nagamune, T., Sortase-Mediated Ligation: A Gift from Gram-Positive Bacteria to Protein Engineering. *Chembiochem* **2009,** *10* (5), 787-798.

37.   Parthasarathy, R.; Subramanian, S.; Boder, E. T., Sortase A as a novel molecular "stapler" for sequence-specific protein conjugation. *Bioconjugate Chem* **2007,** *18* (2), 469-476.

38.   Popp, M. W.; Antos, J. M.; Grotenbreg, G. M.; Spooner, E.; Ploegh, H. L., Sortagging: a versatile method for protein labeling. *Nat Chem Biol* **2007,** *3* (11), 707-708.

39.   Pritz, S.; Wolf, Y.; Kraetke, O.; Klose, J.; Bienert, M.; Beyermann, M., Synthesis of biologically active peptide nucleic acid-peptide conjugates by sortase-mediated ligation. *J Org Chem* **2007,** *72* (10), 3909-3912.

References

40.   Antos, J. M.; Miller, G. M.; Grotenbreg, G. M.; Ploegh, H. L., Lipid Modification of Proteins through Sortase-Catalyzed Transpeptidation. *J Am Chem Soc* **2008,** *130* (48), 16338-16343.

41.   Samantaray, S.; Marathe, U.; Dasgupta, S.; Nandicoori, V. K.; Roy, R. P., Peptide-sugar ligation catalyzed by transpeptidase sortase: A facile approach to neoglycoconjugate synthesis. *J Am Chem Soc* **2008,** *130* (7), 2132-+.

42.   Theile, C. S.; Witte, M. D.; Blom, A. E. M.; Kundrat, L.; Ploegh, H. L.; Guimaraes, C. P., Site-specific N-terminal labeling of proteins using sortase-mediated reactions. *Nat Protoc* **2013,** *8* (9), 1800-1807.

43.   Chan, L. Y.; Cross, H. F.; She, J. K.; Cavalli, G.; Martins, H. F. P.; Neylon, C., Covalent Attachment of Proteins to Solid Supports and Surfaces via Sortase-Mediated Ligation. *Plos One* **2007,** *2* (11).

44.   Ito, T.; Sadamoto, R.; Naruchi, K.; Togame, H.; Takemoto, H.; Kondo, H.; Nishimura, S. I., Highly Oriented Recombinant Glycosyltransferases: Site-Specific Immobilization of Unstable Membrane Proteins by Using Staphylococcus aureus Sortase A. *Biochemistry* **2010,** *49* (11), 2604-2614.

45.   Ham, H. O.; Qu, Z.; Haller, C. A.; Dorr, B. M.; Dai, E. B.; Kim, W.; Liu, D. R.; Chaikof, E. L., In situ regeneration of bioactive coatings enabled by an evolved Staphylococcus aureus sortase A. *Nat Commun* **2016,** *7*.

46.   Warden-Rothman, R.; Caturegli, I.; Popik, V.; Tsourkas, A., Sortase-Tag Expressed Protein Ligation: Combining Protein Purification and Site-Specific Bioconjugation into a Single Step. *Anal Chem* **2013,** *85* (22), 11090-11097.

47.   Witte, M. D.; Wu, T. F.; Guimaraes, C. P.; Theile, C. S.; Blom, A. E. M.; Ingram, J. R.; Li, Z. Y.; Kundrat, L.; Goldberg, S. D.; Ploegh, H. L., Site-specific protein modification using immobilized sortase in batch and continuous-flow systems. *Nat Protoc* **2015,** *10* (3).

48.   Wang, H. H.; Altun, B.; Nwe, K.; Tsourkas, A., Proximity-Based Sortase-Mediated Ligation. *Angew Chem Int Edit* **2017,** *56* (19), 5349-5352.

49.   Strijbis, K.; Spooner, E.; Ploegh, H. L., Protein Ligation in Living Cells Using Sortase. *Traffic* **2012,** *13* (6), 780-789.

50.   Wu, Q.; Ploegh, H. L.; Truttmann, M. C., Hepta-Mutant Staphylococcus aureus Sortase A (SrtA(7m)) as a Tool for in Vivo Protein Labeling in Caenorhabditis elegans. *Acs Chem Biol* **2017,** *12* (3), 664-673.

51.   Glasgow, J.; Salit, M.; Cochran, J., In vivo site-specific protein tagging with diverse amines using an engineered sortase variant. *Abstr Pap Am Chem S* **2017,** *253*.

52.   Cheng, F.; Zhu, L.; Schwaneberg, U., Directed evolution 2.0: improving and deciphering enzyme properties. *Chem Commun* **2015,** *51* (48), 9760-72.

53.   Kuchner, O.; Arnold, F. H., Directed evolution of enzyme catalysts. *Trends Biotechnol* **1997,** *15* (12), 523-530.

54.   Packer, M. S.; Liu, D. R., Methods for the directed evolution of proteins. *Nat Rev Genet* **2015,** *16* (7), 379-394.

55.   Wong, T. S.; Tee, K. L.; Hauer, B.; Schwaneberg, U., Sequence saturation mutagenesis (SeSaM): a novel method for directed evolution. *Nucleic Acids Res* **2004,** *32* (3).

56.   Zhao, H. M.; Arnold, F. H., Optimization of DNA shuffling for high fidelity recombination. *Nucleic Acids Res* **1997,** *25* (6), 1307-1308.

57.   Griffiths, A. D.; Tawfik, D. S., Directed evolution of an extremely fast phosphotriesterase by in vitro compartmentalization. *Embo J* **2003,** *22* (1), 24-35.

58.   Rajpal, A.; Beyaz, N.; Haber, L.; Cappuccilli, G.; Yee, H.; Bhatt, R. R.; Takeuchi, T.; Lerner, R. A.; Crea, R., A general method for greatly improving the affinity of antibodies by using combinatorial libraries. *P Natl Acad Sci USA* **2005,** *102* (24), 8466-8471.

59.   Wang, X. X.; Cho, Y. K.; Shusta, E. V., Mining a yeast library for brain endothelial cell-binding antibodies. *Nat Methods* **2007,** *4* (2), 143-145.

References

60.   Chen, I.; Dorr, B. M.; Liu, D. R., A general strategy for the evolution of bond-forming enzymes using yeast display. *P Natl Acad Sci USA* **2011,** *108* (28), 11399-11404.

61.   Tawfik, D. S.; Griffiths, A. D., Man-made cell-like compartments for molecular evolution. *Nature Biotechnology* **1998,** *16* (7), 652-656.

62.   Korfer, G.; Pitzler, C.; Vojcic, L.; Martinez, R.; Schwaneberg, U., I*n vitro* flow cytometry-based screening platform for cellulase engineering. *Sci. Rep.* **2016,** *6*, 26218: 1-12.

63.   Bessette, P. H.; Rice, J. J.; Daugherty, P. S., Rapid isolation of high-affinity protein binding peptides using bacterial display. *Protein Eng Des Sel* **2004,** *17* (10), 731-739.

64.   Mccafferty, J.; Griffiths, A. D.; Winter, G.; Chiswell, D. J., Phage Antibodies - Filamentous Phage Displaying Antibody Variable Domains. *Nature* **1990,** *348* (6301), 552-554.

65.   Jespers, L. S.; Roberts, A.; Mahler, S. M.; Winter, G.; Hoogenboom, H. R., Guiding the Selection of Human-Antibodies from Phage Display Repertoires to a Single Epitope of an Antigen. *Bio-Technol* **1994,** *12* (9), 899-903.

66.   Wilson, D. S.; Keefe, A. D.; Szostak, J. W., The use of mRNA display to select high-affinity protein-binding peptides. *P Natl Acad Sci USA* **2001,** *98* (7), 3750-3755.

67.   Hanes, J.; Pluckthun, A., In vitro selection and evolution of functional proteins by using ribosome display. *P Natl Acad Sci USA* **1997,** *94* (10), 4937-4942.

68.   Chen, L.; Cohen, J.; Song, X. D.; Zhao, A. S.; Ye, Z.; Feulner, C. J.; Doonan, P.; Somers, W.; Lin, L.; Chen, P. R., Improved variants of SrtA for site-specific conjugation on antibodies and proteins with high efficiency. *Sci.Rep.* **2016,** *6*, 31899: 1-12.

69.   Hirakawa, H.; Ishikawa, S.; Nagamune, T., Design of Ca2+-independent *Staphylococcus aureus* sortase A mutants. *Biotechnol Bioeng* **2012,** *109* (12), 2955-2961.

70.   Wuethrich, I.; Peeters, J. G. C.; Blom, A. E. M.; Theile, C. S.; Li, Z. Y.; Spooner, E.; Ploegh, H. L.; Guimaraes, C. P., Site-Specific Chemoenzymatic Labeling of Aerolysin Enables the Identification of New Aerolysin Receptors. *Plos One* **2014,** *9* (10).

71.   Gianella, P.; Snapp, E. L.; Levy, M., An *in vitro* compartmentalization-based method for the selection of bond-forming enzymes from large libraries. *Biotechnol Bioeng* **2016,** *113* (8), 1647-1657.

72.   Piotukh, K.; Geltinger, B.; Heinrich, N.; Gerth, F.; Beyermann, M.; Freund, C.; Schwarzer, D., Directed Evolution of Sortase A Mutants with Altered Substrate Selectivity Profiles. *J Am Chem Soc* **2011,** *133* (44), 17536-17539.

73.   Cheng, F.; Zhu, L. L.; Schwaneberg, U., Directed evolution 2.0: improving and deciphering enzyme properties. *Chem Commun* **2015,** *51* (48), 9760-9772.

74.   Lulsdorf, N.; Vojcic, L.; Hellmuth, H.; Weber, T. T.; Mumann, N.; Martinez, R.; Schwaneberg, U., A first continuous 4-aminoantipyrine (4-AAP)-based screening system for directed esterase evolution. *Appl Microbiol Biot* **2015,** *99* (12), 5237-5246.

75.   Zhu, L. L.; Cheng, F.; Piatkowski, V.; Schwaneberg, U., Protein Engineering of the Antitumor Enzyme PpADI for Improved Thermal Resistance. *Chembiochem* **2014,** *15* (2), 276-283.

76.   Kruger, R. G.; Dostal, P.; McCafferty, D. G., Development of a high-performance liquid chromatography assay and revision of kinetic parameters for the Staphylococcus aureus sortase transpeptidase SrtA. *Anal Biochem* **2004,** *326* (1), 42-48.

77.   Chen, L.; Cohen, J.; Song, X. D.; Zhao, A. S.; Ye, Z.; Feulner, C. J.; Doonan, P.; Somers, W.; Lin, L.; Chen, P. R., Improved variants of SrtA for site-specific conjugation on antibodies and proteins with high efficiency. *Sci Rep-Uk* **2016,** *6*.

78.   Xu, A. J.; Yang, Y.; Zhang, C. Y., Transpeptidation-directed intramolecular bipartite tetracysteine display for sortase activity assay. *Chem Commun* **2018,** *54* (58), 8116-8119.

79.   Pitzler, C.; Wirtz, G.; Vojcic, L.; Hiltl, S.; Boker, A.; Martinez, R.; Schwaneberg, U., A Fluorescent Hydrogel-Based Flow Cytometry High-Throughput Screening Platform for Hydrolytic Enzymes. *Chem Biol* **2014,** *21* (12), 1733-1742.

80.   Korfer, G.; Pitzler, C.; Vojcic, L.; Martinez, R.; Schwaneberg, U., In vitro flow cytometry-based screening platform for cellulase engineering. *Sci Rep-Uk* **2016,** *6*.

References

81. Ruff, A. J.; Dennig, A.; Wirtz, G.; Blanusa, M.; Schwaneberg, U., Flow Cytometer-Based High-Throughput Screening System for Accelerated Directed Evolution of P450 Monooxygenases. *Acs Catal* **2012,** *2* (12), 2724-2728.

82. Kataoka, K.; Hirota, S.; Maeda, Y.; Kogi, H.; Shinohara, N.; Sekimoto, M.; Sakurai, T., Enhancement of Laccase Activity through the Construction and Breakdown of a Hydrogen Bond at the Type I Copper Center in *Escherichia coli* CueO and the Deletion Mutant Delta alpha 5-7 CueO. *Biochemistry-Us* **2011,** *50* (4), 558-565.

83. Kristin Rübsam; Benjamin Stomps; Alexander Böker; Felix Jakob; Schwaneberg, U., Anchor peptides: A green and versatile method for polypropylene functionalization. *Polymer* **2017,** *116*, 9.

84. Liu, H. F.; Zhu, L. L.; Bocola, M.; Chen, N.; Spiess, A. C.; Schwaneberg, U., Directed laccase evolution for improved ionic liquid resistance. *Green Chem* **2013,** *15* (5), 1348-1355.

85. Rubsam, K.; Stomps, B.; Boker, A.; Jakob, F.; Schwaneberg, U., Anchor peptides: A green and versatile method for polypropylene functionalization. *Polymer* **2017,** *116*, 124-132.

86. Blanusa, M.; Schenk, A.; Sadeghi, H.; Marienhagen, J.; Schwaneberg, U., Phosphorothioate-based ligase-independent gene cloning (PLICing): An enzyme-free and sequence-independent cloning method. *Analytical Biochemistry* **2010,** *406* (2), 141-146.

87. Roberts, S. A.; Weichsel, A.; Grass, G.; Thakali, K.; Hazzard, J. T.; Tollin, G.; Rensing, C.; Montfort, W. R., Crystal structure and electron transfer kinetics of CueO, a multicopper oxidase required for copper homeostasis in *Escherichia coli*. *Proc Natl Acad Sci U S A* **2002,** *99* (5), 2766-2771.

88. Tee, K. L.; Schwaneberg, U., Directed evolution of oxygenases: Screening systems, success stories and challenges. *Comb Chem High T Scr* **2007,** *10* (3), 197-217.

89. Mate, D. M.; Gonzalez-Perez, D.; Falk, M.; Kittl, R.; Pita, M.; De Lacey, A. L.; Ludwig, R.; Shleev, S.; Alcalde, M., Blood Tolerant Laccase by Directed Evolution. *Chem Biol* **2013,** *20* (2), 223-231.

90. Zumarraga, M.; Bulter, T.; Shleev, S.; Polaina, J.; Martinez-Arias, A.; Plow, F. J.; Ballesteros, A.; Alcalde, M., *In vitro* evolution of a fungal laccase in high concentrations of organic cosolvents. *Chem Biol* **2007,** *14* (9), 1052-1064.

91. Guimaraes, C. P.; Witte, M. D.; Theile, C. S.; Bozkurt, G.; Kundrat, L.; Blom, A. E. M.; Ploegh, H. L., Site-specific C-terminal and internal loop labeling of proteins using sortase-mediated reactions. *Nat Protoc* **2013,** *8* (9), 1787-1799.

92. Halaburgi, V. M.; Sharma, S.; Sinha, M.; Singh, T. P.; Karegoudar, T. B., Purification and characterization of a thermostable laccase from the ascomycetes *Cladosporium cladosporioides* and its applications. *Process Biochem* **2011,** *46* (5), 1146-1152.

93. Stephanopoulos, N.; Francis, M. B., Choosing an effective protein bioconjugation strategy. *Nat Chem Biol* **2011,** *7* (12), 876-884.

94. Francis, M. B.; Carrico, I. S., New frontiers in protein bioconjugation Editorial overview. *Curr Opin Chem Biol* **2010,** *14* (6), 771-773.

95. Kalia, J.; Raines, R. T., Advances in Bioconjugation. *Curr Org Chem* **2010,** *14* (2), 138-147.

96. Peng, H.; Rubsam, K.; Jakob, F.; Schwaneberg, U.; Pich, A., Tunable Enzymatic Activity and Enhanced Stability of Cellulase Immobilized in Biohybrid Nanogels. *Biomacromolecules* **2016,** *17* (11), 3619-3631.

97. Kwon, Y.; Coleman, M. A.; Camarero, J. A., Selective immobilization of proteins onto solid supports through split-intein-mediated protein trans-splicing. *Angew Chem Int Edit* **2006,** *45* (11), 1726-1729.

98. Rashidian, M.; Dozier, J. K.; Distefano, M. D., Enzymatic Labeling of Proteins: Techniques and Approaches. *Bioconjugate Chem* **2013,** *24* (8), 1277-1294.

99. Chen, Q.; Sun, Q.; Molino, N. M.; Wang, S. W.; Boder, E. T.; Chen, W., Sortase A-mediated multi-functionalization of protein nanoparticles. *Chem Commun* **2015,** *51* (60), 12107-12110.

100. Zhao, J.; Kardashliev, T.; Ruff, A. J.; Bocola, M.; Schwaneberg, U., Lessons From Diversity of Directed Evolution Experiments by an Analysis of 3,000 Mutations. *Biotechnology and Bioengineering* **2014,** *111* (12), 2380-2389.

References

101.   Islam, S.; Mate, D. M.; Martinez, R.; Jakob, F.; Schwaneberg, U., A robust protocol for directed aryl sulfotransferase evolution toward the carbohydrate building block GlcNAc. *Biotechnol Bioeng* **2018,** *115* (5), 1106-1115.

102.   Aulabaugh, A.; Ding, W. D.; Kapoor, B.; Tabei, K.; Alksne, L.; Dushin, R.; Zatz, T.; Ellestad, G.; Huang, X. Y., Development of an HPLC assay for Staphylococcus aureus sortase: Evidence for the formation of the kinetically competent acyl enzyme intermediate. *Analytical Biochemistry* **2007,** *360* (1), 14-22.

103.   Wong, T. S.; Arnold, F. H.; Schwaneberg, U., Laboratory evolution of cytochrome p450 BM-3 monooxygenase for organic cosolvents. *Biotechnol Bioeng* **2004,** *85* (3), 351-8.

104.   Wu, Z.; Hong, H.; Zhao, X.; Wang, X., Efficient expression of sortase A from Staphylococcus aureus in Escherichia coli and its enzymatic characterizations. *Bioresour Bioprocess* **2017,** *4* (1), 13.

105.   Guerois, R.; Nielsen, J. E.; Serrano, L., Predicting changes in the stability of proteins and protein complexes: a study of more than 1000 mutations. *Journal of molecular biology* **2002,** *320* (2), 369-387.

106.   Roy, S.; Bagchi, B., Comparative study of protein unfolding in aqueous urea and dimethyl sulfoxide solutions: surface polarity, solvent specificity, and sequence of secondary structure melting. *The Journal of Physical Chemistry B* **2014,** *118* (21), 5691-5697.

107.   Zheng, Y.-J.; Ornstein, R. L., A molecular dynamics and quantum mechanics analysis of the effect of DMSO on enzyme structure and dynamics: subtilisin. *J Am Chem Soc* **1996,** *118* (17), 4175-4180.

108.   Akkarawongsa, R.; Pocaro, N. E.; Case, G.; Kolb, A. W.; Brandt, C. R., Multiple Peptides Homologous to Herpes Simplex Virus Type 1 Glycoprotein B Inhibit Viral Infection. *Antimicrobial Agents and Chemotherapy* **2009,** *53* (3), 987-996.

109.   Zou, Z.; Mate, D. M.; Rubsam, K.; Jakob, F.; Schwaneberg, U., Sortase-Mediated High-Throughput Screening Platform for Directed Enzyme Evolution. *Acs Comb Sci* **2018,** *20* (4), 203-211.

110.   Wong, T. S.; Tee, K. L.; Hauer, B.; Schwaneberg, U., Sequence saturation mutagenesis (SeSaM): a novel method for directed evolution. *Nucleic Acids Res* **2004,** *32* (3), e26.

111.   Ruff, A. J.; Kardashliev, T.; Dennig, A.; Schwaneberg, U., The sequence saturation mutagenesis (SeSaM) method. In *Directed Evolution Library Creation: Methods and Protocols*, Gillam, E. M. J.; Copp, J. N.; Ackerley, D., Eds. Springer New York: New York, NY, 2014; pp 45-68.

112.   Krieger, E.; Koraimann, G.; Vriend, G., Increasing the precision of comparative models with YASARA NOVA—a self-parameterizing force field. *Proteins: Structure, Function, and Bioinformatics* **2002,** *47* (3), 393-402.

113.   Van Durme, J.; Delgado, J.; Stricher, F.; Serrano, L.; Schymkowitz, J.; Rousseau, F., A graphical interface for the FoldX forcefield. *Bioinformatics (Oxford, England)* **2011,** *27* (12), 1711-1712.

114.   Zong, Y.; Bice, T. W.; Ton-That, H.; Schneewind, O.; Narayana, S. V., Crystal structures of Staphylococcus aureus sortase A and its substrate complex. *J Biol Chem* **2004,** *279* (30), 31383-31389.

115.   Pronk, S.; Pall, S.; Schulz, R.; Larsson, P.; Bjelkmar, P.; Apostolov, R.; Shirts, M. R.; Smith, J. C.; Kasson, P. M.; van der Spoel, D.; Hess, B.; Lindahl, E., GROMACS 4.5: a high-throughput and highly parallel open source molecular simulation toolkit. *Bioinformatics* **2013,** *29* (7), 845-54.

116.   Berendsen, H. J. C.; van der Spoel, D.; van Drunen, R., GROMACS: A message-passing parallel molecular dynamics implementation. *Computer Physics Communications* **1995,** *91* (1), 43-56.

117.   Van Der Spoel, D.; Lindahl, E.; Hess, B.; Groenhof, G.; Mark, A. E.; Berendsen, H. J., GROMACS: fast, flexible, and free. *J Comput Chem* **2005,** *26* (16), 1701-18.

118.   Schuler, L. D.; Daura, X.; Van Gunsteren, W. F., An improved GROMOS96 force field for aliphatic hydrocarbons in the condensed phase. *Journal of computational chemistry* **2001,** *22* (11), 1205-1218.

119.   Pall, S.; Abraham, M. J.; Kutzner, C.; Hess, B.; Lindahl, E. In *Tackling exascale software challenges in molecular dynamics simulations with GROMACS*, International Conference on Exascale Applications and Software, Springer: 2014; pp 3-27.

References

120.   Oostenbrink, C.; Villa, A.; Mark, A. E.; Van Gunsteren, W. F., A biomolecular force field based on the free enthalpy of hydration and solvation: the GROMOS force-field parameter sets 53A5 and 53A6. *Journal of computational chemistry* **2004,** *25* (13), 1656-1676.

121.   Dolinsky, T. J.; Nielsen, J. E.; McCammon, J. A.; Baker, N. A., PDB2PQR: an automated pipeline for the setup of Poisson–Boltzmann electrostatics calculations. *Nucleic Acids Research* **2004,** *32* (suppl_2), W665-W667.

122.   Dolinsky, T. J.; Czodrowski, P.; Li, H.; Nielsen, J. E.; Jensen, J. H.; Klebe, G.; Baker, N. A., PDB2PQR: expanding and upgrading automated preparation of biomolecular structures for molecular simulations. *Nucleic Acids Research* **2007,** *35* (suppl_2), W522-W525.

123.   Onufriev, A. V.; Alexov, E., Protonation and pK changes in protein-ligand binding. *Quarterly reviews of biophysics* **2013,** *46* (2), 181-209.

124.   Berendsen, H.; Grigera, J.; Straatsma, T., The missing term in effective pair potentials. *Journal of Physical Chemistry* **1987,** *91* (24), 6269-6271.

125.   Essmann, U.; Perera, L.; Berkowitz, M. L.; Darden, T.; Lee, H.; Pedersen, L. G., A smooth particle mesh Ewald method. *The Journal of chemical physics* **1995,** *103* (19), 8577-8593.

126.   Norberg, J.; Nilsson, L., On the Truncation of Long-Range Electrostatic Interactions in DNA. *Biophysical Journal* **2000,** *79* (3), 1537-1553.

127.   Hess, B.; Bekker, H.; Berendsen, H. J.; Fraaije, J. G., LINCS: a linear constraint solver for molecular simulations. *Journal of computational chemistry* **1997,** *18* (12), 1463-1472.

128.   Maiorov, V. N.; Crippen, G. M., Size-independent comparison of protein three-dimensional structures. *Proteins: Structure, Function, and Bioinformatics* **1995,** *22* (3), 273-283.

129.   Walser, R.; Hünenberger, P. H.; van Gunsteren, W. F., Comparison of different schemes to treat long-range electrostatic interactions in molecular dynamics simulations of a protein crystal. *Proteins: Structure, Function, and Bioinformatics* **2001,** *43* (4), 509-519.

130.   Lobanov, M. Y.; Bogatyreva, N.; Galzitskaya, O., Radius of gyration as an indicator of protein structure compactness. *Molecular Biology* **2008,** *42* (4), 623-628.

131.   Luzar, A., Resolving the hydrogen bond dynamics conundrum. *The Journal of Chemical Physics* **2000,** *113* (23), 10663-10675.

132.   Kabsch, W.; Sander, C., Dictionary of protein secondary structure: pattern recognition of hydrogen-bonded and geometrical features. *Biopolymers* **1983,** *22* (12), 2577-2637.

133.   Kulińska, K.; Kuliński, T.; Lyubartsev, A.; Laaksonen, A.; Adamiak, R. W., Spatial distribution functions as a tool in the analysis of ribonucleic acids hydration — molecular dynamics studies. *Computers & Chemistry* **2000,** *24* (3), 451-457.

134.   Eisenhaber, F.; Lijnzaad, P.; Argos, P.; Sander, C.; Scharf, M., The double cubic lattice method: efficient approaches to numerical integration of surface area and volume and to dot surface contouring of molecular assemblies. *Journal of computational chemistry* **1995,** *16* (3), 273-284.

135.   Lindahl, E.; Hess, B.; Van Der Spoel, D., GROMACS 3.0: a package for molecular simulation and trajectory analysis. *Journal of molecular modeling* **2001,** *7* (8), 306-317.

136.   Humphrey, W.; Dalke, A.; Schulten, K., VMD: Visual molecular dynamics. *Journal of Molecular Graphics* **1996,** *14* (1), 33-38.

137.   Schagger, H., Tricine-SDS-PAGE. *Nat Protoc* **2006,** *1* (1), 16-22.

138.   Sheldon, R. A., Enzyme immobilization: The quest for optimum performance. *Adv Synth Catal* **2007,** *349* (8-9), 1289-1307.

139.   Mateo, C.; Palomo, J. M.; Fernandez-Lorente, G.; Guisan, J. M.; Fernandez-Lafuente, R., Improvement of enzyme activity, stability and selectivity via immobilization techniques. *Enzyme Microb Tech* **2007,** *40* (6), 1451-1463.

140.   Datta, S.; Christena, L. R.; Rajaram, Y. R. S., Enzyme immobilization: an overview on techniques and support materials. *3 Biotech* **2013,** *3* (1), 1-9.

References

141. Mohamad, N. R.; Marzuki, N. H. C.; Buang, N. A.; Huyop, F.; Wahab, R. A., An overview of technologies for immobilization of enzymes and surface analysis techniques for immobilized enzymes. *Biotechnol Biotec Eq* **2015,** *29* (2), 205-220.

142. Klinger, D.; Landfester, K., Stimuli-responsive microgels for the loading and release of functional compounds: Fundamental concepts and applications. *Polymer* **2012,** *53* (23), 5209-5231.

143. Sigolaeva, L. V.; Gladyr, S. Y.; Gelissen, A. P. H.; Mergel, O.; Pergushov, D. V.; Kurochkin, I. N.; Plamper, F. A.; Richtering, W., Dual-Stimuli-Sensitive Microgels as a Tool for Stimulated Spongelike Adsorption of Biomaterials for Biosensor Applications. *Biomacromolecules* **2014,** *15* (10), 3735-3745.

144. Appel, E. A.; Loh, X. J.; Jones, S. T.; Biedermann, F.; Dreiss, C. A.; Scherman, O. A., Ultrahigh-Water-Content Supramolecular Hydrogels Exhibiting Multistimuli Responsiveness. *J Am Chem Soc* **2012,** *134* (28), 11767-11773.

145. Cortez-Lemus, N. A.; Licea-Claverie, A., Poly(N-vinylcaprolactam), a comprehensive review on a thermoresponsive polymer becoming popular. *Prog Polym Sci* **2016,** *53*, 1-51.

146. Liu, J.; Debuigne, A.; Detrembleur, C.; Jerome, C., Poly(N-vinylcaprolactam): A Thermoresponsive Macromolecule with Promising Future in Biomedical Field. *Adv Healthc Mater* **2014,** *3* (12), 1941-1968.

147. Hantzschel, N.; Hund, R. D.; Hund, H.; Schrinner, M.; Luck, C.; Pich, A., Hybrid Microgels with Antibacterial Properties. *Macromol Biosci* **2009,** *9* (5), 444-449.

148. Wang, Y.; Nie, J. S.; Chang, B. S.; Sun, Y. F.; Yang, W. L., Poly(vinylcaprolactam)-Based Biodegradable Multiresponsive Microgels for Drug Delivery. *Biomacromolecules* **2013,** *14* (9), 3034-3046.

149. Vihola, H.; Laukkanen, A.; Hirvonen, J.; Tenhu, H., Binding and release of drugs into and from thermosensitive poly(N-vinyl caprolactam) nanoparticles. *Eur J Pharm Sci* **2002,** *16* (1-2), 69-74.

150. Galaev, I. Y.; Mattiasson, B., Affinity Thermoprecipitation of Trypsin Using Soybean Trypsin Inhibitor Conjugated with a Thermo-Reactive Polymer, Poly(N-Vinyl Caprolactam). *Biotechnol Tech* **1992,** *6* (4), 353-358.

151. Kuptsova, S.; Markvicheva, E.; Kochetkov, K.; Belokon, Y.; Rumsh, L.; Zubov, V., Proteases entrapped in hydrogels based on poly(N-vinyl caprolactam) as promising biocatalysts in water/organic systems. *Biocatal Biotransfor* **2000,** *18* (2), 133-149.

152. Srivastava, A.; Kumar, A., Thermoresponsive poly(N-vinylcaprolactam) cryogels: synthesis and its biophysical evaluation for tissue engineering applications. *J Mater Sci-Mater M* **2010,** *21* (11), 2937-2945.

153. Jesionowski, T.; Zdarta, J.; Krajewska, B., Enzyme immobilization by adsorption: a review. *Adsorption* **2014,** *20* (5-6), 801-821.

154. Zhou, Z.; Hartmann, M., Progress in enzyme immobilization in ordered mesoporous materials and related applications. *Chem Soc Rev* **2013,** *42* (9), 3894-3912.

155. Govardhan, C. P., Crosslinking of enzymes for improved stability and performance. *Curr Opin Biotech* **1999,** *10* (4), 331-335.

156. Popp, M. W. L.; Ploegh, H. L., Making and Breaking Peptide Bonds: Protein Engineering Using Sortase. *Angew Chem Int Edit* **2011,** *50* (22), 5024-5032.

157. Cambria, E.; Renggli, K.; Ahrens, C. C.; Cook, C. D.; Kroll, C.; Krueger, A. T.; Imperiali, B.; Griffith, L. G., Covalent Modification of Synthetic Hydrogels with Bioactive Proteins via Sortase-Mediated Ligation. *Biomacromolecules* **2015,** *16* (8), 2316-2326.

158. Hata, Y.; Matsumoto, T.; Tanaka, T.; Kondo, A., C-Terminal-oriented Immobilization of Enzymes Using Sortase A-mediated Technique. *Macromol Biosci* **2015,** *15* (10), 1375-1380.

159. Gau, E.; Mate, D. M.; Zou, Z.; Oppermann, A.; Topel, A.; Jakob, F.; Woll, D.; Schwaneberg, U.; Pich, A., Sortase-Mediated Surface Functionalization of Stimuli-Responsive Microgels. *Biomacromolecules* **2017,** *18* (9), 2789-2798.

References

160.   Lehmann, C.; Sibilla, F.; Maugeri, Z.; Streit, W. R.; de Maria, P. D.; Martinez, R.; Schwaneberg, U., Reengineering CelA2 cellulase for hydrolysis in aqueous solutions of deep eutectic solvents and concentrated seawater. *Green Chem* **2012,** *14* (10), 2719-2726.

161.   Wong, T. S.; Arnold, F. H.; Schwaneberg, U., Laboratory evolution of cytochrome P450BM-3 monooxygenase for organic cosolvents. *Biotechnol Bioeng* **2004,** *85* (3), 351-358.

162.   Joyce, M. G.; Ekanem, I. S.; Roitel, O.; Dunford, A. J.; Neeli, R.; Girvan, H. M.; Baker, G. J.; Curtis, R. A.; Munro, A. W.; Leys, D., The crystal structure of the FAD/NADPH-binding domain of flavocytochrome P450 BM3. *Febs J* **2012,** *279* (9), 1694-1706.

163.   Dubey, N. C.; Tripathi, B. P.; Muller, M.; Stamm, M.; Ionov, L., Bienzymatic Sequential Reaction on Microgel Particles and Their Cofactor Dependent Applications. *Biomacromolecules* **2016,** *17* (5), 1610-1620.

164.   Rodrigues, R. C.; Ortiz, C.; Berenguer-Murcia, A.; Torres, R.; Fernandez-Lafuente, R., Modifying enzyme activity and selectivity by immobilization. *Chem Soc Rev* **2013,** *42* (15), 6290-6307.

165.   Welsch, N.; Wittemann, A.; Ballauff, M., Enhanced Activity of Enzymes Immobilized in Thermoresponsive Core-Shell Microgels. *J Phys Chem B* **2009,** *113* (49), 16039-16045.

166.   Munro, A. W.; Leys, D. G.; McLean, K. J.; Marshall, K. R.; Ost, T. W. B.; Daff, S.; Miles, C. S.; Chapman, S. K.; Lysek, D. A.; Moser, C. C.; Page, C. C.; Dutton, P. L., P450BM3: the very model of a modern flavocytochrome. *Trends Biochem Sci* **2002,** *27* (5), 250-257.

167.   Zhang, H. M.; Yokom, A. L.; Cheng, S.; Su, M.; Hollenberg, P. F.; Southworth, D. R.; Osawa, Y., The full-length cytochrome P450 enzyme CYP102A1 dimerizes at its reductase domains and has flexible heme domains for efficient catalysis. *J Biol Chem* **2018,** *293* (20), 7727-7736.

168.   Zernia, S.; Ott, F.; Bellmann-Sickert, K.; Frank, R.; Klenner, M.; Jahnke, H. G.; Prager, A.; Abel, B.; Robitzki, A.; Beck-Sickinger, A. G., Peptide-Mediated Specific Immobilization of Catalytically Active Cytochrome P450 BM3 Variant. *Bioconjugate Chem* **2016,** *27* (4), 1090-1097.

169.   Roccatano, D.; Wong, T. S.; Schwaneberg, U.; Zacharias, M., Structural and dynamic properties of cytochrome P450 BM-3 in pure water and in a dimethylsulfoxide/water mixture. *Biopolymers* **2005,** *78* (5), 259-67.

170.   Kuper, J.; Tee, K. L.; Wilmanns, M.; Roccatano, D.; Schwaneberg, U.; Wong, T. S., The role of active-site Phe87 in modulating the organic co-solvent tolerance of cytochrome P450 BM3 monooxygenase. *Acta Crystallogr F* **2012,** *68*, 1013-1017.

171.   Ma, X. J.; Liu, L.; Li, Q. Q.; Liu, Y. Y.; Yi, L.; Ma, L. X.; Zhai, C., High-level expression of a bacterial laccase, CueO from Escherichia coli K12 in Pichia pastoris GS115 and its application on the decolorization of synthetic dyes. *Enzyme Microb Tech* **2017,** *103*, 34-41.

172.   Shakya, A. K.; Sami, H.; Srivastava, A.; Kumar, A., Stability of responsive polymer-protein bioconjugates. *Prog Polym Sci* **2010,** *35* (4), 459-486.

173.   Neeli, R.; Girvan, H. M.; Lawrence, A.; Warren, M. J.; Leys, D.; Scrutton, N. S.; Munro, A. W., The dimeric form of flavocytochrome P450BM3 is catalytically functional as a fatty acid hydroxylase. *FEBS letters* **2005,** *579* (25), 5582-5588.

174.   Wong, Y. X.; Yu, J., Laccase-catalyzed decolorization of synthetic dyes. *Water Res* **1999,** *33* (16), 3512-3520.

175.   Couto, S. R.; Herrera, J. L. T., Industrial and biotechnological applications of laccases: A review. *Biotechnol Adv* **2006,** *24* (5), 500-513.

176.   Zhao, J.; Jia, N.; Jaeger, K. E.; Bocola, M.; Schwaneberg, U., Ionic liquid activated Bacillus subtilis lipase A variants through cooperative surface substitutions. *Biotechnol Bioeng* **2015,** *112* (10), 1997-2004.

177.   Häntzschel, N.; Zhang, F.; Eckert, F.; Pich, A.; Winnik, M. A., Poly(N-vinylcaprolactam-co-glycidyl methacrylate) Aqueous Microgels Labeled with Fluorescent LaF3:Eu Nanoparticles. *Langmuir* **2007,** *23* (21), 10793-10800.

Declaration

I hereby declare that all information in this document has been obtained and presented in accordance with academic rules and ethical conduct. I also declare that, as required by these rules and conduct, I have fully cited and referenced all material and results that are not original to this work.

Aachen, 25th of March 2019

_____

Zhi　Zou

Publications

Zou, Z., Alibiglou, Hoda., Mate, D. M., Davari M. D., Jakob, F., & Schwaneberg, U. (2018). Directed sortase A evolution for efficient site-specific bioconjugations in organic co-solvents. *Chemical communications*, 54, 11467-11470.

Zou, Z., Mate, D. M., Rübsam, K., Jakob, F., & Schwaneberg, U. (2018). Sortase-Mediated High-Throughput Screening Platform for Directed Enzyme Evolution. *ACS combinatorial science*, *20*(4), 203-211.

Gau, E.,* Mate, D. M.,* **Zou, Z**., Oppermann, A., Töpel, A., Jakob, F., Schwaneberg, U & Pich, A. (2017). Sortase-mediated surface functionalization of stimuli-responsive microgels. Biomacromolecules,18(9), 2789-2798. * Shared first authorship.

Zhang, L., Cui, H., **Zou, Z**., Mirzaeigarakani, T., Novoa-Henriquez, C., Jooyeh, B & Schwaneberg, U. (2019). Directed Evolution of a Bacterial Laccase (CueO) for Enzymatic Biofuel Cells. Angewandte Chemie. doi.org/10.1002/ange.201814069

Zou, **Z**[#]., Gau E[#]., El-Awaad, I., Jakob, F., Pich, A., & Schwaneberg, U. A Site-specific Enzyme Immobilization Platform on Surface Microgels for Biotechnological Applications (*to be submitted,* [#]shared first authorship)

Author contributions

Zou, **Z**[#]., Gau E[#]., El-Awaad, I., Jakob, F., Pich, A., & Schwaneberg, U. A Site-specific Enzyme Immobilization Platform on Surface of Microgels for Biotechnological Applications (*to be submitted*)

The manuscript prepared by Zhi Zou and Dr. Elisabeth Gau with a shared first authorship. Manuscript preparation and writing were performed by Zhi Zou and Dr. Islam El-Awaad. Zhi Zou performed the experiments of enzymes production, sortase-mediated enzyme immobilization on surface of microgel, activity profiles of immobilized enzymes (e.g kinetics, solvent resistance, pH dependent profile, storage/thermo stabilities and reusability studies) and application of immobilized enzyme in decolourization of dyes. Microgels (GGG-PVCL/GMA and PVCL/GMA-LPETGGRR) were synthesized and charaterized by Dr. Elisabeth Gau. Dr. Felix Jakob and Prof. Dr. Andrij Pich and Prof. Dr. U. Schwaneberg gave advices to the project, participated in the study design and reviewed the manuscript. A detailed chapter is implemented in the Ph.D thesis of Dr. Elisabeth Gau (2019) for the synthesis and characterizations of PVCL/GMA microgels. Zhi Zou included detailed descriptions of sortase-mediated enzyme immobilization on PVCL/GMA microgels in his thesis (Chapter IV). Parts of this chapter will be published.

Zhi Zou

_____

Dr. Elisabeth Gau

_____

Prof. Dr. Ulrich Schwaneberg

_____

Curriculum vitae

Personal data

Name: Zhi Zou

Gender: Male

Date of Birth: 8th August, 1987

Place of Birth: Huanggang, Hubei, China (PRC)

Marital Status: Married

Nationality: Chinese

Education

2014. 10-Present	PhD fellow of *Biotechnology*, RWTH Aachen University, Aachen, Germany
2011.09-2014.06	Master of *Biochemistry and Molecular Biology*, East China University of Science and Technology (ECUST), Shanghai, China (PRC)
2007.09-2011.06	Bachelor of *Bioengineering*, East China University of Science, Wuhan Textile University, Wuhan, China (PRC)
2004.09-2007.06	The first high school of Yingshan, Huanggang, Hubei, China (PRC)
2004.09-2007.06	The middle school of Caopan, Yingshan, Huanggang, Hubei, China (PRC)